

Microwave Electronics

**DESIGN AND DEVELOPMENT OF PLANAR
CHIPLESS RFID TAGS**

A thesis submitted by

SAJITHA V R

*in partial fulfillment of the
requirements for the degree of*

DOCTOR OF PHILOSOPHY

Under the guidance of

Prof. P. MOHANAN



**DEPARTMENT OF ELECTRONICS
FACULTY OF TECHNOLOGY
COCHIN UNIVERSITY OF SCIENCE AND TECHNOLOGY
KOCHI-22, INDIA**

August 2017

Design and Development of Planar Chipless RFID Tags

Ph.D. Thesis under the Faculty of Technology

Author

Sajitha V R

Department of Electronics
Cochin University of Science and Technology
Kochi - 682022
Email: svrk1989@gmail.com

Supervising Guide

Dr. P. Mohanan

UGC-BSR Professor
Department of Electronics
Cochin University of Science and Technology
Kochi - 682022
Email: drmohan@gmail.com

Department of Electronics
Cochin University of Science and Technology
Kochi - 682022

August 2017

Dedicated to the Almighty,

My parents,

Teachers,

Dear ones...





DEPARTMENT OF ELECTRONICS
COCHIN UNIVERSITY OF SCIENCE AND TECHNOLOGY
KOCHI - 682 022

Dr. P. Mohanan
UGC-BSR Professor

Email: drmohan@gmail.com
Ph: 0484 2576418

Certificate

This is to certify that this thesis entitled “**Design and Development of Planar Chipless RFID Tags**” is an authentic record of research work carried out by **Mrs. Sajitha V R** under my supervision in the Department of Electronics, Cochin University of Science and Technology. The results embodied in this thesis or parts of it have not been presented for any other degree. All the relevant corrections and modifications suggested by the audience and recommended by the doctoral committee of the candidate during the presynopsis seminar have been incorporated in the thesis.

Kochi-22
August 2017

Dr. P. Mohanan
(Supervising Teacher)

Declaration

I hereby declare that the work presented in this thesis entitled “**Design and Development of Planar Chipless RFID Tags**” is a bonafide record of the research work done by me under the supervision of Dr. P. Mohanan, UGC-BSR Professor, Department of Electronics, Cochin University of Science and Technology, India and that no part thereof has been presented for the award of any other degree.

Kochi-22
August 2017

Sajitha V R

Words of Gratitude...

I remember with utmost gratefulness ...

My supervising guide, Dr. P. Mohanan, UGC-BSR Professor, Department of Electronics, Cochin University of Science and Technology, for his valuable guidance, advices and timely care extended to me throughout the research period. I could not have imagined having a better advisor for my research study.

Dr. K. Vasudevan, Department of Electronics, Cochin University of Science and Technology for his constant encouragement and concern. His dedication for research is always a leading source of energy.

Dr. C.K. Aanandan, Professor, Department of Electronics, Cochin University of Science and Technology for the advice, discussions and care rented during these years.

Prof. Supriya M. H., Head, Dept. of Electronics for her great support and help during the writing and timely completion of the thesis.

Prof. James Kurian, for his encouragement and cooperation.

Prof. P. R. S. Pillai, Prof. K. T. Mathew and Prof. Tessamma Thomas former professors, Dept. of Electronics for their support and blessings.

My sincere thanks to Dr. K. G. Nair, former Head and founder of Electromagnetics and Antennas Research (CREMA) Laboratory in Department of Electronics, Cochin University of Science and Technology, for establishing full-fledged laboratory that enabled me to do my research work in a well reputed laboratory in the country.

All Faculty members of the department of Electronics for sharing their pearls of wisdom with me during the course of my research.. I thank all the technical, administrative and non-teaching staff of the department for the warm and cordial relations shared and invaluable helps.

My senior researchers Dr. Nijas C.M. Dr. Sarin V.P, Dr. Nishamol M.S., Dr. Sujith R, Dr. Sumi and Dr. Dinesh R for sharing their sound technical and scientific knowledge with me.

Dr. Shameena V.A., Post-Doctoral Fellow, Queens University, U.K., for the wholehearted support during the documentation. Her precious friendship and good humour has had a significant impact on me.

My fellow researchers and best friends at the CREMA lab Mrs. Roshina T.K, Mr. Prakash K.C., Mrs. Sumitha Mathew Mrs. Anitha R, Mr. Vinesh P.V, Mr. Vivek R, Kurup, Mr. Mohammad Ameen, Mr. Manoj M, Ms Remsha M, Ms. Vinisha C.V, Mr. Deepak U, and Mrs. Anila P.V., and for all the immemorable times we spent together.

Mr. Jayakrishnan M.P, and Ms. Nimisha S., Research Fellows, Grenoble University, France for all their untiring support and help during the wee period of my research work,

My research colleagues from the RCS lab, Sreenath S, Lindo A.O, Anju Mathews, Sreekala P.S, Libimol V. A., and Dibin Mary Pulickal for their encouragement.

My colleagues at Centre for Ocean Electronics (CUCENTOL), Microwave Tomography and Material Research Laboratory (MTMR) and Audio and Image Research Lab (AIRL), Department of Electronics, Cochin University of Science and Technology for the supreme cooperation and excellent rapport.

My friends at CUSAT, especially Dr. Prabha C, Anjali Shiju, Binoy Babu, Vipin V P, Vinod V K T, Rijoy, Shari Mohan, Jisha, Jissa, Aswathi, Thasli, for their encouragement and help.

Kerala State Council for Science Technology and Environment (KSCSTE) for supporting my research work financially.

My friends at home town (Thrissur), especially Aathira, Vimitha, Hashmi and Silpa for their encouragement.

My teachers, mentors and my friends at all stages of my education.

My sisters (Saritha and Anitha), grandmother (Karthayayini), Prasannamma, Shanti ammayi, echu ammooma, chimju, chinnu and other family members for being there always as a constant source of energy.

My father (V. K. Radhakrishnan) for being there always as a silent source of energy...

Amma (Anjanavathi) who always gave the highest priority to my education in spite of all hardships.

My Husband (Dipu) for his love, support and care.

My son Ishaan...

My son Devharsh for making me blissful with his charming smile

Above all there is that supreme power whose blessings and kindness without which one single step would not have been possible

Sajitha

Abstract

Chipless RFID is an emerging field which is still in its infancy and expected to be a promising cost effective alternative to conventional RFID. The frequency domain Chipless RFID tags are very attractive in terms of data encoding capacity compared to other developed Chipless tags (except SAW tags). Moreover, they are fully printable, planar, robust and low cost. The thesis is focused on the development of frequency domain Chipless RFID tags. Without any embedded integrated circuits and power sources in the tag, data is encoded using microstrip resonators as spectral signatures. Stepped impedance resonators and Cross loop resonators are presented as the basic elements of the tags. Tags with and without transmitting and receiving antennas are presented. For the tag with antenna, resonators coupled to the transmission line are seen to be more effective than resonators connected to the transmission line. The tag achieved a surface encoding capacity of 1.68 bits/cm^2 on RT Duroid 5880 ($\epsilon_r = 2.2$, $\tan\delta = 0.0009$). Tags without antennas are designed with special focus given to polarization independency, Compactness and high encoding capacity. Two polarization independent tags using cross loop resonator and SIR are developed and surface coding capacity of 1.71 bits/cm^2 and 1.08 bits/cm^2 , respectively are obtained (using RT Duroid 5880 with $\epsilon_r = 2.2$ and $\tan\delta = 0.0009$). SIR based polarization independent tag is modified to get high bit encoding capacity and compactness and the highest surface encoding capacity obtained is 3.54 bits/cm^2 . Time-Frequency domain duality is exploited for tag detection in time domain using UWB Gaussian pulse. Using Matlab, the received data in time domain signal converted into Frequency domain and decoded the tag information. Finally, all the developed tags are tabulated along with their properties.

Contents

Abstract	i
List of Tables	vii
List of Figures	ix
Abbreviations and Symbols	xxi

Chapter 1

INTRODUCTION	01 - 27
1.1 Introduction.....	02
1.2 Components of RFID System.....	05
1.2.1 Reader.....	05
1.2.2 Transponder/Tag	06
1.2.2.1 Passive tags.....	07
1.2.2.2 Semi- passive tags	07
1.2.2.3 Active tags	08
1.2.3 Host computer and middleware.....	09
1.3 Applications of RFID	10
1.4 RFID Vs Optical Barcode	12
1.5 Chipless RFID: New era of RFID.....	13
1.5.1 Time Domain Reflectometry (TDR) Based Chipless RFID Tags	15
1.5.1.1 Non-printable TDR tags: SAW tags	15
1.5.1.2 Printable time domain Chipless RFID tags	17
1.5.2 Spectral signature based/Frequency domain based Chipless RFID tags	19
1.6 Motivation of the thesis.....	21
1.7 Thesis outline.....	22
References.....	25

Chapter 2

METHODOLOGY AND LITERATURE REVIEW OF CHIPLESS RFID TAGS	29 - 83
2.1 Introduction.....	30
2.2 Pre-fabrication studies.....	30
2.3 Fabrication	33
2.4 Tag measurements.....	34
2.5 Literature Survey-Introduction	35
2.6. Review of Frequency domain Chipless RFID tags.....	37
2.6.1 Tags with transmitting/receiving antennas	37
2.6.2 Tags without transmitting/receiving antennas.....	45

2.7	Review on techniques to analyse backscattering from Chipless frequency domain tags	57
2.8	Frequency domain Chipless RFID readers	65
2.9	Conclusion	68
	References.....	68

Chapter 3

CHIPLESS RFID TAGS WITH RECEPTION/TRANSMISSION ANTENNAS85 – 135

3.1	Introduction.....	86
3.2	Data encoding techniques for frequency domain Chipless RFID tags.....	88
3.3	Stepped Impedance Resonators (SIR)	90
3.3.1	Basic Stepped Impedance Resonator.....	92
3.3.1.1	Resonant condition	94
3.3.1.2	Relationship between K, α , fundamental frequency and first harmonic frequency	96
3.3.1.3	Relationship between K and physical size of SIR	97
3.4	A single SIR connected to microstrip transmission line	98
3.4.1	Equivalent circuit of the stepped impedance resonator connected to transmission line.....	100
3.4.2	Selection of Substrate for the tag	105
3.4.3	Optimization of the microstrip resonator and transmission line resonator.....	107
3.5	Multiresonator circuit design using SIR.....	110
3.6	Modified Chipless RFID tag with SIR coupled to transmission line... ..	115
3.6.1	Effect of coupling gap between transmission line	118
3.6.2	Distance between neighboring SIRs.....	119
3.6.3	The multiresonator circuit design using SIRs coupled to microstrip line	120
3.7	Tag antennas	125
3.8	Friss free space transmission formula to calculate free space losses in multiresonator based Chipless RFID system.....	129
3.9	Chipless RFID tag with antennas.....	130
3.10	Conclusion.....	133
	References	133

Chapter 4

MULTISCATTERER BASED CHIPLESS RFID TAGS137 - 198

4.1	Introduction.....	138
4.2	Backscattering from multiscatterer based Chipless RFID tag	139

4.3	Characteristics of the scatterer used in Chipless Frequency domain RFID tags	141
4.3.1	Cross loop resonator	143
4.3.2	Orthogonally aligned SIRs based scatterer	146
4.4	Substrate for the tags	148
4.5	Calibration method	151
4.6	Chipless RFID tag using Cross loop resonator	153
4.6.1	Single cross loop resonator	153
4.6.1.1	Design equation of a single cross loop resonator	154
4.6.1.2	Effect of microstrip width.....	156
4.6.1.3	Study on harmonics	158
4.6.1.4	Effect of substrate height.....	159
4.6.2	Effect of nesting and adjacent resonators	160
4.6.3	Number of nested resonators.....	163
4.6.4	Selection of Coding.....	164
4.6.4.1	8 Bit tag using cross loop resonator.....	165
4.6.4.2	Measurement results and discussions	167
4.6.5	16 bit tag using cross loop resonator	171
4.7	Polarization independent Chipless RFID tag using Stepped impedance resonators	174
4.7.1	Basic scatterer characteristics	174
4.7.1.1	Selection of K and α	174
4.7.1.2	Backscattering from basic scatterer SIR.....	175
4.7.1.3	Effect of substrate height.....	178
4.7.1.4	Effect of coupling from adjacent scatterers	178
4.7.2	Method of Coding	179
4.7.3	Polarization insensitive Chipless RFID tag using Stepped impedance resonator	180
4.7.3.1	Measurements and discussions.....	182
4.7.4	High bit encoded Chipless RFID tag using SIR.....	184
4.7.4.1	Measurement results	187
4.7.5	Modified Compact Chipless RFID tag using SIR	188
4.8	Comparison of different Chipless RFID tags in literature with the tags developed	193
4.9	Conclusion	194
	References.....	195

Chapter 5

TIME DOMAIN ANALYSIS OF

FREQUENCY DOMAIN CHIPLESS RFID TAGS.....199 - 242

5.1	Introduction.....	200
5.1.1	Chipless RFID Reader based on UWB IR.....	201
5.2	Backscattering from frequency domain tags in time domain	204

5.3	Tag performance in time domain using Numerical methods	207
5.3.1	Analysis of Structural Mode and Antenna Mode Scattering	211
5.3.1.1	Hamming window	220
5.4	Steps to Extract Spectral Signature from the Backscattered Signal...	227
5.5	Time Domain Analysis of Measured Time Domain Data from Different Practical Environments.....	229
5.5.1	Tag on plastic box	236
5.5.2	Tag on metal sheet	238
5.6	Conclusion	239
	References.....	240

Chapter 6

CONCLUSION.....	243 -248	
6.1	Introduction.....	244
6.2	Chipless RFID tags with reception/transmission antennas	244
6.3	Multiscatterer based Chipless RFID tags	245
6.4	Time domain analysis of backscattering from frequency domain Chipless tags.....	245
6.5	Comparison of the tags developed in the thesis.....	246
6.6	Future Work.....	247

Appendix

COMPACT CHIP INDUCTOR LOADED

MULTIBAND ANTENNA	249 - 258	
A.1.	Introduction.....	250
A.2.	Antenna Geometry	251
A.3.	Results and Discussions	254
A.4.	Conclusion	257
	References.....	257

LIST OF PUBLICATION	259 - 260
----------------------------------	------------------

RESUME OF AUTHOR	261 – 263
-------------------------------	------------------

List of Tables

Table 1.1:	Classification of RFID tags based on frequency	09
Table 1.2:	History of RFID Development.....	11
Table 1.3:	Comparison between RFID and Barcode	12
Table 3.1:	Dimensions of UIR and SIR resonating at 3.8GHz. Substrate height = 1mm and $\epsilon_r = 2.2$	92
Table 3.2:	Calculated values of inductances and capacitances of equivalent circuit for an SIR having $w_1=0.5$ mm, $w_2=5.89$ mm, $l_1 = 4.77$ mm, $l_2 = 3.99$ mm, substrate height=1mm and $\epsilon_r=2.2$	103
Table 3.3:	Different substrates used for study with their properties	105
Table 3.4:	Resonator and microstrip transmission line dimensions on different substrates detailed in Table 3.3	105
Table 3.5:	Observed Q factor and resonant depth with different substrates (with respect to table 3.3 and table 3.4).....	107
Table 3.6:	Optimization of width w_1 of an SIR designed at 4.1GHz and $K=0.4$, substrate height=1mm and $\epsilon_r=2.2$	108
Table 3.7:	Change in fractional bandwidth (FBW) for transmission line width (W) variation. SIR dimensions: $l_1=5.27$ mm, $l_2=3.99$ mm, $w_1=0.5$ mm, $w_2=5.89$, substrate height=1mm and $\epsilon_r=2.2$	109
Table 3.8:	Parameters of SIRs connected to microstrip line in figure 3.19. Substrate height=1 mm, $\epsilon_r=2.2$	112
Table 3.9:	Variation in fractional bandwidth and resonant dip for different gap between microstrip line and SIR, with respect to figure 3.28.....	119
Table 3.10:	Dimensions of SIRs changed for demonstrating different codes using FSC.....	125
Table 4.1:	Properties of different substrates and the resonator dimensions (with respect to Figure 4.6) on them	149
Table 4.2:	Resonance bandwidth of resonators on different substrates with respect to figure 4.7	150
Table 4.3:	Comparison of resonant frequencies of circular ring and cross loop resonator of same mean perimeter (guided wave length) and microstrip width = 0.5 mm.....	155
Table 4.4:	Individual and effected resonant frequencies of the resonators	162
Table 4.5:	Mean perimeter of the resonators of figure 4.17	166
Table 4.6:	Mean perimeter and the resonant frequencies of the resonators in 16 bit Chipless RFID tag shown in figure 4.22	171

Table 4.7:	Dimensions of SIR shown in Figure 26(a)	176
Table 4.8:	Design parameters of the presented tag (Figure 4.31)	182
Table 4.9:	Dimensions of SIRs constituting the scatterer shown in figure 4.34(a).....	185
Table 4.10:	Comparison of different Chipless RFID tags.....	193
Table 5.11:	Dimensions of the scatterer used in the CST simulation setup. Tag substrate: RT Duroid 5880, $\epsilon_r = 2.2$, height = 1mm	209
Table 6.12:	Different tags developed and their properties	246

List of Figures

Figure 1.1: (a): Great seal of United States and an exploded view of the device. Courtesy: Wikipedia	03
Figure 1.1: (b): Working principle of “The Thing” of Leon Thermin	03
Figure 1.2: Basic Elements of RFID tag	04
Figure 1.3: Block diagram of RFID system.....	05
Figure 1.4: Some of the tags available in the industry	07
Figure 1.5: Applications of RFID	11
Figure 1.6: Working principle of SAW devices based Chipless RFID system Curtsey S. Preradovic et al.	15
Figure 1.7: An Example of Microstrip delay line based time domain Chipless RFID tag	18
Figure 1.8: Different spectral signature based Chipless RFID tags found in literature.....	20
Figure 2.1: HFSS simulation window of multiresonator circuit of Chipless RFID tag. Lumped port excitation is employed at both the ends of microstrip line	31
Figure 2.2 (a): Simulated Chipless RFID tag in CST microwave studio with plane wave excitation. The field probe is polarized along x direction (E- vector) and Propagation is along z direction (K-vector).	32
Figure 2.2 (b): Simulated Chipless RFID tag in Ansoft HFSS with plane wave excitation. Here also the field probe is polarized along x direction (E- vector) vector and propagation is along z direction (K-vector).	33
Figure 2.3: Measurement setup used to read Chipless tags (a) Multiresonator circuit based Chipless RFID tag measurement (b) Multiscatterer based Chipless tag (tags without transmitting and receiving antenna) measurement with one reader antenna (c) Multiscatterer with cross polarized reader antennas	35
Figure 3.1: Block diagram of Chipless RFID tag with reception and transmission antennas	86
Figure 3.2: Some of the Chipless tags with antennas found in literature	87
Figure 3.3: Presence/ absence coding technique (a) presence of resonator is bit 1 and absence is bit 0 (b) presence of resonator is bit 0 and absence is bit 1	88

Figure 3.4: Frequency shift coding technique. Entire frequency spectrum is divided into bands of Δf bandwidth which is further divided into bands of df resolution bandwidth. Each df section is assigned a digit.....	89
Figure 3.5: Evolution of stepped impedance resonator from uniform impedance resonator.....	90
Figure 3.6: Frequency response of UIR and SIR designed at same frequency (dimensions of the structures are given in table 3.1 with respect to figure 3.5)	92
Figure 3.7: Basic SIR Configurations with their design parameters (a) $\lambda_g/4$ (b) $\lambda_g/2$ (c) λ_g	93
Figure 3.8: $\lambda_g/4$ SIR with all design parameters	94
Figure 3.9: Relationship between impedance ratio ($K = Z_2/Z_1$), Length ratio ($\alpha = \theta_2/(\theta_1 + \theta_2)$) and ratio of first harmonic and fundamental frequencies (f_{s1}/f_0)	96
Figure 3.10: Dependence of Impedance ratio on the compactness of resonator [6].....	97
Figure 3.11: (a) Quarter wave resonator connected to transmission line $w_1 = 3.07\text{mm}$, $w_2 = 0.5\text{mm}$, $L = 17.6\text{mm}$, substrate height = 1mm and $\epsilon_r = 2.2$. (b) Transmission characteristics of the structure shown in figure 3.11(a)	98
Figure 3.12: (a) A single SIR connected to microstrip transmission line. $W = 3.07\text{mm}$, $w_1 = 0.5\text{mm}$, $w_2 = 5.89\text{mm}$, $l_1 = 4.77\text{mm}$, $l_2 = 3.99\text{mm}$, substrate height = 1mm, substrate height = 1mm and $\epsilon_r = 2.2$. (b) Transmission characteristics of the structure	99
Figure 3.13: (a) Frequency Response and (b) Current distribution on the SIR shown in figure 3.12	100
Figure 3.14: Equivalent circuit of a microstrip line having an impedance step between high impedance and low impedance sections.....	101
Figure 3.15: Equivalent circuit of SIR connected to 50Ω transmission line (Figure 3.12; $w_1 = 0.5\text{mm}$, $w_2 = 5.89\text{mm}$, $l_1 = 4.77\text{mm}$, $l_2 = 3.99\text{mm}$, substrate height = 1mm and $\epsilon_r = 2.2$) modelled in ADS software. Inductance and capacitance values are detailed in Table 3.2	104
Figure 3.16: Comparison of frequency response obtained for ADS software and HFSS.....	104
Figure 3.17: Performance of resonator designed at 3.2GHz on different substrates. Dimensions are detailed in table 3.4.....	106
Figure 3.18: Response of transmission for different width (W) of transmission line. SIR dimensions: $l_1 = 5.27\text{ mm}$, $l_2 = 3.99\text{ mm}$, $w_1 = 0.5\text{ mm}$, $w_2 = 5.89\text{ mm}$, substrate height = 1 mm and $\epsilon_r = 2.2$	109

Figure 3.19: (a) Geometry of Multiresonator circuit having 8SIRs connected to 50Ω microstrip line. (b) Side view. (c) Fabricated prototype. Dimensions are detailed in table 3.8.....	110
Figure 3.20: Electric field distribution at 3.8 GHz for two different arrangements of adjacent frequency resonators (a) adjacent frequency resonators positioned nearby (b) adjacent frequency resonators positioned apart. R1 is designed at 3.2GHz (K = 0.25, $\alpha = 0.5$, $l_1 = 5.29\text{mm}$, $l_2 = 3.99\text{mm}$, $w_1 = 0.5\text{mm}$, $w_2 = 5.89\text{mm}$) and R2 at 3.8GHz (K = 0.25, $\alpha=0.4$, $l_1 = 5.4\text{mm}$, $l_2 = 2.42\text{mm}$, $w_1 = 0.5\text{mm}$, $w_2 = 5.89\text{mm}$). Substrate height = 1 mm, $\epsilon_r = 2.2$	111
Figure 3.21: Frequency response of two adjacent frequency resonators R1 and R2 for different arrangements with respect to figure 3.20.....	112
Figure 3.22: Measured and simulated frequency response of the multi resonator circuit the eight bit tag shown in figure 3.19	113
Figure 3.23: Geometries for different codes using presence/absence technique (a) 11111111 (b) 01101111 (c) 11111100. Dimensions of the resonators are same as figure 3.19 and detailed in table 3.8.....	114
Figure 3.24: Spectral signature for different codes encoded by the geometries of figure 3.23	114
Figure 3.25: Quarter wave SIR coupled to 50Ω transmission line. SIR dimensions: $l_1 = 4.27\text{mm}$, $l_2 = 3.99\text{mm}$, $w_1 = 0.5\text{mm}$, $w_2 = 5.89$, height = 1mm, $W = 3.071\text{mm}$, substrate height = 1mm, $\epsilon_r=2.2$	115
Figure 3.26: A comparison of frequency response of SIR connected and coupled to transmission line, SIR dimensions: $l_1 = 4.27\text{mm}$, $l_2 = 3.99\text{mm}$, $w_1 = 0.5\text{mm}$, $w_2 = 5.89$, height = 1mm, $W = 3.071\text{mm}$	116
Figure 3.27: (a): Current distribution on SIR coupled to microstrip line at its resonant frequency, SIR dimensions: $l_1 = 5.27\text{mm}$, $l_2 = 3.99\text{mm}$, $w_1 = 0.5\text{mm}$, $w_2 = 5.89$, height = 1mm, $W = 3.071\text{mm}$, substrate height = 1mm, $\epsilon_r=2.2$	117
Figure 4.27: (b): Effect of removal of short to ground at the high impedance end of SIR when it is coupled to microstrip transmission line (with respect to Figure 4.27(a)).....	117
Figure 3.28: Parametric study on different coupling distance between microstrip line and SIR, SIR dimensions: $l_1 = 4.27\text{mm}$, $l_2 = 3.99\text{mm}$, $w_1 = 0.5\text{mm}$, $w_2 = 5.89$, height = 1mm, $W = 3.071\text{mm}$, substrate height = 1mm, $\epsilon_r=2.2$	118
Figure 3.29: Parametric study on distance between two adjacent resonators coupled to microstrip line. $W=3.071\text{mm}$, height = 1mm $\epsilon_r = 2.2$. SIR1 dimensions: $l_1 = 5.27\text{mm}$, $l_2 = 3.99\text{mm}$, $w_1 = 0.5\text{mm}$, $w_2 = 5.89$ mm, SIR2 dimensions: $l_1 = 4.74\text{mm}$, $l_2 = 3.81\text{mm}$, $w_1 = 0.5\text{mm}$, $w_2=3.73$	120

Figure 3.30: Multiresonator circuit with SIRs coupled to microstrip line (SIR dimensions are given in Table 3.8). Microstrip transmission line width=3.071mm, substrate height=1mm, $\epsilon_r=2.2$ mm.....	120
Figure 3.31: Measured and simulated S_{21} of the multiresonator circuit (figure 3.30)	122
Figure 3.32: Different coding combinations for presence/absence coding technique (a) 1111 1111 (b) 0110 1111 (c) 1101 1110. Dimensions of SIRs and transmission line are with respect to figure 3.30 and Table 3.10	122
Figure 3.33: Frequency response of the 8 bit multiresonator circuit for different coding combinations shown in figure 3.32	123
Figure 3.34: Illustration of FSC with $\Delta f=1$ GHz, and $df = 200$ MHz	124
Figure 3.35: Antennas used in frequency domain Chipless tags	125
Figure 3.36: Disc Monopole antenna, $\epsilon_r = 4.3$, $h = 1.6$ mm, $\tan\delta = 0.0018$, $R=19.5$ mm, $w = 3$ mm, $L_{\text{gnd}} = 55$ mm, $w_{\text{gnd}} = 35$ mm, $g=0.6$ mm.....	126
Figure 3.37: Return loss of disc monopole antenna shown in figure 3.36	127
Figure 3.38: Gain of above disc monopole antenna	127
Figure 3.39: The measured radiation pattern of the disc monopole antenna both in (a) H and (b) E plane at different frequencies.	128
Figure 3.40: Schematic of measurement setup used to characterize the tag (also specified in section 2.4).....	130
Figure 3.41: Measured backscattered response of the Chipless RFID tag shown in Figure 3.30 for different codes. The tag parameters are detailed in table 3.10	131
Figure 3.42: Measured backscattered response of the tag shown in figure 3.30 at different distances	132
Figure 4.1: (a) Typical impulse response of RFID tag showing the structural and the antenna modes. (b) Frequency response of the scatterer. The addition of the two modes creates a destructive interference when they are 180° out of phase. Courtesy: A. Vena et al.....	141
Figure 4.2: Single cross loop resonator, $L=4$ mm, $W=3.5$ mm, strip width=0.5mm, substrate height=1mm, $\epsilon_r=2.2$	144
Figure 4.3: Measured backscattering from a cross loop resonator $W=3.5$ mm, $L=4$ mm, strip width=0.5mm, substrate height=1mm, $\epsilon_r=2.2$) for different orientations with respect the axis of tag surface.....	144
Figure 4.4: Comparison between Cross loop resonator and circular ring resonator of same frequency (a) Geometry of cross loop resonator ($W = 2.5$ mm, $L=3.5$ mm) and circular ring (mean radius = 4.9mm). Substrate height =1mm, $\epsilon_r=2.2$ and strip width0.5mm for both geometry (b) Backscattered Electric Field.....	145

Figure 4.5: (a) scatterer geometry, $L_1=5.4\text{mm}$, $L_2 = 2.42\text{mm}$, $W_1 = 0.5\text{mm}$, $W_2 = 5.82\text{mm}$ $\epsilon_r = 2.2$, Substrate height = 1mm (b) Electric field distribution on single SIR and orthogonally aligned SIR based scatterer for X directed excitation (c) Scattering property of a single SIR for different orientations (d) Scattering property of scatterer for different orientations	146
Figure 4.6: Single resonator tag used to study different substrates, imensions L, W and g for different substrates are given in Table 4.1	149
Figure 4.7: Performance of cross loop resonator on different substrates (with reference to figure 4.6 and Table 4.1)	150
Figure 4.8: Current distribution on cross loop resonator ($W=3.5\text{mm}$, $L=4\text{mm}$, strip width= $.5\text{mm}$, substrate height= 1mm and $\epsilon_r=2.2$. Dimensions are with respect to figure 4.6) for different polarizations of incident wave (a) Y polarized (b) 45° tilted (c) X polarized	153
Figure 4.9: (a):Variation in resonance frequency of cross loop resonator for different microstrip widths for constant mean perimeter of 68.4mm , $W=11.5\text{mm}$ and L (With respect to figure 4.6) will be varying according to the microstrip width, substrate height = 1mm , and $\epsilon_r=2.2$	156
Figure 4.9: (b):Current distribution on cross loop resonator for different microstrip width. Mean perimeter is 68.4mm , $W = 11.5\text{mm}$ (with respect to figure 4.9(a)), substrate, height = 1mm and $\epsilon_r = 2.2$. (a) Microstrip width= 0.5mm , (b) Microstrip width = 5mm	157
Figure 4.10: Rotating single cross loop resonator in X-Y plane to see the excitation of first harmonic frequency, $L = 4\text{mm}$, $W = 5.5\text{mm}$, strip width = 0.5mm (L & W are marked with respect to figure 4.6), substrate height= 1mm , $\epsilon_r=2.2$	158
Figure 4.11: Effect of substrate height on cross loop resonator's backscattering, resonator dimensions: microstrip width = 0.5mm , $L = 3.5\text{mm}$, $W = 10\text{mm}$ (L & W are with respect to figure 4.6), $\epsilon_r=2.2$	160
Figure 4.12: Effect of varying gap between resonators, inner resonator dimensions: micrstrip width = 0.5mm , $L = 3.5\text{mm}$, $W = 3.5\text{mm}$, (L & W are with respect to figure 4.6), substrate height = 1mm , $\epsilon_r=2.2$	161
Figure 4.13: Effect of nesting on individual resonators, resonator dimensions: microstrip width = 0.5mm , $L = 3.5\text{mm}$, $W = 3.5\text{mm}$, $g = 0.5\text{mm}$, substrate height = 1mm and $\epsilon_r = 2.2$. R1, R2, R3 are the inner, middle and outer resonators, respectively	162

Figure 4.14: Current distribution on nested resonators at their resonant frequency (with respect to figure 4.13). (a) Outer resonator is excited (b) Middle resonator is excited (c) Inner resonator is excited	162
Figure 4.15: Optimising distance between two resonators R1 and R2. $W_1 = 9.5\text{mm}$, $L_1 = 3.5\text{mm}$, $W_2 = 9.5\text{mm}$, $L_2 = 3.5\text{mm}$, substrate height = 1mm and $\epsilon_r = 2.2$	163
Figure 4.16: Study on number of resonator that can be nested. Resonator dimensions, $L = 3.5\text{mm}$, $W = 3.5\text{mm}$, $g = 0.5\text{mm}$, microstrip width 0.5mm, $\epsilon_r = 2.2$ and height=1mm.....	164
Figure 4.17: Geometry of the 8 bit tag based on cross loop resonators, $L = 3.5\text{mm}$, $W = 3.5\text{mm}$, $L' = 4\text{mm}$, $W' = 3.5\text{mm}$, Substrate height = 1mm, $\epsilon_r = 2.2$	166
Figure 4.18: Different coding combinations simulated using the 8 bit cross loop resonator tag shown in figure 4.17	167
Figure 4.19: Measured noise floor in the measurement environment	168
Figure 4.20: Measured backscattered response from the 8 bit cross loop resonator tag (figure 4.17) for different orientation in x-y plane	169
Figure 4.21: Performance of the tag (shown in figure 4.17) for different distances from the reader antenna (a) Backscattered power (b) Backscattered group delay	170
Figure 4.22: 16 bit tag using cross loop resonator, $\epsilon_r = 2.2$ substrate height = 1mm, $L_1 = 4\text{mm}$, $w_1 = 3.5\text{mm}$, $L_2 = 3.75\text{mm}$, $w_2 = 3.5\text{mm}$, $L_3 = 3.5\text{mm}$, $w_3 = 3.5\text{mm}$, $L_4 = 3.25\text{mm}$ and $w_4 = 3.5\text{mm}$	172
Figure 4.23: Different coding combinations simulated using 16 bit Chipless RFID tag shown in figure 4.22.....	173
Figure 4.24: Measured backscattered power of 16 bit cross loop resonator tag (Shown in figure 4.22) for different distances.....	173
Figure 4.25: Relation between SIR's impedance ratio, length ratio and separation between Fundamental and 1 st harmonic frequency. Courtesy C.M Nijas et al	175
Figure 4.26: (a) Simulated backscattered electric field from a single scatterer for different orientations in x-y plane (b) Measured Backscattered signal from the scatterer for different orientations in x-y plane. Dimensions of SIRs are detailed in Table 4.7 and the parameters are defined according to figure 4.27(a).	176
Figure 4.27: (a): Dimensions of SIR forming the scatterer. Parameter values are given in Table 4.7	176
Figure 4.27: (b): Measured response from single SIR and scatterer. Dimensions are given in Table 4.7 with respect to figure 4.27(a).	177

Figure 4.28: Electric field distribution of Orthogonally joined SIR (a) X polarized wave (b) Ypolarized wave (c) 45° tilted wave. Dimensions are given in Table 4.7 with respect to figure 4.27(a).	177
Figure 4.29: The performance of SIR based scatterer for different substrate heights. $\epsilon_r = 2.2$, $L_1 = 4.74\text{mm}$, $L_2 = 3.81\text{mm}$, $W_1 = 0.5\text{mm}$ and $W_2 = 3.73\text{mm}$ (Dimensions are specified with respect to Figure 4.27(a)).	178
Figure 4.30: Optimization of distance between two scatterers. S1 dimensions: $L_1 = 5.27\text{mm}$, $W_1 = 0.5\text{mm}$, $L_2 = 3.99\text{mm}$, $W_2 = 5.89\text{mm}$, S2 dimensions: $L_1 = 5.2\text{mm}$, $W_1 = 0.5\text{mm}$, $L_2 = 2.83\text{mm}$ $W_2 = 2.16\text{mm}$	179
Figure 4.31: Geometry of the 8 bit polarization independent tag. Tag dimensions are $6.3 \times 3.8 \times 0.1 \text{ cm}^3$. $\epsilon_r = 2.2$ Resonator dimensions are given in table 4.8	181
Figure 4.32: Measured backscattered response of 8 bit tag of figure 4.31 (a) Magnitude response (b) Group delay	183
Figure 4.33: Performance of the tag (Shown in Figure 4.31) for different distances.....	183
Figure 4.34: (a) Geometry of a single scatterer of high bit encoded tag. Substrate height = 1mm and $\epsilon_r = 2.2$. Dimensions of SIRs constituting the scatterer are given in Table 4.9 (b) Response of the scatterer of Figure 34(a) for different polarizations of incident wave.....	185
Figure 4.35: Geometry of the high bit encoded tag Dimensions: $3.9 \times 3.6 \times 0.1 \text{ cm}^3$. $\epsilon_r = 2.2$. Resonator dimensions are given in table 4.8.....	186
Figure 4.36: Measured responses of high bit encoded tag (shown in figure 4.35) (a) magnitude response for 3 different orientations (b) Group delay.....	187
Figure 4.37: Transformation of the basic scatterer to compact form. Substrate height = 1mm and $\epsilon_r = 2.2$, $L_1 = 4.74\text{mm}$, $L_2 = 3.81\text{mm}$, $W_1 = 0.5\text{mm}$, $W_2 = 3.73\text{mm}$	188
Figure 4.38: Comparison between the magnitude response of the basic scatterer and its compact form. Substrate height = 1mm and $\epsilon_r = 2.2$, $L_1 = 4.74\text{mm}$, $L_2 = 3.89\text{mm}$, $W_1 = 0.5\text{mm}$, $W_2 = 3.73\text{mm}$ (figure 4.37).....	189
Figure 4.39: Geometry of compact polarization independent tag. Resonator dimensions are tabulated in Table 4.8. Dimension of the tag is $3 \times 4 \times 0.1\text{cm}^3$	190
Figure 4.40: Measured backscattered response of the compact polarization independent tag shown in 4.39. Dimensions are shown in Table 4.8.	191

Figure 4.41: Performance of compact polarization independent tag (Figure 4.39) at different distances.....	191
Figure 4.42: Geometry of compact high bit encoded Chipless RFID tag whose resonator dimensions are given in Table 4.8. Dimension of the tag is $3 \times 2.5 \times 0.1$ cm ³	192
Figure 4.43: Measured response of high bit encoded Chipless RFID tag shown in figure 4.42 for different orientations	192
Figure 5.2: Gaussian pulse and its derivatives (a) waveforms in the time domain and (b) Power spectral densities	202
Figure 5.3: Temporal Chipless RFID reader based on UWB interrogation signals. Courtesy: Smail Tedjini et al.	203
Figure 5.4: Block diagram of a Chipless reader based on equivalent time sampling. Courtesy: Smail Tedjini et al.	204
Figure 5.5: UWB IR based Chipless RFID system.....	205
Figure 6.5: Simulation setup used in CST for time domain analysis of frequency spectra based RFID tag with two Polarization independent scatterers. The probe is placed at 10 cm away from the tag. The dimensions of scatterers are detailed in table 5.1.....	208
Figure 5.7: (a) Modulated Gaussian excitation pulse (b) Normalized amplitude spectrum of the pulse shown in figure 5.6(a).....	210
Figure 5.8: Signal picked up by the electric probe placed in front of the source and 10cm away from the tag.....	210
Figure 5.9: Structural mode and antenna mode in the backscattered signal from the tag. An enlarged view of antenna mode is shown on the right side.....	211
Figure 5.10: Normalized frequency spectrum of structural mode and antenna mode filtered from the backscattered signal from a 2scatterer tag (Table 5.1) placed 10cm away from the source	212
Figure 5.11: Spectral signature of the tag (Detailed in table 5.1) obtained from time and frequency domain analysis	213
Figure 5.12: (a) Backscattered signal from the tag placed at 50 cm (b) Time Vs Frequency analysis of the backscattered signal in (a) when the resolution time is 0.09ns and window size is 0.16ns	214
Figure 5.13: Backscattered signal from the tag (detailed in table 5.1) after removing the forward transmitted signal (Delay = 3.2ns). Concept of window size and resolution time are shown.....	215
Figure 5.14: (a): Time Vs Frequency analysis when the resolution time is 0.09ns and window size is 0.16ns. (b) resolution time is 0.06ns and window size is 19.8ns, Delay=3.2ns.....	216

Figure 5.15: Frequency Vs Time plot for a 2 scatterer tag (Table 5.1) at 50cm from the source (a) with structural mode., delay = 3.2ns (b) Without structural mode, delay = 4.2ns. In both cases window size is 19.8ns and resolution time is 0.06ns	218
Figure 5.16: Frequency Vs Time plot for a 2 scatterer tag (Table 5.1) at 50cm from the source, Delay = 4.2ns (a): Window size = 1.98ns. (b) Window size = 3.96ns. (c) Window size = 7.92ns. (d) Window size = 19.8ns. In all the cases resolution time is 0.06ns	218
Figure 5.17: PSD Vs Frequency- Time plot for a 2 scatterer tag (Table 5.1) at 50cm from the source, Delay = 4.2ns (a): Window size = 1.98ns. (b) Window size = 3.96ns. (c) Window size = 7.92ns. (d) Window size = 19.8ns. in all the cases resolution time is 0.06ns	219
Figure 5.18: Frequency time Plot of backscatter analysis (a) with hamming window. (b) Without hamming window. In both cases the window size is 7.92ns and resolution time is 0.06ns, Delay = 4.2ns	221
Figure 5.19: Power Spectrum Density plot of backscatter analysis (a) with hamming window. (b) Without hamming window. In both cases the window size is 7.92ns and resolution time is 0.06ns, Delay = 4.2ns.....	222
Figure 5.20: Frequency time Plot of backscatter analysis (a) with hamming window, window size = 7.92ns. (b) Without hamming window, window size = 19.8ns. Resolution time for both cases is 0.06ns, delay = 4.2ns.....	222
Figure 5.21: (a) frequency Vs time plot, window size = 7.96ns, resolution time = 0.06ns. (b) Frequency Vs time plot, window size = 19.8ns, resolution time=0.06ns, (c) PSD amplitude variation with frequency and time, window size = 7.96ns, resolution time = 0.06ns. (d) PSD amplitude variation with frequency and time, window size =19.8ns, resolution time = 0.06ns	223
Figure 5.22: Frequency time plot of backscattering from the 2 scatterer tag placed 100cm from the source(processed without hamming window) (a) Window size = 7.96ns, resolution time = 0.06ns (b) window size = 39.6na, resolution time = 0.06ns.....	224
Figure 5.23: Frequency time plot of backscattering from the 2 scatterer tag placed 100cm from the source(processed with hamming window) (a) Window size = 7.96ns, resolution time = 0.06ns (b) window size =19.8ns, resolution time= 0.06ns.....	225
Figure 5.24: Frequency time plot of backscattering from the 2 scatterer tag with structural mode, window size =19.8ns, resolution time = 0.06ns (a) tag placed at 20cm (b) tag placed at 100cm	225

Figure 5.25: Frequency Vs time plot and PSD amplitude Vs time-frequency plot of backscattering from the 2 scatterer tag placed at 100cm from the source for different delay time. window size =19.8ns, resolution time = 0.06ns (a), (b) delay= 2.04ns. (c), (d) delay = 6.93ns. (e), (f) delay = 7.52ns	226
Figure 5.26: Backscattered signal in time domain measured from an 8bit Tag (Figure 4.31 and table 4.8) placed at 50cm from the reader antenna	229
Figure 5.27: Backscattering from the tag (Figure 4.31 and table 4.8) at different distances measured in frequency domain	230
Figure 5.28: Backscattered signal from the above mentioned 8 bit tag with and without delay time. Delay =11.26ns	231
Figure 5.29: Frequency-time plot of figure 5.27 for different delay time. Window size = 94ns, resolution time = 0.14ns (a) No delay (b) delay = 4.7ns (c) delay = 9.4ns (d) delay = 11.28ns	231
Figure 5.30: Spectrum of antenna mode extracted using time domain analysis when tag is placed at different distances	232
Figure 5.31: Frequency-time plot of extracted antenna mode of the 8bit tag for different window sizes, Resolution time=0.14ns, Delay time =11.28ns. (a) window size =18.8ns (b) window size = 47ns (c) window size = 94ns (d) window size = 470ns	233
Figure 5.32: Power Spectral Density variation plot of extracted antenna mode of the 8bit tag for different window sizes, Resolution time = 0.14ns, Delay time =11.28ns. (a) window size = 18.8ns (b) window size = 47ns (c) window size = 94ns (d) window size = 470ns	234
Figure 5.33: Frequency-Time plot of extracted antenna mode of the 8bit tag for different, Resolution time. Window size = 94ns, Delay time =11.28ns. (a) Resolution time = 0.56ns (b) Resolution time = 0.42ns (c) Resolution time = 0.28ns (d) Resolution time =0.14ns.....	235
Figure 5.34: Power Spectral Density variation plot of extracted antenna mode of the 8bit tag for different, Resolution time. Window size 94ns, Delay time =11.28ns. (a) Resolution time = 0.56ns (b) Resolution time = 0.42ns (c) Resolution time = 0.28ns (d) Resolution time =0.14ns	236
Figure 5.35: Measurement setup of tag fixed on plastic box	237
Figure 5.36: Extracted antenna mode spectrum of tag fixed on a plastic box using time domain analysis (a) tag response at different distances (b) Frequency time plot and PSD variation plot of antenna mode spectrum. Window size = 93.8ns, resolution time = 0.14ns.....	237

Figure 5.37: Measurement setup of tag fixed on metal sheet	238
Figure 5.38: Extracted antenna mode spectrum of tag fixed on a metal sheet using time domain analysis (a) tag response at different distances (b) 2D and 3D frequency – time plot of antenna mode spectrum. Window size = 93.8ns, resolution time = 0.19ns.....	239
Figure A.1: Coaxial fed antenna with single rectangular patch connected to circular patch through chip inductor (IND). R = 7mm, L = 3mm, W = 1.5mm, substrate height =1.6mm and $\epsilon_r = 4.4$	251
Figure A.2: Different S11 characteristics for different inductor values. Central circular and outer rectangular patch dimensions are same as figure A.1.....	252
Figure A.3: (a) Effect of different length of outer rectangular patch on reflection coefficient for a width of 1.5mm. (b) Effect of different width on reflection coefficient for a length of 3mm. In both cases chip inductor value is 1.2nH.	253
Figure A.4: Geometry of the proposed multiband antenna. R=7mm, W1 = 5mm, L1 = 4mm, W2 = 5mm, L2 = 3mm, W3 = 3mm, L3 = 3mm, W4 = 1.5mm, L4 = 3mm, IND1= 4.7nH, IND2 = 3.3nH, IND3 = 2.2nH, IND4 = 1.8nH.....	254
Figure A.5: Simulated and measured reflection coefficient of the multi band antenna shown in figure A.4.....	255
Figure A.6: Measured radiation pattern of the proposed antenna on two planes (x-y & x-z) (a) 2.28GHz (b) 2.82GHz (c) 3.96GHz (d) 5GHz.....	256

||| List of Abbreviations and Symbols |||

ADS	Advanced Design System
CMT	Characteristic Mode Theory
CNR	Complex Natural Frequency
CPW	Coplanar Waveguide
CST MWS	Computer Simulation tool Microwave Studio
EAS	Electronic Article Surveillance
EBG	Electronic Band Gap
EM	Electromagnetic
EMI	Electromagnetic Interference
EPC	Electronic Product code
FBW	Fractional BandWidth
FFT	Fast Fourier Transform
FMCW	Frequency Modulated Continuous Wave
FSC	Frequency Shift Coding
FSS	Frequency Selective Surfaces
GUI	Graphical User Interface
HF	High frequency
HFSS	High Frequency Structure Simulator
HIS	High Impedance Surface
IDT	Inter Digital Transducer
IEEE	Institute of Electrical and Electronics Engineers
IFF	Identification of Friend and Foe
LF	Low Frequency
LNA	Low noise amplifiers
LP	Log Periodic
ML	Maximum likelihood
NFMPM	Narrow frequency matrix pencil method
OCR	Optical Character Recognition
PNA	Programmable Network Analyser
RCS	Radar Cross Section
RF	Radio Frequency
RFID	Radio Frequency Identification
SAR	Synthetic Aperture Radar
SAW	Surface Acoustic Wave
SFMPM	Short-Frequency Matrix Pencil Method
SSI	Selective Spectral Interrogation
STFT	Short Time Fourier Transform

STMPM	Short Time Matrix Pencil Method
TDR	Time Domain Reflectometry
TFTC	Thin Film Transistor Circuits
UHF	Ultra High Frequency
UWB IR	Ultra-Wide Band Impulse Radar
VCO	Voltage controlled oscillators
VSWR	Voltage Standing Wave Ratio

Notations

c	Velocity of light
h	Height of the dielectric substrate
K	Impedance Ratio
Q	Quality factor
S_{11}	Reflection coefficient scattering parameter
S_{21}	Transmission coefficient scattering parameter
Z	impedance
Z_0	Characteristic Impedance
Z_{in}	Input impedance
β	Phase constant
γ	Propagation constant
δ	Skin depth
ϵ_{eff}	effective permittivity of the substrate
ϵ_r	Relative permittivity of the substrate
λ	Free space wavelength
λ_g	Guide wavelength
σ	Conductivity of copper
ω	angular frequency
Ω	Resistance
α	Length ratio

.....❧.....

Contents	1.1. Introduction
	1.2. RFID System
	1.3. Applications of RFID
	1.4. RFID, The Electromagnetic Barcode Vs Optical Barcode
	1.5. Chipless RFID: New era of RFID
	1.6. Motivation of the thesis
	1.7. Thesis outline

This chapter highlights an introduction about the conventional RFID technology. The basic electronic building blocks and working principle of RFID system is discussed in detail. A comparison of RFID and optical barcode is also presented in this chapter. The need and evolution of Chipless RFID technology is narrated. A general classification of Chipless RFID tags is provided. Organization of thesis is given at the end of the chapter

1.1. Introduction

Automatic identification is an ever interested topic which finds countless applications in different fields like industrial, medical, banking, day to day life etc., Barcodes, Optical Character Recognition (OCR), fingerprint, smart cards, RFID systems, voice identification etc., are some of the existing automatic identification systems [1]. Among them Radio Frequency Identification (RFID) is a contactless, non-line of sight technology which relies on Radio Frequency (RF) waves for communication. Being originated in World war-II to identify friend and foe aircrafts, this technology extended to several other domains. With the updates in the Electronics and information technology RFID developed as an integral part to fulfil the needs of mankind. Electronic article surveillance, Supply chain management, vehicle tracking, animal tracking, fare collection, factory automation, health care etc., are some of applications [2-8] of RFID.

RFID is one among the many technologies developed to meet the needs of World War I & II. Identification of Friend and Foe (IFF) was done by attaching a transmitting antenna to friend aircrafts which reflects back particular signal to the radar base stations thus informing their identity. ‘The Thing’ developed by Leon Theremin in 1945 was another interesting form of RFID in the context of World War II. Figure 1.1(a) shows its front view and its exploded view. It was a tool developed for Soviet Union to spy the conversations in U.S Embassy and was hidden in the Great Seal and presented to the U.S. ambassador in Moscow [11]. The working of ‘the thing’ is shown in figure 1.1(b) and is as follows. The sound waves from the scene make vibrations in the diaphragm connected to the resonant cavity

which is coupled to an antenna. This will change the impedance of cavity according to the sound waves and thus modulates the antenna load accordingly.



Figure 1.1(a): Great seal of United States and an exploded view of the device.
 Courtesy: Wikipedia

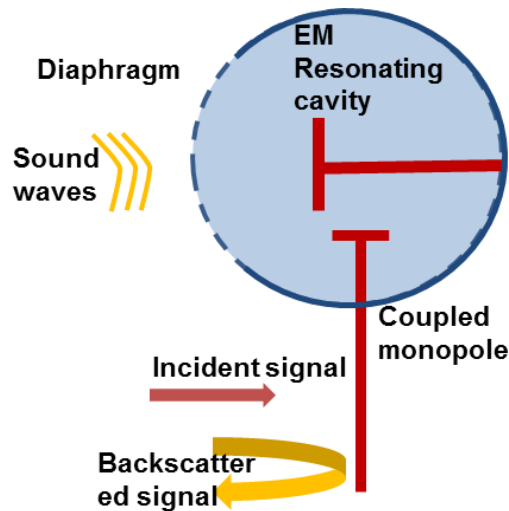


Figure 1.1(b): Working principle of “The Thing” of Leon Thermin

The electromagnetic wave transmitted from the reader (in this case located in car parked outside U.S Embassy) induces currents on the tag antenna and get modulated with the sound waves. The backscattered signal from this spying

tool is demodulated at the receiver. Though “the thing” had been used for spying not for identification, it is considered as the predecessor of RFID because the device was likewise passive, being energized by electromagnetic waves from an outside source.

The basic theory of RFID is reflected power communication or backscatter modulation [12] and is developed on the heels of RADAR. The technology is a combination of different aspects of radio broadcasting and RADAR. Basic radar operation enables to know whether there is an object present or not. If the target to be detected is subjected to some sort of modulation, the identity of the target can be obtained from the backscattered power. More clearly, the information embedded in the reflected power from loaded scatterers [13] is used to identify the target. Tag, the data carrying device attached to the object to be tracked or identified is the scatterer here. The operation of conventional RFID tag is depicted in figure 1.2. Radio waves transmitted by the reader antenna will be received by the tag antenna and is modulated by the tag’s data which is stored in the silicon chip connected as a variable load to the tag antenna. The modulated RF wave will be retransmitted or backscattered towards the reader antenna. The backscattered signal is processed for the identification of the target.

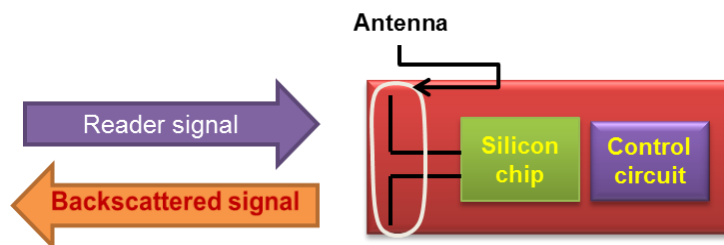


Figure 1.2: Basic Elements of RFID tag

1.2. Components of RFID System

Typically an RFID system consists of a reader/interrogator which is usually connected to a computer with internet and multiple number of tags/transponders [14]. The basic block diagram of RFID system is shown in figure 1.3. A brief description of each component is given here.



Figure 1.3: Block diagram of RFID system

1.2.1. Reader

Reader/Interrogator/Scanner Sends and receives electromagnetic data to and from the tags that enter its field of view. The reader houses decoder, RF module and one or more antennas. One side of the reader is connected to the computer which will process the detected data and the other side with antenna or antennas to communicate with the tags. The reader antenna would be continuously scanning or observing its operating area and once one or more tag enters the reading zone, it gets the identity of tag/tags. The decoded identity is then passed to the computer. So the reader can be viewed as a device connecting tags and host computer.

The complexity and functions of the reader, size, number and gain of reader antenna, all depends on the specific application for which it is

designed. The reader can be fixed (in a room or factory) or portable (like the one integrated in handheld scanner).

1.2.2. Transponder/Tag [15]

Tags are the data carrying devices attached to the object to be detected. Conventional RFID tags consist of an antenna which is connected to a silicon chip, the associated control circuits and the substrate on which all the other components are printed or attached. The whole device can be used as such or can be encapsulated with different materials depending upon the application. The tag antenna receives the electromagnetic waves at its frequency once it is within reader's reading zone; modulates it with the tag's identity stored in the chip and backscatters the modulated wave towards the reader antenna.

Tag's identity is stored in the silicon chip in conventional RFID technology. Due to the availability of several bytes of data, the identification code can include more information other than a simple serial number which identifies the tag like that in Electronic Product code (EPC).

The tags can be read only, read-write and write once-read many type depending on the application. Conventional RFID tags are classified into three as Passive, Semi-passive and Active tags depending on the method used to activate the tag. Some of the tags available in the industry are shown in figure 1.4.

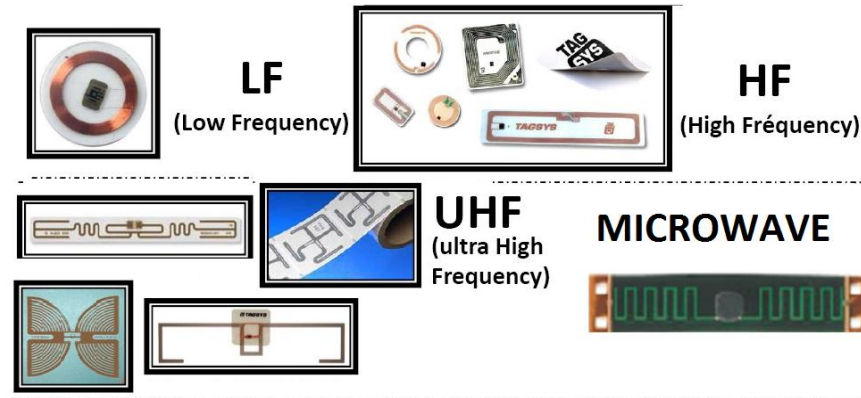


Figure 1.4: Some of the tags available in the industry

1.2.2.1. Passive tags

Passive tags house an antenna, silicon chips and the associated control circuits. No battery is provided to power the tag. The silicon chip and the control circuits are energised from the incident reader's signal. These tags are less expensive (Tag prices range from a few pennies to \$10) due to the absence of battery but they would offer short reading ranges (typically less than 3 meters) and slow reading speeds. But these tags have longer shelf life and can use any frequency band. They are generally used to tag low cost items and are not reusable.

1.2.2.2. Semi- passive tags

The semi- passive tags work similar to the passive tags that they also use power from the reader signal to communicate with it. The difference is that they house a battery to power the chip electronics within the tag just like battery in watches and are also known as battery assisted tags. Semi-passive tags also have short reading ranges and slow reading speeds but offer better performance than passive tags. Battery assisted tags usually

provide more memory than passive tags. These are generally used when some sensing function is also needed to be included in the low cost tags. The presence of the battery makes this tag a little more expensive than passive tags (\$10 to \$50). Although the battery life limits the tags life, semi passive tags have longer shelf life than active tags. Usually they use UHF frequency band.

1.2.2.3. Active tags

Active tags contain an on board battery to broadcast the RF waves and to power the electronics within the tag. They also contain an RF transmitter and transmit their data independently without relying on the reader signal. These tags use two frequencies for the transmission and reception (down link and uplink). Sensing applications can also be effectively incorporated in these types of tag. Active tags are most reliable and they provide greater reading ranges (1000m), speeds and memory. But the tags are expensive than the other two tags (\$20 to over \$100) due to the presence of battery and other related circuits. For these tags battery life limits the tag's life though precautions like sleeping mode are available. Active tags can use UHF and microwave frequency bands.

Conventional RFID tags use unlicensed spectrum space i.e., ISM bands. However, the exact frequency may change according to the regulations of different countries. The frequency of operation is also greatly dependent on the application. Generally it can use any of the four bands like Low Frequency (LF), High frequency (HF), Ultra High Frequency (UHF) and microwave and are given in the table 1.1 [16]. LF and HF tags are less affected by the environmental effects like water content or presence of metals whereas UHF and microwaves don't penetrate into the metal, fluids and dust. RFID tags in

these bands depend on their working environment. Both HF and UHF RFID are used for item level tagging and pallet tracking applications. HF offers a smaller reading range. However, it offers a better performance in terms of reading since it is based on near field coupling. In contrast, UHF RFID offers a better read range in comparison to HF RFID. However, since the reading is based on propagation of radio waves, the performance is limited in this case.

Table 1.1: Classification of RFID tags based on frequency

Typical RFID frequency	LF(125-134 KHz)	HF (13.56 MHz)	UHF (433 MHz, 860-960 MHz)	Microwave (2.45 GHz~, 5.8 GHz)
Communication range	< 0.5m	≤1.5m	1-10m	3m≤
Data transfer rate	Low	Low to moderate	Moderate, moderate to high	High
Reader cost	Low	Medium	High	Very high
Coupling	Inductive	Inductive	Backscattering	backscattering

1.2.3. Host computer and middleware

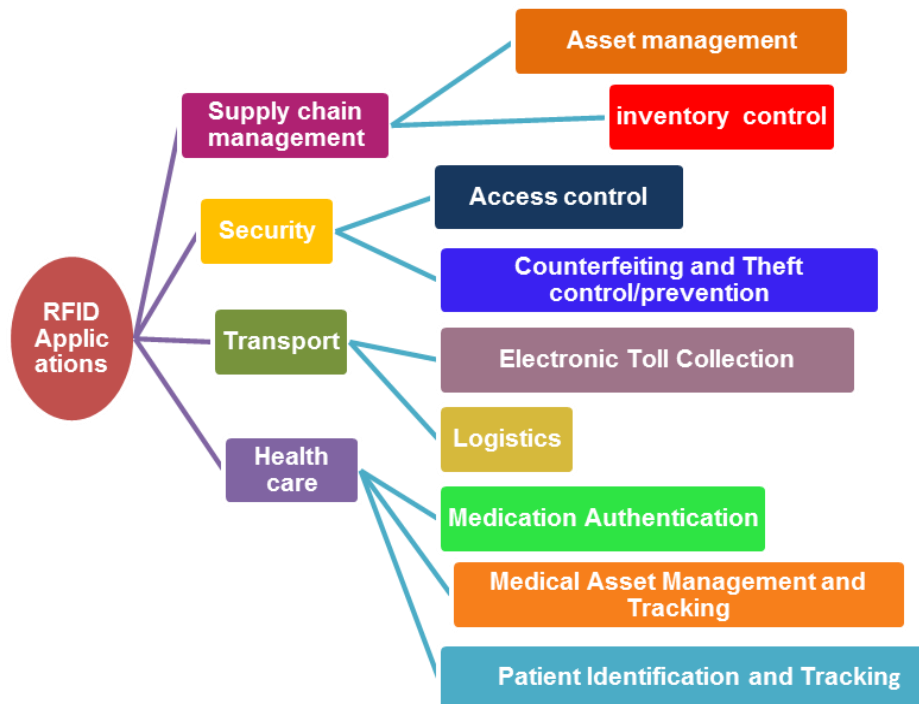
RFID reader is connected to a host computer through a software interface known as middleware. The middleware maintains the interface and the software protocol to encode and decode the identification data from the reader into a mainframe or personal computer. The decoded data from the reader is given to the computer for further processing according to the application and make it useful for the end user. This block of the RFID system includes software to monitor, configure and control the reader hardware and hence reader functions. The computer is connected to internet so that features like remote identification can be supported.

1.3. Applications of RFID [2] - [10]

Commercial applications of RFID have been found place in market since 1960's. Sensormatic and Checkpoint are two among the early manufactures of RFID applications. Electronic Article Surveillance (EAS) equipment developed to counter theft of merchandise was the first and most wide spread commercial RFID application. These types of systems often use 1bit tags; only the presence or absence of a tag could be detected, but the tags are less expensive and provided effective antitheft measures. These systems used either microwave (generation of harmonics using a semiconductor) or inductive (resonant circuits) technology. The 1970s were characterized primarily by developmental work of RFID systems intending applications like animal tracking, vehicle tracking, and factory automation. The 1980s became the decade for full implementation of RFID technology, though interests developed somewhat differently in various parts of the world. RFID has been successfully implemented in transportation, personal access, animal tracking, toll collection etc. A key to the rapid expansion of RFID applications was the development of the personal computer (PC) that allowed economically convenient data access and management from RFID systems. Since 1990's wide spread deployment of RFID has been continuing in various fields of everyday life. Its applications are increasing and are updated with the technology advancements. It can replace or can be co-functioned with any existing automatic identification technologies and for this reason RFID is one among world's top ten technologies. Some of its popular applications including supply chain management and transport are shown in figure 1.5.

Table 1.2: History of RFID Development [8]

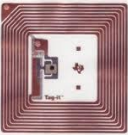

The Decades of RFID	
Decade	Event
1940–1950	Radar is refined and used, As a major World War II development effort RFID is invented in 1948.
1950–1960	Early explorations of RFID technology, laboratory experiments.
1960–1970	Development of the theory of RFID. Start of applications and field trials.
1970–1980	Explosion of RFID development. Tests of RFID accelerate. Very early adopter Implementations of RFID.
1980–1990	Commercial applications of RFID enter mainstream.
1990–2000	Emergence of standards. RFID widely deployed. RFID becomes a part of everyday life.
2000–	RFID explosion continues

**Figure 1.5: Applications of RFID**

1.4. RFID Vs Optical Barcode [1] - [10]

Optical barcodes have major role in product identification in markets and is used worldwide. These are very cheaper than any other identification systems. They can be printed directly on paper or plastic materials and can perform with the same accuracy in different working environments. Two types of barcode: 1D (represent data in the widths and the spacing of the lines) & 2D (data in patterns of squares, dots, hexagon and other geometric pattern) are common in use [5]. 2D barcodes have more data capacity (maximum capacity 128 bits) than 1D(maximum capacity 41 bits) and the former is used in applications where more information is needed like in industrial products and the latter is used in household products.

Table 1.3: Comparison between RFID and Barcode

 RFID	 Barcode
Electronic device	Printed symbol
Uses RF waves	Uses light
Sensitive to EMI(noise), metal and water	Not sensitive to EMI(noise), metal, water
Non line of sight	Line of sight
No human labour needed in most cases	human labour needed in most cases
Can be hidden, protected	Subject to dirt, abrasion etc.
Read multiple tags simultaneously	Read only one tag at a time
Small to large reading range can be obtained depending on the application	Small reading ranges and crucial positioning is required
Strong authentication (access control, non-duplication)	No authentication, except encryption
\$0.1 to \$200+ tags, expensive reader	Virtually free label, inexpensive reader
Emerging for some uses, mature in other areas	Mature- Ubiquitous

Though barcodes are widely adopted identification technology, it has many limitations. RFID technology by itself or combined with optical barcodes has overcome these limitations and also opened new horizons of identification. The most advantage of RFID technology over barcodes is non line of sight communication. A comparison of barcodes and RFID is given in the table 1.3.

Though the RFID technology is offering many advantages over barcodes, it is far away from the point to replace barcodes. As already mentioned, the reason behind this is the cost. Researches are actively conducting in this field to reduce the cost of RFID systems. No significant advancements have been achieved in this regard but a suggested approach is Chipless RFID tags introduced in the next section and is the topic of the thesis.

1.5. Chipless RFID: New era of RFID [11], [14]

Despite the fact that the use of RFID tags with an IC is a well-established and broadly used technology, the need for an all passive technology exhibiting very low cost, high robustness and the ability to be used in severe environments is very attractive and highly desirable for many applications. Chipless RFID system is a system whose transponders or tags do not contain silicon chip. This can drastically reduce the cost. With the chipped RFID tags, the cost of silicon chip is inevitable. The cost of RFID tag is due to the substrate, handling of the die and placing them onto label. By eliminating integrated circuits from the tags the cost can be reduced significantly with a lossless low cost substrate. Besides the similarity in function with optical barcodes, these RF barcodes are envisaged with more

advantages like non-line of sight readability, automated reading, incorporation of sensors, etc. It is an emerging technology and active researches are going on in this field to raise this technology into a commercially and economically acceptable level. Still a long way has to be climb to reach the aim.

The Chipless RFID tags do not require an IC and communication protocol. The challenge is how to encode data without a chip within an all passive structure using a low cost substrate. Chipless RFID tags are viewed like radar targets and the system simply relies on the radar principle with the tag information encoded in the reflected wave as an electromagnetic signature of the structure. The electromagnetic signature depends on the size and shape of the tag. So this signature, added by the tag to the reflected power serves like a unique ID of the tag.

Chipless RFID tags are classified according to the way in which the identity of the tags is encoded [11]. The first one defines a set of symbols as Chipless tags and uses their electromagnetic properties as their signature or ID. The second technique is to use a compact and simple RF circuit to encode data. This design should have an antenna to communicate with reader and RF processing unit. The second approach has strong similarity with RF filter design. The third technique combines features of first and second. Here, the antenna and filtering functions are combined in RF circuits with strong scattering properties.

RFID tags are also classified according to the domain in which the identity is stored. They are time domain reflectometry based Chipless RFID tags, spectral signature based Chipless RFID tags and phase/amplitude backscatter modulation based Chipless RFID tags [11].

1.5.1. Time Domain Reflectometry (TDR) Based Chipless RFID Tags [14]

As the name implies, in this type of tag data is encoded in the time domain. This type of tags are interrogated by an extremely short duration broad band RF pulse lasting only a few Pico seconds. Data is encoded by the tag by creating a reflection of the interrogation pulse in different time intervals. So there should be structures in the signal path to create discontinuities that in turn create reflections. These tags have the advantages of better noise immunity, long reading range, and low cost. But at the same time there are disadvantages like lower encoding capacity and difficulty to generate and detect narrow UWB pulses. The time domain tags are again classified into printable and non-printable tags.

1.5.1.1. Non-printable TDR tags: SAW tags [17] - [18]

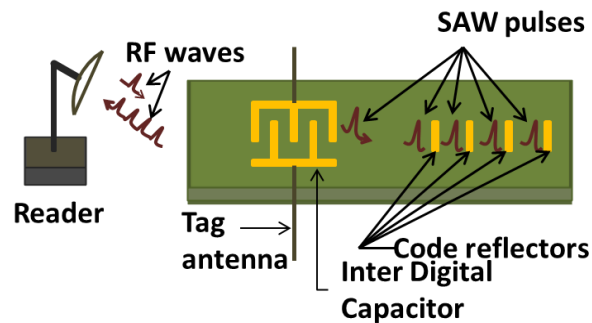


Figure 1.6: Working principle of SAW devices based Chipless RFID system Curtsey S.Preradovic et al. [15]

This type of tags relies on SAW (Surface Acoustic Wave) devices. SAW devices are based on the unique characteristics of piezoelectric materials that allow transformation of electromagnetic waves into much slower acoustic waves. These fully passive tags merely reflect the reader

signal in a coded form that represent their identity. Reflecting reader signal in coded format means reflections at predetermined time intervals, which is accomplished by using SAW delay lines. SAW delay lines boast low losses, large delay times and small dimensions.

Piezoelectricity is the operation principle behind SAW devices and is a coupling between a material's electrical and mechanical properties. A piezoelectric crystal experiences a mechanical distortion when an electric field is applied. Interdigital capacitors (IDT) are inevitable part of SAW tags and are used to convert or transduce electrical waves to acoustic waves or vice versa. Figure 1.6 depicts the principle of operation of a reflector based SAW tag. The interrogation pulse emitted by the reader is picked up by the reader antenna that is directly linked to an IDT. The IDT transforms the electrical signal to surface acoustic wave, which is a mechanical wave of particle displacements. The generated SAW pulse then propagates along the surface of the substrate, which is usually made of a strong piezoelectric material. At precisely determined positions on the substrate is embedded with so called code reflectors usually made of one or a few narrow PEC (Perfect Electric Conductor) strips. The propagating mechanical wave gets partially transmitted and partially reflected by the above mentioned reflectors. The reflected SAW returning to the IDT thus bears a code, based on the positions of the reflectors. The modulation used here is based on time delay between reflected pulses and hence is pulse position modulation. Similarly the phase and amplitude of the reflected signal can also be modulated to encode information. The IDT reconverts the reflected SAWs returning towards it to electrical form which is retransmitted by the tag antenna. The response is then detected and decoded by the reader.

SAW tags offer many advantages over conventional chipped RFID tags like compactness, robustness, ability to withstand in harsh environments, better read range comparing fully passive chipped systems etc. These are the only Chipless tags commercially available in the market to the date and offer a data capacity of 128 bits. Successful researches are taking place in this field to enhance the properties and to reduce the cost of SAW tags.

Comparing Chipless RFID tags under research, these tags are costlier, not fully printable due to the presence of piezoelectric material. Active researches are going on to make both technologies competent with the chipped ones.

1.5.1.2. Printable time domain Chipless RFID tags [19] - [21]

Printable time domain tags include Thin Film Transistor Circuit (TFTC) tags and microstrip delay line. TFTC tags can be printed on low cost plastic at high speed. Comparing Chipless tags they offer more functionality since they include most of the functions of integrated circuits but consume more power and manufacturing cost. The delay line based tags consist of a microstrip discontinuity after a section of delay line. The operation of these tags is similar to SAW tags and these tags can be viewed as microstrip counter part of SAW tag. The tag when excited by a short RF pulse retransmits echoes of the same due to discontinuities in the propagation path. The discontinuities placed at predefined distances determine the delay between echoes of interrogation signal and hence the identity of the tag. Time encoding can also be done by terminating transmission lines by different loads. An example of microstrip delay line based tag is shown in figure 1.7.

One key feature of the time domain tags is the two backscattering modes from the tag antenna. One is the structural mode and the other is the antenna mode. The structural mode is inherent to each antenna and is independent of antenna loads. Antenna mode backscattering is a load dependent scattering and changes with impedance of load [29], [30]. While examining antenna or tag backscattering, the early time pulse is the structural mode and the late time pulse is the antenna mode. Controlling the time difference between structural and antenna modes (by controlling the length of transmission line) and controlling the phase difference between different antenna modes are the techniques used for coding in time domain reflectometry based tags.

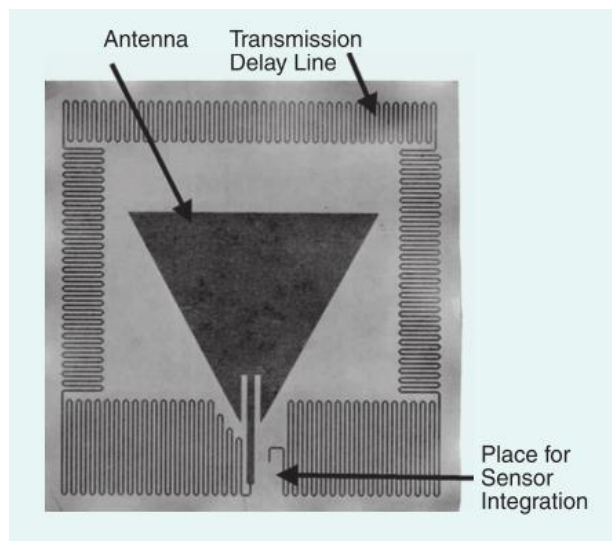


Figure 1.7: An Example of Microstrip delay line based time domain Chipless RFID tag [17]

The time domain tags are simple and immune to noise. These tags use narrow band of frequency and due to the availability of high emission for short frequency bands, UWB tags offer greater reading ranges than other

Chipless RFID systems. Left handed artificial delay lines are under active research to use in time domain tags which in turn increase the information density by reducing the size. But the disadvantage is lower data encoding capacity. Generation of short pulses, width of which determines the shortest delay between echoes and hence the coding capacity is a difficult task with time domain tags. Also the length of delay lines to provide long delay is a limiting factor in terms of tag size.

Though the time domain tags offer better reading range and immunity to noise, researchers are most interested in frequency domain tags. This is because of the fact that frequency domain tags can encode more number of bits than the time domain tags (except SAW tags). Duality between time and frequency domains enables to use Time domain reading techniques to read frequency domain tags and hence to enhance their performance.

1.5.2. Spectral signature based/Frequency domain based Chipless RFID tags [11], [14]

This type of tag encodes data or identity in the spectrum or frequency domain using resonant structures. The presence or absence of a resonant peak or dip indicates a data bit. Resonant peaks or dips can be either phase jumps or amplitude jumps. Spectral signature based tags are fully printable, planar, low cost and robust. These tags also have higher encoding capacity than time domain tags. But large spectrum requirements, wideband RF readers and exact tag orientation with reader antenna are some draw backs of frequency domain tags. Understanding the advantages of high encoding aspect of frequency domain tags, researches are going on to overcome the disadvantages of this class of tags.

Depending upon the nature of tag, spectral signature based tags can be classified into two: chemical and planar. Chemical tags have deposition of chemicals on low cost paper substrates. These chemicals upon the incidence of electromagnetic waves resonate at different frequencies. Though these tags are extremely low cost, they operate at low frequencies (a few kilo hertz) [22]. Planar tags are made of microstrip, coplanar and strip line technologies. They can be printed on thin, thick or flexible substrates depending upon the application. Multiple scatterers [23], multiple resonators coupled to microstrip transmission line [24], space filling curves [25], LC resonators, multiresonant antennas [26] etc., are used as the basic elements of frequency domain based Chipless RFID tags. With these resonant structures data bits can also be encoded in phase- frequency domain [31] and it can be viewed as a type of frequency domain coding. To increase coding capacity data can be coded in multiple domains [32]. Some of spectral signature based tags reported in literature are shown in figure 1.8.

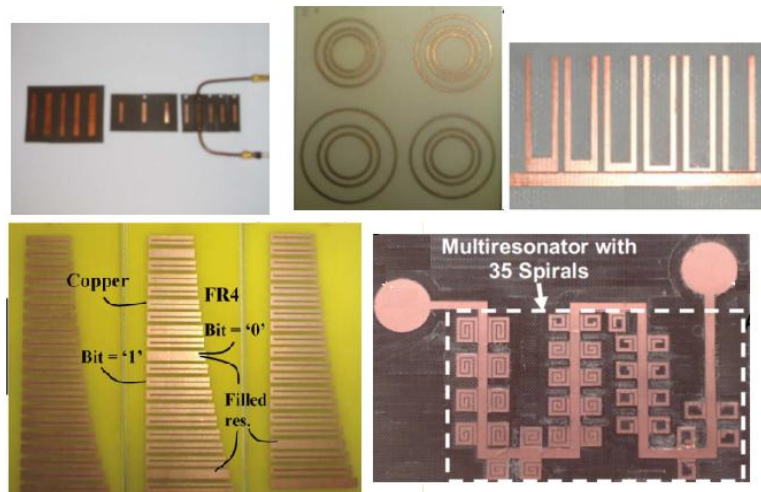


Figure 1.8: Different spectral signature based Chipless RFID tags found in literature [23], [24], [32], [33]

1.6. Motivation of the thesis

Chipless RFID is an emerging field which is still in its infancy and expected to be a promising cost effective alternative to conventional RFID. If the technology and researches turn effective, it also offer a better replacement of optical barcodes with improved features like fully automated and non-line of sight identification. The frequency domain Chipless RFID tags are very attractive in terms of data encoding capacity compared to other developed Chipless tags (except SAW tags). Moreover, they are fully printable, planar, robust and low cost. Time domain tags at the same time have better resistance to noise and offer better reading ranges with flexible positioning freedom.

Most of the frequency domain tags proposed in the literature should obey stringent positioning with respect to the reader. Less readable range and limited frequency spectrum availability are the other dominant disadvantages of frequency domain tags. Also, frequency modulated continuous wave readers designed for reading frequency domain tags are very expensive due to the requirement of wide band VCOs [27], [28]. For time domain tags, the disadvantages are the lower bit encoding capacity, difficulty to generate narrow width pulse and the size.

The dual nature of time and frequency domains enables to combine technologies of both domains so that benefits of both can be incorporated in the tag. The idea is to use time domain techniques to read or post process frequency domain tags or data. A hand full of such techniques is proposed in the literature.

The main concerns of this thesis include identification of effective resonating structures for frequency domain tags with distinguished features that can mitigate some of its limitations. Also a study on time domain techniques that improve the performance of frequency domain tags is also considered.

1.7. Thesis outline

Chapter 1: Introduction

This chapter provides an introduction to the conventional RFID system, its basic working principle and its applications. Evolution of Chipless RFID system, a general classification of the Chipless RFID tags and commercially available Chipless tags are given special narration in the chapter. The motivation of this thesis and an outline of the entire thesis are also provided in the chapter.

Chapter 2: Methodology and literature review of Chipless RFID tags

This Chapter deals with the methodology of research and the tools used in the study. It includes the software used for prefabrication studies, fabrication procedure for prototyping the tags and measurement setups. Literature survey on frequency domain Chipless tags and time domain techniques to post process backscattering from frequency domain tags is provided. Finally Chipless RFID tag reader architecture is also reviewed from the literature.

Chapter 3: Chipless RFID tags with reception/transmission antennas

This chapter presents frequency domain Chipless RFID tags in which multiresonators are coupled to the transmission line connecting transmitting and receiving antennas. Quarter wave Stepped Impedance Resonator is the basic element constituting the proposed tag. A brief report on SIR characteristics are provided in this chapter. Performances of resonators connected to and coupled to the transmission line are compared. Parametric studies to optimize tag performance are conducted and finally measurements of the tag composed of multiresonating circuits, transmission and receiving antennas are performed.

Chapter 4: Multiscatterer based Chipless RFID tags

This chapter deals with Chipless frequency domain tags in which scatterers perform the function of transmitting and receiving antennas in addition to filtering function (to add their signature in the backscattered spectrum). Two types of scatterers are presented that are suitable for multiscatterer based Chipless RFID tags with distinguished properties. Focus is given to polarization insensitivity, high bit encoding capacity and compactness of the tag. Different parametric studies are included for the optimization of the tag. Finally the tag performance is validated through measurement results and discussed elaborately.

Chapter 5: Time domain analysis of frequency domain Chipless RFID tags

UWB IR (Ultra Wide Band Impulse Radar) technology based reading techniques are summarized in this chapter. Time domain analysis of backscattered signal from the tag is presented in the chapter. Quality of antenna mode extraction is improved by using hamming window. Validation of the results is conducted by analyzing the backscattered data measured using PNA E8362B.

Chapter 6: Conclusion

This chapter gives the summary and conclusion of the overall work and a brief description on the scope for future investigations.

The thesis also includes the bibliography and a list of publications by the author in the related field

Appendix

Appendix presents a compact chip inductor loaded microstrip patch antenna for multiband application. The antenna is fabricated on a substrate of dielectric constant 4.4 and thickness 1.6 mm. The proposed antenna is of circular geometry with a circular patch of radius 7mm surrounded by four different inductors which are connected to small rectangular metal patches.

References

- [1] RFID Design Principles, Harvey Lehpamer, Second Edition, Artech House, London 2012.
- [2] Y. Xiao, S. Yu, K. Wu, Q. Ni, C. Janecek and J. Nordstad, "Radio Frequency identification: Technologies, Applications, and Research Issues", *Wireless Communications and Mobile Computing Wirel. Commun. Mob. Comput.* 2007.
- [3] E. Perret, S. Tedjini and R.S. Nair, "Design of Antennas for UHF RFID Tags", *Proc. of the IEEE*, Vol.100, No. 7, pp.2330-2340.
- [4] G. R.T. White, G. Gardiner, G. Prabhakar, and A. A. Razak, "A Comparison of Barcoding and RFID Technologies in Practice," *Journal of Information, Information Technology, and Organizations*, Vol. 2, pp.119-132, 2007.
- [5] M.R. H. Khandokar, G. Tangim, M. K. Islam and M. N. I. Maruf, "Simultaneously Multiple 3D Barcodes Identification Using Radio Frequency", 2nd International Conference on Signal Processing Systems (ICSPS), pp.633-636, 2010.
- [6] R. Das, "An Introduction to RFID and Tagging Technologies", IDTechEx, White paper, Cambridge, UK., 2002, <http://www.idtechex.com>
- [7] M Robert and Bob Violino, "The History of RFID technology", *RFID Journal*, <http://www.rfidjournal.com/articles/view1338>, 2005.
- [8] Arkansas Radio Compliance Retail Suppliers: Available online. <http://rfid.uark.edu/2060.asp>.
- [9] LAREN RFID, Whitepaper, "A Basic Introduction to RFID Technology and Its Use in the Supply Chain", Jan 2004.
- [10] IEIMobile, Whitepaper, RFID Technology: Introduction and Application, www.ieimobile.com.
- [11] Smail Tedjini, Nemaï Karmakar, Etienne Perret, Arnaud Vena, Randika Koswatta, and Rubayet E-Azim, "Hold the Chip" *IEEE microwave magazine*, August 2013.
- [12] H. Stockman, "Communication by means of reflected power," *Proc. IRE*, pp. 1196–1204, Oct. 1948.

- [13] Prof. Roger and F. Harrington, Theory of Loaded Scatterers, Proc. IEE, Vol. III, No. 4, pp.617-623, April 1964.
- [14] S. Preradovic, N. C. Karmakar, “Chipless RFID: Barcode of the future”, IEEE Microwave Magazine, vol. 11, no. 7, pp:87–97, December 2010.
- [15] S. Preradovic and N. C. Karmakar, “RFID Transponders – A Review” Proceedings of 4th International Conference on Electrical and Computer Engineering ICECE 2006, Dhaka, Bangladesh, pp 96-99, 19-21 December 2006.
- [16] Stephen A. Weis, “RFID (Radio Frequency Identification): Principles and Applications”, System, Vol.2, No.3, 2007.
- [17] S. Harmal and V. P. Plessky, “Development and Implementation of RFID Technology”, I-Tech Education and Publishing Vienna, Austria, February 2009, Open Access Database www.intechweb.org.
- [18] V. P. Plessky and L. M. Reindl “Review on SAW RFID Tags”, IEEE Trans Ultrason Ferroelectr Freq Control, Vol. 57, No. 3, pp. 654-68, Mar 2010.
- [19] A. Chamarti and K. Varahramayan, “Transmission Delay Line- Based ID Generation Circuit for RFID Applications,” IEEE Micro- wave Wireless Compon. Lett., vol. 16, No.11, pp. 588–590, Nov. 2006.
- [20] J. Vemagiri, A. Chamarti, M. Agarwal, and K. Varahramyan, “Transmission Line Delay-Based Radio Frequency Identification (RFID) Tag”, Microwave Opt. Technol. Lett., Vol.49, No.8, pp. 1900– 1904, 2007.
- [21] S. Shretha, J. Vemagiri, M. Agarwal, and K. Varahramyan, “Trans- Mission Line Reflection And Delay-Based ID Generation Scheme For RFID And Other Applications,” International Journal of Radio Frequency Identification Technology and Applications , Vol. 1, No. 4, pp. 401–416, 2007.
- [22] R. Das, “Chipless RFID—The End Game,” IDTechEx, Cambridge, MA, Internet article, Feb. 2006. [Online]. Available: <http://www.idtechex.com/products/en/articles/00000435.asp>, (accessed Apr. 2008).
- [23] A.Vena, E. Perret and S. Tedjini, “Design Rules For Chipless RFID Tags Based On Multiple Scatterers,” Annals of Telecommunications - Annales Des Télécommunications, Vol.68, pp. 361-374, 2013.

-
- [24] S. Preradovic, I. Balbin, N. C. Karmakar, and G. F. Swiegers, "Multiresonator-Based Chipless RFID System For Low-Cost Item Tracking," *IEEE Trans. Microwave Theory Tech.*, Vol. 57, No. 5, pp. 1411–1419, May 2009.
- [25] J. McVay, A. Hoorfar, and N. Engheta, "Space-Filling Curve RFID Tags," *IEEE Radio and Wireless Symp. Dig.*, San Diego, pp. 199–202, Jan. 17–19 2006.
- [26] I. Balbin and N. Karmakar, "Novel Chipless RFID Tag For Conveyor Belt Tracking Using Multi-Resonant Dipole Antenna," in *Proc. 39th European Microwave Conf.*, Rome, Italy, pp. 1109–1112, Sept. 2009.
- [27] S. Preradovic and N. C. Karmakar, "Design Of Short Range Chipless RFID Reader Prototype," in *Proc. 5th International Conference on Intelligent Sensors, Sensor Networks and Information Processing (ISSNIP)*, Melbourne, Australia, pp. 307–312, Dec. 2009.
- [28] R. V. Koswatta and N. C. Karmakar, "A Novel Reader Architecture Based On UWB Chirp Signal Interrogation for Multiresonator-Based Chipless RFID Tag Reading," *IEEE Trans. Microw. Theory Tech.*, Vol. 60, No. 9, pp. 2925–2933, Sept. 2012.
- [29] R. Ling and P. Ufimtsev, "Scattering of Electromagnetic Waves by A Metallic Object Partially Immersed In A Semi-Infinite Dielectric Medium," *IEEE Transactions on Antennas and Propagation*, Vol. 49, No.2, Feb 2001.
- [30] P.V. Nikitin, "Theory and Measurement of Backscattering from RFID Tags," *IEEE Transactions on Antennas and Propagation*, Vol. 48, No. 6, pp. 212- 218, December 2006.
- [31] I. Balbin and N. Karmakar, "Phase-Encoded Chipless RFID Transponder for Large-Scale Low-Cost Applications," *IEEE Microwave and Wireless Components Letters*, Vol. 19, No. 8, pp. 509-511, August 2009.
- [32] A. Vena, E. Perret and S. Tedjini, "Chipless RFID Tag Using Hybrid Coding Technique", *IEEE Transactions on Microwave Theory and Techniques*, Vol. 59, No. 12, pp 3356-3364 December 2011.

.....✂.....

**METHODOLOGY AND LITERATURE REVIEW
OF CHIPLESS RFID TAGS**

Contents	2.1. <i>Introduction</i>
	2.2. <i>Pre-fabrication studies on RFID Tags</i>
	2.3. <i>Fabrication of RFID tags</i>
	2.4. <i>Tag measurement set-ups</i>
	2.5. <i>Literature Survey-Introduction</i>
	2.6. <i>Review of Frequency domain Chipless RFID tags</i>
	2.7. <i>Review on techniques to analyse backscattering from Chipless frequency domain tags</i>
	2.8. <i>Frequency domain Chipless RFID readers</i>
	2.9. <i>Conclusion</i>

This chapter includes software tools employed for simulation studies, fabrication procedure of the tags and measurement system. Ansoft HFSS and CST Microwave Studio are used for the simulation studies and the tags are fabricated using photolithographic process. The main instrument used for the tag detection is the vector network analyser. Post processing of the received data is done in MATLAB. The chapter also presents a survey on the Chipless RFID tags, reported in the literature. The techniques to improve tag performance are also surveyed. Finally, reader architecture and reading techniques are also reviewed.

2.1. Introduction

Chipless RFID is an emerging technology in the field of automatic identification and the objective is to reduce the tag price by eliminating the integrated circuits from the tag. This thesis highlights the design and development of frequency domain Chipless RFID tags. This chapter presents the software tools used for prefabrication studies, fabrication procedure for the tags, measurement setup and a thorough survey of the previous works.

Literature survey part is organized into three sections. First section is concerned with the survey of two classes of frequency domain Chipless RFID tags; Tags with transmitting/receiving antennas and Tags without transmitting/receiving antennas. Second section deals with the review of the time domain techniques used to improve frequency domain tag detection. The last part of literature review is a survey on the reported frequency domain Chipless RFID readers.

2.2. Pre-fabrication studies

For the simulation and optimization of Chipless RFID tag geometries, professional softwares Ansoft HFSS (High Frequency Structure Simulator) and CST Microwave studio are used. HFSS is a Finite Element Method (FEM) based solver for electromagnetic structures. Multiresonator based Chipless tags are studied in HFSS using its PEC and radiation boundaries. Lumped or waveguide port excitation can be used for the studies of two port multiresonating circuit and the resonant characteristics are studied by observing the S_{21} (transmission coefficient). The simulation setup is shown in figure 2.1. The geometry of the multiresonator circuit is drawn using the drawing tools and by specifying material properties and boundaries for 3D

or 2D elements in the HFSS window. After that, suitable port excitation and boundaries have to be assigned. A radiation boundary filled with air is used and the size of air column is defined equal to quarter of the free space wavelength of the lowest frequency of operation. The simulation engine is invoked by adding solution setup and then defining a suitable frequency sweep. Discrete type frequency sweep is defined for accurate results and the solution frequency is selected as the highest operating frequency of the multifrequency structure. The vector and scalar representation of E, H, and J fields of the excited tag geometry under consideration provides good insight into the performance of the tag.

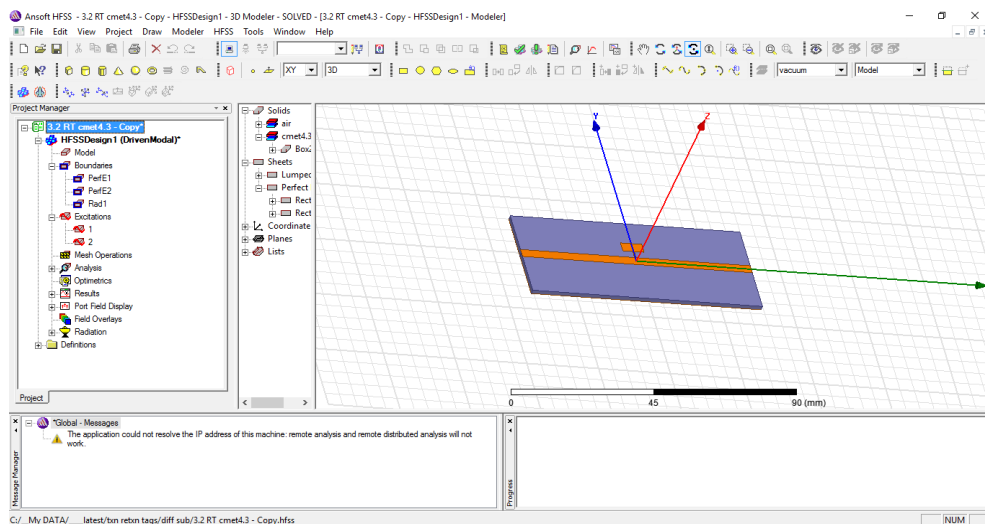


Figure 2.1: HFSS simulation window for the multiresonator circuit of Chipless RFID tag. Lumped port excitation is employed at both the ends of microstrip line

Multiscatterer based tags or the second class of tags concerned in this thesis are studied using both HFSS and CST microwave studio and the simulation setups are shown in figure 2.2. The tag structure is drawn in CST

by specifying the coordinates for each point of structure in the built in GUI(Graphical User Interface). When the structure is drawn, dielectrics and metallization are assigned. CST provides pre-defined templates that suit for problems in which parameters such as boundary conditions, mesh size, type etc. are pre-defined or that can be user defined. Once the tag structure is modelled, plane wave excitation is given to excite the Chipless tag and then the frequency sweep is defined for the required frequency spectrum. Electric probe is then defined at the required distance to measure the backscattered electric field both in time and frequency domains. The transient solver is executed to start the simulation. The parametrization and optimization tools in CST can optimize parameters such as the dimensions or position of a component and the material properties. The position and gap between resonators on the tag surface are optimized for minimum coupling effects and the most suitable substrate is also identified.

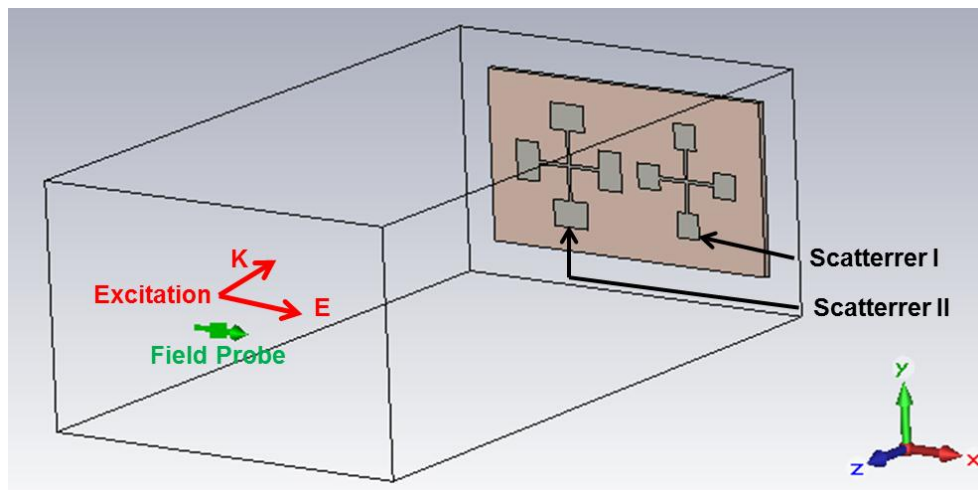


Figure 2.2(a): Simulated Chipless RFID tag in CST microwave studio with plane wave excitation. The field probe is polarized along x direction (E- vector) and Propagation is along z direction (K-vector).

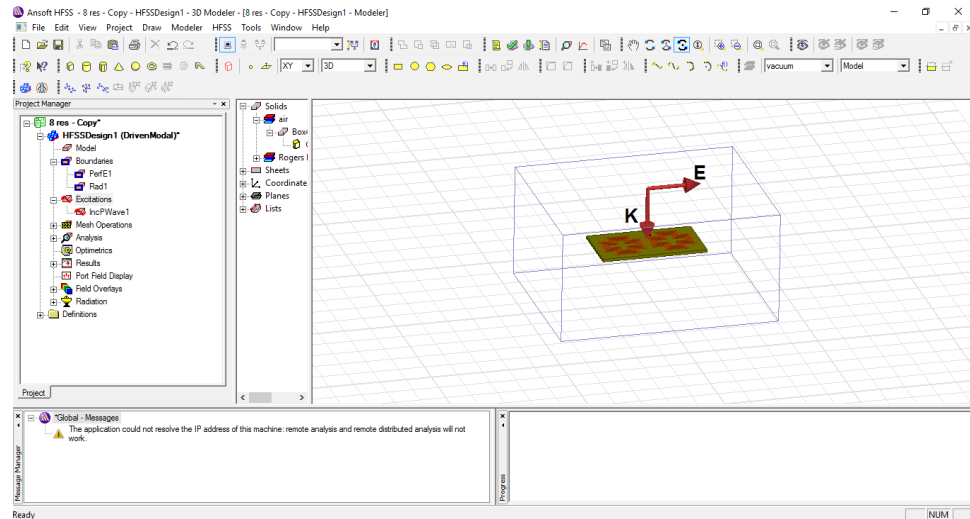


Figure 2.2(b): Simulated Chipless RFID tag in Ansoft HFSS with plane wave excitation. Here also, the field probe is polarized along x direction (E- vector) and propagation is along z direction (K-vector).

2.3. Fabrication

RT Duroid 5880 ($\epsilon_r = 2.2$ and $\tan\delta = 0.0009$) is selected as the substrate for the tags based on the prefabrication studies. Prototype of the tag is fabricated using photolithographic process. Using chemical etching process the unwanted metal regions are removed. For this first a negative mask of the tag geometry is created. Then the substrate's copper surface has to be cleaned thoroughly to remove oxide layer or any kind of impurities. The clean substrate is then dipped in negative photo resist and dried to get a thin film of the photo resist on the laminate. It is then exposed to ultra violet (UV) radiation through the negative mask for 20 minutes. UV exposure hardens the exposed portions. The substrate is then immersed in the developer solution and agitated for a few minutes. It is then washed in Ferric Chloride (FeCl_3) solution to remove the unwanted metal portions.

FeCl_3 dissolves the copper parts which are not hardened during UV exposure. Finally, the laminate is washed in Acetone solution to remove the hardened negative photo resist.

2.4. Tag measurements

The tag measurements were done by using the network analyzer as the reader. Measurements are carried out at the antenna research facility at CREMA, Dept. of Electronics, CUSAT. The test facilities available include Network Analyzers (R&S ZVB20 and Agilent PNA E8362B), spectrum analyzer, automated antenna positioner, broadband double ridged horn antennas (2-20 GHz) and anechoic chamber.

For the concerned frequency domain Chipless RFID tags, both frequency and time domain measurements are needed. The important measurements to be conducted are S_{11} (Reflection coefficient), S_{21} (transmission coefficient) and group delay in frequency domain and backscattering in time domain. Both frequency and time domain measurements are taken using Agilent PNA E8362B with 0dBm transmitted power and medium gain horn antennas. The network analyser is calibrated using the standard calibration kit before performing the measurements and the calibration can be stored and recalled at any time.

Two types of measurement setup are needed for the tags proposed in the thesis. First type of tag is multiresonator based Chipless tag with cross polarized transmitting-receiving antennas. For this type of tag, reader (analyzer) should be provided with two cross polarized antennas corresponding to the tag antennas and the measured quantity is S_{21} (Figure 2.3(a)). The

second type of tag proposed has no transmitting/receiving antennas and with a single antenna at the reader side, S_{11} is measured (figure 2.3(b)). This type of tag can also be designed to encode data in two polarizations and the measurement setup should contain two mutually perpendicular antennas at the reader side since both S_{11} and S_{22} are to be measured (figure 2.3(c)). For spectral signature based tags, measuring backscattering in time domain is also significant. The measurement setup is same as detailed above and a transformation to time domain is needed. Cross polarized antennas at the reader is needed in some cases for the second class of tags when data is encoded in both polarizations. Different measurement setups used in the thesis are shown in figure 2.3.

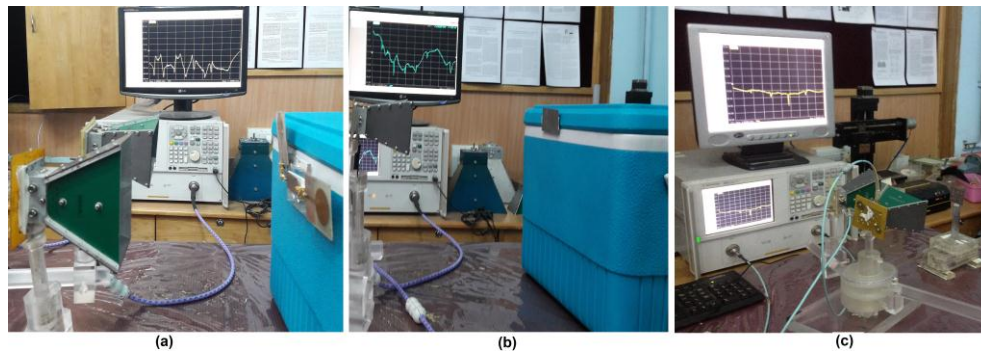


Figure 2.3: Measurement setup used to read Chipless tags (a) Multiresonator circuit based Chipless RFID tag measurement (b) Multiscatterer based Chipless tag (tags without transmitting and receiving antenna) measurement with one reader antenna (c) Multiscatterer with cross polarized reader antennas

2.5. Literature Survey-Introduction

As already stated in the introductory chapter, the Chipless RFID is an emerging technology and is an attempt to reduce the cost of RFID tags by

eliminating the silicon chip. Without the chip, the major concern with Chipless tags is how to encode data. Based on the type of encoding technique the tags are classified as Chipless Tags in time and frequency domains. Definitions and other sub classifications are already detailed in the previous chapter.

The first Chipless RFID tag reported [1] is a time domain tag based on SAW technology. Data is encoded according to the location of reflections from the tag in time domain and hence using the pulse position modulation. The SAW tag developed subsequently by RFSAW [1-3] is the only commercially available Chipless RFID tag with a coding capacity of 256 bits and reading range of the order of a few meters. The tag is operated at 2.54 GHz and uses a power of 10mW. The SAW based tags are a good alternative to chipped RFID tags. But the piezoelectric crystal made these tags not fully printable, bulky and costly.

Several time domain tags are developed subsequently based on TFTC (Thin Film Transistor Circuits) [4-5] and delay lines [6-9]. In [6] information is encoded as impedance mismatches along a transmission line. It is similar in coding to passive SAW tags whose reader listens to the reflections of transmitted pulse and their timings. Though this type of tag can obtain the planar nature and better resistance to noise, they can only encode a few data bits. The disadvantages of time domain tags and their principle of operation are already briefed in the introductory chapter. A narration about time domain tags is done in this survey just to show the evolution of this young technology started with time domain tags.

2.6. Review of Frequency domain Chipless RFID tags

As the name implies, frequency domain tag encodes data in the frequency domain as magnitude dips/peaks. Tags in which data is coded as phase frequency signatures can also be included in the frequency domain tags. Frequency domain tags generally employ two types of coding, Presence/absence coding and Frequency Shift Coding (FSC). The former has a 1:1 correspondence between data bits and resonances. Presence of a resonance represents bit 1 and absence represents bit 0 and vice versa. A single resonator can represent only two states. In frequency shift coding the resonance presented by a single resonator is made to vary in a band of frequency. Each slot in the band can represent one state. Thus the data encoding can be increased by using FSC.

A third type of coding in frequency domain is possible if the resonator employed has control over its harmonics. Then multiple bits can be represented by a single resonator. This technique also aids in enhancing the coding capacity of the Chipless Transponders. Multiple bits/per resonator can also be achieved with multiband resonators which have independent control over their individual bands.

Following two sections present an extensive survey on frequency domain Chipless RFID tags. The section '2.6.1' deals with frequency domain tags with antennas and section '2.6.2' deals with frequency domain tags without antennas.

2.6.1. Tags with transmitting/receiving antennas

A Chipless RFID tag encoding data as phase-frequency signature which is achieved by reactively terminating the tag antenna is presented in

[10]. A typical L-C ladder implemented in microstrip technology is used to reactively terminate the tag antenna. The technique offers operations with low transmit power, more resistance to multipath propagation and interference. An algorithm to extract the phase frequency signature from the composite backscattered signal is also presented.

The concept of frequency signature based Chipless RFID tag with cross polarized tag antennas is introduced by S.Preradovic et al. [11-13]. A multifrequency signal (between 2-2.5 GHz) generated in the reader is the interrogation signal and data is encoded in both magnitude and phase of the signal when it passes through the multiresonator circuit (cascaded spiral resonators) on the tag surface. Monopole circular disc antenna with simple geometry and relatively wide bandwidth is used as the tag antenna. The received and retransmitted signals are cross polarized in order to achieve good isolation between them. The read range of this system is more than 10 cm with an interrogation power level of -28 dBm. Data in phase of the signal is useful in noisy environments. A complete Chipless RFID system which is suitable for low cost item tracking is detailed in [14]. 35 bit Chipless RFID tag prototype having 1:1 correspondence for data bits is demonstrated on Taconic TLX-0 ($\epsilon_r = 2.45$, $h = 0.787$ mm, $\tan\delta = 0.0019$) substrate with a size of 88 mm \times 65 mm. The tag is designed to operate in between 3.1- 7 GHz. For the ease of coding, a technique of shorting of spiral resonators (which effectively shifts the resonance to higher frequency) is also presented. The paper also details performance of tag antenna (disc loaded monopole antenna) and the reader antenna (LPDA-Log Periodic Antenna). The tag offers a read range of 10cm for magnitude coding and

40cm for phase coding. The tag also claims to be useful in applications like low-cost item tagging such as banknotes and secured documents.

The design, analysis and measurement results of a novel 6-bit Chipless RFID tag based on dual multiresonant dipole antenna are presented in [15]. Here the multi-resonator circuit and the second antenna on the tag reported in [14] had been replaced with the dual multiresonant antenna. The multiresonant antenna acts as a group of loop antennas arranged in parallel. The tag uses the spectrum between 3.1-5 GHz and the main advantage is size reduction.

A fully printable Chipless RFID tag designed on Taconic TF290 ($\epsilon_r = 2.9$, $h = 90 \mu\text{m}$, $\tan\delta = 0.0028$) with multiple stop band spiral resonator is presented in [16]. The substrate used has very similar characteristics to plastic and paper. The usage of flexible and thin substrates causes substantial drop in spiral resonator quality factor. To overcome this adverse effect corner coupling and spiral repetition are adopted. The tag is designed to operate in between 5 and 10.7 GHz. S. Prerdovic et. al proposes [17] a similar tag but with improved features like less sensitivity to tag orientation and more compactness. The presented tag has a single antenna loaded with spiral EBGs. The authors claim that operation of the tag is based on backscattering rather than re-transmission. To get freedom in tag orientation, it is advised to have a circularly polarized reader antenna. Resonator repetition and corner coupling are also suggested for the design on flexible and thin substrates.

Another Chipless RFID tag having transmitting and receiving antenna aligned to same polarization is proposed in [18]. The tag has a single

bandstop resonator. By varying the position of slot on the resonator, frequency can be varied over 2-2.7 GHz. By using frequency shift coding, within the assigned spectrum with a resolution of 100 MHz, it can access eight combinations and hence has 3-bits encoding capacity. The transmitting and retransmitting antennas are wideband tapered monopoles.

An interesting application of Chipless RFID system for intelligent traffic information system is presented in [19]. The system used the tag presented in [14] and is embedded in the road for this application. The reader antennas (Planar disc loaded monopole antennas with UWB bandwidth 3.1-7 GHz) are placed under the vehicle and the reader is installed in the vehicle. Detailed review of Chipless RFID tag reader is provided in later part of this chapter. With the same microstrip spiral resonators on thin substrates, an RFID system for paper/plastic item tagging is demonstrated in [20].

A novel fully passive ID generation circuit based on spectral signatures is proposed in [21]. The paper employs frequency re-usage to yield more bits per bandwidth. Compared to time domain based Chipless tags, frequency domain tags have higher encoding capacity and reduced size. But the definite bandwidth required even for very high Q resonators (about 20 MHz) and the occurrence of higher order modes of resonance are the factors limiting the total usable bandwidth. The technique of frequency reuse is a good solution for the utilization of limited available bandwidth more efficiently. In this paper with this technique, 8 bits are encoded in the spectrum 4.5 GHz-6 GHz to validate the concept. The tag consists of cross polarized receiving and transmitting antennas, one broadband power divider, a time delay circuit and two multiresonator circuits (constituted by the high

Q spiral resonators). The readout signal consists of two retransmitted signals, each from the two multi resonator sections which are delayed by a time determined by the delay circuit.

Chipless millimeter wave based RFID (MMID) tags are proposed in [22-23]. The frequency range is around 30 GHz. Compact size, better isolation between reader's interrogation signal and greater reading ranges are advantages of the proposed MMID. Slots loaded in the patch antennas are the encoding elements of MMID proposed in [23].

Stub loaded dual band resonators are integrated in the Chipless RFID tag in [24] and can encode 3^N words with N resonators. Rhomboid antenna with integrated stepped adapter is used in the tag to ensure increased bandwidth and improvement in return loss. Background subtraction and time gating are employed to enhance the read range. Background subtraction is an effective calibration technique that consists of subtracting the measurement of a scene data including the calibration tag (identical to the designed tag but without resonators) from the measurement of the tag data. Time gating effectively minimizes multipath effects by neglecting the multiple reflections at the objects in the measurement scene. Another compact quarter wave open stub loaded Chipless tag is reported in [25]. The width of transmission line for optimum performance is calculated and an impedance transformer is used to minimize impedance mismatch with transmission line feeding the tag antenna. The tag antenna used is a circular monopole disc antenna. A low loss substrate with dielectric constant of 4.4 and $\tan\delta = 0.0018$ is used for the tag design and the frequency band of operation is between 2-4 GHz.

A Chipless UWB RFID system employing uniplanar Chipless tags is proposed in [26]. The tag consists of two UWB monopole antennas connected by coplanar waveguide and multiresonators embedded on the coplanar waveguide. The multiresonators are designed in the frequency band 3 to 6 GHz. The reader antennas employed are high gain Vivaldi antennas. Cross polarization of the receiving and transmitting antennas and usage of copper plate in between the reader antennas are presented to reduce the mutual coupling effects between transmission and reception.

The concept of prototyping Chipless RFID tag based on Surface Integrated Waveguides for microwave identification is illustrated in [27]. The tag is based on a single high Q (366) substrate integrated cavity resonator. Data is encoded as frequency signature in the reader signal by varying the effective dielectric constant of the substrate by the air holes made inside the resonator structure. The SIW based tag operates in the frequency range of 10.5-11 GHz and it has the advantages of low cost, compactness and passive. The concept is transferrable easily to other low cost substrates.

A multiresonator circuit based on dual band modified complementary split ring resonator is presented in [28]. The modified complementary split ring resonator is embedded in the transmission line and is capable of encoding multiple bits per resonator. Symmetric alignment of the resonators with respect to the feed line is presented as a means to suppress the second harmonic and hence to enhance the total realizable bandwidth. Triangular microstrip filter is used along with circular UWB disc monopole antennas to form Chipless RFID tag (frequency band 3.5-4.3 GHz) in [29].

Presence/absence coding is used and the resonance is removed from the spectrum simply by making a slot in the resonator.

Multiresonators based on defected ground structures are employed to constitute Chipless RFID tag in [30]. The tag claims to have excellent band notch characteristics and is capable of avoiding error arising from the re-radiation from normal resonators. The prototypes of the tag are fabricated on both thick FR4 and thin polyamide substrates and are found to be working. Open circuited stub multiresonators positioned within bifurcated transmission line [31] and open loop multiresonator circuit [32] based Chipless RFID tags are reported as suitable candidates for nearfield identification and security systems because of their high Q and compact size. Another work reported introduces meandered microstrip transmission line resonator as a modification to open stub resonators to constitute a 6 bit Chipless tag operating in the frequency range of 3-5 GHz [33]. Meander complementary split ring resonators that have reduced size are employed in [34] to form electrically small (due to their quasi-static resonance) tag.

Chipless RFID tags are generally designed in GHz frequencies to reduce the size of the tag. In [35], it is reported a micro-electro-mechanical system based Chipless tag that can operate at standard UHF band. The tag is fabricated using basic MEMs fabrication process and the backscattered signal is patterned by an array of MEMS-switching modules with different pull-in voltages. An N-bit tag with 2N MEMs switches is also presented.

An open ring microstrip resonator which can act as multiresonant element of Chipless RFID tag in combination with cross polarized transmission and reception antennas is presented in [36]. With a single

resonator a 3 bit tag is realized. The resonances of Open ring resonator are adjusted by changing the relative position of ring gap and excitation port. The tag is prototyped on RO3010 50mil Rogers substrate ($\tan\delta = 0.0022$ and $\epsilon_r = 10.2$) and it is suggested that further compactness can be achieved by including high dielectric constant material in the center of the ring.

A unipolar L shaped defected ground structure resonator based Chipless RFID tag operating in the range 3.1-6.1 GHz is reported in [37]. Though such a single resonator has 1 bit coding correspondence, the coding capacity is increased by increasing the number of resonators in parallel with tag size. Again cross polarized UWB monopole antennas are suggested with the resonator to form the complete tag. The multiresonator circuit of [38] is based on half wave length shorted stub resonators and in [39] it is based on Archimedean spirals. Spur line [40] and microstrip E shaped [41] resonator based Chipless tags are also reported in a similar way

Modified coplanar waveguide circular monopole antennas combined with a 7 bit multiresonator to form Chipless RFID tag is reported in [42]. The circular monopole antenna is modified with two steps and an offset circular slot. The antenna claimed to have good impedance matching with stable radiation characteristics over the selected band of operation 6-8 GHz. In [43], the same antenna is demonstrated with quarter wave open stub resonators. In [44], the mutiresonator circuit is formed by printing rectangular slotted split ring on the back of the substrate and is connected to 50Ω transmission line. The metamaterial based resonator is an attempt to realize compact tags and is realized on fleece substrate ($\epsilon_r = 1.35$, $\tan\delta = 0.025$ and $h = 1$ mm).

2.6.2. Tags without transmitting/receiving antennas

These types of tags have no antennas embedded with them for the reception and retransmission of reader interrogation signal and data encoded signal. The functions of reception, filtering (data encoding), and retransmission are assigned to each of the multiple resonators scattered on the surface of Chipless tag. The following section reviews such tags and the characteristics of resonators that should be selected for the design of them.

The first tag of this category or might be the first frequency domain Chipless RFID tag is reported in [45], [46]. The paper presents the tag as a wireless equivalent of optical barcodes. The tag is formed of arrays of microstrip dipole-like structures that function as resonant bandpass or band stop filters tuned to predetermined frequencies. Enhancement of coding capacity by straddling many frequency bands and resonator width variation to control the resonance frequency are proposed to constitute a practical RF barcode. Detection of the tag is done by measuring the reflection from the tag and by analyzing the frequency content. The tag is realized on Taconics TLY-5 substrate ($h = 0.53\text{mm}$, $\epsilon_r = 2.2$ and $\tan\delta = 0.001$).

As already stated, tags encoding data as phase-frequency signature are also included in the category of frequency domain Chipless RFID tags. Such tags are more robust in presence of multipath and clutter. In [47] and [48] data is encoded as phase frequency signatures without any reception and retransmission antennas. Stacked multi-layer patches are used as basic scatterer in [47]. In the case of stacked patch resonators when the upper patch is resonant, the middle patch functions as a ground plane and for the middle patch the bottom acts as a ground plane. Since the frequency is

swept between resonances the magnitude of backscattering from such patches is relatively constant but the phase variation/delay is substantial. The structure claimed to have the potential to be used in multipath and clutter environment because of its inherent low structural scattering. A 3bit Chipless RFID tag is developed using the basic principle of vector backscattered signals from multiple planar reflectors in [48]. The tag consists of square stub loaded microstrip patch antennas. The phase of the backscattered signal changes in a predictable way for the changes in the length of the loaded stub and a unique code is extracted with a phase shift of 30° . The substrate used for prototyping the tag is Taconic TLX-0 ($h = 0.787$ mm $\epsilon_r = 2.45$).

A Chipless RFID tag suitable for secure identification systems like in credit cards (data transfer by contact) is reported in [49]. Giving importance to security and larger data encoding capacity a 23 bit tag is developed with the dimensions of credit card employing dipole like resonators [45]. Data is encoded by varying the length in addition to width to enhance coding capacity. Measurement is based on metallic cavity perturbation to get resolution of the order of 2MHz unlike the bistatic measurement of [45]. Various combinations of split ring resonator (SRR) are used to generate electromagnetic code in [50]. The SRR array used in the tag has frequency selective behavior and tuning of resonators to different frequencies is accomplished by varying the SRR parameters and the directions of the gaps. Performance of the tag on polycarbonate sheet is also effectively reported and the tag is read by placing it between two waveguides.

Unlike the most reported chipless frequency domain tags, a 10 bit tag operating in the HF/VHF band using the sympathetic oscillations of array of

LC resonators is reported in [51]. The tag reported has a successful reading range of 21 cm, good resistance to water contained environment (unlike GHz range frequencies) and is reconfigurable. Letters of alphabets when etched with metallic strips on dielectric substrate create unique signature and are therefore used in [52] to encode data in frequency domain. Electromagnetic signatures of 26 letters in Ariel font 24mm are also presented.

Chipless tag to replace the holographic band on banknotes is reported in [53] and is based on split-ring resonators. The tag is suitable for paper based materials and is demonstrated by printing SRR based patterns on paper. Phase deviation technique is used in [54] to encode data using single sided C shaped multiple phase shifters and a 10 bit tag is demonstrated. Coding capacity of the Chipless tag in [55] is enhanced by using both phase and magnitude to encode the information. The tag is based on single sided C shaped resonator which has an uncoupled resonant and an anti-resonant modes. Coding capacity of 22.9 bits is obtained with a few resonators having a small area of $2 \times 4 \text{ cm}^2$. A compact dual polarized Chipless RFID tag is presented in [56]. The tag is composed of single sided rectangular patches loaded with slots. Mutual coupling between adjacent frequency resonators is reduced by placing slots of adjacent frequencies on adjacent patches. Bandwidth utilization is doubled by using similar patches in both polarizations. Since the ground plane is absent and the tag is able to reradiate in both front and back directions, different reading methods are demonstrated with dual polarized antennas and with dual polarized waveguides. Tag rotations are limited to small angles so as to resist cross polar levels.

A compact single layer 20 bit tag is reported with a novel detuning technique [57]. Detuning is most needed in single layer Chipless tags since they are more sensitive to the material of tagged item. It is achieved here by employing two resonators to probe the effective permittivity of the surrounding environment. The resonators of the proposed tag can be configured easily by filling or not filling them depending on the binary code to be implemented. The same tag is also claimed to extend to a capacity of 40 bits within a surface smaller than a credit card. Another highly compact and single layer tag with similar detuning technique is reported in [58]. The tag employed coplanar strip line resonators with one side as a short circuit and other side as an open circuit. Multiple bits in one resonator and Frequency shift coding are also adopted to improve coding capacity.

In [59], polarization diversity is used for the first time in the Chipless tag to encode data and is based on split ring resonators having strong polarization sensitivity. The tag utilizes narrow frequency bands and is robust to the detuning effect of tagged item due to the presence of ground plane. It is also reported for its effectiveness as a rotation sensor. For reading, a polarization agile antenna is needed at the reader side. A backscattering based Chipless RFID tag using triangle microstrip filter operating in 4-7 GHz is presented [60]. The tag is less sensitive to orientation and is easy to configure for coding by introducing simple opening on the sides.

Chipless Frequency domain tags insensitive to polarization are reported in [61] and [62]. The tag [61] uses circular ring resonators and [62]

uses circular patch loaded with multiple slot ring resonator. The ring nature enables nesting of resonators and makes the tag more compact. Polarization insensitive tags provide a lot of freedom in positioning of the tag with respect to the reader interrogation signal. Both the tags utilize entire UWB from 3.1 GHz to 10.6 GHz and the former is prototyped on RO4003 substrate ($\epsilon_r = 3.55$, $\tan\delta = 0.0027$) and the latter is on Taconic TLX-9 ($\epsilon_r = 2.5$, $\tan\delta = 0.0019$). In [62], it is stated that the symmetric and continuous nature of the resonator inhibit the even and odd harmonic current paths from occurring. Also the tag has no ground and provide signature in both front and back directions.

Chipless RFID tag printed on paper substrates is reported [63]. The tag uses phase modulation which is achieved by employing reconfigurable coplanar LC resonators. The tag is realized using all printing technique and overprinting is used to enhance conductivity of the tag. LC resonator in the tag is formed by a single loop inductor and an interdigital capacitor (IDC). The IDC permits single surface fabrication and capacitance modification by connecting or disconnecting a finger. The coding is achieved without changing the inductor structure and changing IDC structure. The size of inductor is selected in match with the tag reader antenna and that of capacitor is decided in accordance with resonance frequency and should be small enough to be accommodated by the inductor. A split wheel resonator based tag is presented in [64]. Tag could be made linearly polarized as well as polarization independent, by positioning of split and axial symmetry present in the split wheel resonator. Taconic TLX-0 substrate is used to prototype the tag and tag is easily configurable to encode data by simple layout modification.

Electromagnetic imaging technique is reported in [65] to form Chipless RFID tag in the millimetre wave range. Data encoding is based on diffraction of electromagnetic waves by a carefully positioned conductive strip. Synthetic Aperture Radar (SAR) technique is suggested to get high resolution and the proposed tag has an encoding capacity of 2 bits/cm² in 100 MHz bandwidth. Size reduced unit cells derived from U folded dipole loaded with meander line inductor or interdigital capacitor are used to constitute uniplanar Chipless RFID tag [66]. Loading of interdigital capacitor or meander line inductor is relied to bring size reduction.

A Chipless RFID tag in [67] is formed by multiresonant metamaterial absorbers. High impedance surfaces (HIS) comprising of frequency selective surfaces are used as metamaterial absorbers and concentric loop resonators function as unit cells. The number of bits encoded in the tag can be increased without much increase in tag size. The symmetry of unit cells made the tag polarization independent and the tag can be mounted on metallic objects because of the isolation provided by the ground.

Tailorable band rejection property of log-periodic (LP) antennas is used [68] to form Chipless RFID tag. Large number of dipole radiators on the LP aperture is used to encode data. Functioning of LP antenna as both radiator and coding element makes the tag design simple. The tag is frequency scalable so that designing at millimetre wave is feasible. Also it is broadband in nature due to the intrinsic property of LP radiator. In [69] space angle information is used to encode data and the scatterer is identified by the complex scattered field in two perpendicular directions.

A Chipless RFID tag (3-6 GHz) inkjet printed on a polyamide substrate using both conductive and resistive ink is reported in [70]. The conductive ink contains silver nanoparticles that will contribute to radiating performance and the resistive ink containing carbon nanotubes makes the printing near-transparent. The usage of organic ink makes the configuration flexible and easy to reconfigure. Also, the resistive properties of the organic ink allow amplitude shift coding technique along with frequency domain coding to enhance coding capacity. The basic resonator is a double rhombic loop resonator. Chipless RFID tag employing sewn scatterers on cotton textile is presented in [71]. The scatterer is sewn by computer aided sewing machine using electro thread plated with silver. Sewn stretchable sensor can also be realized on the tag and preliminary results are also reported. The results are validated in the frequency band 3-6 GHz. A 19 bit Chipless RFID tag realized using the flexography technique on paper substrate is reported in [72]. The tag is designed to operate within the UWB with comparable size with similar tags. Performance comparison with chemical etching and catalyst inkjet printing is also provided in the paper.

A depolarizing Chipless RFID tag for robust detection is reported by Vena et al. [73]. Multiple scatterers on the tag surface depolarizes the incident wave and backscatters in an orthogonal direction. Backscattering in orthogonal direction claims to enhance the detection capability of the tag. A reading system based on UWB impulse radar is also presented.

An experimental validation of the LP based tag is reported by Gupta et al. [68] and is discussed in detail with special emphasis to the design flexibility in [74]. The multi-octave bandwidth property of LP antenna has

been effectively utilized for the design of Chipless RFID tags. A study on influence of mutual coupling on scatterer based frequency domain tag is conducted in [75] employing inductively/capacitively loaded U- folded dipoles. A 20 U-slot resonators in metallic plate which has improved RCS than its complementary array of U folded dipoles is demonstrated in [76]. Distribution of the resonators to get minimal coupling and detuning effects is also studied.

Cross RCS- based uniplanar Chipless RFID system is reported in [77] - [78]. Well designed and carefully oriented conductive strip and meander line are the key elements of the tag and would act like EM-polarizers. The RFID tag is operating in the 60 GHz band and has high data encoding capacity in a small area equal to or less than a credit card. The tags reported are robust against multipath and clutter effects. SAR (Synthetic Aperture Radar) based reader as well as signal processing techniques are also suggested for the presented tags. A grounded periodic surface is used to encode data as the phase difference between reflection coefficient of incident TE and TM plane waves [79]. The tag is having relatively small foot print and could avoid use of any calibration techniques with considerable performance.

A uniplanar orientation independent Chipless RFID tag formed by circular patch loaded with multiple discretized circular slot resonators is reported in [80]. The resonator is compact comparing the corresponding circular slot resonator and eliminates 2nd and 3rd harmonic frequencies. The tag is designed in a frequency band of 6-14 GHz. The substrate used is Taconic TLX-9 ($\epsilon_r = 2.5$, $\tan\delta = 0.0019$) with a thickness of 0.5 mm.

Multibit data capacity per resonator is achieved in [81] by utilizing scattering from an array of perpendicularly polarized identical split wheel resonators. The tag is based on those identical split wheel resonators of mutually orthogonal polarization which do not interfere in their fundamental mode. The technique of re-usage of the same frequency band is utilized to increase the data encoding capacity.

A multiresonant FSS based Chipless RFID tag using Matryoshkas geometry is reported in [82]. The geometry unlike from concentric ring stays open and interconnected as a single ring increases the resonant length and exhibits multiresonant behavior.

Complex-natural-resonance-based design of Chipless RFID tag having high-density of data is reported in [83]. The late time response from the tag is the summation of complex natural resonances (CNR) that are aspect independent parameters of the tag. Encoding and decoding of the data is successfully carried out by properly embedding and extracting the CNRs. The low profile tag presented here is designed in the frequency band 3.1-10.6 GHz and has 24 quarter-wavelength open-ended slot resonators inserted into a metallic object. The damping factor of the resonators which is a function of slot width is chosen as low as possible to confine the overall structure to a narrow spectrum. The design has the advantages of acceptable RCS (improved RCS due to the uniform metallic part of the tag) and high Q resonant frequencies. The distance between slots is decreased to improve quality factor and coupling between adjacent resonators is not changing much when nulling a bit. Effects of different parameters on structure are used to optimize the dimensions of the tag. Backscattered signal from the tag is

processed using short time matrix method which is a time- frequency approach having better performance compared to Prony and matrix pencil method. The pole diagram representation is also presented here to get more insight of the electromagnetic behavior.

Multibit encoded Chipless RFID tag reported by Nijas [84], perhaps is the highest bit encoded microstrip Chipless frequency domain tag reported so far. The basic resonator of the tag is stepped impedance resonator (SIR) and a single SIR can represent four different combinations (00, 01, 10, and 11) by suitably applying different boundary conditions and by using both fundamental and first harmonic frequencies. A tag comprising N number of such resonators therefore represents 2^{2N} combinations. Study on the scattering property of the tag for different angular directions is presented. The property of SIR, for the independent control over harmonic frequencies is effectively utilized in the tag. Structural information of the tag is encoded in both magnitude and group delay of the backscattered signal. 79 bit data is encoded using 5 resonators with the aid of frequency shift coding technique. A simple post processing technique of the backscattered signal based on difference operation is also reported to enhance detection in noisy environment.

A high capacity polarization independent tag employing angle based encoding of data is presented in [85]. The basic scatterer is V-shaped resonator and data is encoded with respect to the space angle between the V-shape. Tag identity is decoded by measuring the scattered field in two orthogonally polarized directions. A single scatterer can encode 3 bits of data and is sensitive to the reader even in the tilted positions. Both UIR (Uniform Impedance Resonator) and SIR (Stepped Impedance resonators)

are used as the scatterers by introducing suitable bends in the geometry to have V- shape and hence to define a space angle in between. Both vertically and horizontally polarized I shaped slot resonator of different lengths are employed in [86] to form dual polarized as well as orientation insensitive Chipless RFID tag. I slot resonators do not produce the second harmonics but create the third harmonic for symmetric excitation. These resonators add signature to both phase and magnitude of backscattered signal and the resonators are easily reconfigurable. For the reader side of the proposed system, a low profile wideband dual polarized aperture coupled microstrip patch antenna is employed. The tags developed are single layer and are directly printable using conductive ink.

A new coding technique based on the control of RCS magnitude of depolarizing tags together with frequency coding is reported in [87] to increase coding capacity of Chipless RFID tag. A specific auto-compensation approach is also reported to reduce the dependency of RCS magnitude coding to the environment. An FSS (frequency selective surface) based Chipless RFID tag on PET and paper substrates are reported along with a new semi-automatic reader technique for reducing the time per tag [88]. A proposal for the application of the tag in evacuation procedures under crisis is also suggested. The tag is also reported to have orientation insensitivity. Another Chipless RFID tag in which encoding is done as phase-frequency signature in the backscattered signal using HIS (High Impedance Surface) is presented in [89]. The tag is based on metallic nested rectangular loops printed on the surface of a grounded substrate and having stubs of varying lengths attached in the four corners of the rectangular rings.

A Chipless RFID tag based on cross dipole elements and which gives emphasis to coding efficiency, operating bandwidth preservation, compactness and detection robustness is reported in [90]. Smart arrangement of resonators adds to detection robustness of the tag by reducing interfering reflections from environment. In [91] a transparent, stretchable Chipless RFID tag is realized on polydimethylsiloxane elastomer ($\epsilon_r = 2.8$, $\tan\delta = 0.02$). Highly conductive silicon nanowires used in the tag make it useful in RFID strain sensors. A Chipless RFID tag with increased data encoding capacity is proposed in [92] which uses the same frequency spectrum in both polarization. Polarization sensitive closed loop ring resonators are the basic encoding particles of the reported tag realized on RO4003 substrate ($\epsilon_r = 3.5$, $\tan\delta = 0.0027$).

A two layer printed Chipless RFID tag realized on Teslin paper using inkjet printing technique is reported in [93] for the specific applications requiring date and time identification. The tag is based on nested loop resonators with circular inner wall and truncated rectangular outer wall. The resonator geometry reduces mutual coupling effects between multiple resonators. Surface coding density of 3.56 bits/cm^2 is obtained for the tag. This is good value compared to the so far reported Chipless tags on paper substrate. Another Chipless RFID tag realized on low cost flexible materials using screen printing is reported in [94]. The tag is based on FSS and the inherent high RCS response of FSS structures provides enhanced reading range (3.5 m). The unit element is a multi-octagonal ring structure consisting of concentric octagonal rings with an additional octagonal patch at the centre. Effects of bending and folding of the flexible tag is also corroborated. The symmetric nature of resonators assures orientation insensitivity to the tag.

Comparison of methods like inter element rearrangement of resonators and element geometry modifications like tapering of edges to reduce coupling effects between resonators is conducted in [95]. In [96] orientation insensitivity is added to the Chipless RFID tag by relying on circularly polarized reader signal. Detection robustness is enhanced by introducing depolarizing effect on the backscattered signal. The tag is based on ladder shaped resonators. Performance comparison of several uniplanar capacitively loaded scatterers for frequency domain Chipless tag is conducted in [97] and from that a thin spiral three arm scatterer based tag is also corroborated. The idea of an unclonable Chipless RFID based on manufacturing variations is reported for the first time [98]. The basic resonators are concentric slot resonators. Resonant frequency of these resonators is sensitive to slot parameters as well as to the substrate dielectric constant. The substrate dielectric constant could be varied during manufacturing and hence is varied to encode IDs in frequency.

2.7. Review on techniques to analyse backscattering from Chipless frequency domain tags

Backscattering from Chipless frequency domain RFID tags can be recorded either in time or frequency domain. This is possible due to the duality existing between both the domains and due to the availability of powerful transforms between the domains. Application of time domain techniques on backscattered data from frequency domain tags helps to accommodate advantages of the time domain tags like better noise resistivity and freedom in orientation. Backscattering from a tag in time domain is constituted mainly by two components namely early time response (structural mode) and late time response (antenna mode). The

structural mode or early time response is inherent to any reflective object and it has a broadband response and a short time existence. It does not contain any information regarding the scatterers/resonators on the tag surface. It is arising due to the specular reflections emanating from the local current distributions on the discontinuities in the tag surface. Interaction between these local current distributions in the early time leads to late time response which is spread over time. Late time response represents the source free response of the tag and is directly related to the stored energy retransmitted from the scatterers on the tag surface, their quality factor and their resonant parameters. In Chipless frequency domain tags, these antenna modes in late time response are controlled and processed to decode the tag ID. In the literature various techniques to process these modes are reported.

Pole- residue representation of scattering from a finite body is used for the design and backscattering analysis of Chipless RFID tags in [99]. Decoding of data is done by recording backscattered time domain wave and then extracting the poles and residues. The time domain impulse response is obtained by taking IFFT of scattering parameters in frequency domain. Late time response free from source effects is obtained by employing gating to time domain waveform. From the gated time domain, data poles and residues are extracted using matrix pencil method. A method to improve noise reduction using matrix pencil method is given in [100]. It proposes autocorrelation function that could reduce random signals including noise to extract poles more accurately. In [101] Data encoding is considered in context of complex natural frequencies of the structure and data retrieval is done using Singularity expansion method based concepts along with target identification techniques. The paper also provides background information

for singularity based coding needed for Chipless RFID tags. Singularity expansion method is based on the assumption that an object's response to electromagnetic excitation can be defined completely by the singularities in complex frequency plane. The inherent pole singularities representing aspect independent source free (natural) solutions of the Chipless RFID tag can be controlled by changing the parameters of resonator embedded on the tag surface. Real and imaginary parts of Complex frequency poles are extracted from the late time response using matrix pencil method (which has considerable noise resistance than Prony's method). Notched-elliptical dipole tag is considered in the paper and its successful detection via its scattered fields in time domain is reported . A space- time-frequency target identification technique which enables the detection of Chipless RFID tag in multi-object scattering environment is reported in [102]. Here the poles are separated based on time and direction of scattered fields. Concept of time variant time window is applied to the matrix pencil method to improve the accuracy of pole detection. A four element receiving antenna array at the reader side is suggested as method for location finding with collision avoidance.

Moving average filtering as a simple de-noising technique is used in [103] to enhance the performance of dedicated low cost Chipless RFID reader. The selection of the technique is justified by its simplicity in implementation and suitability for removing random noise. Validation of the technique is done for a mid-range microcontroller. In [104] zeros of derivative of the group delay of the received signal are used for the detection. A filtering based on prolate spheroidal wave function is employed to filter the received signal and hence to accurately determine the zeros. The filtering method also reduces the noise in group delay.

Time domain analysis of frequency domain Chipless RFID tag and the components of backscattered time domain signal are given in [105]. Structural and antenna modes are clearly identified and meandering of transmission line is illustrated as an effective way to increase the separation between two modes. Windowing of antenna mode is done to extract the frequency signature of the tag. Analysis of backscattering in time domain of a Chipless RFID tag interrogated by an ultra-wideband impulse radar based reader is reported in [106]. The backscattering is explained using a semi analytical model and is validated by measurement results. The method does not need calibration and provide increased degree of freedom in the tag alignment with respect to the reader. A novel detection method named selective spectral interrogation (SSI) is also reported together with peak detection algorithm for the precise extraction of spectral signature of the tag. SSI is based on a set of interrogation pulses, each designed to maximize the unique resonance of the tag. In [107] spectral signature of Chipless RFID tag is represented in signal space. The frequency signature of the tag is specified using a set of orthonormal basis functions and the tag detection is based on minimum distance detection from the signal space representation of frequency signatures.

An effective collision avoidance methodology useful for a multi-tag environment is accounted in [108]. The method utilizes linear frequency modulated signal for interrogation and employs fractional Fourier transform technique for time-frequency analysis of received signals. The received signal at the reader side is analysed as a summation of a number of chirp signals where the number corresponds to the number of tags present in the measuring environment. In the presented method, the received signal is first

transformed to fractional domain from which the number of tags in the reading zone is estimated. Then windowing is performed (number of times equal to the number of tags present) in the fractional domain itself in order to avoid overlapping of tag responses. The separated responses after windowing are restored to time domain using inverse fractional Fourier transform and the frequency spectrum is obtained through Fourier transform. Another collision detection algorithm is reported in [109] based on FMCW-RADAR technique which involves calculation of the time difference of arrival of tag responses from different distances. The method converts the received multi-response signal to an intermediate frequency (IF) signal using a mixer and examines the IF spectrum to get the information about the number of tags.

In [110], a localization technique for frequency domain Chipless RFID tags based on UWB-IR ranging technique is described. Backscattered signal from the reading zone containing multiple tags is collected by means of multiple receivers. RTOF (roundtrip time of flight) calculation and time gating analysis for frequency domain Chipless RFID tag is also presented. A comparison of delay of structural mode and the interrogation pulse yields the RTOF and relative ranges between the tag and the receiver and then linear least square approximation is employed to find out the tag position. The tag mode RCS or antenna mode is processed to get the tag ID. Proper windowing of both RCS modes are used to determine the tag position and ID. Sets of equations are reported based on trilateration localization to aid the calculations. The reported calibration process are claimed to be useful for eliminating background noise, obtaining reference data for tag and RTOF reference.

The embedded poles of a Chipless RFID tag is extracted using short time matrix pencil method (STMPM) in [111]. STMPM is based on moving a right duration time window through the entire signal by small time steps and then employing matrix pencil method to extract the poles. Differentiation between the early time and late time response is done based on the time index obtained for the extracted singularities. Robustness of the technique in noisy environment can be enhanced by averaging complex poles over the time. An anti-collision algorithm for frequency domain Chipless RFID tags based on STMPM is presented in [112]. STMPM is used here to extract the turn-on times and complex natural resonances of the poles. Here tags are marked with definite resonances denoting the background additional to resonances corresponding to tag ID. Round trip times of the tags are taken as the turn-on time of complex natural resonances of the tags. A method for determining the position of Chipless RFID tag by measuring angular position from multiple scanning antennas is reported in [113].

A design of high density Chipless RFID tag based on complex natural resonances is described in [114]. Here the late time response containing the ID part of Chipless RFID tag is analysed as the summation of CNRs with some weighted residues. Also, application of STMPM, extraction of turn-on times, damping factors, and resonant frequencies of poles are explained clearly.

Apart from data encoding, an analysis based on CNRs is effectively used to develop a space-time-frequency anti-collision algorithm to detect multiple Chipless RFID tags present in the reader's antenna main beam in [115]. Identification of multiple multibit tag is given emphasis here and a

new method for obtaining accurate turn on times and CNRs of the tag is reported. For time-frequency analysis STMPM is used and a space-frequency representation is found by employing short-frequency matrix pencil method (SFMPM) realizing the duality between late time response in the time domain and early time response in the frequency domain. An accurate space-frequency technique for Chipless RFID tag localization is described in [116]. Division of reader zone into triangular unit areas and distribution of three antennas to each unit cell are relied in the measurement setup. Distance of the tag from the antennas is found from the space-frequency diagram by applying narrow frequency matrix pencil method (NFMPM) to the frequency response of the tag.

The more advanced application of fractional Fourier transform and usage of minimum distance detection are reported in [117], [118] for the detection of multiple frequency domain tags without collision. The time shifting and index additivity of fractional Fourier operator are explored to achieve better detection in a multi-tag scenario. Maximum likelihood (ML) technique is used in [119] - [121] for detection and channel estimation of Chipless RFID tags. The technique derives a decision by comparing the received signal with all possible combinations. In [122], the fact that the total received Radar Cross Section (RCS) is directly proportional to the number of Chipless tags located within the interrogation zone of the tag reader is used for counting the tagged objects.

Range of detection of Chipless RFID tag is improved [123] by receiver diversity with maximal ratio combining (MRC) at the reader side. It is demonstrated that the detection range has improved considerably by

increasing the number of antennas at the reader side without increasing the transmitting power.

Design of Chipless RFID tags using characteristic mode theory (CMT) is described in [124]. The paper explains CMT as a generalized Eigen-mode expansion method and illustrates its efficient use in the design and analysis of Chipless RFID tags. The quality factor, resonant frequency and the characteristic fields from the tag are monitored based on this theory. It is also demonstrated that CMT is an effective tool for analyzing the coupling mechanism between resonators, its effect on the quality factor and effect of low Q resonances of the structure. A solution for the challenges in distinguishing early and late time responses of multibit tags having closely placed scatterers is explained in [125]. The method consists of sliding a window along the time axis and then the application of STMPM to distinguish the poles corresponding to early time and the late time responses. The paper reports that the damping factor of poles is equal to zero when the early time response is located at the centre of the sliding window. Also the poles of early time, unlike the late time poles vary as the window slides along the time axis. These observations are used to distinguish the early time response. Based on window based singular value decomposition and adaptive energy detection two smart notch detection techniques are presented in [126] to improve Chipless RFID (frequency domain) system readability. The techniques are reported to have immunity to environmental effects like cluttering, fading and multipath components. A study on determination of theoretical detection ranges of UWB Chipless RFID tags is reported in [127] and the detection ranges are estimated based on both continuous wave based radar technique and the impulse radio based

radar technique. In [128], a mathematical framework for Notch Position Modulation scheme which is presented as Medium access control (MAC) algorithm to handle multi-tag identification for frequency domain Chipless system is described. An advanced UWB signaling scheme is also reported for maximizing transmitted power and correspondingly the reading range.

A method avoiding common calibration techniques but ensuring enhancements in tag detection is reported in [129]. The method is based on differential encoding achieved by subtracting the tag response measured simultaneously using two orthogonally polarized antennas. Before applying the subtraction, the time domain response is subjected to filtering to remove unwanted antenna coupling and multipath effects. The method is more practical than the other calibration techniques needing more reference measurements. Another method to avoid calibration with reference measurements is reported in [130]. The method utilizes short time Fourier transform (STFT) and is applied to depolarizing Chipless RFID tag measurements realizing the fact that they have long time signatures than the normal frequency domain Chipless tags.

A 3D localization method for frequency domain Chipless RFID tags is reported in [131] and is utilizing the time domain RCS, delay time and the relative positions of reader antenna for its calculations.

2.8. Frequency domain Chipless RFID readers

The reader is the complicated part of the Chipless RFID system where there exists a master-slave relationship between the reader and the tag. The Chipless tag cannot make any response without the interrogation from reader and is the reason behind the master (reader) – slave (tag) saying. The

duality between time and frequency domain enables the development of two classes of frequency domain Chipless RFID readers. The one class of readers decodes tag ID directly from frequency domain measurements while the other takes measurements in time domain.

S. Preradovic et al. reported 3 generations of Chipless RFID readers that are taking measurements in frequency domain directly [132] - [134]. The first generation reader is reported to detect amplitude only and the second generation reader is able to detect both phase and amplitude. Both generations operates over a narrowband (2-2.5 GHz) and have a capacity of 5 bit reading. The third generation reader operates over a wide band of frequencies from 5-11 GHz and is capable of reading 23 bits of data. General blocks of all the 3 generations include a digital section and an RF section. The digital section deals with the necessary signal processing of transmitted and received signals and consists of microprocessor, memory block, ADCs, DACs, and communication block for the software applications. The RF section includes voltage controlled oscillators (VCO), Low noise amplifiers (LNA), demodulator (gain/phase detector) and antenna. Two VCOs are used in the RF section of these readers; one is for generation of interrogation signal and the other in the mixer to down convert the backscattered signal to an intermediate frequency signal. The VCOs makes the system very expensive. These readers also need reference tag measurements and recalibration for dynamic environmental conditions. No additional signal processing techniques are used in the readers.

Design and implementation of digital control section for a UWB Chipless RFID reader is reported in [135]. The same system can read tags

with different data capacity and can control multiple RF sections. In [136], it reports a direct frequency domain Chipless tag reader architecture based on coherent frequency modulated continuous wave radar that can decode tag ID both from amplitude and phase of the backscattered signal. Hilbert transform based signal processing is also reported to improve and simplify detection. The reader relies on a single VCO and hence results in low cost design. Without any calibration tags accurate detection of 9 bit tag is performed. Ultra-wideband chirp signal interrogation based reader architecture to detect dual polarized Chipless RFID tags is described in [137]. This architecture also doesn't require calibration tags and needs a single VCO. A UWB reflect array antenna system enhancing the Chipless RFID reader performance is reported in [138]. The basic cell used in the design is the double circular ring and antenna panel has 100 elements. A dual polarized aperture coupled microstrip patch antenna array for a millimeter wave Chipless RFID reader is reported in [139].

The dual relationship between frequency domain and time domain is effectively utilized in [106] to read frequency domain tags using UWB-IR based interrogation. The reader architecture reported does not require any wideband VCOs and hence is low cost than the frequency modulated continuous-wave based readers. Also it does not require any calibration tags and ground planes, provides greater degree of freedom in tag - reader alignment and improves the reading range considerably. Realization cost of the UWB-IR based reader reported in [140] is reduced by using equivalent time approach (based on reproducibility of the measurement) in the design and repeating the tag interrogation sequence. [141] reports low sampling noise Chipless RFID reader based on the same equivalent time approach.

2.9. Conclusion

Tools for the pre-fabrication studies of research work, fabrication procedure and measurement facilities are presented in this chapter. A detailed survey on two main classes of frequency domain Chipless RFID tags is conducted. Also various time domain techniques and Chipless RFID tag reader architecture in the literature are also reviewed in this chapter.

References

- [1] C. S. Hartmann, "A global SAW ID tag with large data capacity," IEEE Ultrasonics Symposium 2002 Proceedings., vol. 1, No. c, pp. 65–69, 2002.
- [2] R. Das, "Chipless RFID—The End Game," IDTechEx, Cambridge, MA, Internet article, Feb. 2006. [Online]. Available: <http://www.idtechex.com/products/en/articles/00000435.asp>.
- [3] S. Harma, V. P. Plessky, C. S. Hartmann and W. Steichen, "SAW RFID tag with reduced size", IEEE Ultrasonics Symposium 2006, pp:2389-2392, Vancouver, Canada, Oct. 2006
- [4] R. Das and P. Harrop. (2006, Mar.). Chip-less RFID forecasts, technologies&players2006-2016.IDTechEx[Online].Available:<http://www.idtechex.com/products/en/view.asp?productcategoryid=96>.)
- [5] Advanced Industrial Science and Technology (AIST), (2010, Mar). Printing of organic thin-film transistor arrays on flexible substrates [Online]. Available: http://www.aist.go.jp/aist_e/latest_research/2008/20080728/20080728.html.
- [6] Lu Zhang, Saul Rodriguez, Hannu Tenhunen, and Li-Rong Zheng, "An Innovative Fully Printable RFID Technology Based on High Speed Time-Domain Reflections," Conference on High Density Microsystem Design and Packaging and Component Failure Analysis, 2006. HDP'06, pp. 166 - 170, 2006.

- [7] A. Chamarti and K. Varahramyan, "Transmission delay line- based ID generation circuit for RFID applications," *IEEE Micro- wave Wireless Compon. Lett.*, Vol. 16, No. 11, pp. 588–590, Nov. 2006.
- [8] J. Vemagiri, A. Chamarti, M. Agarwal, and K. Varahramyan, "Transmission Line Delay-Based Radio Frequency Identification (RFID) Tag," *Microwave Opt. Technol. Lett.*, Vol. 49, No. 8, pp. 1900 - 1904, 2007.
- [9] S. Shretha, J. Vemagiri, M. Agarwal, and K. Varahramyan, "Trans- Mission Line Reflection And Delay-Based ID Generation Scheme For RFID And Other Applications," *International Journal of Radio Frequency Identification Technology and Applications.*, Vol. 1, No. 4, pp. 401–416, 2007.
- [10] S. Mukherjee, "Chipless Radio Frequency Identification by Remote Measurement of Complex Impedance," *37th European Microwave Conference*, pp.249-252, October 2007.
- [11] S. Preradovic, I. Balbin, N. C. Karmakar and G. Swiegers, "A Novel Chipless RFID System Based On Planar Multiresonators For Barcode Replacement," *2008 IEEE International Conference on RFID*, pp:289-296, 16-17 April 2008.
- [12] S. Preradovic, I. Balbin, N. C. Karmakar and G. Swiegers, "Chipless Frequency Signature Based RFID Transponders," *Proceedings of the 38th European Microwave Conference*, Amsterdam, The Netherlands, pp 1723-1726, October 2008.
- [13] S. Preradovic, I. Balbin and N. C. Karmakar, "The Development and Design of a Novel Chipless RFID System for Low-Cost Item Tracking," *Asia-Pacific Microwave Conference*, pp. 1-4, 2008.
- [14] S. Preradovic, I. Balbin, N. C. Karmakar and G. Swiegers, "Multiresonator-Based Chipless RFID System for Low-Cost Item Tracking", *IEEE Transactions on Microwave Theory and Techniques*, Vol. 57, No. 5, pp - 1411-1419, May 2009.
- [15] I. Balbin and N. C. Karmakar, "Novel Chipless RFID Tag for Conveyor Belt Tracking using Multi-Resonant Dipole Antenna," *39th European Microwave Conference*, pp. 1109 - 1112, 2008.

- [16] S. Preradovic and N. C. Karmakar, "Design of Chipless RFID Tag for Operation on Flexible Laminates," *IEEE Antennas and Wireless Propagation Letters*, Vol. 9, pp. 207-210, 2010.
- [17] S. Preradovic and N. C. Karmakar, "4th Generation Multiresonator-Based Chipless RFID Tag Utilizing Spiral EBGs", *The 40th European Microwave Conference*, pp. 1746 - 1749, 2010.
- [18] T. Kim, U. Kim, J. Kwon, and J. Choi, "Design of a Novel Chipless RFID Tag Using a Simple Bandstop Resonator," *Asia-Pacific Microwave Conference*, pp.2264-2267, 2010.
- [19] S. Preradovic and N. C. Karmakar, "Chipless RFID for Intelligent Traffic Information System," *IEEE International Symposium on Antennas and Propagation (APSURSI)*, pp-992-995, 2011.
- [20] S. Preradovic, S. M. Roy, and N. C. Karmakar, "RFID System Based on Fully Printable Chipless Tag for Paper-/Plastic-Item Tagging," *IEEE Antennas and Propagation Magazine*, Vol. 53, No. 5, pp. 16-32, October 2011.
- [21] Md. Shakil Bhuiyan, R. E Azim and N. C. Karmakar "A Novel Frequency Reused Based ID Generation Circuit for Chipless RFID Applications," *Asia-Pacific Microwave Conference*, pp.1470-1473, 2011.
- [22] S. Preradovic and N. C. Karmakar, "Chipless Millimeter Wave Identification (MMID) Tag at 30 GHz," *41st European Microwave Conference*, Manchester, UK, pp.123-126, October 2011.
- [23] N. C Karmakar and C. K. Pern, "Mm-Wave Chipless RFID Tag For Low-Cost Item Tagging," *Asia-Pacific Microwave Conference*, pp.1462-1465, 2011.
- [24] D. Girbau, J. Lorenzo, A. Lázaro, C. Ferrater and R. Villarino," *Frequency-Coded Chipless RFID Tag Based on Dual-Band Resonators*," *IEEE Antennas and Wireless Propagation Letters*, Vol. 11, pp.126-128, 2012
- [25] C. M. Nijas, R. Dinesh, U. Deepak, A. Rasheed, S. Mridula, K. Vasudevan, and P. Mohanan, " Chipless RFID Tag Using Multiple Microstrip Open Stub Resonators," *IEEE Transactions On Antennas and Propagation*, Vol. 60, No. 9, pp.4429-4431, September 2012.

- [26] Y. F. Weng, S. W. Cheung, T. I. Yuk and L. Liu, "Design of Chipless UWB RFID System Using A CPW Multiresonator", *IEEE Antennas and Propagation Magazine*, Vol. 55, No. 1, pp. 13-31, February 2013.
- [27] H. El. Matbouly, N. Boubekeur and F. Domingue, "A Novel Chipless Identification Tag Based on a Substrate Integrated Cavity Resonator", *IEEE Microwave And Wireless Components Letters*, Vol. 23, No. 1, pp.52-54, January 2013.
- [28] Md. S. Bhuiyan, AKM Azad and N. C. Karmakar , "Dual-band Modified Complementary Split Ring Resonator (MCSR) Based Multiresonator Circuit for Chipless RFID Tag," *IEEE Eighth International Conference on Intelligent Sensors, Sensor Networks and Information Processing*, pp.277-281,2013.
- [29] S.H. Zainud-Deen, M Abo El-Hassan, HA. Malhai, K.H Awadalla, "Simple Microstrip Bandstop Resonators for Chipless RFID Tag," *30th National Radio Science Conference (NRSC 2013)*, pp.74-81, April 2013.
- [30] Seok-Jae Lee, Jongsik Lim, OaJ Ahn and Sang-Min Han, "Flexible Microwave Chipless Tag System Based on DGS Resonators," *IEEE 14th Annual Wireless and Microwave Technology Conference (WAMICON)*, 2013.
- [31] R. Dinesh, P V Anila, C M Nijas, M Sumi and P Mohanan, "Modified Open Stub MultiResonator Based Chipless Rfid Tag," *2014 URSI General Assembly and Scientific Symposium, Beijing, China on August 16-23, 2014*.
- [32] R. Dinesh, P V Anila, C M Nijas, M Sumi and P Mohanan "Open Loop MultiResonator Based Chipless RFID Tag" *2014 URSI General Assembly and Scientific Symposium, Beijing, China on August 16-23, 2014*.
- [33] M. E. Jalil, Md Kamal, A Rahim, Noor A. Samsuri and R. Dewan, "Chipless RFID Tag based on Meandered Line Resonator *IEEE Asia-Pacific Conference on Applied Electromagnetics (APACE)*, pp. 203 - 206, 2014.
- [34] Soumaya Sakouhi, Raggad Hedi, Rachida Bedira and Ali Gharsallah, "A novel Meander Complementary Split Ring Resonator-based RFID Chipless Tag," *2014 Mediterranean Microwave Symposium (MMS2014)*, pp.1-5, 8-10 December,2014.

- [35] A. Attaran, R. Rashidzadeh and R. Muscedere, “Chipless RFID tag using RF MEMS switch,” *ELECTRONICS LETTERS*, Vol. 50, No. 23, pp. 1720–1722, 6th November 2014.
- [36] U. M. Iranzo, B. Moradi and J. G. Garcia, “Open Ring Resonator Structure for Compact Chipless RFID Tags,” 2015 IEEE MTT-S International Microwave Symposium (IMS), 2015.
- [37] M. Khaliel, Md. El-Hadidy and Thomas Kaiser, “Printable Depolarizing Chipless RFID Tag Based on DGS Resonators for Suppressing the Clutter Effects,” 9th European Conference on Antennas and Propagation (EuCAP), pp. 1-5, 2015.
- [38] M Sumi, R Dinesh , C.M. Nijas, S. Mridula and P. Mohanan , “Frequency signature based Chipless RFID tag using shorted stub resonators” IEEE 4th Asia-Pacific Conference on Antennas and Propagation (APCAP), pp.296-299, 2015.
- [39] Hillner de P. A. Ferreira, Alexandre J. R. Serres, Georgina Karla de F. Serres, Francisco M. de Assis, and Alfrêdo Gomes Neto “Archimedean Spiral Multiresonator for Chipless RFID Tag Using Frequency-Coded Decimal Method,” SBMO/IEEE MTT-S International Microwave and Optoelectronics Conference (IMOC), pp. 1-4, 2015.
- [40] M Sumi, R Dinesh , C.M. Nijas, S. Mridula and P. Mohanan, “High Bit Encoding Chipless RFID Tag Using Multiple E-Shaped Microstrip Resonators,” *Progress In Electromagnetics Research B*, Vol. 61, pp.185–196, Nov. 2014.
- [41] M Sumi, R Dinesh , C.M. Nijas, S. Mridula and P. Mohanan, “Frequency Coded Chipless RFID Tag Using Spurline Resonators,” *Radio engineering*, Vol. 23, pp. 203-207, April 2014.
- [42] Md. A. Ashraf, O. M. Haraz, Md. R. AlShareef, Hatim M. Behairy and S. Alshebeili, “Design of A Chipless UWB RFID Tag Using CPW Circular Monopole Antennas and Multi-Resonators” IEEE International Conference on Ubiquitous Wireless Broadband (ICUWB), Montreal, Canada, 4-7th October, pp. 1-4, 2015.

- [43] O. M. Haraz, Md. A. Ashraf, Md. R. AlShareef, Hatim M. Behairy and S. Alshebeili "UWB Monopole Antenna Chipless RFID Tags Using 8-Bit Open Circuit Stub Resonators," 21st International Conference on Microwave, Radar and Wireless Communications (MIKON), Nadwislanska St, Krakow, 9-11 May, pp. 1-4, 2016.
- [44] M. E. Jalil, Noor Asmawati Samsuri, Md Kamal A Rahim and R. Dewan, "Compact Chipless RFID Metamaterial Based Structure Using Textile Material," 2015 International Symposium on Antennas and Propagation (ISAP), Hobart, Tasmania, Australia, 09 - 12 Nov, pp. 1-4, 2015.
- [45] I. Jalaly and I. D. Robertson, "RF Barcodes Using Multiple Multiple Frequency Bands", IEEE MTT-S Digest, June 2005, pp.139-142.
- [46] I. Jalaly and I. D. Robertson, "Capacitively-Tuned Split Microstrip Resonators for RFID Barcodes", 2005 European Microwave Conference, Paris, France, Vol. 2, Oct 2005. S. Mukherjee, "Chipless RFID using stacked multilayer patches Applied Electromagnetics Conference (AEMC), pp. 1-4, Dec. 2009.
- [47] I. Balbin and N. C. Karmakar, "Phase-encoded chipless RFID transponder for large-scale low-cost applications," IEEE Microw. Wireless Compon. Lett., Vol. 19, No. 8, pp. 509-511, Aug. 2009.
- [48] V. Deepu, A. Vena, E. Perret and S. Tedjini, "New RF identification technology for secure applications," in IEEE Int. Conf. on RFID-Technology and Applications(RFID-TA), Guangzhou, China. pp. 159-63, 17-19 Jun.2010.
- [49] H-S. Jang, W-G. Lim, K-S. Oh, S-M. Moon and J-W. Yu, "Design of Low-Cost Chipless System Using Printable Chipless Tag With Electromagnetic Code," IEEE Microwave And Wireless Components Letters, Vol. 20, No. 11, pp. 640-642, November 2010.
- [50] Botao Shao, Qiang Chen, Ran Liu and Li-Rong Zheng,, "A reconfigurable chipless RFID tag based on sympathetic oscillation for liquid-bearing applications," IEEE RFID 2011 Conference, Orlando, Florida, USA, 12-14April, 2011, pp. 170-175.

- [51] T. Singh, S. Tedjini, E. Perret, and A. Vena, "A frequency signature based method for the RF identification of letters," in Proc. Int. Conf. RFID, Orlando, FL, 12-14 Apr. 2011, pp. 1–5.
- [52] W. S. Lee, H. S. Jang, K. S. Oh and J. W. Yu, "Design of Chipless Tag with Electromagnetic Code for Paper-based Banknote Classification", Proceedings of the Asia-Pacific Microwave Conference, pp. 1406-1409, 2011.
- [53] A.Vena, E. Perret, and S. Tedjini, "RFID Chipless Tag Based On Multiple Phase Shifters," presented at the IEEE MTT-S Int. Microwave Symp. Dig., Baltimore, MD, Jun. 5–10, 2011.
- [54] A. Vena, E. Perret, and S. Tedjini, "Chipless RFID tag using hybrid coding technique," IEEE Transactions On Microwave Theory and Techniques, Vol. 59, No. 12, pp. 3356–3364, Dec. 2011.
- [55] M. A. Islam and N. C. Karmakar, "A Novel Compact Printable Dual-Polarized Chipless RFID System," IEEE Transactions on Microwave Theory and Techniques, vol. 60, No.7, pp. 2142-2151, July 2012.
- [56] A. Vena, E. Perret and S. Tedjini, "A Fully Printable Chipless RFID Tag With Detuning Correction Technique", IEEE Microwave and Wireless Components Letters, Vol. 22, No. 4, pp. 209-211, April 2012.
- [57] A. Vena, E. Perret, and S. Tedjini, "Design of compact and auto compensated single layer chipless RFID tag," IEEE Transactions On Microwave Theory and Techniques., vol. 60, pp. 2913–2924, Sept. 2012.
- [58] A.Vena, E. Perret, and S. Tedjini, "A compact chipless RFID tag using polarization diversity for encoding and sensing," IEEE Int. Conf. RFID, Orlando, FL, Apr. 3–5, 2012, pp. 191–197.
- [59] H. Zainud-Deent, M. Abo El-Hassan, H.A. Malhet and K.H. Awadalla, "Novel Chipless Tag with Electromagnetic Codes", Middle East Conference on Antennas and Propagation (MECAP), 2012, Dec. 29-31, 2012.
- [60] A. Vena, E. Perret, and S. Tedjini, "High capacity chipless RFID tag insensitive to the polarization," IEEE Trans. Antennas Propag., Vol. 60, No. 10, pp. 4509–4515, Oct. 2012.

- [61] Md. Aminul Islam, Yixian Yap, Nemai Karmakar and A K M Azad, "Orientation Independent Compact Chipless RFID Tag", 2012 IEEE International Conference on RFID-Technologies and Applications, RFID-TA 2012, pp. 137-141.
- [62] Botao Shao, Yasar Amin, Qiang Chen, Ran Liu and Li-Rong Zheng, "Directly-printed packaging paper based chipless RFID tag with coplanar LC resonator," IEEE Antennas and Wireless Propagation Letters, Vol. 12, pp. 325-328, December 2013.
- [63] Md. Shakil Bhuiyan and Nemai Karmakar, "Chipless RFID Tag based on Split-wheel Resonators," 2013 7th European Conference on Antennas and Propagation (EuCAP), pp.3054-3057.
- [64] M. Zomorodi, N.C.Karmakar and S. G. Bansal, "Introduction of Electromagnetic Image-based Chipless RFID System," Proceedings of the 2013 IEEE 8th International Conference on Intelligent Sensors, Sensor Networks and Information Processing: Sensing the Future, ISSNIP, pp.443-448.
- [65] M. Polivka and J. Machac, "Novel Size-Reduced Unit Cells for Uniplanar Chipless RFID Tags," 2013 Asia-Pacific Microwave Conference Proceedings, pp.908-910.
- [66] F. Costa, S. Genovesi, and A. Monorchio, "A Chipless RFID Based on Multiresonant High-Impedance Surfaces," IEEE Transactions On Microwave Theory And Techniques, Vol. 61, No. 1, pp.146-152, January 2013.
- [67] S. Gupta and Li Jun Jiang, "Chipless RFID Tags based on Multiple Band-rejected Planar Log-Periodic Antennas," IEEE Antennas and Propagation Society, AP-S International Symposium (Digest), pp.1120-1121,2013.
- [68] L. Yan, W. Zhang, Runbo Ma and X. Chen, "Chipless RFID Tag Based on Space Angle Information," IEEE MTT-S International Microwave Workshop Series on RF and Wireless Technologies for Biomedical and Healthcare Applications (IMWS-BIO), pp. 30-32, 2013.
- [69] A.Vena, A. Ali. Babar, L. Sydänheimo, M. M. Tentzeris and Leena Ukkonen, "753A Novel Near-Transparent ASK-Reconfigurable Inkjet-Printed Chipless RFID Tag," IEEE Antennas and Wireless Propagation Letters, Vol. 12, pp. 753-756, 2013.

- [70] A. Vena, E. Moradi, K. Koski, A. Ali Babar, L. Sydänheimo and Leena Ukkonen, “Design and Realization of Stretchable Sewn Chipless RFID Tags and Sensors for Wearable Applications,” 2013 IEEE International Conference on RFID, pp. 176-183, 2013.
- [71] A. Vena, E. Perret, S. Tedjini, G. E. P.Tourtollet, A. Delattre, F. Garet, and Y. Boutant, “Design of Chipless RFID Tags Printed on Paper by Flexography,” IEEE Transactions On Antennas And Propagation, Vol. 61, No. 12, pp. 5868-5877, December 2013.
- [72] A. Vena, E. Perret and S. Tedjni, “A Depolarizing Chipless RFID Tag for Robust Detection and Its FCC Compliant UWB Reading System”, IEEE Transactions On Microwave Theory And Techniques, Vol. 61, No. 8, pp.2982-2994, August 2013.
- [73] S. Gupta, Gui Jun Li, R.C. Roberts and Li Jun Jiang, “Log-periodic dipole array antenna as chipless RFID tag,” Electronics Letters, Vol. 50, No. 5, pp. 339–341, February 2014.
- [74] M. Polivka and J. Machac, “Influence of Mutual Coupling on Performance of Small Scatterers for Chipless RFID Tags,” Proceedings of 24th International Conference Radioelektronika, RADIOELEKTRONIKA 2014, April 2014.
- [75] M. Polivka, M. Svanda, and J. Machac, “Chipless RFID Tag with an Improved RCS Response,” Proceedings of the 44th European Microwave Conference, Rome, Italy, pp.770-773, 6-9 Oct 2014.
- [76] Md. Zomorodi and N. C. Karmakar, “Cross-RCS Based, High Data Capacity, Chipless RFID System,” IEEE MTT-S International Microwave Symposium Digest, 1-6 June 2014.
- [77] Md. Zomorodi and N. C. Karmakar, “Cross-Polarized Printable Chipless RFID Tag with Superior Data Capacity,” 44th European Microwave Conference, Rome, Italy, pp-766-769, 6-9 Oct 2014.
- [78] S. Genovesi, F. Costa, A. Monorchio and G. Manara. “Phase-Only Encoding for Novel Chipless RFID Tag,” 2014 IEEE RFID Technology and Applications Conference, RFID-TA 2014, pp.68-71.

- [79] Marcos Martinez, Daniel van der Weide, “Compact Slot-Based Chipless RFID Tag,” 2014 IEEE RFID Technology and Applications Conference, RFID-TA 2014, pp.233-236.
- [80] Md. Shakil Bhuiyan and N. C. Karmakar, “A Spectrally Efficient Chipless RFID Tag Based on Split-wheel Resonator,” The 2014 International Workshop on Antenna Technology, pp.11- 14.
- [81] Alfrêdo Gomes Neto, Adaildo Gomes DAssunção Junior and Jefferson Costa e Silva, “A Proposed Geometry for Multi-Resonant Frequency Selective Surfaces”, Proceedings of the 44th European Microwave Conference, pp.897-900, 6-9 Oct. 2014.
- [82] R. Rezaiesarlak and M. Manteghi, “Complex-Natural-Resonance-Based Design of Chipless RFID Tag for High-Density Data,” IEEE Transactions on Antennas and Propagation, Vol. 62, No. 2, pp.898-904, February 2014.
- [83] C. M. Nijas, U. Deepak, P. V. Vinesh, R. Sujith, S. Mridula, K.Vasudevan and P. Mohanan, “Low-Cost Multiple-Bit Encoded Chipless RFID Tag Using Stepped Impedance Resonator,” IEEE Transactions On Antennas And Propagation, Vol. 62, No. 9, pp.4762-4470, September 2014.
- [84] C. Feng, W. Zhang, Li Li, L. Han, X. Chen, and R. Ma, “Angle-Based Chipless RFID Tag With High Capacity and Insensitivity to Polarization,” IEEE Transactions On Antennas And Propagation, Vol. 63, No. 4, pp.1789-1997, April 2015.
- [85] Md. A. Islam and N. C. Karmakar, “Compact Printable Chipless RFID Systems,” IEEE Transactions On Microwave Theory And Techniques, Vol. 63, No. 11, pp. 3785-3793, November 2015.
- [86] O. Rance, R. Siragusa, P. Lemaltre-Auger and E. Perret, “Toward RCS Magnitude Level Coding for Chipless RFID,” IEEE Transactions On Microwave Theory And Techniques, Vol. 64, No. 7, pp. 2315-2325, July 2016.
- [87] D. Betancourt, R. Nair, K. Haase, G. Schmidt, M. Bellmann, D. Höft, A. Hübler, and F. Ellinger, “Square-shape fully printed chipless RFID tag and its applications in evacuation procedures,” 9th European Conference on Antennas and Propagation, EuCAP , pp.3-7, 2015.

- [88] S. Genovesi, F. Costa, A. Monorchio and G. Manara, "A Novel Phase Encoding Technique Exploiting Linear or Circular Polarization," 9th European Conference on Antennas and Propagation (EuCAP), pp.3-5, 2015.
- [89] M. Khaliel, A. El-Awamry, A. Fawky, Md. El-Hadidy and T. Kaiser, "A Novel Co/Cross-Polarizing Chipless RFID Tags for High Coding Capacity and Robust Detection," IEEE Antennas and Propagation Society, AP-S International Symposium (Digest), pp.159-160, October 2015.
- [90] Taehee Jang and L. Jay Guo, "Transparent and Stretchable Chipless RFID Fabricated Using Silver Nanowire and 3D Printed Mask," IEEE Antennas and Propagation Society, AP-S International Symposium (Digest), pp. 312-313, October 2015.
- [91] M.M. Khan, F. A. Tahir and H. M. Cheema, "High Capacity Polarization Sensitive Chipless RFID Tag," IEEE Antennas and Propagation Society, AP-S International Symposium (Digest), pp.1770-1771, October 2015.
- [92] M. M. Khan, F. A. Tahir, M. F. Farooqui, A. Shamim, and H. M. Cheema, "3.56-bits/cm Compact Inkjet Printed and Application specific Chipless RFID Tag," IEEE Antennas And Wireless Propagation Letters, Vol. 15, pp.1109-1112, 2016.
- [93] D. Betancourt, K. Haase, A. Hübler, and F. Ellinger, "Bending and Folding Effect Study of Flexible Fully Printed and Late-Stage Codified Octagonal Chipless RFID Tags," IEEE Transactions On Antennas And Propagation, Vol. 64, No. 7, pp. 2815-2823, July 2016.
- [94] Milan Svanda, Jan Machac, Milan Polivka and Jaroslav Havlicek, "A Comparison of Two Ways to Reducing the Mutual Coupling of Chipless RFID Tag Scatterers," 21st International Conference on Microwave, Radar and Wireless Communications (MIKON), pp. 2-5, 2016.
- [95] M. Martinez and D. van der. Weide, "Circular Polarization on Depolarizing Chipless RFID Tags," IEEE Radio and Wireless Symposium (RWS) RWS, pp.145-147, 2016.
- [96] J. Havlicek, M. Polivka, M. Svanda, and Jan Machac, "Capacitively Loaded Dipoles for Chipless RFID Transponder," 26th International Conference Radioelektronika (RADIOELEKTRONIKA), pp 446 - 449, 2016.

- [97] Kun Yang, Domenic Forte, and Mark M. Tehranipoor, "UCR: An Unclonable Chipless RFID Tag," IEEE International Symposium on Hardware Oriented Security and Trust (HOST), pp. 7-12, 2016.
- [98] A. Blischak, M. Manteghi, "Pole residue techniques for chipless RFID detection," IEEE Antennas and Propagation Society International Symposium APSURSI 2009, Charleston, USA, pp.1-4, June 2009.
- [99] M. Manteghi, "A novel approach to improve noise reduction in the matrix pencil algorithm for chipless rfid tag detection," IEEEAntennas and Propagation Society International Symposium (APSURSI), 2010, pp. 1-4, July 2010.
- [100] A.T. Blischak and M. Manteghi, "Embedded Singularity Chipless RFID Tags", IEEE Transactions On Antennas And Propagation, Vol. 59, No. 11, pp. 3961-3968, November 2011.
- [101] M. Manteghi, "A Space-Time-Frequency Target Identification Technique for Chipless RFID Applications," IEEEAntennas and Propagation Society International Symposium (APSURSI), pp. 3350-3351, 2011.
- [102] R. Koswatta and N. C. Karmakar, "Moving Average Filtering Technique for Signal Processing in Digital Section of UWB Chipless RFID Reader," Proceedings of Asia-Pacific Microwave Conference, pp.1304-1307, December 2010.
- [103] W. Dullaert, L. Reichardt and H. Rogier, "Improved Detection Scheme for Chipless RFIDs Using Prolate Spheroidal Wave Function Based Noise Filtering," IEEE Antennas and Wireless Propagation Letters, Vol. 10, pp.472-475, 2011.
- [104] P. Kalansuriya and N. Karmakar, "Time domain analysis of a backscattering frequency signature based chipless RFID tag," 2011 Asia-Pacific Microwave Conference Proceedings (APMC), pp. 183-186, 2011.
- [105] P. Kalansuriya, N. C. Karmakar, and E.Viterbo, "On the Detection of Frequency-Spectra-Based Chipless RFID Using UWB Impulsed Interrogation," IEEE Transactions On Microwave Theory And Techniques, Vol. 60, No. 12, pp. 4187-4197, December 2012.

- [106] Kalansuriya, P., Karmakar, N.C. and Viterbo, E., “Signal Space Representation of Chipless RFID Tag Frequency Signatures,” IEEE Global Telecommunications Conference (GLOBECOM 2011), pp. 1-5, 5-9 Dec. 2011.
- [107] R. E. Azim and N. C. Karmakar, “A collision avoidance methodology for chipless RFID tags,” 2011 Asia-Pacific Microwave Conference (APMC), pp. 1514-1517, 2011.
- [108] R. E. Azim and N. C. Karmakar, “Efficient Collision Detection Method in Chipless RFID systems,” 7th International Conference on Electrical and Computer Engineering, Dhaka, Bangladesh, pp.830-832, 20-22 Dec. 2012.
- [109] R. E-Azim Anee and Nemaï C. Karmakar, “Chipless RFID Tag Localization,” IEEE Transactions On Microwave Theory And Techniques, Vol. 61, No. 11, pp. 4008-4017, November 2013.
- [110] R. Rezaiesarlak and M. Manteghi, “Short-Time Matrix Pencil Method for Chipless RFID Detection Applications,” IEEE Transactions On Antennas And Propagation, Vol. 61, No. 5, pp. 2801-2806, May 2013.
- [111] R. Rezaiesarlak and M. Manteghi, “A new anti-collision algorithm for identifying chipless rfid tags,” 2013 IEEE Antennas and Propagation Society International Symposium (APSURSI), pp. 1722– 1723, July 2013.
- [112] S. M. A. Motakabber M. I. Ibrahimy and A. H. M. Zahirul Alam, “Development of a Position Detection Technique for UWB Chipless RFID Tagged Object,” 2013 International Conference on Computing, Electrical And Electronic Engineering (ICCEEE), pp. 735-738, 2013.
- [113] Reza Rezaiesarlak and Majid Manteghi, “Complex-Natural-Resonance-Based Design of Chipless RFID Tag for High-Density Data”, IEEE Transactions on Antennas and Propagation, Vol. 62, No. 2, pp. 898-904, February, 2014.
- [114] R. Rezaiesarlak and M. Manteghi, “A Space–Time–Frequency Anticollision Algorithm for Identifying Chipless RFID Tags,” IEEE Transactions On Antennas And Propagation, Vol. 62, No. 3, pp. 1425-1432, March 2014.

- [115] R. Rezaiesarlak and M. Manteghi, "A Space-Frequency Technique for Chipless RFID Tag Localization", *IEEE Transactions on Antennas And Propagation*, Vol. 62, No. 11, 5790-5797, November 2014.
- [116] Camila D. R. Lopes, Edmar C. Gurjão and Francisco M. de Assis, "Optimized Recovery of Collided Chipless RFID Signals using Fractional Fourier Transform," *IEEE RFID Technology and Applications Conference, RFID-TA*, pp. 91-96, 2014.
- [117] Camila D. R. Lopes, Edmar C. Gurjão and Francisco M. de Assis, "Performance of Fractional Fourier Transform for Separation of Chipless RFID Collided Signal," *International Telecommunications Symposium (ITS)*, pp.1-5, 2014.
- [118] C. Divarathne and N. C. Karmakar, "ML Detection based SISO Chipless RFID Tag Reading," *44th European Microwave Conference, Rome, Italy*, pp. 762-765, 6-9 Oct 2014.
- [119] C. Divarathne and N. C. Karmakar, "A Maximum Likelihood Based Tag Detection Technique for MIMO Chipless RFID Systems," *IEEE International Microwave and RF Conference (IMaRC)*, pp. 5-8, 2014.
- [120] C. Divarathne and N. C. Karmakar, "An Advanced Tag Detection Technique for Chipless RFID Systems," *45th European Microwave Conference, Paris, France*, pp. 251-254, 7-10 Sept 2015.
- [121] M. Barahona, D. Betancourt, and F. Ellinger, "Decoding of Multiple Same-coded In-line Placed Chipless RFID Tags," *IEEE Conference on Antenna Measurements and Applications, CAMA*, pp.1-4, 2014.
- [122] K. Mahmud and S.P. Majumder, "Improvement of the Detection Range of a Chipless RFID for UWB system Using Receiver Diversity with Maximal Ratio Combining," *8th International Conference on Electrical and Computer Engineering, Dhaka, Bangladesh*, pp. 761-764, 20-22 December 2014.
- [123] R. Rezaiesarlak and M. Manteghi, "Design of Chipless RFID Tags Based on Characteristic Mode Theory (CMT)," *IEEE Transactions on Antennas And Propagation*, Vol. 63, No. 2, pp. 711-718, February 2015.

- [124] R. Rezaiesarlak and M. Manteghi, "Accurate Extraction of Early-/Late-Time Responses Using Short-Time Matrix Pencil Method for Transient Analysis of Scatterers," *IEEE Transactions On Antennas And Propagation*, Vol. 63, No. 11, pp. 4995-5002, November 2015.
- [125] A. El-Awamry, A. Fawky, Md. El-Hadidy and T. Kaiser, "Smart Notch Detection Techniques for Robust Frequency Coded Chipless RFID Systems," 9th European Conference on Antennas and Propagation (EuCAP), pp.1-5, 2015.
- [126] A.Vena, E. Perret, B. Sorli and S. Tedjini, "Theoretical Study on Detection Distance for Chipless RFID Systems According to Transmit Power Regulation Standards," 9th European Conference on Antennas and Propagation (EuCAP), pp.1-4, 2015.
- [127] M. El-Hadidy, A. El-Awamry, A. Fawky, M. Khaliel and T. Kaiser, "A Novel Collision Avoidance MAC Protocol for Multi-Tag UWB Chipless RFID Systems Based on Notch Position Modulation," 9th European Conference on Antennas and Propagation (EuCAP), pp. 1-5,2015.
- [128] F. Costa, S. Genovesi and A. Monorchio, "Normalization-Free Chipless RFIDs by Using Dual-Polarized Interrogation," *IEEE Transactions On Microwave Theory And Techniques*, Vol. 64, No. 1, pp. 310-318, January 2016.
- [129] A. Ramos, E. Perret, O. Rance, S. Tedjini, A. Lázaro and D. Girbau, "Temporal Separation Detection for Chipless Depolarizing Frequency-Coded RFID," *IEEE Transactions On Microwave Theory And Techniques*, Vol. 64, No. 7, pp. 2326-2337, July 2016.
- [130] Naibo Zhang, Mingjun Hu, Lingmin Shao, and Jun Yang, "Localization of Printed Chipless RFID in 3-D Space," *IEEE Microwave And Wireless Components Letters*, Vol. 26, No. 5, pp. 373-375, May 2016.
- [131] S. Preradovic and N. Karmakar, "Design of Short Range Chipless RFID Reader Prototype," *International Conference on Intelligent Sensors, Sensor Networks and Information Processing (ISSNIP)*, pp.307-312, 2009.
- [132] S. Preradovic and N. Karmakar, "Multiresonator based chipless RFID tag and dedicated RFID Reader," *IEEE MTT-S Int. Microw. Symp. Dig., Anaheim, CA*, pp. 1520–1523, 2010.

- [133] S. Preradovic and N. Karmakar, "Chipless RFID: Bar code of the future," *IEEE Microw. Mag.*, Vol. 11, No. 7, pp. 87–97, Dec. 2010.
- [134] Randika Koswatta and Nemai C. Karmakar, "Development of Digital Control Section of RFID Reader for Multibit Chipless RFID Tag Reading," 6th International Conference on Electrical and Computer Engineering, ICECE, Dhaka, Bangladesh, pp. 554-557, 18-20 December 2010.
- [135] R. V. Koswatta and N. C. Karmakar, "A Novel Reader Architecture Based on UWB Chirp Signal Interrogation for Multiresonator-Based Chipless RFID Tag Reading," *IEEE Transactions On Microwave Theory And Techniques*, Vol. 60, No. 9, pp. 2925-2933, September 2012.
- [136] Md. A. Islam, AKM. Azad and N. C. Karmakar, "A Novel Reader Architecture for Chipless RFID Tags" *Asia-Pacific Symposium on Electromagnetic Compatibility (APEMC)*, pp. 1 - 4, 2013
- [137] M.Khaliel, A. Fawky, Md. El-Hadidy, T. Kaiser, "UWB Reflectarray Antenna for Chipless RFID Applications," 31st National Radio Science Conference (NRSC2014, Faculty of Engineering, Ain Shams University, Egypt, pp.17-20) 28-30April, 2014.
- [138] Md. A. Islam and N.C Karmakar, "A 4×4 Dual Polarized mm-Wave ACMPA Array for a Universal mm-Wave Chipless RFID Tag Reader," *IEEE Transactions On Antennas And Propagation*, Vol. 63, No. 4, pp. 1633-1640, April 2015.
- [139] M. Garbati, R. Siragusa, E. Perret, A. Vena, C. Halopé, "High Performance Chipless RFID Reader Based on IR-UWB Technology," 9th European Conference on Antennas and Propagation (EuCAP), pp.1-5, 2015
- [140] M. Garbati, R. Siragusa, E. Perret and C. Halope, "Low Cost Low Sampling Noise UWB Chipless RFID Reader," *IEEE MTT-S International Microwave Symposium*, pp.1-5, 2015.

.....✂.....

**CHIPLESS RFID TAGS WITH
RECEPTION/TRANSMISSION ANTENNAS**

Contents	3.1. <i>Introduction</i>
	3.2. <i>Data encoding techniques for frequency domain Chipless RFID tags</i>
	3.3. <i>Stepped Impedance Resonators</i>
	3.4. <i>A Single SIR connected to microstrip transmission line</i>
	3.5. <i>Multiresonator circuit</i>
	3.6. <i>Modified Chipless RFID tag with SIR coupled to transmission line</i>
	3.7. <i>Tag antennas</i>
	3.8. <i>Friss-free space transmission formulae</i>
	3.9. <i>Chipless RFID tag with antennas</i>
	3.10. <i>Conclusion</i>

This chapter presents Chipless RFID tags with embedded antennas in them for reception and transmission of reader signal by the tag. Tags have multiple resonators coupled/connected to microstrip line in between the transmitting and receiving antennas. The basic resonator proposed is the quarter wave stepped impedance resonator. The tag utilizes the entire UWB which increases the data encoding capacity. Frequency Shift coding is also applied to increase the efficiency of spectrum usage. Prototype of the tag is fabricated on RT Duroid 5880 ($\epsilon_r = 2.2$, $\tan\delta = 0.0009$) and the measured results are compared with the simulated one. Characteristics of UWB antenna used in the tag are also given in the chapter.

3.1. Introduction

In the literature survey part of the thesis, classification of frequency domain tags based on the presence/absence of transmission and retransmission antenna is mentioned. This chapter is devoted for tags with embedded antennas. The basic data encoding part of this type of tags is the multiresonator circuit connected in between the receiving and retransmitting antennas. The UWB electromagnetic wave transmitted from the reader antenna will be received by the tag's receiving antenna (Rx) which is then guided to the tag's transmitting antenna (Tx) through multiresonator circuits connected to the transmission line. Block diagram of the tag with antennas is shown in figure 3.1.

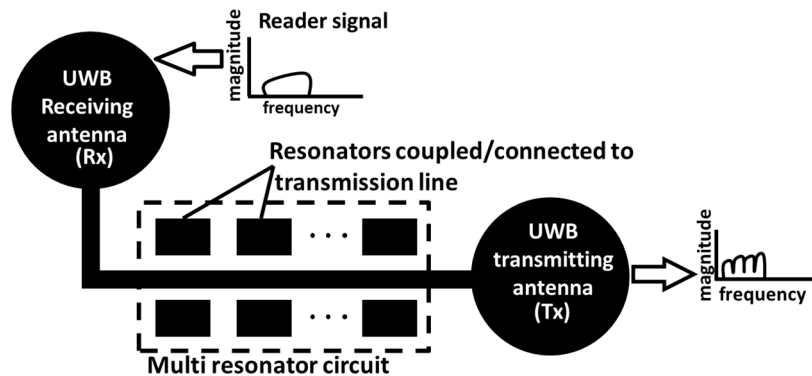


Figure 3.1: Block diagram of Chipless RFID tag with reception and transmission antennas

The multiresonators are either connected or coupled to the transmission line in between the Tx and Rx antennas. The coupled or connected resonators become resonant at their resonant frequencies within the UWB frequencies. The resonators thus absorb the EM energy corresponds to their resonant

frequency to produce a notch in the retransmitted signal. The notch is considered as logic 1 and absence of resonator as logic 0. The absence of the frequency in the output is considered as logic 1 and the reverse case is logic 0 [1]. Apart from this presence or absence of notch, the resonators can be tuned in an assigned band to increase data encoding capacity.

Though the Chipless RFID technology is still in its infancy, a variety of resonators for these tags are available in the literature. High Q compact resonators are preferred for the multiresonator circuits due to increased coupling, increased efficiency in spectrum usage etc. Some of the resonators proposed in the literature are shown in figure 3.2.

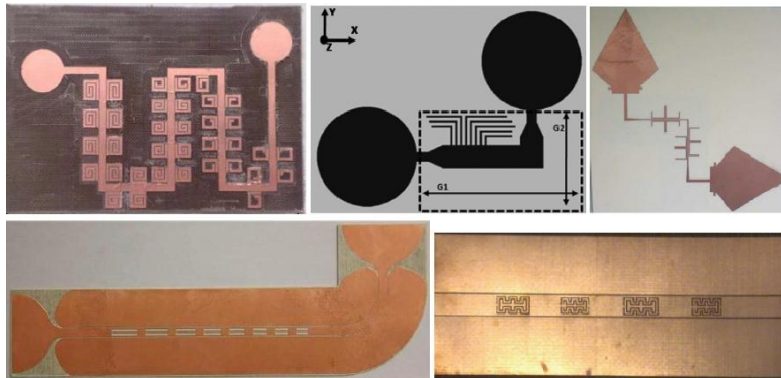


Figure 3.2: Some of the Chipless tags with antennas found in literature
[1], [2], [3], [4], [5]

The resonator proposed in this chapter is microstrip quarter wave stepped impedance resonator. The resonator is very dominant in filter applications due to its unique properties and flexible design. An overview of the stepped impedance resonators is provided in this chapter.

3.2 Data encoding techniques for frequency domain Chipless RFID tags

The two methods commonly employed for data encoding in frequency domain tags are Presence/absence coding and Frequency shift coding. As mentioned in the previous section, the former technique is very simple that the presence or absence of a resonator and hence the respective resonance in the frequency spectrum would be considered as bit 0 or bit 1 and vice versa. The technique has 1:1 correspondence between the number of bits and the number of resonators in the tag. This type of coding is illustrated in figure 3.3. The ease of removal of a resonance without much alteration to the geometry adds an advantage to this coding technique along with the desirable properties like high Q and compact size. The total bit encoding capacity with N resonators is N and can access 2^N items. So the total number of resonators, resonance bandwidth and the available spectrum are the major factors determining the encoding capacity. An increased number of resonators inversely affect the compactness of the tag. With normal resonators, frequency spectrum up to first harmonic frequency (twice the fundamental frequency) of the lowest frequency resonator is the normally available spectrum.

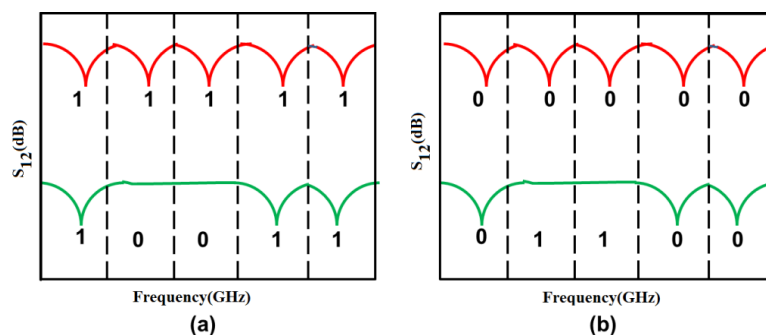


Figure 3.3: Presence/ absence coding technique (a) presence of resonator is bit 1 and absence is bit 0 (b) presence of resonator is bit 0 and absence is bit 1

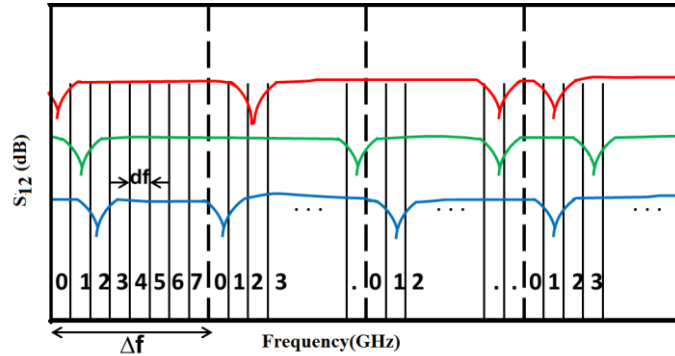


Figure 3.4: Frequency shift coding technique. Entire frequency spectrum is divided into bands of Δf bandwidth which is further divided into bands of df resolution bandwidth. Each df section is assigned a digit

Frequency shift coding technique (illustrated in figure 3.4) is like assigning multiple bits for a single resonator. The entire frequency spectrum would be divided into a number of sub bands (Δf) equal to the number of resonators. Each of these sub bands are again divided into further smaller subbands (df). This second division (df) is dependent on the resonance bandwidth of each resonator. For high Q, narrow bandwidth resonators, df would be even smaller and is known as the resolution bandwidth. Each resolution bandwidth is assigned a digit. Then each resonator is tuned in its allocated bandwidth and takes the digit corresponding to frequency division in which it appears. Δf and df can vary with resonator. Thus the total encoding capacity of frequency shift coding systems is given below.

$$T_b = \log_2 \prod_{i=1}^N \left(\frac{\Delta f_i}{df_i} \right) \dots\dots\dots (3.1)$$

where N is the number of resonators, Δf_i is the bandwidth allotted for ' i^{th} ' resonator and df_i is the resolution bandwidth assigned to the same.

3.3 Stepped Impedance Resonators (SIR) [6]

Stepped impedance resonators are cascaded transmission line of different impedance steps along the length of transmission line. They provide great advantage compared to uniform impedance transmission (UIR) lines like control over harmonic frequencies with compact and high flexibility in design. Evolution of stepped impedance resonator from half wavelength transmission lines is shown in figure 3.5.

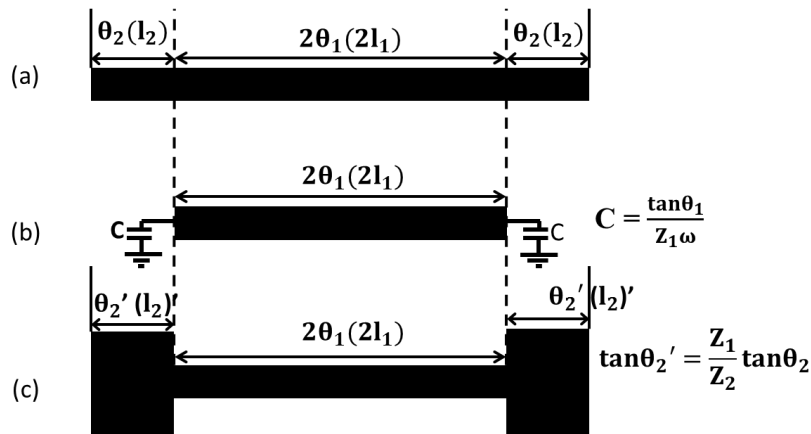


Figure 3.5: Evolution of stepped impedance resonator from uniform impedance resonator

The capacitance loading of UIRs is a common practice in the VHF band to control its harmonic frequencies and to make the structure more compact. Loading capacitance at the open ends of uniform impedance transmission line as shown in figure 3.5(b) is relied to control harmonic frequencies which otherwise appear at the integer multiples of fundamental resonant frequency. The value of capacitor should be $C = \frac{\tan\theta_1}{Z_1\omega}$ where ω is the angular resonant frequency, Z_1 and θ_1 are the characteristic impedance

and angular length corresponding to the physical length l_1 of the UIR shown in figure 3.5(a). This lumped capacitance technique brings size reduction and control over harmonic. However, lumped element capacitor is lossy above 1 GHz.

The same electrical characteristics can be obtained using an open ended transmission line having different impedance, Z_2 . All the three resonators in figure 3.5 will resonate at the same frequency if $Z_1 \tan \theta'_2 = Z_2 \tan \theta_2$ where Z_1 and θ_1 are the characteristic impedance and angular length corresponding to the physical length l_1 and Z_2 and θ_2 are the characteristic impedance and angular length corresponding to the physical length l_2 . Resonator in figure 3.5(c) will be most compact if $Z_2 < Z_1$ and $\theta'_2 < \theta_2$. The stepped impedance transmission line resonators mitigate the losses at high frequency. Compact size with high Q is the major advantage of SIR.

Since the thesis is concentrated on planar Chipless RFID tags, microstrip SIRs have been elaborately discussed in this chapter. The frequency response of half wavelength UIR and the SIR resonating at the same frequency are shown in figure 3.6. The dimensions are detailed in table 3.1. The response is simulated in CST with plane wave excitation. From the table the difference in dimensions of SIR and UIR is obvious. Overall length of the UIR is 26.32 mm whereas that for the SIR is only 7.81 mm. Also the response shows that the SIR provides higher Q than the corresponding UIR.

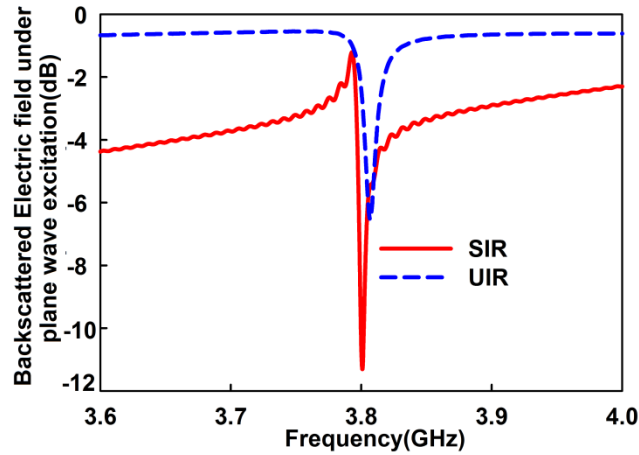


Figure 3.6: Frequency response of UIR and SIR designed at same frequency (dimensions of the structures are given in table 3.1 with respect to figure 3.5)

Table 3.1: Dimensions of UIR and SIR resonating at 3.8 GHz. Substrate height = 1 mm and $\epsilon_r = 2.2$

Structure	Length (mm)		Width (mm)		Overall dimension of the resonator (mm)
UIR	26.32		0.5		26.32
SIR	$l_1 = 5.39$	$l_2 = 2.42$	$w_1 = 0.5$	$w_2 = 5.89$	7.81

3.3.1. Basic Stepped Impedance Resonator

Basic stepped impedance resonator configurations are shown in figure 3.7. They are $\lambda_g/4$, $\lambda_g/2$, λ_g stepped impedance resonators. The angular length (θ_1 and θ_2) and characteristic impedance (Z_1 and Z_2) of the sections corresponding to l_1 and l_2 transmission lines are also shown in the figure 3.7.

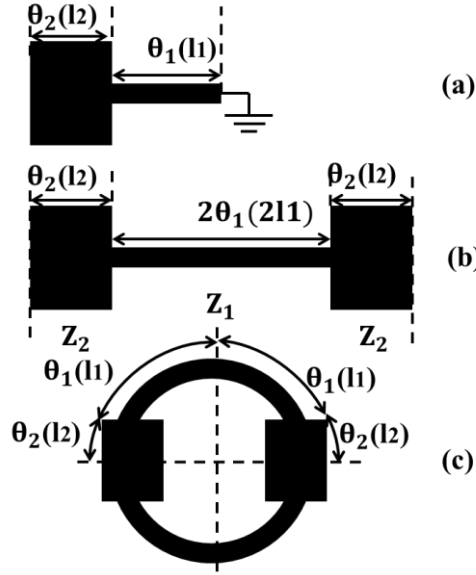


Figure 3.7: Basic SIR Configurations with their design parameters (a) $\lambda_g/4$ (b) $\lambda_g/2$ (c) λ_g

Obviously the basic element of three types of SIRs is a non-uniform transmission line having both open and short circuited ends and a step junction in between. Both $\lambda_g/2$ and λ_g resonators can be viewed as a combination of multiple number of this fundamental $\lambda_g/4$ elements. The division of $\lambda_g/2$ and λ_g into fundamental elements is shown in figure 3.7(b) and (c) by marking l_1 and l_2 . From the figure it is clear that two $\lambda_g/4$ SIRs are joined to form $\lambda_g/2$ resonator and λ_g resonator could be viewed as combination of two $\lambda_g/2$ resonators or as combination of 4 $\lambda_g/4$ resonators. So analysis of the fundamental element ($\lambda_g/4$) is enough to describe the characteristic of both $\lambda_g/2$ and λ_g resonators. Resonant conditions and other important characteristics of the fundamental $\lambda_g/4$ SIR is given in the following sections.

The most important electrical parameter of SIR is termed as impedance ratio (K). It is defined as the ratio of transmission line impedances Z_2 to Z_1 .

$$K = \frac{Z_2}{Z_1} \dots\dots\dots (3.2)$$

3.3.1.1. Resonant condition

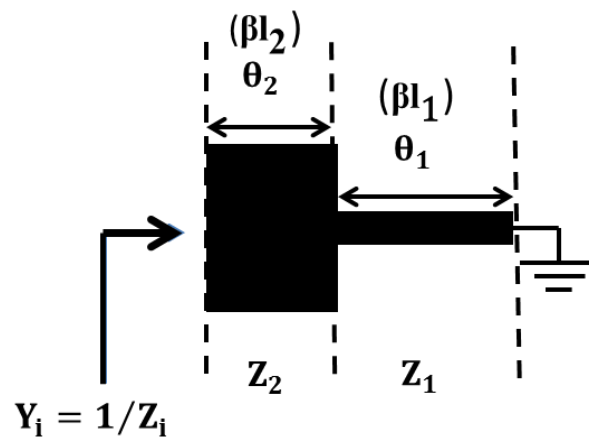


Figure 3.8: $\lambda_g/4$ SIR with all design parameters

Condition for resonance of SIR is addressed in this section. The expression for input impedance (Z_i) of the basic $\lambda_g/4$ SIR shown in figure 3.8 is derived using transmission line theory as given below [6-9].

The input impedance of a lossless transmission line is

$$Z_i = jZ_2 \frac{Z_1 \tan \theta_1 + Z_2 \tan \theta_2}{Z_2 - Z_1 \tan \theta_1 \tan \theta_2} \dots\dots\dots (3.3)$$

By letting input admittance, $Y_i = 0$ the parallel resonant condition is obtained as

$$Z_2 - Z_1 \tan\theta_1 \tan\theta_2 = 0 \dots\dots\dots (3.4)$$

$$\tan\theta_1 \tan\theta_2 = \frac{Z_2}{Z_1} = K \dots\dots\dots (3.5)$$

For the case of uniform impedance resonator, the length of the transmission line determines the condition for resonance. But from the resonance condition of SIR stated above, it is clear that the length and impedance ratio have significant influence on the resonance condition.

Further, the condition for odd and even modes can also be derived separately [10] as

$$K \cdot \cot\theta_2 = \tan\theta_1 \text{ for odd modes}(f_0, fs_2, \dots) \dots\dots\dots (3.6)$$

$$K \cdot \cot\theta_2 = -\cot\theta_1 \text{ for even modes}(fs_1, fs_3, \dots) \dots\dots\dots (3.7)$$

Where $f_0, fs_1, fs_2, fs_3 \dots$ are the fundamental and higher harmonic frequencies. Equations (3.6) and (3.7) are further arranged as equations (3.8) and (3.9), respectively by defining a new term length ratio, α .

$$K \cdot \cot(\alpha \cdot \theta_t) = \tan((1 - \alpha) \cdot \theta_t) \dots\dots\dots (3.8)$$

$$K \cdot \cot(\alpha \cdot \theta_t) = -\cot((1 - \alpha) \cdot \theta_t) \dots\dots\dots (3.9)$$

Where the length ratio, $\alpha = \theta_2 / (\theta_1 + \theta_2)$ and total electrical length $\theta_t = \theta_1 + \theta_2$.

From the above equations, it is obvious that the selection of K and α determines the fundamental and higher harmonic frequencies. Value of θ_t for odd and even modes can be calculated separately by solving transcendental equations (3.8) and (3.9). The resonant modes of SIR can be found using the relation $\frac{f_0}{\theta_t} = \frac{fs_1}{\theta_t}$ where θ_t corresponds to total electrical

length of the respective resonant mode. The effect of step junction at the high impedance and low impedance junction is neglected in the present analysis.

3.3.1.2. Relationship between K , α , fundamental frequency and first harmonic frequency

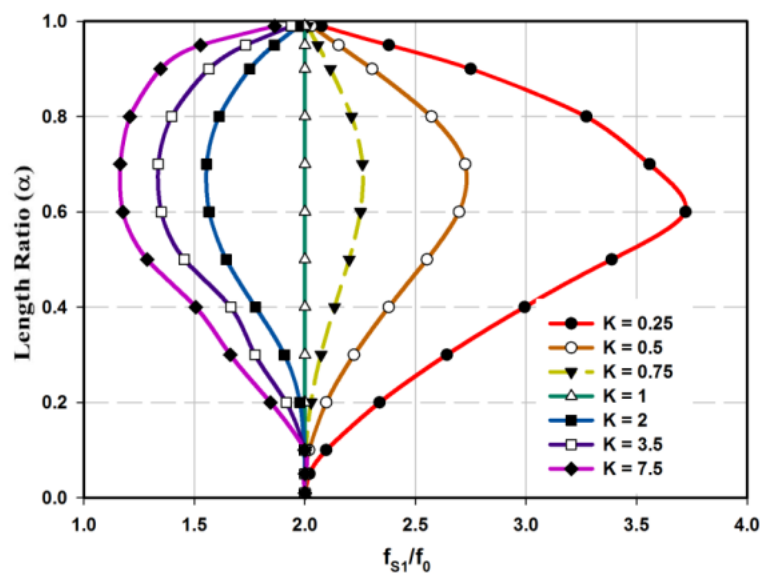


Figure 3.9: Relationship between impedance ratio ($K = Z_2/Z_1$), Length ratio ($\alpha = \theta_2/(\theta_1 + \theta_2)$) and ratio of first harmonic and fundamental frequencies (f_{s1}/f_0) [6]

The relationship between impedance ratio, length ratio and the separation between fundamental and first harmonic frequency is shown in figure 3.9. From the figure, it is clear that the proper selection of impedance and length ratio defines accurately the separation between the fundamental and first harmonic frequency. For Chipless frequency domain RFID tags, the worst problem reported in the literature is the limited frequency spectrum due to the occurrence of first harmonic frequency. This affects the data encoding

capacity badly. By the above mentioned property of SIR, even the entire UWB (3.1 GHz-10.6 GHz) spectrum can be made available for encoding data. For example, if the lowest frequency resonator is designed at 3.2 GHz, the selection of K and α as 0.25 and 0.6, respectively shifts the first harmonic frequency out of UWB ($f_{s1}/f_0 > 4$, beyond 10.6 GHz).

3.3.1.3. Relationship between K and physical size of SIR

As said earlier, the importance of the parameter ‘impedance ratio’ is not just confined in determining the separation between fundamental and higher harmonic frequencies. Selection of K also determines the compactness of the resonator. This is shown in figure 3.10. From the figure, it is noted that the resonator length will be short compared to a conventional UIR for $K < 1$ and long for $K > 1$. The resonator length can be shortened by choosing smaller values of K while the maximum resonator length is limited to twice that of corresponding UIR [6]. Compactness is always a desirable feature for resonators designed for Chipless RFID tags. So $K < 1$ SIR is used for the present study.

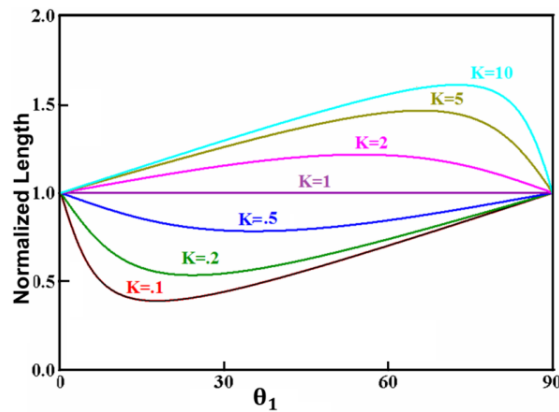


Figure 3.10: Dependence of Impedance ratio on the compactness of resonator [6]

3.4. A single SIR connected to microstrip transmission line

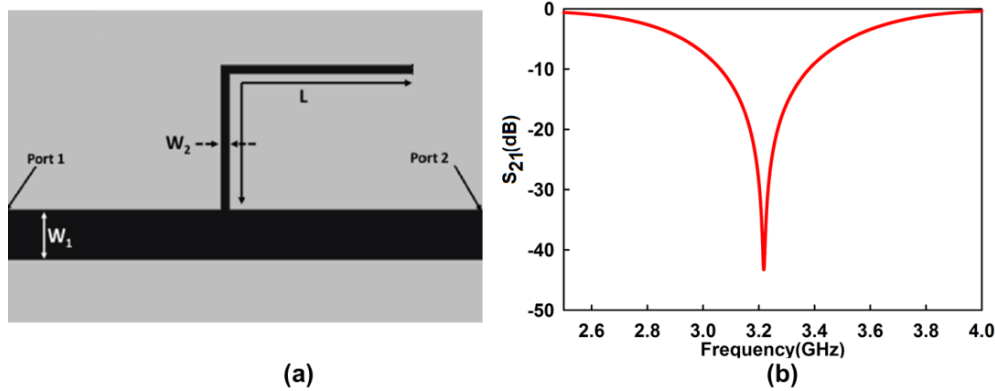


Figure 3.11: (a) Quarter wave resonator connected to transmission line $w_1 = 3.07$ mm, $w_2 = 0.5$ mm, $L = 17.6$ mm, substrate height = 1 mm and $\epsilon_r = 2.2$. (b) Transmission characteristics of the structure shown in figure 3.11(a)

Nijas et al. [2] proposed a spectral signature based tag using quarter wave open stub resonator connected to transmission line. The basic encoding element of the tag and its S_{21} characteristics are shown in figure 3.11(a) and (b), respectively. The Chipless RFID tag presented in this chapter is motivated from this structure with an added advantage of increased spectrum availability with an impedance step in the microstrip resonator. The presented tag uses stepped impedance resonator instead of open stub resonator. As discussed in the previous sections, the flexible design and control over harmonic frequency of this resonator brings a lot of advantage to the design of Chipless RFID tag. Moreover, the resonator length can be made short compared to quarter-wave open stub resonator. A 17.6 mm long open stub resonates at 3.2 GHz whereas a quarter-wave SIR of the same frequency can have greater, smaller or even equal lengths depending on the impedance ratio chosen. Such an SIR which is shorter than

open stub resonating at 3.2 GHz is shown in the following figure and is discussed subsequently.

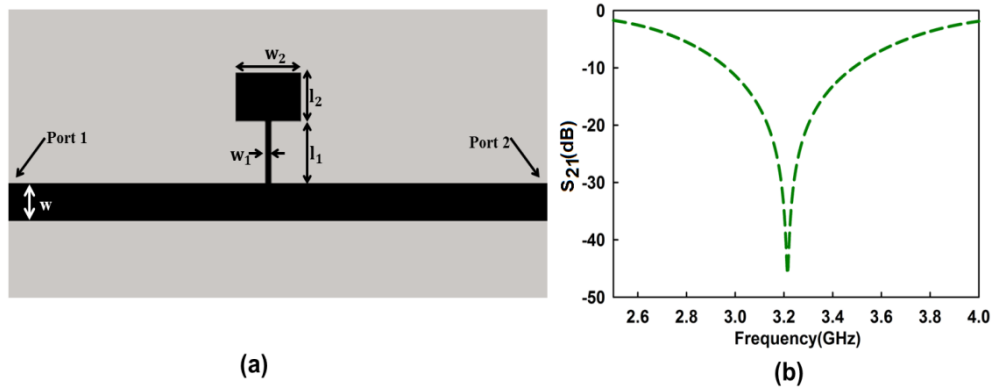


Figure 3.12: (a) A single SIR connected to microstrip transmission line. $W = 3.07$ mm, $w_1 = 0.5$ mm, $w_2 = 5.89$ mm, $l_1 = 4.77$ mm, $l_2 = 3.99$ mm, substrate height = 1 mm, substrate height = 1 mm and $\epsilon_r = 2.2$. (b) Transmission characteristics of the structure

Figure 3.12(a) and (b) shows a single quarter wave SIR connected to transmission line and its transmission characteristics, respectively. The substrate used is RT Duroid 5880 with substrate height 1mm, permittivity 2.2, and $\tan\delta = 0.0009$. The impedance of microstrip line is 50Ω . The SIR dimensions are also shown in figure 3.12. The frequency response of transmission coefficient (S_{21}) over the entire UWB and the surface current distribution are shown in figure 3.13(a) and (b), respectively. From the quarter-wave ($\lambda g/4$) current distribution, the mode of excitation is the fundamental one.

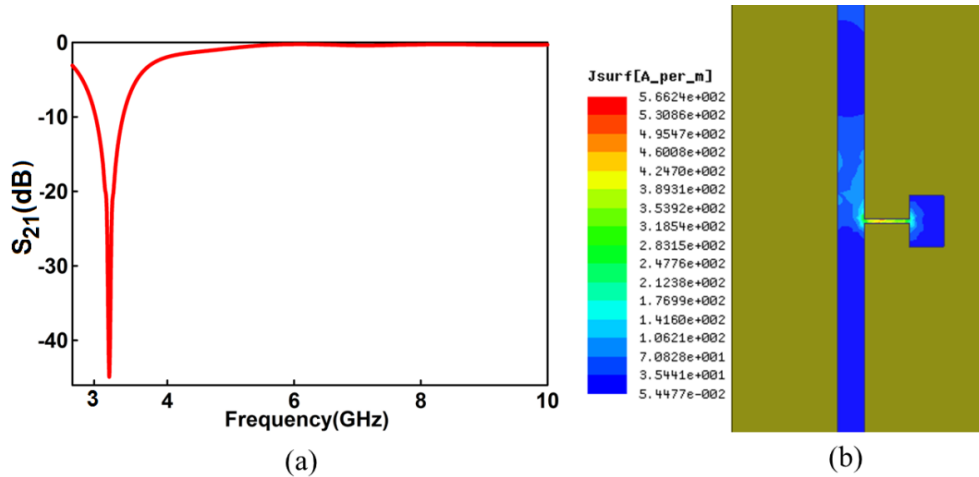


Figure 3.13: (a) Frequency Response and (b) Current distribution on the SIR shown in figure 3.12

The resonator frequency response is given for the entire UWB in figure 3.13(a). The band gap between the first harmonic and the fundamental resonant frequency can be controlled as per the selection of impedance and length ratio. In the above case, the fundamental resonance alone is seen in the frequency band up to 10 GHz. This observation validates the rejection of first harmonic in the entire UWB frequency band. This is the beauty of using SIR as a resonator.

3.4.1. Equivalent circuit of the stepped impedance resonator connected to transmission line

Equivalent circuit of stepped impedance transmission line can be derived by knowing the capacitance and inductance of each section in the microstrip line. Effects of open end fringing and microstrip step are also to be incorporated into the analysis for the accurate calculation of resonant frequency. The distributed resistance of the stepped impedance resonator is taken as zero i.e., stepped impedance resonator is assumed to

be lossless. Equivalent circuit of the microstrip line having an impedance step in between is shown in figure 3.14. L_{s1} , C_{p1} and L_{s2} , C_{p2} are the series inductance and shunt capacitance of the high impedance and low impedance sections of the microstrip line, respectively. L_1 , L_2 and C are the inductances and capacitance incorporated to bring the effect of impedance step. Δc is shunt capacitance due to open end fringing field. Expressions for the unknown inductances and capacitances are given below [11]-[16].

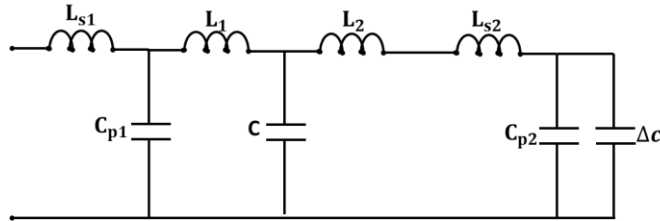


Figure 3.14: Equivalent circuit of a microstrip line having an impedance step between high impedance and low impedance sections

Series inductance and shunt capacitance of a microstrip transmission line (L_{s1} , C_{p1} and L_{s2} , C_{p2}) can be calculated using equations given below [11]

$$Z_0 = \frac{87}{\sqrt{\epsilon_r + 1.41}} \ln \left[\frac{5.98.h}{0.8.W+t} \right] \Omega \dots\dots\dots (3.10)$$

$$C_p = \frac{2.64.10^{-11}(\epsilon_r + 1.41)}{\ln[5.98.h/(0.8.W+t)]} \text{ pF/m} \dots\dots\dots (3.11)$$

$$L_s = c.Z_0^2 \text{ nH/m} \dots\dots\dots (3.12)$$

where ϵ_r , h , W , t are the permittivity, height of substrate, width of microstrip line and thickness of the metal, respectively. Parallel capacitance and series

inductances concerned with a symmetrical impedance step can be computed by [12]

$$C = 0.00137 \cdot h \cdot \frac{\sqrt{\epsilon_{re1}}}{Z_{c1}} \left(1 - \frac{W_2}{W_1}\right) \left(\frac{\epsilon_{re1}+0.3}{\epsilon_{re1}-0.258}\right) \left(\frac{W_1/h+0.264}{W_1/h+0.8}\right) \text{ (pF) .. (3.13)}$$

$$L_1 = \frac{L_{W1}}{L_{W1}+L_{W2}} L, \quad L_2 = \frac{L_{W2}}{L_{W1}+L_{W2}} L \dots\dots\dots (3.14)$$

where $L_{Wi} = Z_{ci} \sqrt{\epsilon_{rei}}/c$, $L = 0.000987 \cdot h \cdot \left(1 - \frac{Z_{c1}}{Z_{c2}} \sqrt{\frac{\epsilon_{re1}}{\epsilon_{re2}}}\right)^2$ (nH)

Where L_{Wi} for $i= 1, 2$ are the inductances per unit length, Z_{ci} and ϵ_{rei} denote the characteristic impedance and effective dielectric constant corresponding to width W_i for $i= 1, 2$. c is the velocity of light in free space, and h is the substrate thickness.

Capacitance associated with open end fringing effects of microstrip line is given by [13]

$\Delta c = \frac{\Delta l \sqrt{\epsilon_{re}}}{c Z_c}$ where Δl is the extended length due to fringing field and is given by

$$\frac{\Delta l}{h} = \frac{\xi_1 \xi_2 \xi_3}{\xi_4} \dots\dots\dots (3.14)$$

where $\xi_1 = 0.434907 \frac{\epsilon_{re}^{0.81+0.26(W/h)^{0.8544}+0.236}}{\epsilon_{re}^{0.81+0.189(W/h)^{0.8544}+0.87}}$

$$\xi_2 = 1 + \frac{(W/h)^{0.371}}{2.35\epsilon_r + 1}$$

$$\xi_3 = 1 + \frac{0.527 \tan^{-1}[0.084(W/h)^{1.9413/\xi_2}]}{\epsilon_{re}^{0.9236}}$$

$$\xi_4 = 1 + 0.037 \tan^{-1}[0.067(W/h)^{1.456}]\{6 - 5 \exp[0.036(1 - \epsilon_r)]\}$$

$$\xi_5 = 1 - 0.218\exp(-7.5W/h)$$

where ϵ_{re} is the effective dielectric constant of microstrip line.

The calculated values of inductances and capacitances of stepped impedance resonator are detailed in Table 3.2.

Table 3.2: Calculated values of inductances and capacitances of equivalent circuit for an SIR having $w_1 = 0.5$ mm, $w_2 = 5.89$ mm, $l_1 = 4.77$ mm, $l_2 = 3.99$ mm, substrate height = 1 mm and $\epsilon_r = 2.2$

L_{s2} (pF)	0.046
C_{p2} (nH)	0.412
L_1 (nH)	0.866
C (pF)	0.686
L_2 (nH)	0.127
L_{s1} (pF)	1.043
C_{p1} (nH)	0.704
Δc (pF)	0.014

The lumped element equivalent circuit of stepped impedance resonator with 50Ω transmission line is modelled in Agilent ADS software with values given in table 3.2. The frequency response obtained in ADS is validated with HFSS simulation. The equivalent circuit designed in ADS software connected across the 50Ω transmission line is shown in figure 3.15. Comparison of frequency response between equivalent circuit and 3D numerical result is shown in figure 3.16. Equivalent circuit response shows good agreement with numerical results.

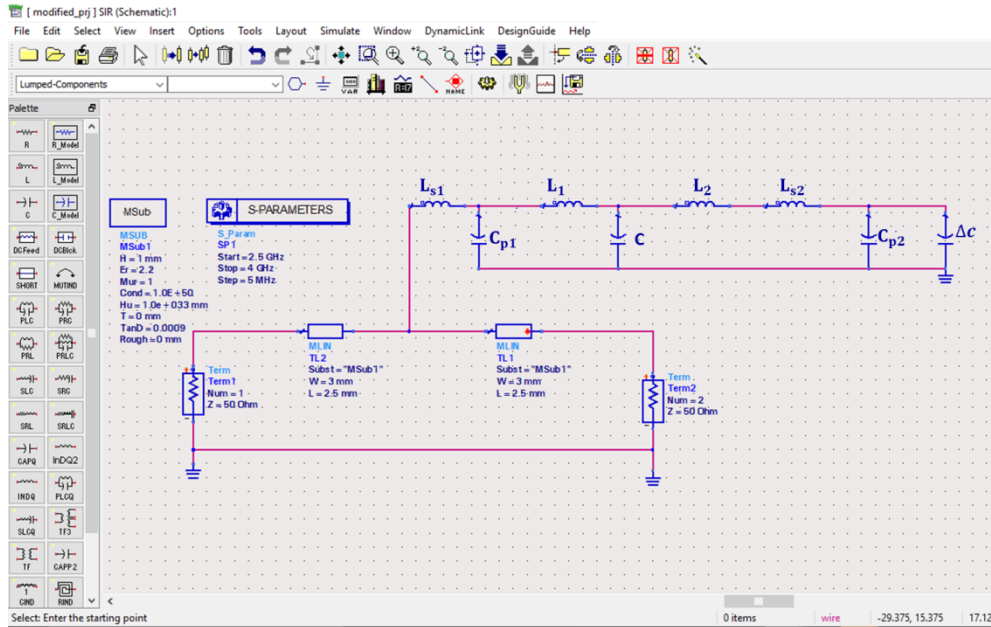


Figure 3.15: Equivalent circuit of SIR connected to 50Ω transmission line (Figure 3.12; $w_1 = 0.5$ mm, $w_2 = 5.89$ mm, $l_1 = 4.77$ mm, $l_2 = 3.99$ mm, substrate height = 1mm and $\epsilon_r = 2.2$) modelled in ADS software. Inductance and capacitance values are detailed in Table 3.2

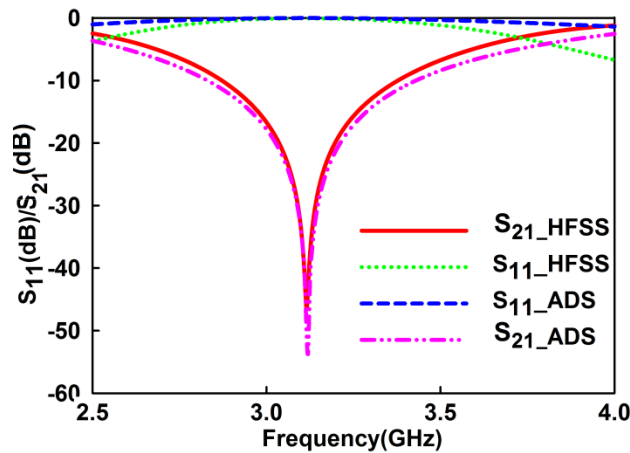


Figure 3.16: Comparison of frequency response obtained for ADS software and HFSS

3.4.2. Selection of Substrate for the tag

The performance of the tag on different substrates is studied by designing a resonator at 3.2 GHz connected to microstrip transmission line. The substrates used are tabulated in table 3.3 along with their dielectric constant, loss tangent and thickness.

Table 3.3: Different substrates used for study with their properties

Substrate	Dielectric constant	Loss tangent	Substrate Height(mm)
CMET_4.3(*)	4.3	0.0018	1.6
CMET_6.5(*)	6.5	0.002	1
FR4 EPOXY	4.4	0.025	1
RT DUROID	2.2	0.0009	1

(*Substrates indigenously developed by Center for Materials for Electronics Technology (CMET), Thrissur, Kerala, India.)

Dimensions of resonators on different substrates are given in table 3.4. High Q resonances (narrow resonances) are observed for low loss substrates ($\ll \tan\delta$) [16]. A high permittivity substrate offers a more compact resonator [16]. Also, loss tangent of a dielectric is inversely related to the permittivity.

Table 3.4: Resonator and microstrip transmission line dimensions on different substrates detailed in Table 3.3

Substrate	Txn line width, W(mm)	l_1 (mm)	l_2 (mm)	w_1 (mm)	w_2 (mm)
CMET_4.3	3.07	2.72	3.51	0.5	7.45
CMET_6.5	1.4	3.07	2.35	0.5	5.65
FR4 EPOXY	1.91	3.65	2.87	0.5	5.75
RT DUROID	3.07	4.77	3.99	0.5	5.89

Experimental transmission coefficients for the circuit designed on different substrates are shown in figure 3.17 and the observed characteristics are given in the table 3.5. From the results it is clear that the lossy FR4 provides the smallest Q[22] and the low loss RT Duroid 5880 shows the highest Q. CMET_6.5 provides the most compact resonator dimensions (Table 3.4) owing to its high dielectric constant with a Q factor of 215.82. As mentioned earlier, high Q resonators are most desirable as the number of bits that could be encoded per frequency spectrum can be maximized with them. Also, resonators with high Q increase the time of existence of resonance, ease identification in noisy surroundings and provides better reading ranges. In this context, considering the best spectrum utilization and better reading ranges offered by high Q resonators, RT Duroid 5880 is selected for the tag design.

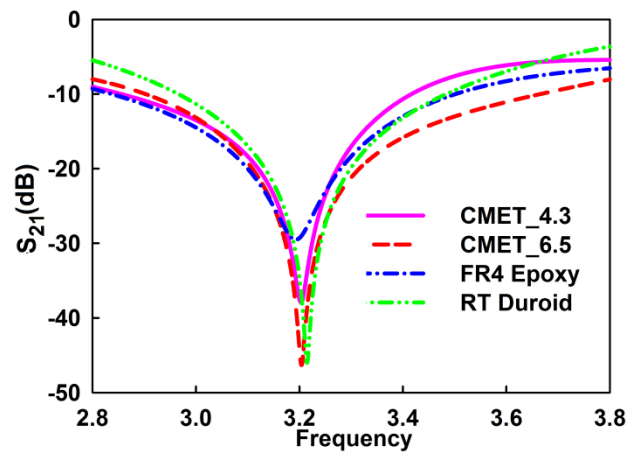


Figure 3.17: Performance of resonator designed at 3.2 GHz on different substrates. Dimensions are detailed in table 3.4

Table 3.5: Observed Q factor and resonant depth with different substrates (with respect to table 3.3 and table 3.4)

Substrate	Q factor [22]	Resonant depth(dB)
CMET_4.3	169.46	-37.93
CMET_6.5	215.82	-45.99
FR4 EPOXY	52.005	-29.52
RT DUROID	376.79	-45.89

3.4.3. Optimization of the microstrip resonator and transmission line resonator

For making the structure more compact, $K < 1$ SIR is selected for the tag design. For the design of the resonators, the width of l_1 (w_1) is fixed at 0.5 mm. This width is seen as optimum for compact design. Optimization study of the width w_1 is tabulated in table 3.6. When w_1 is less than 0.5 mm, value of w_2 is very near to w_1 . This makes it difficult to realize the step junction in our inhouse etching setup. From table 3.6, it is also noted that very low values of w_1 result in longer l_1 and l_2 . That is for $w_1 = 0.2$ mm ($K = 0.4$ and $\alpha = 0.4$) the overall length of the resonator is 8.6 mm while that for $w_1 = 1$ mm the resonator length is 8 mm. Another observation from the table is that increment in w_1 results increment in w_2 . It can be justified by examining the values of w_2 for $w_1 = 0.2$ mm and 1 mm given in table 3.6. Here, w_2 is 2.05 mm and 4.65 mm for the 0.2 mm and 1 mm case, respectively. Though this increment in width reduces the overall length of the resonator, compactness will not be achieved due to the increment in w_2 . These observations are true for different values of length ratio and are given in table 3.6. As a compromise, w_1 is fixed at 0.5 mm.

As stated earlier, value of K and α are selected according to the required separation between fundamental and first harmonic frequency, keeping in mind the compactness of the structure.

Table 3.6: Optimization of width w_1 of an SIR designed at 4.1 GHz and $K = 0.4$, substrate height = 1 mm and $\epsilon_r = 2.2$

$w_1(\text{mm})$	$w_2(\text{mm})$	$\alpha = 0.4$		$\alpha = 0.5$		$\alpha = 0.6$	
		$l_1(\text{mm})$	$l_2(\text{mm})$	$l_1(\text{mm})$	$l_2(\text{mm})$	$l_1(\text{mm})$	$l_2(\text{mm})$
0.2	2.05	5.18	3.41	4.10	4.34	3.12	5.37
0.3	2.45	5.14	3.35	4.06	4.27	3.09	5.30
0.4	2.8	5.11	3.30	4.04	4.21	3.08	5.24
0.5	3.13	5.09	3.25	4.02	4.16	3.06	5.18
0.6	3.5	5.07	3.19	4.00	4.10	3.04	5.12
0.8	4.07	5.03	3.11	3.97	4.01	3.02	5.02
0.9	4.38	5.01	3.06	3.96	3.97	3.00	4.97
1.0	4.65	5.00	3.02	3.94	3.93	2.99	4.93

Width of transmission line is varied to study its effect on resonance. The results are shown in figure 3.18. Of course, the frequency shifts downwards with increment in width owing to the overall increment in size. There is slight decrease in 10 dB fractional bandwidth of resonances as the width of transmission line increases where the fractional bandwidth is calculated as $((\Delta f/f_0)*100)$. Change in fractional bandwidth for different transmission line width is shown in table 3.7. For an SIR connected to transmission line, this change is not as substantial as for the open stub resonator [2] connected to transmission line (for open stub resonator FBW changes from 39.42% to 12.57% for widths from 2 mm to 7 mm). Also, increased width of the transmission line reduces the compactness of the tag.

Impedance transformers are also needed to match with the antenna feed lines. So it is decided to design uniform width transmission line of 50Ω (3.071 mm).

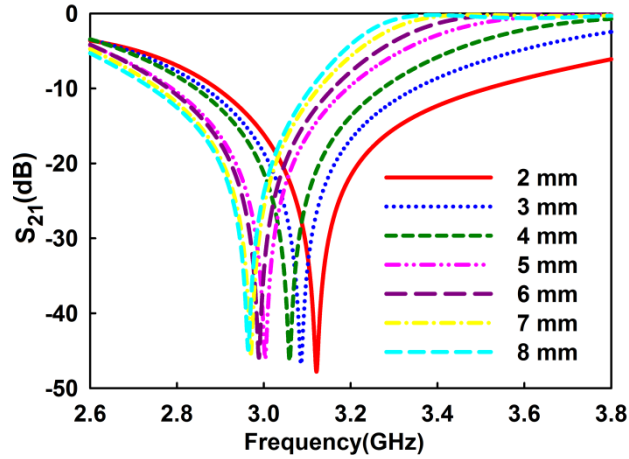


Figure 3.18: Response of transmission for different width (W) of transmission line. SIR dimensions: $l_1 = 5.27$ mm, $l_2 = 3.99$ mm, $w_1 = 0.5$ mm, $w_2 = 5.89$, substrate height = 1 mm and $\epsilon_r = 2.2$.

Table 3.7: Change in fractional bandwidth (FBW) for transmission line width (W) variation. SIR dimensions: $l_1 = 5.27$ mm, $l_2 = 3.99$ mm, $w_1 = 0.5$ mm, $w_2 = 5.89$, substrate height = 1 mm and $\epsilon_r = 2.2$

Width (mm)	FBW (%)
2	19.90
3	15.65
4	13.97
5	13.40
6	12.64
7	12.37
8	12.30

3.5. Multiresonator circuit design using SIR

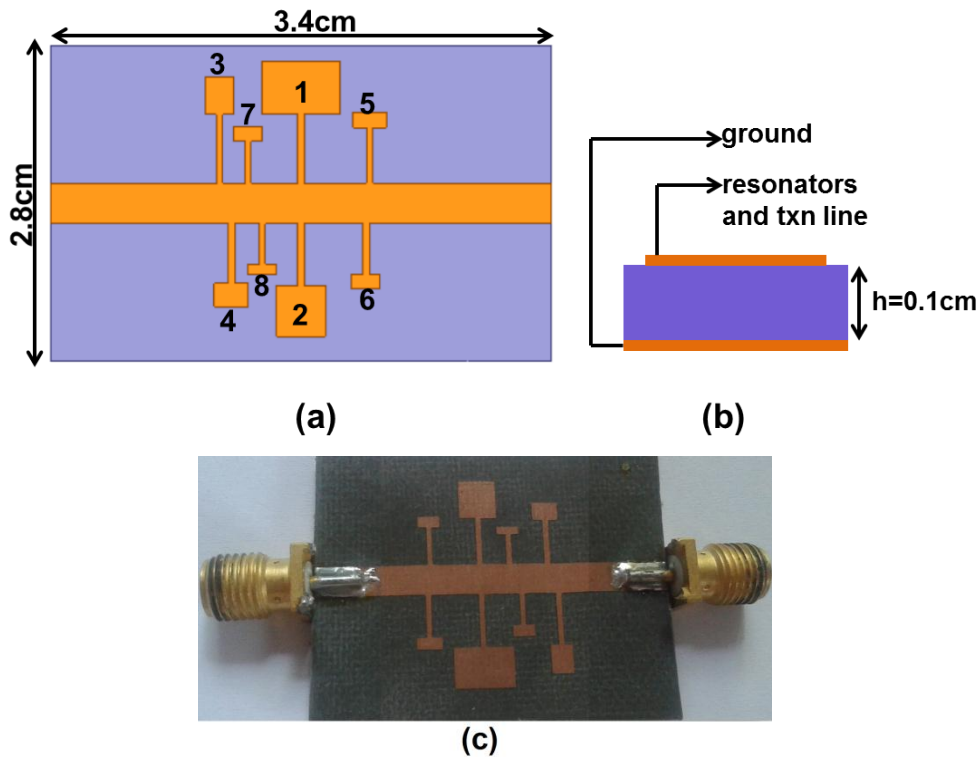


Figure 3.19: (a) Geometry of Multiresonator circuit having 8 SIRs connected to 50Ω microstrip line. (b) Side view. (c) Fabricated prototype. Dimensions are detailed in table 3.8.

Figure 3.19 shows the multiresonator circuit designed for the Chipless RFID tag. The circuit contains 8 resonators connected to transmission line. The resonators are positioned in the transmission line so that adjacent frequency resonators are separated. This arrangement does minimize the coupling between adjacent frequencies and is demonstrated in figures 3.20 - 3.21.

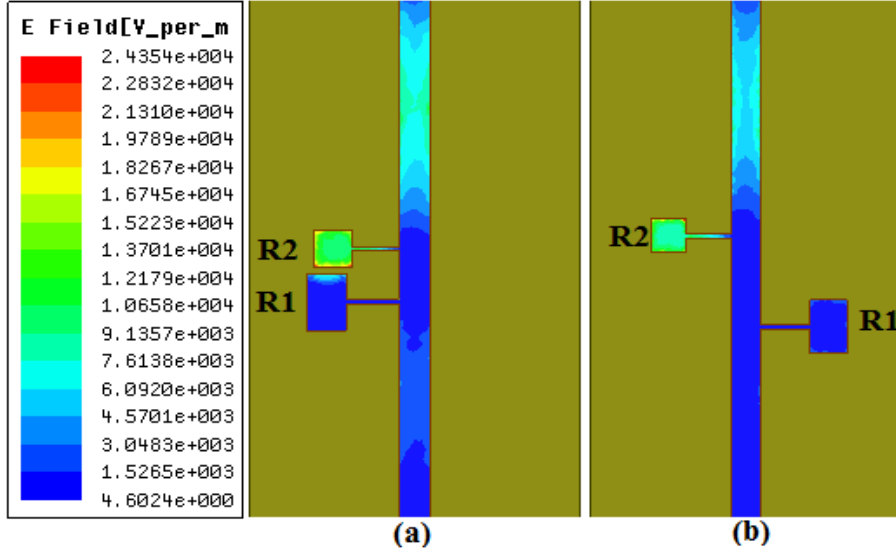


Figure 3.20: Electric field distribution at 3.8 GHz for two different arrangements of adjacent frequency resonators (a) adjacent frequency resonators positioned nearby (b) adjacent frequency resonators positioned apart. R1 is designed at 3.2 GHz ($K = 0.25$, $\alpha = 0.5$, $l_1 = 5.29$ mm, $l_2 = 3.99$ mm, $w_1 = 0.5$ mm, $w_2 = 5.89$ mm) and R2 at 3.8 GHz ($K = 0.25$, $\alpha = 0.4$, $l_1 = 5.4$ mm, $l_2 = 2.42$ mm, $w_1 = 0.5$ mm, $w_2 = 5.89$ mm). Substrate height = 1 mm, $\epsilon_r = 2.2$

R1 and R2 represent two resonators operating at 3.2 GHz and 3.8 GHz, respectively. Their individual frequencies and the shift in frequencies according to the positioning are shown in figure 3.21. From figure 3.21, it is clear that better isolation is ensured when the adjacent frequency resonators are placed apart. For that case, resonances experience minimum shift in frequency. The reason would be clear after examining the electric field distribution at one of the resonant frequency, say 3.8 GHz. When the resonators are nearby electric field coupling between them is obviously higher than the other case and if frequencies are too close there is chance of merging of resonances into one. So for the tag design, resonators need to be placed such a way that no adjacent frequency resonators came nearby.

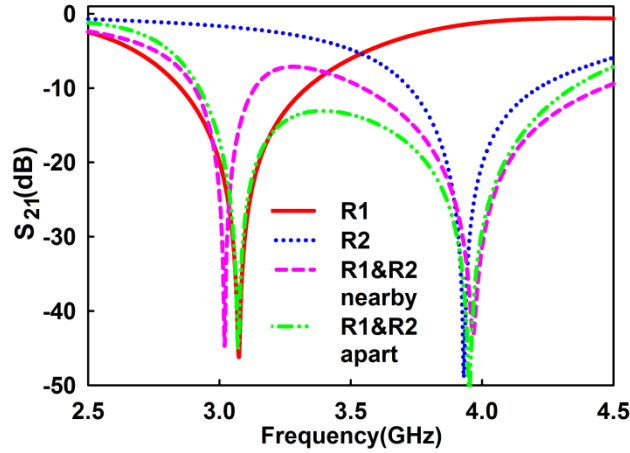


Figure 3.21: Frequency response of two adjacent frequency resonators R1 and R2 for different arrangements with respect to figure 3.20

The dimensions and other design parameters of stepped impedance resonators are given in table 3.8. K and α value are different for each resonator according to the separation needed between the fundamental and first harmonic frequency.

Table 3.8: Parameters of SIRs connected to microstrip line in figure 3.19. Substrate height =1 mm, $\epsilon_r = 2.2$

Parameters	Resonators							
	I	II	III	IV	V	VI	VII	VIII
K	0.25	0.35	0.5	0.45	0.45	0.5	0.5	0.5
α	0.5	0.5	0.4	0.35	0.3	0.3	0.35	0.3
l_1 (mm)	5.27	4.74	5.2	4.52	4.22	3.85	3.18	3.08
l_2 (mm)	3.99	3.81	2.83	1.78	1.18	1.08	1.13	0.754
w_1 (mm)	0.5	0.5	0.5	0.5	0.5	0.5	.5	0.5
w_2 (mm)	5.89	3.73	2.16	2.56	2.56	2.16	2.16	2.16

The simulated and measured S_{21} without transmitting and receiving antennas for an eight bit tag are shown in figure 3.22. For this case, the multiresonator circuit is directly connected to ports through probes. The only noise present will be due to the mismatch and losses of probes connected.

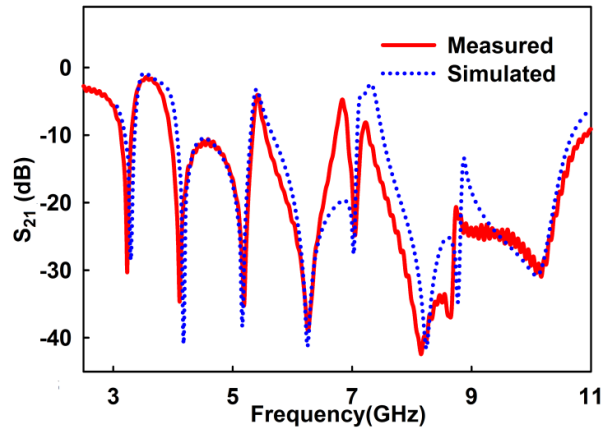


Figure 3.22: Measured and simulated frequency response of the multi resonator circuit of the eight bit tag shown in figure 3.19

The S_{21} plot shows 8 resonances over the band from 3.1 GHz to 10.6 GHz. All the resonators are present in the tag and the shown S_{21} represents an all bit ‘on’ combination. Slight shift in the resonance frequencies can be due to the slight coupling of multiple resonators. The resonances can be tuned for another combination either by the presence/absence technique or by the frequency shift coding. From the figure 3.22, it can be noted that the resonances are wider and hence the determination of resolution bandwidth for each resonance is difficult in case of frequency shift coding technique. For this reason, the presence/absence technique is preferred for the tag design. For removing a resonance from the spectrum, the corresponding resonator is simply disconnected from the transmission line. The resulting

$\lambda/4$ SIR will always get excited at its first harmonic frequency which is out of the used spectrum (to excite in the fundamental mode either a short circuit or a connection to the microstrip line is needed). The different coding combinations in tag geometry are shown in figure 3.23. Corresponding Spectral signatures are shown in figure 3.24.

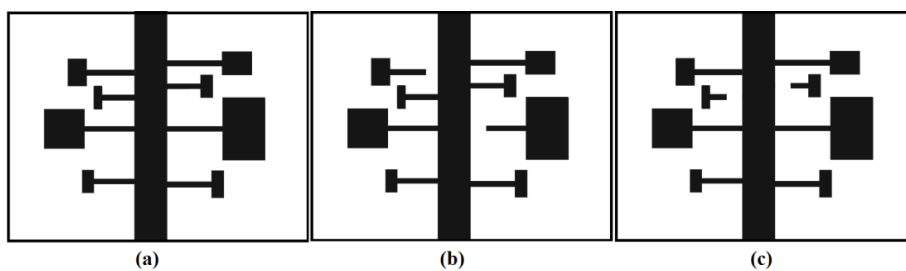


Figure 3.23: Geometries for different codes using presence/absence technique (a) 11111111 (b) 01101111 (c) 11111100. Dimensions of the resonators are same as figure 3.19 and detailed in table 3.8

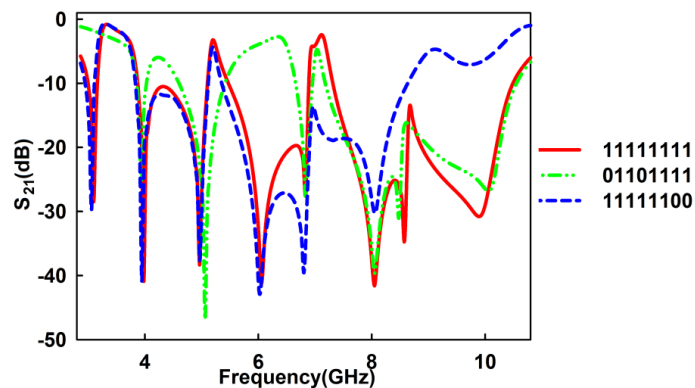


Figure 3.24: Spectral signature for different codes encoded by the geometries of figure 3.23

At the higher end of UWB, the resonances become feeble in appearance and are difficult to identify in a noisy environment. These feeble resonances at the higher frequency end of the UWB can be justified by the inherent losses and dispersion of microstrip structures with increasing frequency [12].

With the SIRs connected to the microstrip line, it is not possible to utilize the full advantages of design flexibility owned by the Stepped Impedance resonators. Also the efficiency in spectrum utilization is at its minimum due to the inability to use frequency shift coding technique. This can be improved by another configuration with the same $\lambda/4$ SIRs. The new configuration is constituted by a set of SIRs coupled rather than connected to the microstrip transmission line. The advantage of the modified structure is demonstrated in the following section.

3.6. Modified Chipless RFID tag with SIR coupled to transmission line

The geometry of the multiresonator circuit is modified for better performance. The resonators are coupled to the transmission line rather than directly connected to it as shown in figure 3.25.

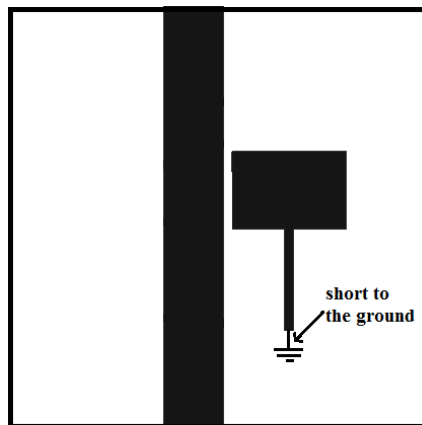


Figure 3.25: Quarter wave SIR coupled to 50Ω transmission line. SIR dimensions: $l_1 = 4.27$ mm, $l_2 = 3.99$ mm, $w_1 = 0.5$ mm, $w_2 = 5.89$, height = 1 mm, $W = 3.071$ mm, substrate height = 1 mm, $\epsilon_r = 2.2$

The high Q nature of stepped impedance resonators provides good coupling with the line. The spectral signature of such a configuration shows a much better resonance than a connected resonator at the same frequency. A comparison of frequency response of SIR connected and coupled to transmission line is shown in figure 3.26.

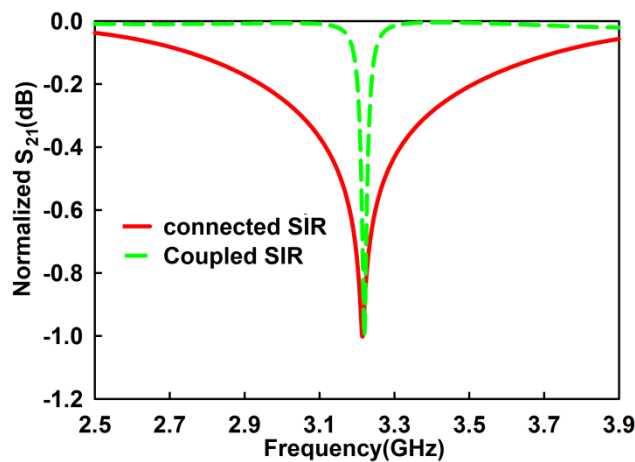


Figure 3.26: A comparison of frequency response of SIR connected and coupled to transmission line, SIR dimensions: $l_1 = 4.27$ mm, $l_2 = 3.99$ mm, $w_1 = 0.5$ mm, $w_2 = 5.89$, height = 1 mm, $W = 3.071$ mm

The resonance bandwidth is narrower for coupled SIR though the dip of resonance is lesser. The 10 dB fractional bandwidth for coupled and connected SIR is 0.28% and 14.85%, respectively. Calculated Q is also large for the coupled case and is 436.25 while that for connected is 376.79. As stated previously narrow bandwidth resonance is an important factor which have direct relation to bit encoding capacity per spectrum of frequency domain Chipless RFID tags and high Q enables better detection in noisy environment.

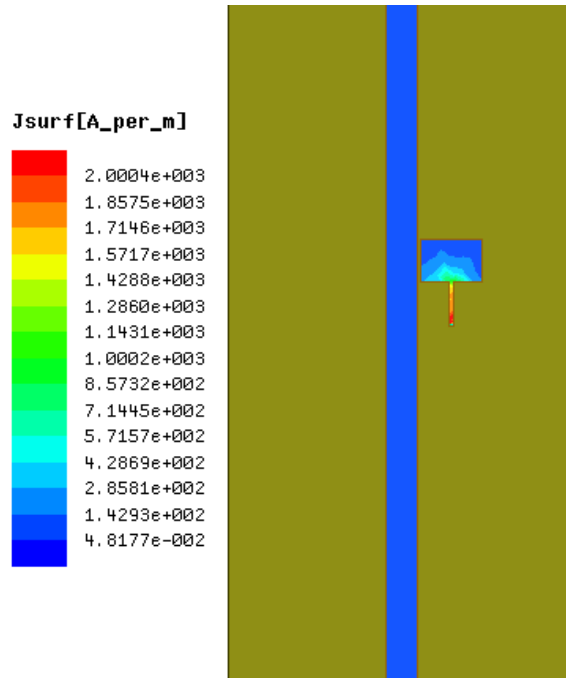


Figure 3.27(a): Current distribution on SIR coupled to microstrip line at its resonant frequency, SIR dimensions: $l_1 = 4.27$ mm, $l_2 = 3.99$ mm, $w_1 = 0.5$ mm, $w_2 = 5.89$, height = 1 mm, $W = 3.071$ mm, substrate height = 1 mm, $\epsilon_r = 2.2$

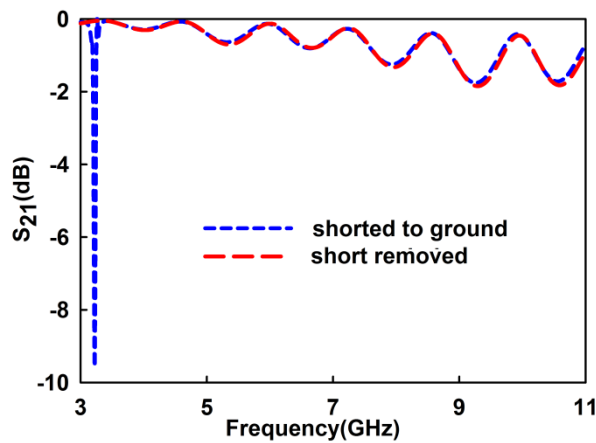


Figure 4.27(b): Effect of removal of short to ground at the high impedance end of SIR when it is coupled to microstrip transmission line (with respect to Figure 4.27(a)).

Current distribution on the resonator at its resonance frequency is shown in figure 3.27(a). The resonator is excited at its fundamental mode and the distribution is quarter wave. Removing the short circuit to ground prevents the fundamental mode from appearing in the used spectrum (Shown in figure 3.27(b)). Without the short, the lowest frequency that is appearing would be the first harmonic frequency which is set beyond the spectrum of interest. This adds another advantage of easy coding. The resonance can be removed simply by removing the short to ground in case of employing presence/absence coding technique. Frequency shift coding is also suitable for this type of tag considering the reduced bandwidth and flexible design of the resonator.

3.6.1. Effect of coupling gap between transmission line

The gap between transmission line and the resonator is optimized observing the performance for different gaps between two. The results are shown in figure 3.28.

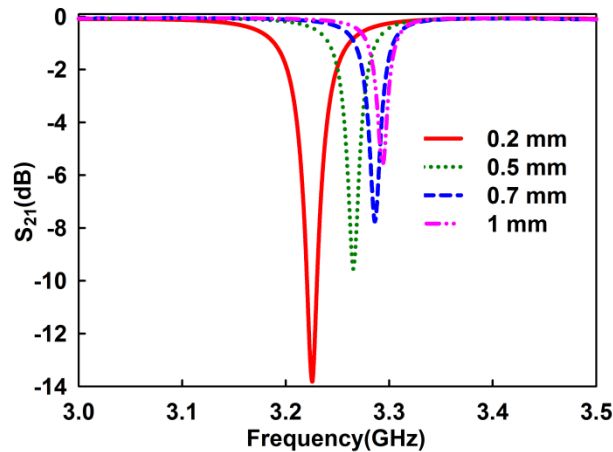


Figure 3.28: Parametric study on different coupling distance between microstrip line and SIR, SIR dimensions: $l_1 = 4.27$ mm, $l_2 = 3.99$ mm, $w_1 = 0.5$ mm, $w_2 = 5.89$ mm, height = 1 mm, $W = 3.071$ mm, substrate height = 1 mm, $\epsilon_r = 2.2$

Table 3.9: Variation in fractional bandwidth and resonant dip for different gap between microstrip line and SIR, with respect to figure 3.28

Gap (mm)	FBW %	Resonance dip (dB)	Q factor
0.2	1.1	-13.79	436.54
0.5	0.67	-9.53	412.25
0.7	0.54	-7.75	367.15
1	0.36	-5.38	311.73

As expected, it is clear from the figure that the attenuation is greater for minimum separation due to the strong coupling of the resonator to the microstrip line. The variations in 10 dB fractional bandwidth and resonant depth for different gaps are tabulated in table 3.9. It is observed that the fractional bandwidth is minimum for larger separation but depth of resonance is decreasing drastically even for small increment in the gap value. This decrease is also observed with the Q values for the gaps from 0.2 mm to 1 mm as given in table 3.9 and is from 436.54 to 311.73. So a separation of 0.2 mm satisfying high attenuation and high Q is selected for the tag design which is more compact also.

3.6.2. Distance between neighboring SIRs

The distance between SIRs is selected to avoid coupling effects between them. The study on distance between two SIRs, SIR1 and SIR 2 designed at 3.2 GHz and 4.1 GHz, respectively is shown in figure 3.29. The figure shows performance of individual resonators when they are present alone. Small separation may lead to couplings resulting in shift in resonances as can be seen for the case of 0.2 mm. Separations greater than 0.3 mm offer minimum coupling effects. So care is taken to provide a separation greater than 0.3 mm.

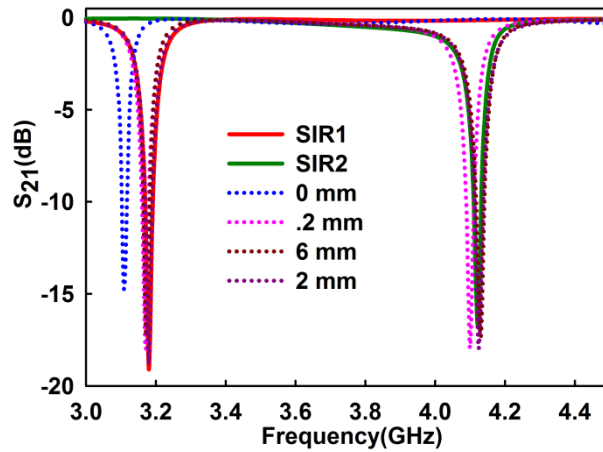


Figure 3.29: parametric study on distance between two adjacent resonators coupled to microstrip line. $W = 3.071$ mm, height = 1 mm $\epsilon_r = 2.2$. SIR1 dimensions: $l_1 = 4.27$ mm, $l_2 = 3.99$ mm, $w_1 = 0.5$ mm, $w_2 = 5.89$, SIR2 dimensions: $l_1 = 4.74$ mm, $l_2 = 3.81$ mm, $w_1 = 0.5$ mm, $w_2 = 3.73$ mm.

3.6.3. The multiresonator circuit design using SIRs coupled to microstrip line

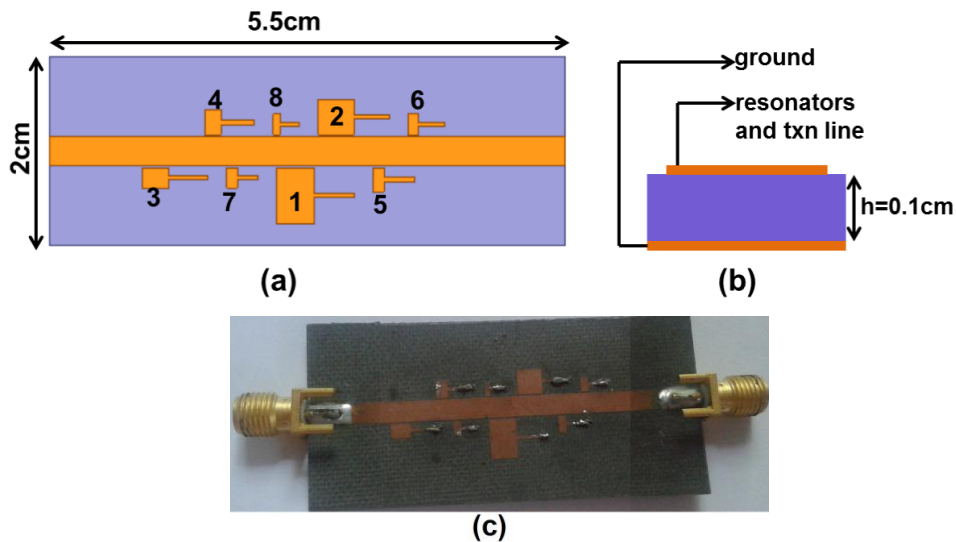


Figure 3.30: Multiresonator circuit with SIRs coupled to microstrip line (SIR dimensions are given in Table 3.10). Microstrip transmission line width = 3.071 mm, substrate height = 1 mm, $\epsilon_r = 2.2$ mm

Table 3.10: Parameters of SIRs of the multiresonator circuit shown in figure 3.30

Parameters	Resonators							
	I	II	III	IV	V	VI	VII	VIII
F(GHz)	3.2	4.1	5.2	6.3	7.4	8.4	9.3	10.5
K	0.25	0.35	0.5	0.45	0.45	0.5	0.5	0.5
α	0.5	0.5	0.4	0.35	0.3	0.3	0.35	0.3
l_1 (mm)	4.27	3.74	4.2	3.52	3.22	3.28	2.58	2.52
l_2 (mm)	3.99	3.81	2.83	1.78	1.18	1.08	1.13	0.754
w_1 (mm)	0.5	0.5	0.5	0.5	0.5	0.5	0.5	0.5
w_2 (mm)	5.89	3.73	2.16	2.56	2.56	2.16	2.16	2.16

The geometry of the multiresonator circuit with eight SIRs coupled to microstrip transmission line is shown in figure 3.30. The dimensions of SIRs are given in table 3.10. The measured S_{21} of the multiresonator circuit is shown in figure 3.31. The simulated S_{21} is also shown for comparison. For the all eight resonators present in the geometry, eight resonances can be seen in the spectrum. Minimum coupling effects due to multiple resonators are anticipated in the tag performance due to the positioning of resonators. The coupling effects between multiple resonators and that between the adjacent frequency resonators however present and result in slight shift in resonant frequency.

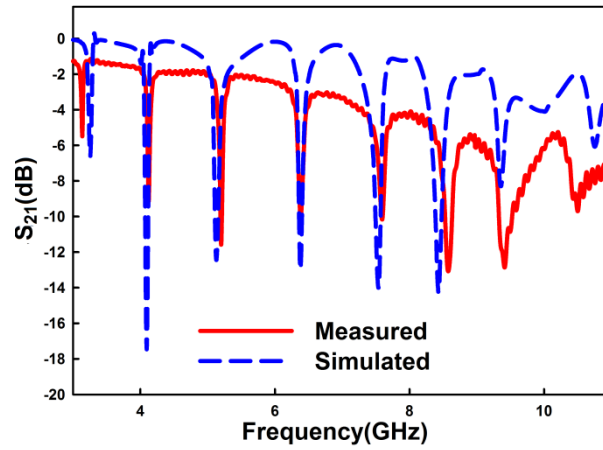


Figure 3.31: Measured and simulated S_{21} of the multiresonator circuit (figure 3.30)

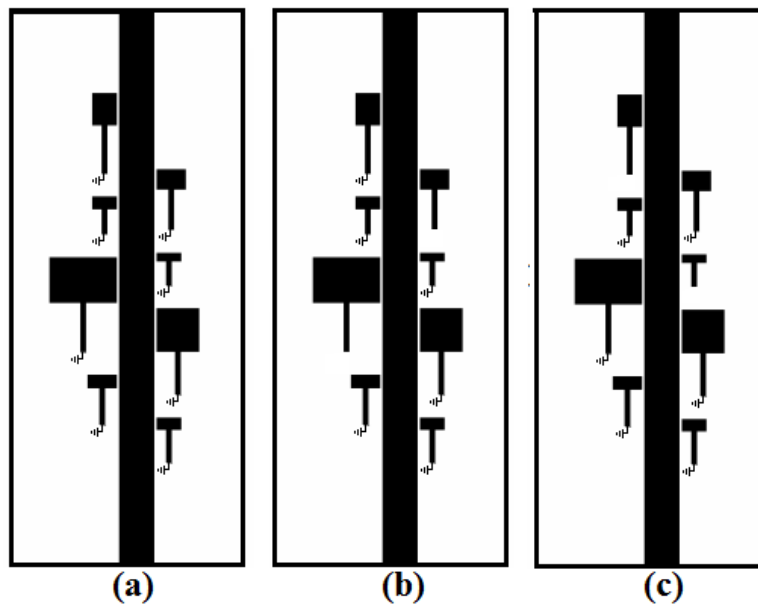


Figure 3.32: Different coding combinations for presence/absence coding technique (a) 1111 1111 (b) 0110 1111 (c) 1101 1110. Dimensions of SIRs and transmission line are with respect to figure 3.30 and Table 3.10

Different coding combinations for presence/absence technique are shown in figure 3.32. In present/absence coding technique, coding can be done simply by shorting/opening the high impedance end. Spectral signatures for different coding combinations of figure 3.32 are shown in figure 3.33. For this case the maximum coding capacity with 8 resonators is 256.

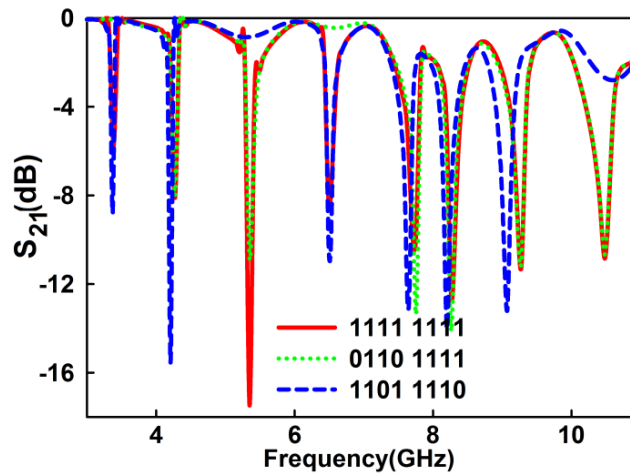


Figure 3.33: Frequency response of the 8 bit multiresonator circuit for different coding combinations shown in figure 3.32

The geometry is best suited for frequency shift coding (detailed in section 3.2) also. The flexible design of SIRs is effectively utilized in frequency shift coding technique to increase the coding capacity. In FSC, each resonator is tuned in an assigned sub-band with a definite resolution bandwidth. FSC for the multiresonator circuit of figure 30 is illustrated below. For 8 resonator the entire spectrum from 3.1-11.1 GHz is divided in to 8 frequency bands with $\Delta f = 1$ GHz and $df = 200$ MHz. Each sub section of the band Δf is assigned digits 0, 1, 2, 3, 4. Frequency response and SIRs

with changed dimensions to form different codes are shown in figure 3.34 and table 3.11, respectively.

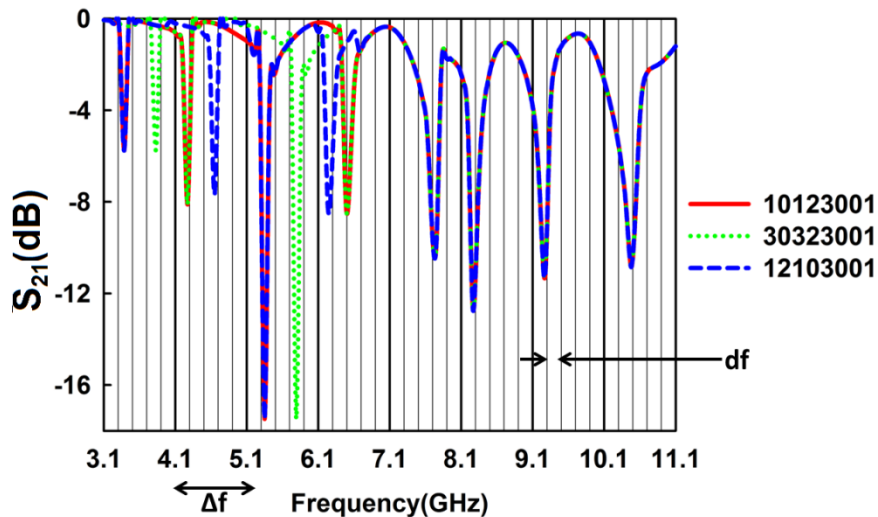


Figure 3.34: Illustration of FSC with $\Delta f = 1$ GHz, and $df = 200$ MHz.

With this type of coding, the total bit encoding capacity obtained (equation 3.1) is 18.58. On close examination on the spectral signature, it is clear that for lower frequency resonators smaller resolution can also be assigned. The resolution bandwidth is determined by the bandwidth of each resonance. As the frequency increases, though the fractional bandwidth remains the same, bandwidth of resonances would increase. Assignment of smaller resolution bandwidth for lower frequency resonators will further increase the coding capacity. For example, if the first four resonators of the multiresonator circuit are assigned a resolution of 100MHz and for the remaining the same 200MHz, the total bit encoding capacity can be enhanced to 22.57.

Table 3.11: Dimensions of SIRs changed for demonstrating different codes using FSC

Parameters	I'	II'	III'	IV'
F(GHz)	3.8	4.6	5.8	6.25
K	0.25	0.35	0.45	0.45
α	0.4	0.5	0.3	0.35
l_1 (mm)	4.4	3.24	4.4	3.58
l_2 (mm)	2.42	3.41	1.66	1.8
w_1 (mm)	0.5	0.5	0.5	0.5
w_2 (mm)	5.89	3.15	2.56	2.62

3.7. Tag antennas

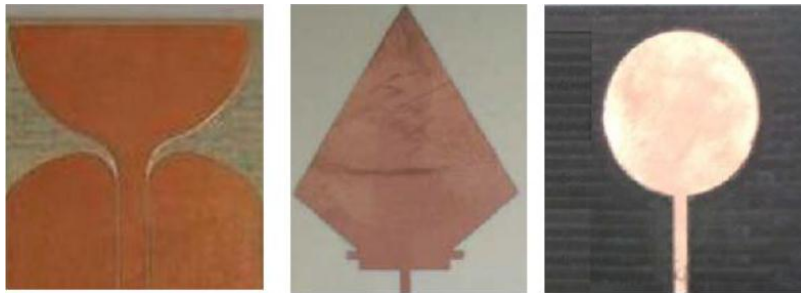


Figure 3.35: Antennas used in frequency domain Chipless tags [4], [3], [1]

Some of the antennas used in frequency domain Chipless tags are shown in figure 3.35. CPW or microstrip feed can be used for the antennas. The overall size of the antenna is determined by the lowest operating frequency, permittivity and geometry of the tag. Each has its advantage as well as disadvantage. As the thesis is dealing with ultra-wide band frequency domain tags, planar UWB antennas are needed for the tags [17]. The tag antenna needs to have an omnidirectional pattern unlike the highly

directional reader antenna. It should also possess substantial impedance match over the operating bandwidth of Chipless RFID tag. Linear polarization property is mandatory since cross polarized antenna arrangement for reception and transmission antennas at the reader side has been used to reduce mutual coupling between antennas. Moreover, radiation pattern should be same throughout the spectrum. Of course simple layout, compactness and fully printable geometries are most desirable characteristics of Chipless RFID tag antennas.

Giving emphasis to a simple layout, disc monopole UWB antenna [18] is selected as the tag antenna. The UWB characteristic of the disc monopole antenna is accomplished by the overlapping of the antenna modes that are closely occupied in the spectrum. The geometry of the disc monopole antenna along with the design parameters are shown in figure 3.36.

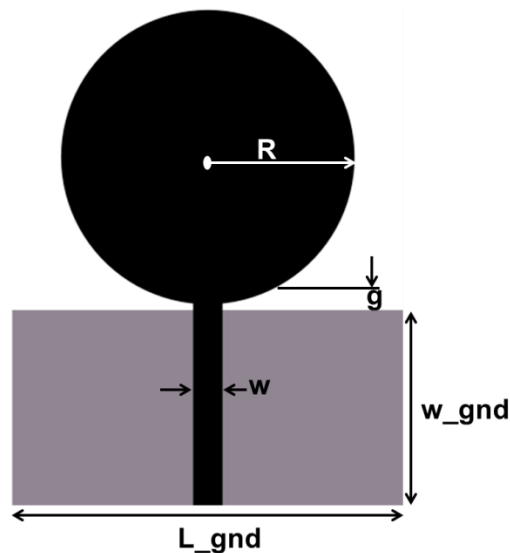


Figure 3.36: Disc Monopole antenna, $\epsilon_r = 4.3$, $h = 1.6$ mm, $\tan\delta = 0.0018$, $R = 19.5$ mm, $w = 3$ mm, $L_{\text{gnd}} = 55$ mm, $w_{\text{gnd}} = 35$ mm, $g = 0.6$ mm

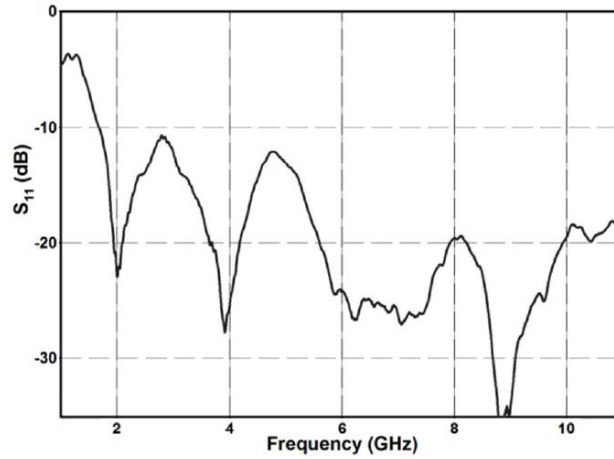


Figure 3.37: Return loss of disc monopole antenna shown in figure 3.36

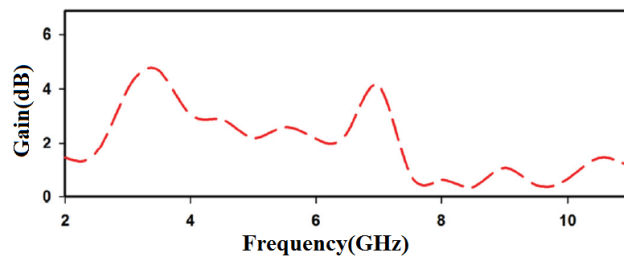


Figure 3.38: Gain of above disc monopole antenna

The measured return loss and gain of the antenna are shown in figure 3.37 and 3.38, respectively. The antenna possesses good impedance match throughout the entire UWB. The measured radiation pattern of the disc monopole antenna both in H and E plane are shown in figure 3.39 at different frequencies. The excitation of higher order modes influences the antenna radiation pattern and consequently there is a distortion in the E plane figure of eight pattern. More clearly, at the fundamental mode of operation the antenna operates in standing wave oscillation. As frequency of operation increases antenna operates in a hybrid mode in which both

standing and travelling waves are present. At higher frequencies travelling waves are more dominant hence there will be distortion to the corresponding radiation pattern [21]. As the higher frequency distortion is common to all UWB antennas the only choice is to select an antenna with better performance. Some papers propose methods to improve radiation characteristics like dual microstrip transitions [18]. Such method should be used to improve the performance at high frequency end of UWB.

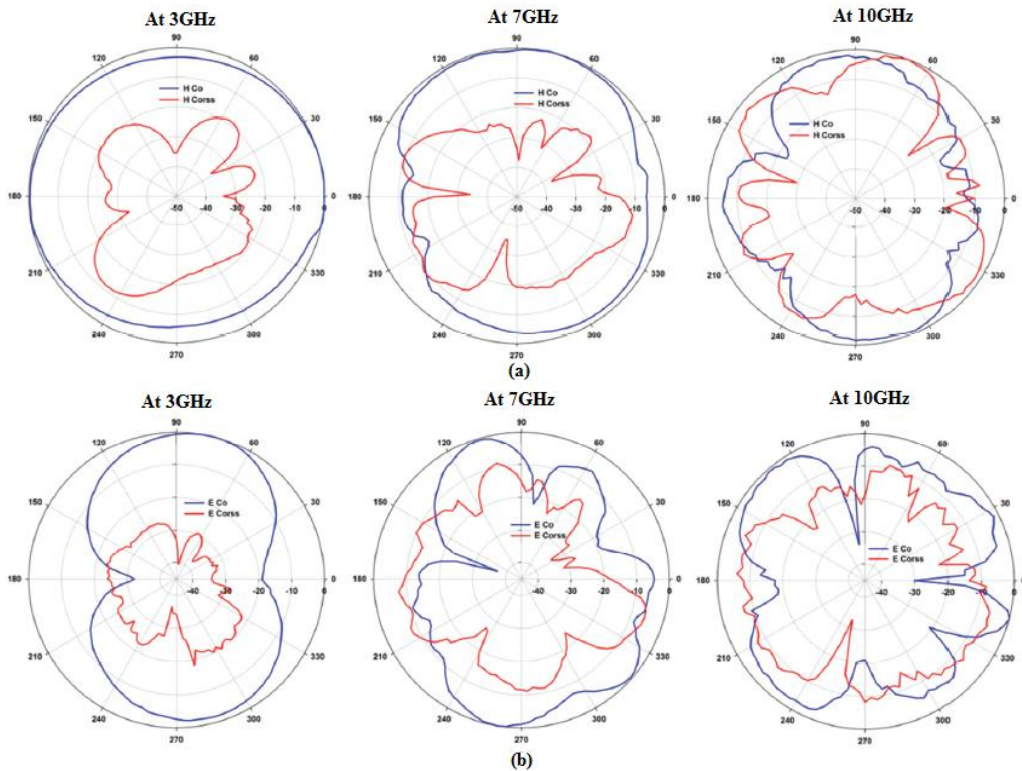


Figure 3.39: The measured radiation pattern of the disc monopole antenna both in (a) H and (b) E plane at different frequencies.

3.8. Friss free space transmission formula to calculate free space losses in multiresonator based Chipless RFID system

Friss free space transmission formulae can be used to calculate the expected power levels at the reader receiving antenna from the Chipless tags in a lossless environment [19]. The power density of the signal reaching the tag in free space is given by

$$S = \frac{P_t G_r}{4\pi r^2} \dots\dots\dots (3.15)$$

Where P_t is the transmitted power, G_r is the gain of the reader transmitting antenna and r is the distance between the tag and reader antenna. The power collected by the transponder antenna is defined as

$$P_a = S A_e = \frac{S \lambda^2 G_t}{4\pi} \dots\dots\dots (3.16)$$

Where A_e is the effective area of the tag antenna, G_t is the gain of the tag antenna and λ is the operating wavelength. Both antennas used by the RFID reader for transmission and reception are assumed to be identical in this calculation. Similarly receiving and transmitting antennas in the tag is also taken as identical. With these assumptions, the signal received by the reader from the tag is

$$P_r = \frac{P_t G_t^2 G_r^2 \lambda^4 L(f)}{(4\pi r)^4} \dots\dots\dots (3.17)$$

Where $L(f)$ is the insertion loss of the tag's multi resonating circuit as a function of frequency f . To successfully identify the signal, the received signal strength P_r should be greater than the noise floor. Polarization isolation between the reader antennas and environment conditions like

interference from wireless systems, scattering from stationary objects, etc. are the factors determining the noise floor in Chipless RFID systems.

3.9. Chipless RFID tag with antennas

In the preceding sections, the components of Chipless RFID tag: multiresonator circuit and tag antennas are individually discussed and analysed. Here the Chipless RFID system as a whole is presented. As discussed in chapter 2, PNA E8362B along with two horn antennas is employed as the reader. The reader antennas are cross polarized like the tag antennas. The schematic of entire measurement setup is shown in figure 3.40.

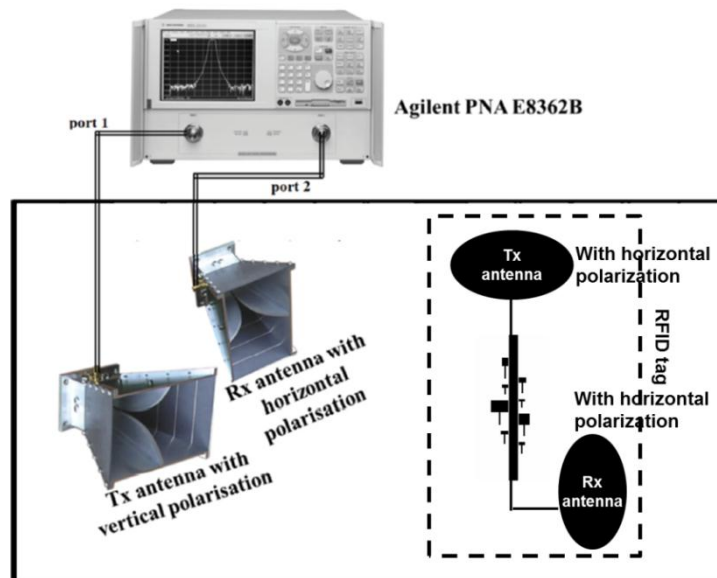


Figure 3.40: Schematic of measurement setup used to characterize the tag (specified in section 2.4)

Measured backscattered response of the Chipless RFID tag is shown in figure 3.41. The typical responses of the RFID tag for the codes 1111 1111, 0110 1111, and 1101 1110 are shown in the figure 3.41. As it is seen

all the bits can be identified from the backscattered magnitude. The performance at the highest frequency is deteriorated even when connecting the multiresonator circuit directly to the ports without the tag antennas. This decreased performance can be justified by the inherent microstrip losses at high frequencies. Further, decreased performance at the higher frequency resonances is due to the distorted radiation pattern of the disc monopole antenna at the higher frequencies.

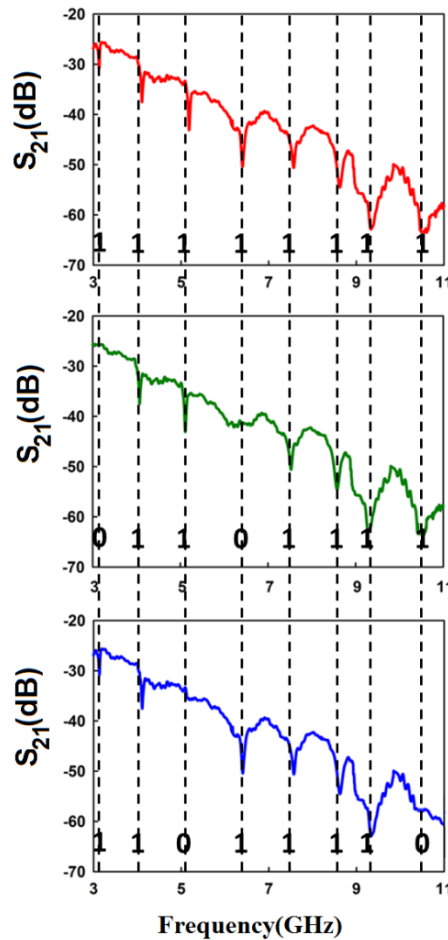


Figure 3.41: Measured backscattered response of the Chipless RFID tag shown in figure 3.30 for different codes. The tag parameters are detailed in table 3.10

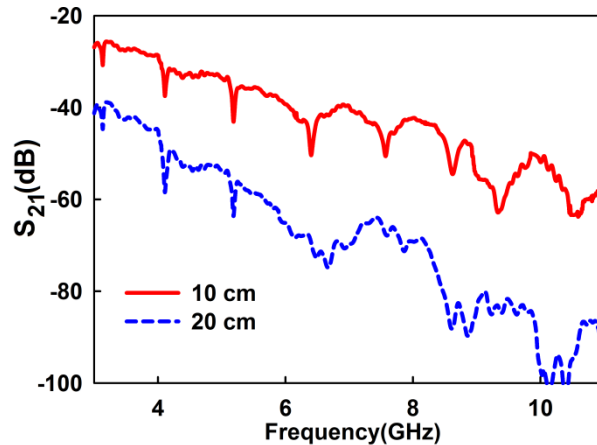


Figure 3.42: Measured backscattered response of the tag shown in figure 3.30 at different distances

The successful read range of the tag is 10 cm from the reader (shown in figure 3.42). The lower frequencies can be read at more distances than the higher frequencies. This is due to the poor radiation characteristics of tag antenna at higher frequencies. Coming to the tag antenna, it is a bitter task to find an antenna with a stable and constant radiation pattern throughout the frequency spectrum. Proposed system can be used for very near field automatic identification systems with the presented disc monopole antenna. With the realization of more efficient UWB antenna having much stable and good radiation characteristics throughout the entire band, the read range of the tag can be enhanced. By providing proper arrangements in the reader the tag can be proposed as a better alternative for barcode technology.

3.10. Conclusion

A Chipless RFID tag with multiple stepped impedance resonators is proposed in this chapter. Quarter wave SIR ($K < 1$) at its fundamental mode is used for the compactness and coding. The proposed system, owing the SIR's control over harmonic frequencies can use a larger spectrum for data encoding comparing similar tags in literature. For Chipless RFID tags, SIRs coupled to microstrip line is shown to have more advantages than directly connected to the line. Equivalent circuit model and different parametric studies are conducted on the resonator. The method presented in this chapter can be effectively implemented using low cost substrate materials which in turn reduce the overall cost.

References

- [1] S. Preradovic, I. Balbin, N. C. Karmakar and G. Swiegers, "Multiresonator-Based Chipless RFID System for Low-Cost Item Tracking," *IEEE Transactions on Microwave Theory and Techniques*, Vol. 57, No. 5, pp -1411-1419, May 2009.
- [2] C. M. Nijas, R. Dinesh, U. Deepak, Abdul Rasheed, S. Mridula, K. Vasudevan, and P. Mohanan, "Chipless RFID Tag Using Multiple Microstrip Open Stub Resonators," *IEEE Transactions On Antennas And Propagation*, Vol. 60, No. 9, pp.4429-4432, September 2012.
- [3] David Girbau, Javier Lorenzo, Antonio Lázaro, Carles Ferrater, and Ramón Villarino, "Frequency-Coded Chipless RFID Tag Based on Dual-Band Resonators," *IEEE Antennas And Wireless Propagation Letters*, Vol. 11, pp.126-128, 2012.
- [4] Y. F. Weng, S. W. Cheung, T. I. Yuk, and L. Liu, "Design of Chipless UWB RFID System Using A CPW Multi-Resonator," *IEEE Antennas and Propagation Magazine*, Vol. 55, No. 1, pp.13-31, February 2013.

- [5] Md. Shakil Bhuiyan, R. E Azim and N. C. Karmakar “A Novel Frequency Reused Based ID Generation Circuit for Chipless RFID Applications,” Asia-Pacific Microwave Conference, pp.1470-1473, 2011.
- [6] M. Makimoto and S. Yamashita, “Microwave Resonators and Filters for Wireless Communication, Theory, Design and Application,” Springer eries in Advanced Microelectronics, Vol. 4, 2001.
- [7] Chi-Feng Chen, Ting-Yi Huang, Chi-Ping Chou, and Ruey-Beei Wu “Microstrip Diplexers Design With Common Resonator Sections for Compact Size But High Isolation,” IEEE Transactions On Microwave Theory And Techniques, Vol. 54, No. 5, pp. 1945 – 1952, May, 2006.
- [8] Sheng-Yuan Lee, “Optimum Resonant Conditions of Stepped Impedance Resonators,” Microwave Conference, 2005 European, 4- 6 Oct., 2005.
- [9] M. Kirsching, R. H. Jansen, and N. H. L. Koster, “Accurate model for open end effect of microstrip lines,” Electronics Letters, Vol. 17, pp. 123-125, Feb. 1981.
- [10] S. Lee, “Optimum Resonant Conditions of Stepped Impedance Resonators”, 35th European Microwave Conference 2005, Vol.1, pp. 417-420, 2005.
- [11] M. Kirsching, R. H. Jansen, and N. H. L. Koster, “Accurate model for open end effect of microstrip lines,” Electronics Letters, 17, pp.123-125, Feb.1981.
- [12] K. C. Gupta, R Garg, I Bhal and P. Bhartis, Microstrip Lines and slotlines” Second edition, Artech House, Boston, 1996.
- [13] Antonije R. DjordjeviC and Tapan K. Sarkar, “Closed-Form Formulas for Frequency-Dependent Resistance and Inductance per Unit Length of Microstrip and Strip Transmission Lines,” IEEE Transactions on Microwave Theory and Techniques, Vol. 42, No. 2, February 1994.
- [14] K. C. Gupta, R. Gag, and R. Chadha, Computer-Aided Design of Microwave Circuiis. Boston: Artech, 1981.
- [15] F. E. Gardiol, Introduction to Microwaves. Boston: Artech. 1984

- [16] Jia-Sheng Hong and M J Lancaster “Microstrip Filters for RF/Microwave Applications” A Wiley-Interscience publication, pp.112-120, 2001.
- [17] K. Y. Yazdandoost and R. Kohno, “Ultra wideband antenna”, IEEE Communication Magazine, Vol. 42, No. 6, pp:S29-S32, 2004
- [18] A. Alipour and H. R. Hassani, “A novel omni-directional UWB monopole antenna,” IEEE Transactions on Antennas and Propagation, Vol. 56, No. 12, pp: 3854-3857, Dec. 2008
- [19] M. N. Srifi , S. K. Podilchak , M. Essaaidi and Y.M.M. Antar, ” Planar Circular Disc Monopole Antennas Using Compact Impedance Matching Networks for Ultra-Wideband (UWB) Applications,” Asia Pacific Microwave Conference , pp. 782-785, 2009.
- [20] C. A. Balanis, Antenna Theory: Analysis and Design, 2nd ed. New York: Wiley, 1982
- [21] S. Preradovic, Chipless RFID System for Barcode Replacement, PhD thesis, Monash University, December 2009.
- [22] Aps Khanna and Y. Garault, “Determination of Loaded, Unloaded, and External Quality Factors of a dielectric Resonator Coupled to a Microstrip Line,” IEEE Transactions On Microwavs Theory And Techniques, Vol. -31, No. 3, pp. 261-264, March 1983.

.....✂.....

MULTISCATTERER BASED CHIPLESS RFID TAGS

C o n t e n t s	4.1. <i>Introduction</i>
	4.2. <i>Backscattering from multiscatterer based Chipless RFID tag</i>
	4.3. <i>Characteristics of the scatterer used in Chipless Frequency domain RFID tags</i>
	4.4. <i>Substrate for the tags</i>
	4.5. <i>Calibration method</i>
	4.6. <i>Chipless RFID tag using Cross loop resonator</i>
	4.7. <i>Polarization independent Chipless RFID tag using Stepped impedance resonators</i>
	4.8. <i>Comparison of different Chipless RFID tags in literature with the tags developed</i>
	4.9. <i>Conclusion</i>

Design and development of Polarization independent multiscatterer based Chipless RFID tags are discussed in this chapter. Backscattering phenomenon from Chipless Tags, calibration method and requirements of the multiscatterers to form efficient tags are also discussed. Two polarization independent tags, one using cross loop resonator and the other using stepped impedance resonators as basic scatterer are proposed in this chapter. Parametric analysis of basic resonators is presented to get optimum multiresonant characteristics. Depending on the application, emphasis is given to various tag properties like polarization insensitivity, high bit encoding capacity, size, and maximum reader ranges.

4.1. Introduction

The presence of transmitting and receiving antennas and the transmission line in the multiresonator based Chipless RFID tag(tags with transmitting-receiving antennas and resonators coupled to microstrip line) [1-5] increases the tag size and structural complexity. The transmitting and receiving antennas which occupy more than 50% of the tag surface area and whose inconsistent radiation characteristics in the operating UWB are the major problems with the multiresonator based Chipless RFID tags. Moreover, the multiresonator coupling to the microstripline and the mutual coupling between resonators should also be considered in the tag design. In this context we have to consider the efficiency of the multiscatterer based Chipless RFID tags [6-12]. These tags have more attractive features like availability of better readable range, effective calibration techniques and applicability of effective time domain techniques for processing the backscattered signal. Moreover, they are akin to the concept of electromagnetic barcodes.

The multiscatterer based tag simply eliminates the trans receiving antennas and transmission lines. This will reduce the overall size of the tag. This type of tags combines all the three functions of reception, transmission and filtering in each scatterer [13]. Thus the tag generates a spectral signature similar to multiresonator based Chipless RFID tag with less structural complexity. The Multiple scatterers selected should have very high Q so that they can effectively add their signature to the frequency spectrum of the reader. Upon the incidence of the reader signal, currents are induced on the multiscatterers at their resonant frequencies. These currents

in the scatterers reradiate along with the backscattered signal as the signature of the tag and can be detected and decoded by the reader. The selection of basic scatterer is very crucial because it defines the effective use of bandwidth, polarization sensitivity, readable range etc.. Resonators with narrow bandwidth or with high selectivity are most interested for frequency domain Chipless RFID tags to enhance the coding capacity. The selectivity or Q factor depends on conduction, dielectric, surface wave and radiation losses [15]. Thin substrates with low loss tangent and small metal thickness are suitable for Chipless RFID tags to meet the high Q requirements.

There are numerous multiscatterer based Chipless RFID tags reported and many are narrated in the literature review chapter of this thesis. Most of the reported tags should meet stringent polarization alignment with respect to the polarization of the incident wave. Polarization independent or orientation independent Chipless RFID tags offer more freedom in positioning and detection. Detection in cross polar level adds to considerable reduction in noise [8]. Only a few works on polarization insensitivity are available in the literature [15, 16, 17]. So developing Chipless RFID tags with polarization insensitivity along with other desirable properties of multiscatterer based Chipless RFID tags deserves significant research. This chapter focuses on the development of polarization independent tags with high data encoding capacity.

4.2. Backscattering from multiscatterer based Chipless RFID tag

Multiscatterer based Chipless RFID tag contains carefully aligned high Q resonators without any antennas. Chipless frequency domain tags require high Q resonators embedded on them to create bit patterns with

resonant dips/peaks in the frequency response captured by the reader in response to these tags. These tags can be viewed like radar targets but with unique IDs. The IDs are stored as electromagnetic signature in the backscattered signal from the tag. Due to the duality between time and frequency domain, frequency domain tags can be analyzed in time domain also. If the backscattered signals are observed in frequency domain directly, the bit pattern will be dominant and is represented by the resonant peaks/dips. If it is analyzed in time domain, a conversion from time domain to frequency domain is needed to extract the ID.

Time domain approach to detect or interpret response of frequency domain tags is more reliable and noise resistant [18-19]. The time domain response from a Chipless RFID tag has mainly two components named as structural mode and antenna mode. When the incident pulse illuminates scatterers on the tag, specular reflections from the scattering centers are scattered around. These reflections are due to the local current distribution on the discontinuities on the scatterer. This reflection which resembles the incident pulse constitutes the structural mode or early time response. After the incident pulse passes through the tag completely, there will be an interaction between local current distributions produced during the early time. These interactions converge to natural current modes of the scatterer and results in late time response or antenna mode [18]. A. Vena et al. also explained the scattering mechanism behind multiscatterer based Chipless RFID tag in a much simple way [13]. The structural mode depends only on the geometry of the tag while the antenna mode depends on the Q factor and other resonant characteristics of the scatterers embedded on the tag.

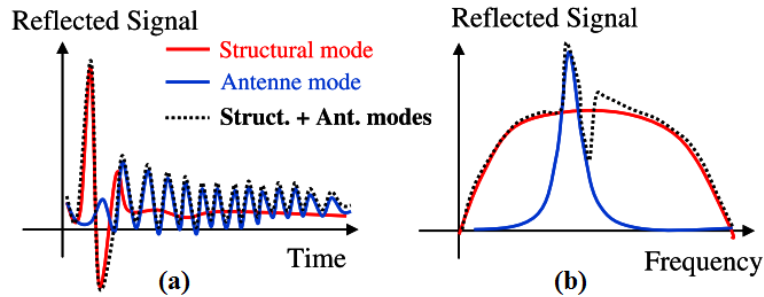


Figure 4.1: (a) Typical impulse response of RFID tag showing the structural and the antenna modes. (b) Frequency response of the scatterer. The addition of the two modes creates a destructive interference when they are 180° out of phase. Courtesy: A. Vena et al. [13].

Figure 4.1 shows the two modes or responses contained in the backscattered signal from the Chipless RFID tag. As seen from the figure, the total response of the tag is a superposition of structural mode (which is characterized by a constant level along the magnitude as well as phase) and antenna mode with a very selective response. It is not possible to encode any data in structural mode but it can be used as a reference for determining the starting time of antenna mode and for locating the tag.

4.3. Characteristics of the scatterer used in Chipless Frequency domain RFID tags

Elements of Multiscatterer based Chipless tags have to perform multiple functions like transmission, reception, and filtering. Because of this multiple functionality assigned to each scatterer, the selection of the basic scatterer is very important for the performance of the tag. The desired properties for scatterers are detailed below.

- High Q: High Q factor or narrow bandwidth of the basic resonator is a desirable characteristic of frequency domain Chipless RFID

tags. With high Q, more number of bits can be encoded in a given spectrum. Also sharp narrow resonances can be identified more easily even in noisy surroundings. This can also be considered as an advantage to achieve better reading ranges.

- Compact size: Compactness of the resonator is also a plus point in the modern gadgets. Compactness can be easily achieved by using nested resonators [15], [17].
- Harmonics: Control over the higher harmonics is another favourite factor regarding the selection of scatterers. If the ratio between higher harmonics and the fundamental frequency can be controlled independently, a wide spectrum can be used for data encoding. Also, this control enables to define multiple bits per resonator [10]. Only a few resonators are reported in the literature with such a degree of freedom.
- The number of bits per resonator: The number of bits per resonator is another preferred property which may increase the coding capacity of the tag. Compact and flexible multiband resonators [5] with control over harmonic frequencies can offer this property.
- Polarization: Polarization independent RFID tag is a desirable feature of Chipless RFID system. This property defines the tag's ability to respond without concerning the polarization of the reader signal. With polarization insensitive tags, restrictions on tag orientation with respect to the reader antenna would be mitigated. Alignment of the trans receiving antennas at the reader side can be chosen independently to offer minimum coupling

effects between them since the tag is being insensitive to their polarization. Compact symmetric resonators, symmetric repeated distribution of resonators [17], [11], [16], [15] etc. are the methods utilized to attain polarization independency.

- Isolation: Isolation between resonances is a crucial factor which is very difficult to achieve. Careful positioning of the resonators is the only relied way to reduce coupling between resonators. It would be advantageous if such a geometry could be realized.

This chapter gives emphasis to polarization insensitivity of the tag to the incident reader signal and therefore the selected structures are symmetric in x-y plane. Two types of microstrip multiscatterer based Chipless RFID tags are proposed in this thesis, one is cross loop resonator and the other is Stepped impedance resonator tags. Both type of tags offer polarization insensitivity either by geometry or by arrangement.

The simulation setup (Section 2.2) and measurement setup (Section 2.4) mentioned in this chapter are detailed in chapter 2. Both CST microwave studio and Ansoft HFSS are used for the simulation studies. Plane wave excitation is used in both tools. Backscattered field is measured using an electric probe oriented along the plane wave polarization and placed in front of the plane wave source.

4.3.1. Cross loop resonator

Geometry of the cross loop resonator is shown in figure 4.2. The structure is symmetric in x-y plane and hence it will generate a response independent of its orientation in x-y plane. Besides from the symmetric

appearance, the polarization independency of the structure is verified by measuring the backscattered signal from a single scatterer for different angles. The response is given in figure 4.3. As it is clear from the figure the resonance is detected in the backscattered signal for all the orientations of the tag in the x-y plane.

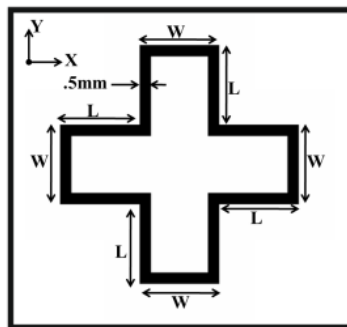


Figure 4.2: Single cross loop resonator, $L = 4$ mm, $W = 3.5$ mm, strip width = 0.5 mm, substrate height = 1 mm, $\epsilon_r = 2.2$

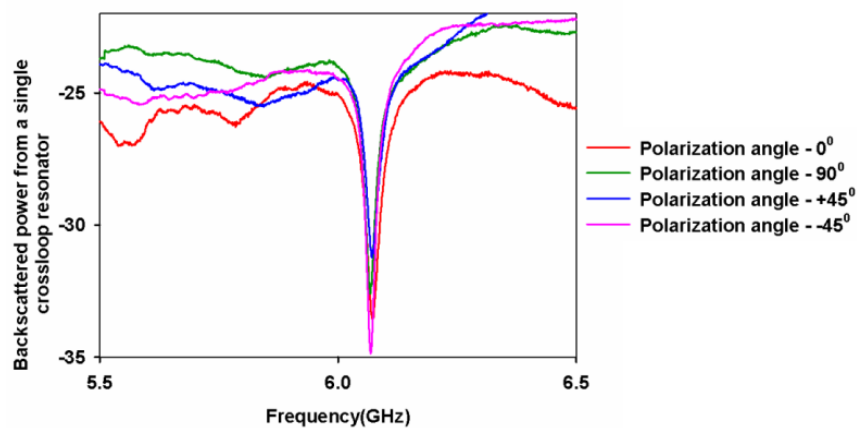


Figure 4.3: Measured backscattering from a cross loop resonator ($W = 3.5$ mm, $L = 4$ mm, strip width = 0.5 mm, substrate height = 1 mm, $\epsilon_r = 2.2$) for different orientations with respect the axis of tag surface

Detailed explanations about the current distribution and resonant frequency of the resonator are provided later in this chapter. The zig-zag nature of the cross loop is the advantage of the resonator compared to the circular ring as it brings considerable reduction in surface area occupied.

The cross loop resonator is compared with a circular ring resonator operating at the same frequency (7.47 GHz) and is shown in figure 4.4. Figure 4.4(a) shows the dimensions of the resonators resonating at the same frequency and 4.4(b) shows the simulated frequency response of both resonators. An area reduction of approximately 54% is obtained for cross loop resonator. Moreover, the reduced area can be utilized for embedding other electronic components. The loop nature supports nesting [17] of resonators and thus offers a compact tag.

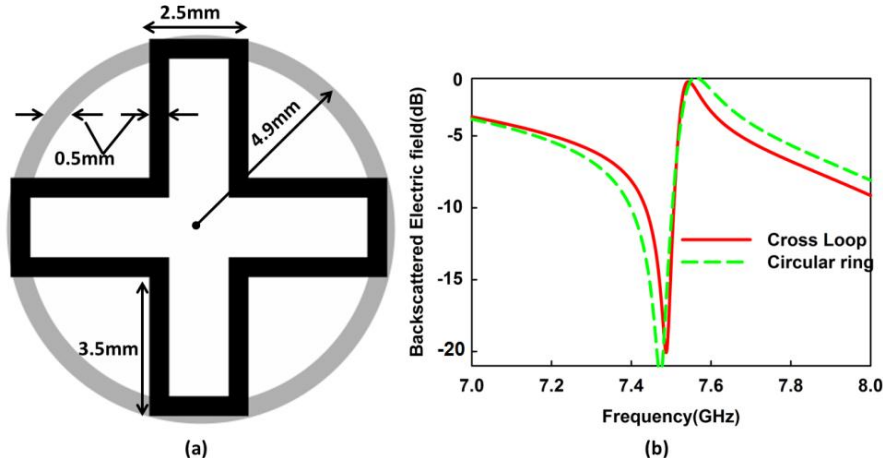


Figure 4.4: Comparison between Cross loop resonator and circular ring resonator of same frequency (a) Geometry of cross loop resonator ($W = 2.5$ mm, $L = 3.5$ mm) and circular ring (mean radius = 4.9 mm). Substrate height = 1 mm, $\epsilon_r = 2.2$ and strip width 0.5 mm for both geometry (b) Backscattered Electric Field

The cross loop resonator is polarization independent and offers reduction in surface area occupied but it doesn't have any mechanism to control the higher harmonic frequencies. So the first harmonic of the lowest frequency resonator should be expected at twice the fundamental frequency. Hence spectrum available for the tag is limited between the lowest frequency and its first harmonic.

4.3.2. Orthogonally aligned SIRs based scatterer

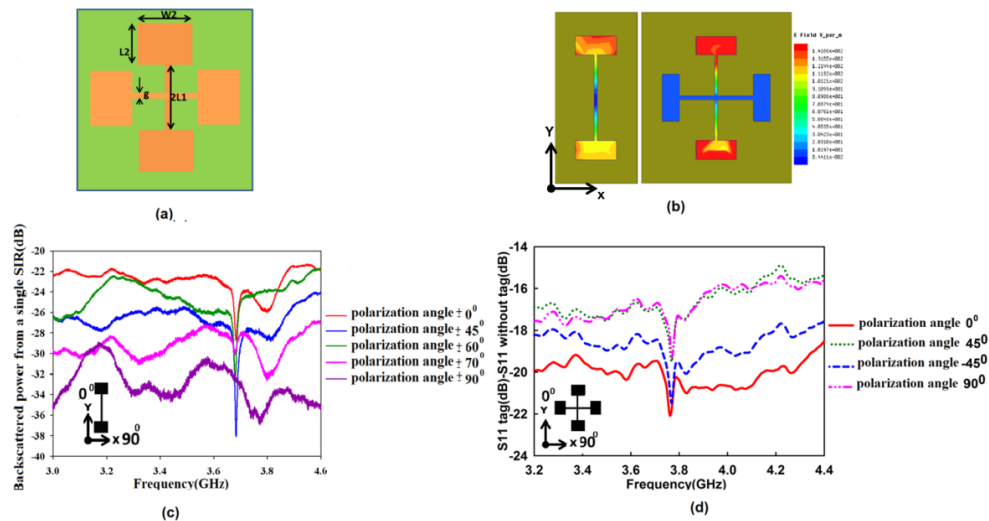


Figure 4.5: (a) scatterer geometry, $L_1 = 5.4$ mm, $L_2 = 2.42$ mm, $W_1 = 0.5$ mm, $W_2 = 5.82$ mm $\epsilon_r = 2.2$, Substrate height = 1 mm (b) Electric field distribution on single SIR and orthogonally aligned SIR based scatterer for X directed excitation (c) Scattering property of a single SIR for different orientations (d) Scattering property of scatterer for different orientations

The basic scatterer (shown in figure 4.5(a)) consists of two identical $\lambda/2$ stepped impedance resonators which are orthogonally placed in such a way that they cut each other at the electric field zero point (shown in figure

4.5(b)). The scattering property of a single SIR (3.7 GHz) for different angles in x-y plane is shown in figure 4.5(c). It can be seen that up to $\pm 60^\circ$ angular rotations, SIR responds to the incident wave (say y polarized for this case) with the same resonance. After that the resonance gradually diminishes from the spectrum and at 90° , the resonator will be completely insensitive to the incident wave. When two identical resonators orthogonally joined to form the scatterer, it will behave as a polarization insensitive system and responds for all polarization of incident wave. Measured scattering from the scatterer is shown in figure 4.5(d)

Electromagnetic devices with multiple resonators of course suffer from coupling effects from adjacent resonators. If the resonators of these particular scatterers are placed simply orthogonal without joining each other, the coupling effects encountered by each resonator will be different. Different environments encountered by the SIRs may make them resonate differently. So that polarization insensitivity can't be ensured by simply aligning two identical SIRs in two polarization orientations. By joining them at their voltage minimum at least the same coupling/adjacent conditions can be ensured for the two SIRs of a single scatterer.

This SIR based scatterer offers all the advantages of SIRs like flexibility in design, compactness, and above all control over harmonic frequencies. By this geometrical arrangement it constitutes a polarization insensitive tag.

4.4. Substrate for the tags

It is clear from the above sections that narrow resonances (high Q) are required for coding data in the frequency domain. The total quality factor [17] is mainly affected by the radiation loss, the conduction loss and the dielectric loss. Radiation loss is useful for the tag antennas (if present) but for the resonator it should be minimum. The conduction and dielectric losses have to be as small as possible. The conduction losses are low for highly conductive materials like copper. Also, compact and low cost tags are most desirable. Selection of substrate for the fabrication of Chipless RFID tag is significant in fulfilling the above requirements. Low loss substrate offers better storage of energy in the resonators at their resonance which may constitute High Q. These narrow resonances with considerable resonant depths/peaks can be distinguished easily from the noise. Dielectric constant of the substrate is another factor which has significance in tag performance. The higher the dielectric constant more will be the confinement of electric field within the substrate and hence narrow peaks/depths at resonances. Also, high dielectric constant substrates offer compact resonators. But the inverse relationship between loss tangent ($\tan\delta = \sigma/\omega\epsilon$, where σ is the conductivity and ω is the angular resonant frequency) and dielectric constant demands the selection of substrate as a compromise between all the above stated properties

Properties of different substrates used in the studies and the dimensions of resonator employed are detailed in table 4.1 with respect to figure 4.6. Performance of scatterers on different substrates is shown in figure 4.7

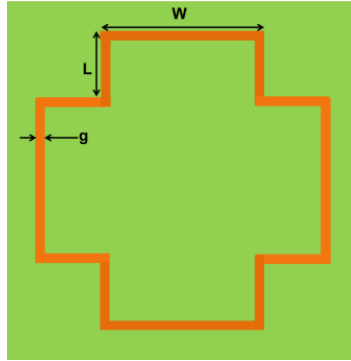


Figure 4.6: Single resonator tag used to study different substrates, imensions L , W and g for different substrates are given in table 4.1

Table 4.1: Properties of different substrates and the resonator dimensions (with respect to Figure 4.6) on them

Substrate	ϵ_r	$\tan\delta$	Substrate height(mm)	W(mm)	L(mm)	g(mm)
FR4	4.3	0.025	1	6	3.5	0.5
RT DUROID	2.2	0.0009	1	9.5	3.5	0.5
CMET_4.3	4.3	0.0018	1.6	6.4	3.5	0.5
CMET_6.5	6.5	0.002	1	4.46	3.5	0.5

As seen from figure 4.7, the substrate with highest loss tangent among the group (FR4) shows a feeble resonance. Such a resonance is very difficult to identify. Though FR4 has higher dielectric constant than the other substrates, its lossy nature deteriorates the performance. Low loss nature of other substrates enables better performance though with a lower dielectric constant. RT Duroid 5880 is showing the most narrow and deep resonance owing to its low loss nature. Considering the contribution of narrow band resonators in bit encoding capacity per bandwidth RT Duroid 5880 is the

better choice. High permittivity substrate CMET_6.5 offers more compact resonators but the inverse relation between permittivity and loss tangent leads to wider resonance and hence lower spectrum utilization. The resonant bandwidth of resonators on each substrate is given table 4.2.

Table 4.2: Resonance bandwidth of resonators on different substrates with respect to figure 4.7

Substrate	Resonance bandwidth(MHz)
FR4	150
RT DUROID	30
CMET_4.3	110
CMET_6.5	180

From Table 4.2, it could be seen that RT Duroid 5880 is giving the least bandwidth and giving emphasis to sharp and narrow resonances, RT Duroid 5880 is selected for the tag design.

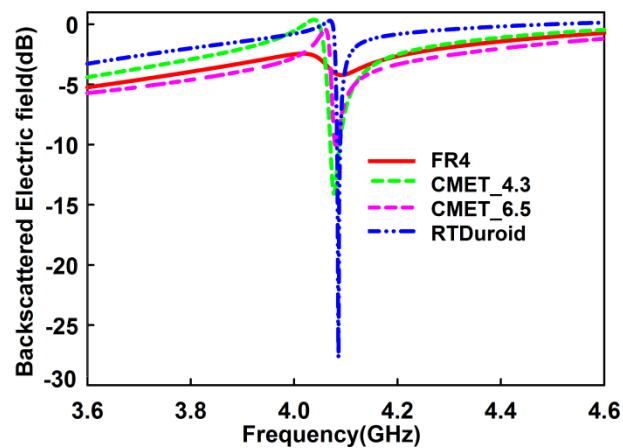


Figure 4.7: Performance of cross loop resonator on different substrates (with reference to figure 4.6 and Table 4.1)

Effect of objects on which tags are attached can be eliminated with grounded tags. Also, backscattering along the boresight direction is enhanced with the presence of ground. From the literature survey it can be seen that the grounded tags offer better performance in terms of noise reduction and reading range. So the microstrip version of tag is preferred in this thesis than the coplanar version.

4.5. Calibration method

As already stated, the principle behind RFID depends on reflected power from the scatterer. The reflected or backscattered power received by the reader contains many other components other than the data. The other components include reflection from surrounding objects like fixed objects, nearby wireless equipment and reflection from the reader antenna due to impedance mismatch. Therefore an effective calibration method should be used to easily detect the data. The method used is subtracting the measured data without tag from the measured data with tag [10], [20].

The effectiveness of the calibration method can be understood by analyzing the components of backscattering. The first and predominant component in the backscattered energy is due to antenna impedance mismatch resulted in reflection of transmitted pulse and this component will decay to zero gradually with time. Immediately after the incidence of transmitted pulse on the tag, the component arising is the structural mode $Y_S(t)$ that is due to the geometry of the tag especially by the ground plane. Following the structural mode is the antenna mode $Y_A(t)$ that contains the identity information. Apart from the above stated components, there will be

reflections from the fixed objects in the surrounding and white noise ($W_N(t)$) which may vary with time.

The noise in the tag measurement is due to the fixed objects and the white noise. The amplitude of the signal received from the room is represented by

$$Y_{\text{without tag}}(t) = Y_N(t) = Y_R(t) + W_N(t) \dots\dots\dots (4.1)$$

Where $Y_R(t)$ include reflection due to antenna mismatch and reflections from surroundings and $W_N(t)$ is the white noise present at the time. Similarly, the amplitude of the signal received with tag is given by,

$$Y_{\text{with tag}}(t) = Y_S(t) + Y_A(t) + Y_R(t) + W_N'(t) \dots\dots\dots (4.2)$$

where $Y_S(t)$ is the structural mode from the tag and $Y_A(t)$ is the antenna mode from the tag.

By subtracting (4.1) from (4.2)

$$Y(t) = Y_S(t) + Y_A(t) + W_N''(t) \dots\dots\dots (4.3)$$

Where $W_N''(t) = W_N'(t) - W_N(t)$

So the subtraction or calibration eliminates all the reflections and the signal contains the structural mode, antenna mode and a component due to white noise. Measurements are carried out outside the anechoic chamber with sufficient averaging to minimize the white noise level.

4.6. Chipless RFID tag using Cross loop resonator

A compact Chipless Polarization independent RFID tag using cross loop resonator as the basic element is presented in this section. The loop nature, symmetry and the compactness are the advantages of the proposed scatterer. The loop nature supports nesting of resonators and adds to the compactness of the tag. Symmetric geometry of the scatterer makes the tag polarization independent. The prototype of the tag is fabricated on RT Duroid 5880 substrate with $\epsilon_r = 2.2$, $\tan\delta = 0.0009$, $h = 1$ mm.

4.6.1. Single cross loop resonator

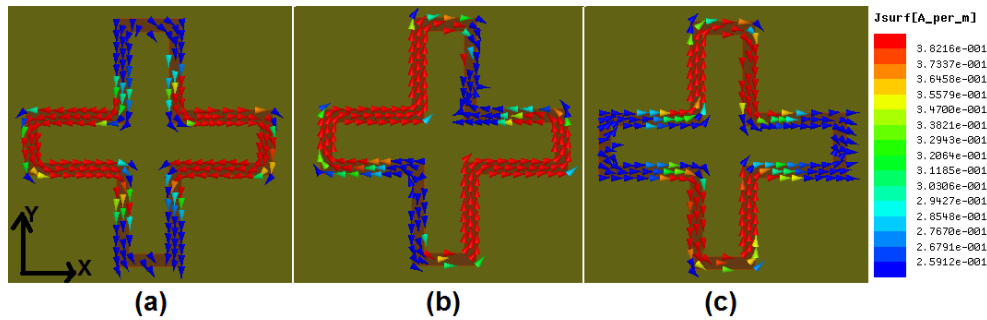


Figure 4.8: Current distribution on cross loop resonator ($W = 3.5$ mm, $L = 4$ mm, strip width = 0.5 mm, substrate height = 1 mm and $\epsilon_r = 2.2$. Dimensions are with respect to figure 4.6) for different polarizations of incident wave (a) Y polarized (b) 45° tilted (c) X polarized

The cross loop which is basically a closed ring only support waves that have integral multiple of guided wavelength equal to the mean perimeter. The simulated current distribution on a single cross loop resonator is shown in figure 4.8. One full wavelength of current distribution is noticed along the perimeter. The current distribution remains lambda though the positions of current minimum or maximum change according to

the polarization of incident wave. Any variation from the symmetry of ring may lead to the excitation of degenerate modes that leads to distinct resonant frequencies which otherwise appear as a single resonance. Degenerate modes [20] in ring resonators are modes that can be present simultaneously, independent of each other and are orthogonal to each other. They can exist at the same frequency and can be considered as two waves progressing in clockwise and anticlockwise direction. For symmetric resonators, only one of the modes will be excited. Any deviation from symmetry causes the two modes to excite and the split in the resonant frequency will be obvious [20]. In this particular tag design, symmetry of the resonator is very significant due to special attention given to the polarization insensitivity.

4.6.1.1. Design equation of a single cross loop resonator

From the current distribution discussed in previous section, it is clear that the cross loop resonator is a full wavelength (λ) resonator like the ring resonator. But it will not resonate exactly at the resonant wavelength equal to its perimeter. For a circular ring resonator, this variation can be accounted by defining an effective dielectric constant that includes the effects of fringing fields. Apart from the fringing fields, the deviation of resonant wavelength from guided wavelength is influenced by the corners and bends in the geometry. An approximate design equation of cross loop resonator can be developed by conducting a comparison between the ring and cross loop resonator and then by adding a correction to the design equation of circular ring resonator. A comparison of different cross loop resonator and circular loop having same perimeter and width is given in table 4.3. Percentage error in

frequency is also calculated as $\left\{ \left[\frac{(f_{cross\ loop} - f_{circular\ ring})}{f_{circular\ ring}} \right] * 100 \right\} \%$. The cross loop resonant frequency can be approximated by adding the calculated %error to the frequency of circular ring of same perimeter.

The resonant frequency of circular ring is calculated using the equation [17] written below

$$f_{circular\ ring} = \frac{c}{2\pi R [0.965 + 19.2R - 1372R^2] \sqrt{\epsilon_{eff}}} \dots\dots\dots (4.4)$$

Where R is the radius of circular ring and ϵ_{eff} is the effective dielectric constant of the microstrip line having width w, height h and permittivity ϵ_r . The modified Equation 4.5 can be used to determine the resonant frequency of cross loop resonator analytically. The equation is valid for values of ‘R’ in between 9 and 4 mm and for a width 0.5 mm [17].

Table 4.3: Comparison of resonant frequencies of circular ring and cross loop resonator of same mean perimeter (guided wave length) and microstrip width = 0.5 mm

f cross loop (GHz)	f circular ring (GHz)	Mean perimeter (mm)	% error
2.74	2.52	90	8.73
3.03	2.75	82	9.57
3.36	3.05	74	10.16
3.77	3.41	66	10.56
4.32	3.86	58	11.92
5.07	4.52	50	12.17
6.10	5.41	42	12.75
7.62	6.65	34	14.59

From table 4.3, it is seen that the deviation in frequency between circular ring and cross loop resonator is increasing with frequency. This is due to the fact that the effect of corners and bends become more dominant at higher frequencies [20]. So, with respect to table 4.3 frequency of cross loop resonator can be approximated by adding an average % error of 11.3%.

$$f_{cross\ loop} = f_{circular\ ring} + 0.113 \dots\dots\dots (4.5)$$

4.6.1.2. Effect of microstrip width

In [20], it is stated that when the width of the microstrip ring resonator is comparable to $\lambda_g/2$, higher order modes will be excited. It is also stated that the dispersion of ϵ_r is low for high impedance microstrip lines and the reverse is the case for low impedance lines. So in terms of compactness and frequency stable response, thin microstrip resonators are preferred.

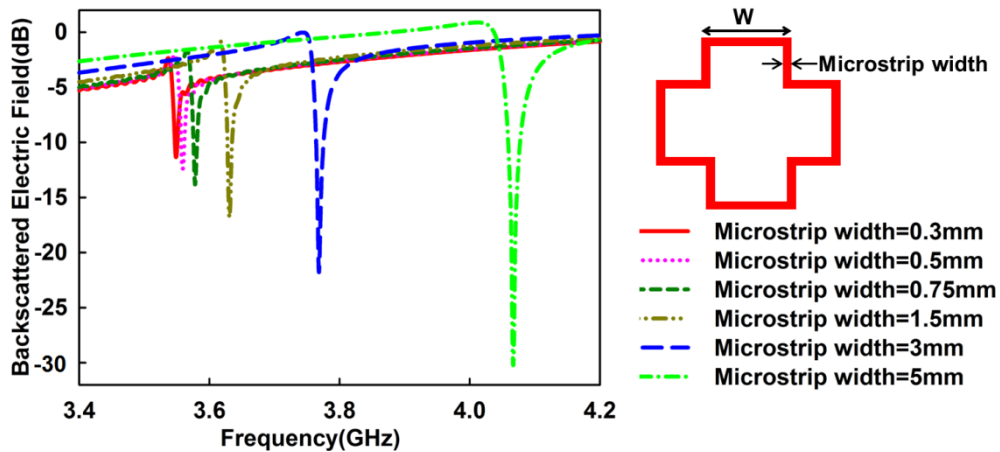


Figure 4.9(a): Variation in resonance frequency of cross loop resonator for different microstrip widths for constant mean perimeter of 68.4 mm, $W = 11.5$ mm and L (With respect to figure 4.6) will be varying according to the microstrip width, substrate height = 1 mm, and $\epsilon_r = 2.2$.

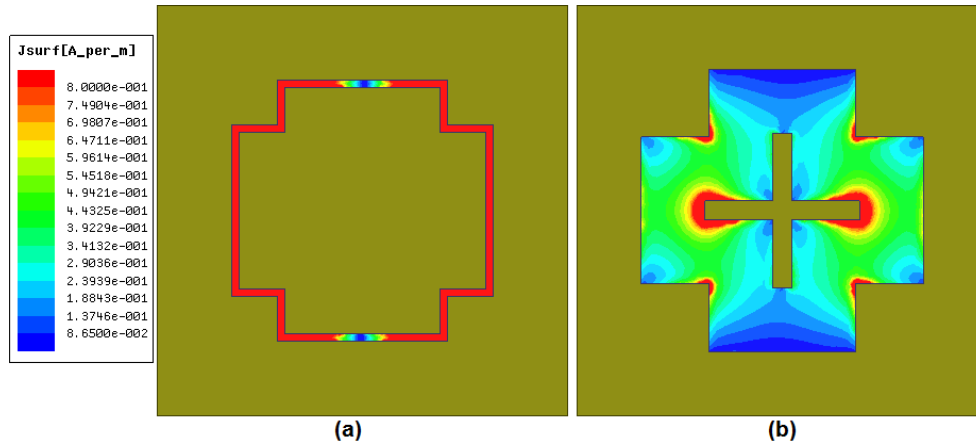


Figure 4.9(b): Current distribution on cross loop resonator for different microstrip width. Mean perimeter is 68.4 mm, $W = 11.5$ mm (with respect to figure 4.9(a)), substrate, height = 1 mm and $\epsilon_r = 2.2$.
(a) Microstrip width = 0.5 mm, **(b)** Microstrip width = 5 mm

The effect of varying width of the microstrip resonator for a constant perimeter of 68.4 mm is shown in figure 4.9(a). From the figure it can be seen that as the width increases the resonator frequency shift upwards. This can be justified by viewing the surface current density on the resonators with width 0.5 mm and 5 mm shown in figure 4.9(b). It is seen in figure 4.9(b) that for 0.5 mm width the current distribution is almost constant along the width of the microstrip and with 5 mm width, the current density tends to concentrate more towards the inner perimeter. So for wider resonators the inner perimeter has more influence on the resonant frequency. Due to the large microstrip width, the inner perimeter is substantially smaller than the mean perimeter of the resonator. This is the reason behind the upward shift in resonant frequency. It is seen in the figure 4.9(a) that the resonant dip is increasing with the microstrip width. But, due to the dispersion of ϵ_r for low impedance microstrip resonators and inherent microstrip losses [20] at higher

frequencies, the shifted resonances of thick microstrip resonators are wider. Narrow bandwidth resonances are preferred to encode more bits in the spectrum. So, considering the compactness of the tag and more number of bits per spectrum, a width of 0.5 mm is selected as the optimum width of the microstrip resonator.

4.6.1.3. Study on harmonics

The cross loop resonator doesn't have any mechanism to control the higher order modes. So the presence of first harmonic frequency at twice the fundamental frequency is anticipated. Slight shift from the exact multiple is seen for all type of resonators. From the simulation results for plane wave incidence, it is found that no harmonics are generated for symmetric excitation [21]. Any deviation from the symmetry of alignment, there is chance for the excitation of first harmonic frequency. Simulation results are shown below in figure 4.10.

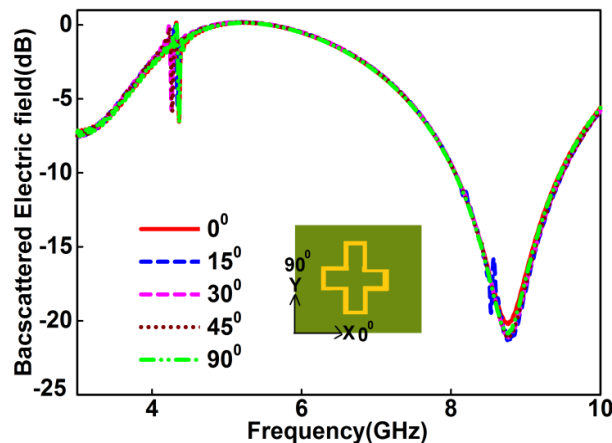


Figure 4.10: Rotating single cross loop resonator in X-Y plane to see the excitation of first harmonic frequency, $L = 4$ mm, $W = 5.5$ mm, strip width = 0.5 mm (L & W are marked with respect to figure 4.6), substrate height = 1 mm, $\epsilon_r = 2.2$

It is seen in the figure that harmonic frequency is excited for a rotation of 15° in the x-y plane. Since any authentic method is not reliable to have control over harmonic frequency and symmetric excitation cannot be ensured practically, frequency range of operation is selected in between the lowest resonant frequency of tag and its first harmonic frequency.

4.6.1.4. Effect of substrate height

The height of substrate has significant contribution towards the performance of Chipless RFID tags. The heights that offer identifiable resonance peaks/depths and high quality factor are required. At the same time, compact and thin tags are always desirable. For microstrip resonators, as the height increases the confinement of field within the resonator decreases and the radiation tendency increases [22]. As a result, the resonance becomes wider and too weak to identify. The bits which are represented by these resonances become less identifiable. Also, the number of bits that can be encoded in the frequency domain decreases as the bandwidth of individual resonance increases. Simulation results for different heights of RT Duroid 5880 substrate are shown in figure 4.11. From the figure, it is clear that for heights 0.3 mm and 0.5 mm the resonances are feeble even for low loss RT Duroid 5880 substrate. As height increases, resonances become more clear and deeper, but the bandwidth increases. Beyond 1.6 mm height, the resonance becomes wider and depth decreases. Height of 1 mm is selected as optimum and is readily available in market. So RT Duroid 5880 with 1 mm height is selected for the tag design.

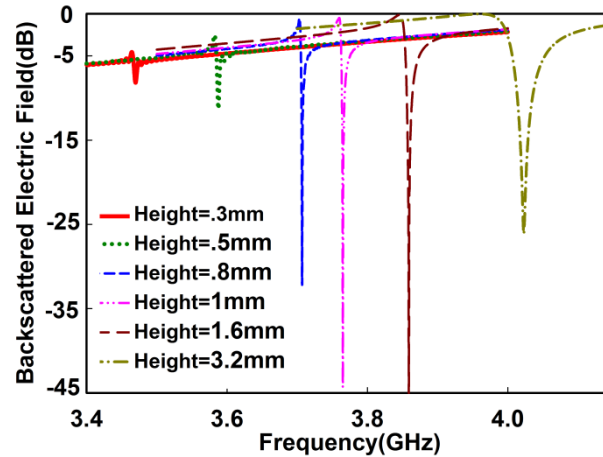


Figure 4.11: Effect of substrate height on cross loop resonator's backscattering, resonator dimensions: microstrip width = 0.5 mm, L = 3.5 mm, W = 10 mm (L & W are with respect to figure 4.6), $\epsilon_r = 2.2$

4.6.2. Effect of nesting and adjacent resonators

When resonators are nested there would be shift in the resonant frequency due to the coupling effect between nested resonators. Gap between the nested resonators is varied and the results are observed to select the optimum gap. The responses are shown in figure 4.12. It is found that for gaps greater than 0.25 mm, resonators show distinct frequencies with slight shifts. Since it has been developed for RFID applications these shifts are tolerable because the responses of all combinations of resonators are pre-recorded. Due to the difficulty to fabricate uniform 0.25 mm gap and also to ensure the backscattering from inner resonator 0.5 mm gap is selected for the present tag design.

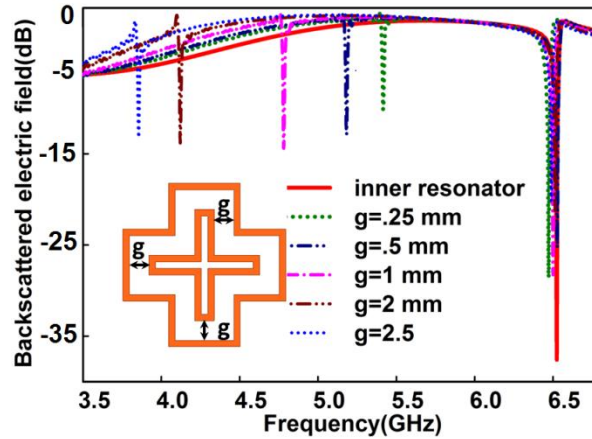


Figure 4.12: Effect of varying gap between resonators, inner resonator dimensions: microstrip width = 0.5 mm, $L = 3.5$ mm, $W = 3.5$ mm, (L & W are with respect to figure 4.6), substrate height = 1 mm, $\epsilon_r = 2.2$

Effect of nesting on different resonators in a nested group of 3 resonators is shown in figure 4.13. In the figure, inherent resonant behaviors of individual resonators are also plotted. When the nested resonators are present, it is found in the simulation result that, the innermost resonator/highest frequency resonance remains almost unchanged. But there is a downward shift in outer resonances. The shift in resonant frequency could be accounted by viewing the current distribution (shown in figure 4.14) on the nested resonators. From the current distribution it is clear that the coupling effects encountered by the inner most resonator is minimum as there is no resonator inner to it to couple with. Also from figure 4.13, it is seen that the depth of resonance of outer resonators is decreasing with the number of nested resonators. Individual resonant frequencies of 3 resonators together with their nested combinations are tabulated in table 4.4.

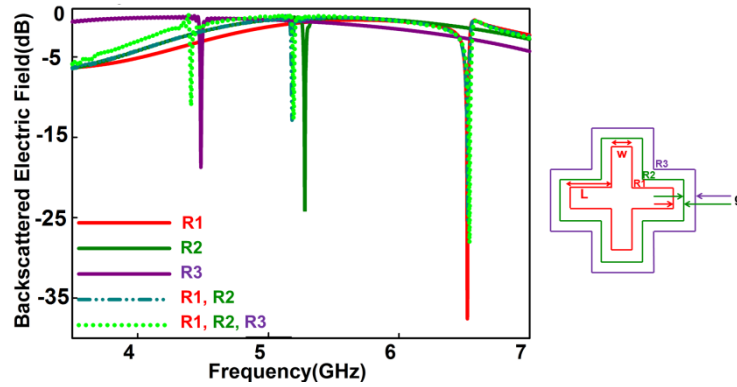


Figure 4.13: Effect of nesting on individual resonators, resonator dimensions: microstrip width =0.5 mm, L = 3.5 mm, W = 3.5 mm, g = 0.5 mm, substrate height = 1 mm and $\epsilon_r = 2.2$. R1, R2, R3 are the inner, middle and outer resonators, respectively

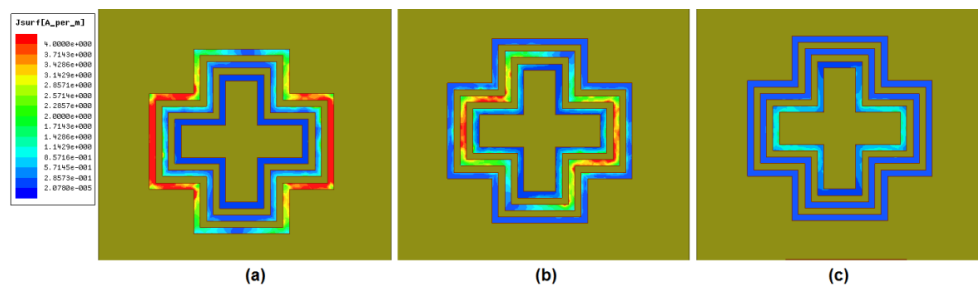


Figure 4.14: Current distribution on nested resonators at their resonant frequency (with respect to figure 4.13). (a) Outer resonator is excited (b) Middle resonator is excited (c) Inner resonator is excited

Table 4.4: Individual and effected resonant frequencies of the resonators

Resonators present	Inner most, R1(GHz)	Middle, R2(GHz)	Outer, R3(GHz)
Individual response	6.52	5.27	4.48
Middle & inner	6.52	5.17	Not present
All the three	6.53	5.19	4.41

Space between adjacent resonators is also important since it has direct involvement in determining the compactness of the tag. The optimum gap between adjacent resonators is determined by simulating different gap between resonators. The result is shown in figure 4.15.

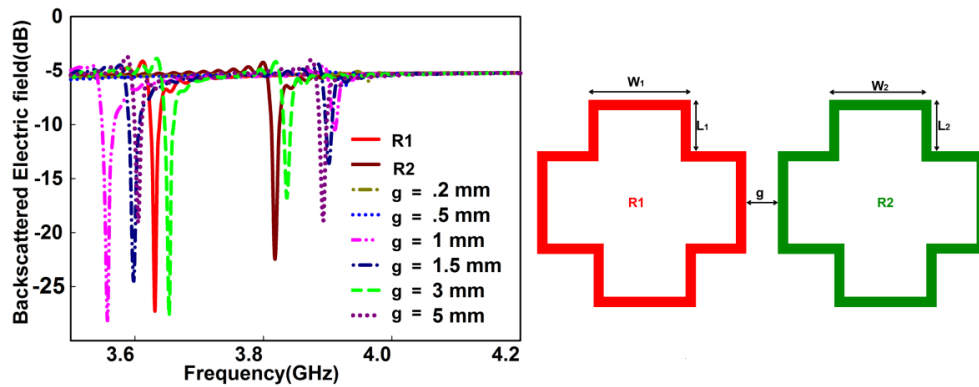


Figure 4. 15: Optimising distance between two resonators R1 and R2.
 $W_1 = 9.5 \text{ mm}$, $L_1 = 3.5 \text{ mm}$, $W_2 = 9.5 \text{ mm}$, $L_2 = 3.5 \text{ mm}$,
 substrate height = 1 mm and $\epsilon_r = 2.2$

From the figure it is clear that, for small gaps up to 0.5 mm the resonances appear as single (if frequencies are close) or cannot be distinguished. For the distances 1 mm onward, separate resonances can be observed. But the shift from original resonance frequency is large. So for the resonators to resonate independently, large separation is needed both in space and frequency. To get a compact tag, 3 mm spacing is taken as optimum distance. Also, for better performance care is taken not to have resonators nearby

4.6.3. Number of nested resonators

The number of resonators that could be nested is studied by varying the number of nested resonators. The results with different number of nested

resonators are shown in figure 4.16. It is found that the outer resonance decreases in magnitude as nesting increases. Also, up to four resonators the resonances have considerable magnitude. Beyond that it becomes very weak and is difficult to detect. As it is seen, the problem is severe with the outermost resonator. For the innermost resonator the magnitude remains almost unchanged with nesting. It is noticed that up to 4 resonators nested in a group, it is possible to achieve a tolerable magnitude for outer resonators.

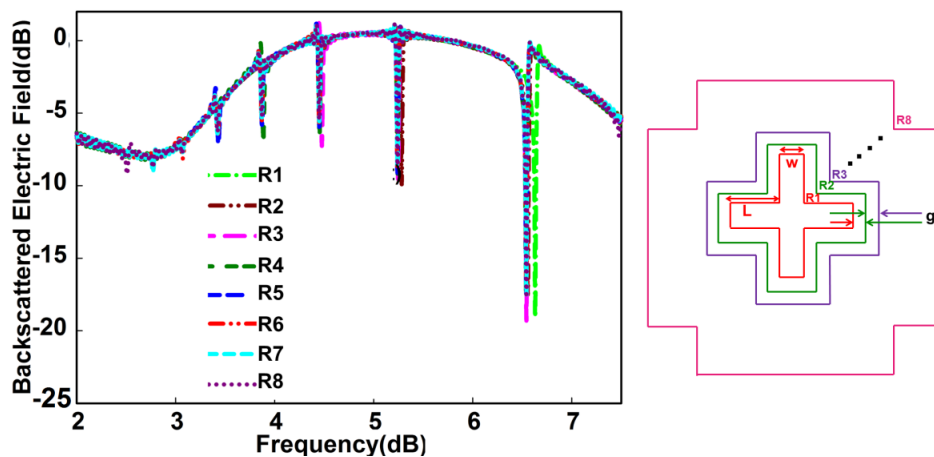


Figure 4.16: Study on number of resonator that can be nested. Resonator dimensions, $L = 3.5$ mm, $W = 3.5$ mm, $g = 0.5$ mm, microstrip width = 0.5 mm, $\epsilon_r = 2.2$ and height = 1 mm

4.6.4. Selection of Coding

For nested resonators, the influence of presence or absence of other resonators is a little more obvious than other resonators. It is impossible to assign a fixed frequency to each bit without slight shift. Because of this, all the combinations of frequencies should be pre-determined, stored and each received code has to be compared with the stored ones. Frequency shift coding technique is difficult to imply due to the above problem. The coding

reliable for this tag is presence or absence technique which has a 1:1 correspondence with the number of bits. To increase the coding capacity, the only solution is to increase the number of resonators. The nesting property utilizes the tag surface efficiently and hence offers compactness.

4.6.4.1. 8 Bit tag using cross loop resonator

A Chipless RFID tag with a coding capacity of 8 bits using cross loop resonator is discussed in this section. The geometry of the tag is evolved by carefully positioning resonators as different nested sets. Two sets of such nested cross loop resonators are arranged nearby at optimum locations to form an eight bit tag. Each set consists of four resonators. The resonators are nested with a gap of 0.5 mm and individual sets are separated with a distance not less than 3 mm. The gaps between nested resonators and the adjacent sets are selected as a compromise between the compactness and isolation between resonators. To reduce the coupling effects or interference between adjacent resonators, they are nested in a way so that no resonators of adjacent frequencies are placed adjacently. By taking the above mentioned positioning precautions, the interference between resonators are reduced considerably.

After determining the range of frequencies that is intended to use, the lower/first frequency resonator in the desired band is selected. Since cross loop resonator doesn't have any control over higher harmonic frequencies, the bandwidth available would be limited in between the selected lower frequency and its first harmonic frequency. As the last step, fix the number of resonators or bits needed and align them accordingly in different nested groups.

For the present tag the frequency range is selected in between 3.5 GHz and 6.8 GHz. The innermost resonator of the first set or the highest resonance is selected at 6.6 GHz. The second highest frequency resonator (6.04 GHz) is the innermost resonator of the second set and so on. The tag geometry is shown in figure 4.17. The tag has dimensions of 4.5cm \times 2.3cm. The perimeter of each resonator in the ascending order of frequency is given in table 4.5. The adjacent frequency resonators fall in separate nested set and the alternative in the same set.

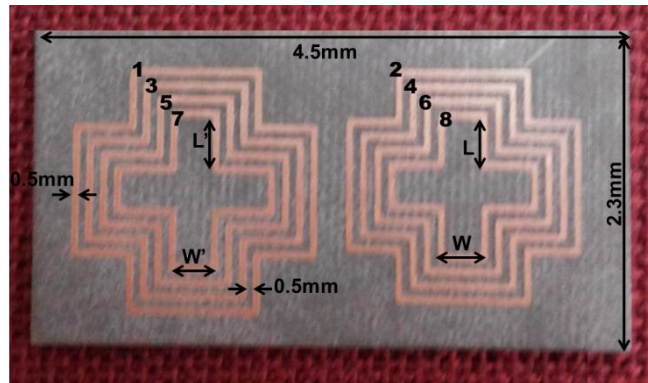


Figure 4.17: Geometry of the 8 bit tag based on cross loop resonators, $L = 3.5$ mm, $W = 3.5$ mm, $L' = 4$ mm, $W' = 3.5$ mm, Substrate height = 1 mm, $\epsilon_r = 2.2$

Table 4.5: Mean perimeter of the resonators of figure 4.17

Resonator	λ_g (mm)	F(GHz)
1	68	3.68
2	64	3.89
3	60	4.23
4	56	4.53
5	52	4.92
6	48	5.34
7	44	6.04
8	40	6.66

The simulation is done in CST with plane wave excitation. The backscattered field is measured with a probe. The simulated frequency response of the tag is shown in figure 4.18. The simulated response for the codes 1111 1111, 1111 1110 and 1110 0111 are displayed in the figure. The MSB is represented by lowest resonance frequency and the LSB by highest resonance frequency. The '1' corresponds to a resonance and the '0' absence of the same.

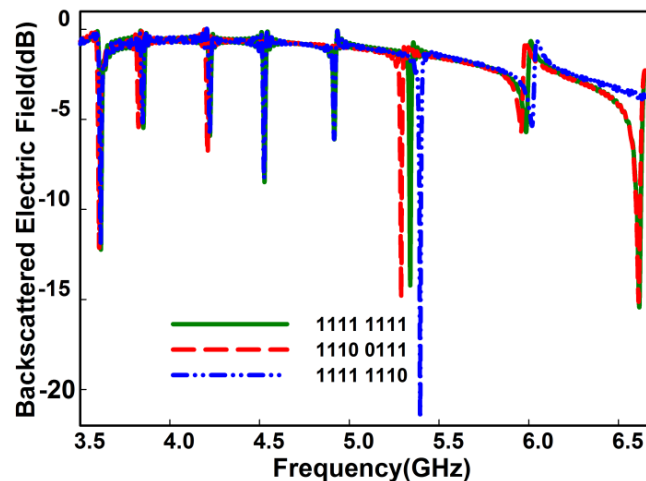


Figure 4.18: Different coding combinations simulated using the 8 bit cross loop resonator tag shown in figure 4.17

4.6.4.2. Measurement results and discussions

An eight bit Chipless RFID tag based on cross loop resonator is fabricated and measurements are carried out. The calibration method mentioned earlier removes the effects of surrounding stationary objects except the time varying white noise. The backscattering based Chipless RFID is basically based on the radar cross section technique. The only

difference is that the Chipless tag is based on the late time response which accounts for the presence of resonators on the tag.

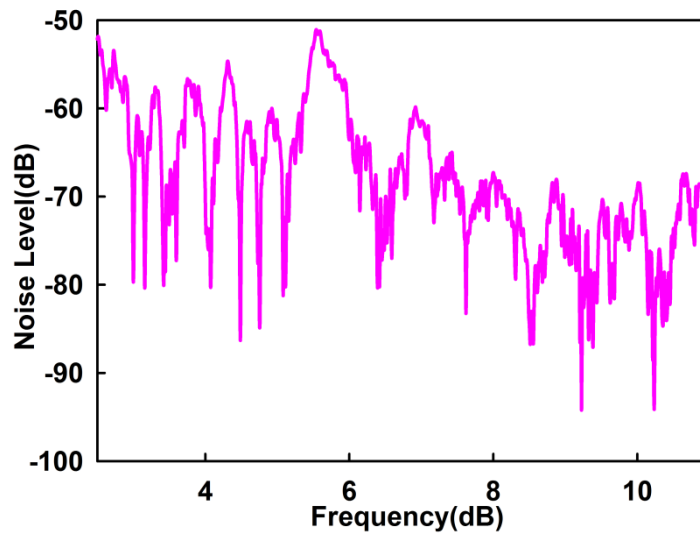


Figure 4.19: Measured noise floor in the measurement environment

Noise level in the measurement environment is shown in the figure 4.19. It is very clear that the detection is very difficult. The noise level can be minimized by subtracting S_{11} of the medium gain horn antenna measured in a previous time without the tag from the same with the tag. The backscattering from the tag should be better than this level for the effective extraction of the encoded data. The backscattering from the tag depends on many factors like transmitted power, reader antenna gain, distance between reader and tag. The relation between the factors determining the backscattering from the tag is detailed in [23]. Agilent PNA E8362B with 0dBm (1mW) power and a medium gain horn is used as the reader (as discussed in chapter 2.4).

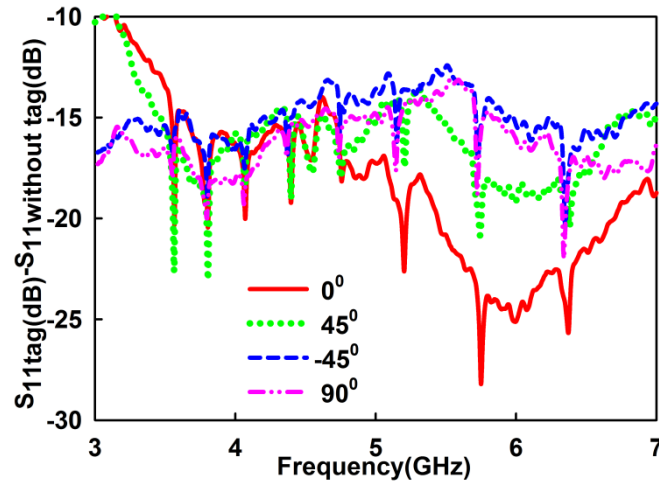


Figure 4.20: Measured backscattered response from the 8 bit cross loop resonator tag (figure 4.17) for different orientation in x-y plane

Magnitude response from the eight bit cross loop resonator based tag for different orientations is shown in figure 4.20. As in the case of a single scatterer, the tag with eight such scatterers is also presenting its all resonances for all the orientations. Presence/absence coding is used due to the before mentioned limitations. Presence of a resonance is denoted as a bit in this case and an all bit combination, i.e., 1111 1111 is the id encoded in the tag. All the presence and absence combinations of resonators should have stored for comparison with the received IDs. This is due to the increased coupling effects resulting from the nested nature. These coupling effects as concluded from the studies mentioned before, cause shifts in frequencies that could not be accountable in an assigned resolution bandwidth.

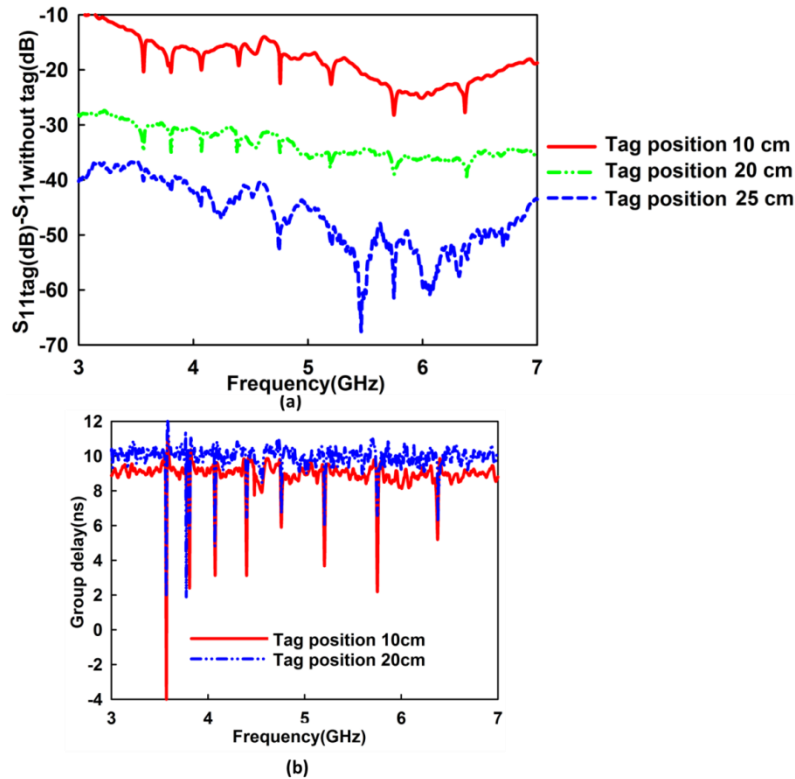


Figure 4.21: Performance of the tag (shown in figure 4.17) for different distances from the reader antenna (a) Backscattered power (b) Backscattered group delay

With 8 resonators in the tag, the system can tag 2^8 items. The size of the tag is $4.2 \times 2.3 \times 0.1 \text{ cm}^3$. So the surface coding capacity is 0.83 bits/cm^2 .

The performance of the tag for different distances between the tag and the reader is also shown in figure 4.21(a) and (b). The tag is working faithfully up to 20 cm. Beyond this distance the backscattering from the tag become equal or less than the noise floor shown in figure 4.19. So the data bits cannot be detected normally. This much distance is achievable with a power level of only 1mW and surely it can be enhanced by increased power levels. Group delay from the tag is also measured and is shown in figure

4.21(b). The data bits are well identifiable in the group delay measurement also.

4.6.5. 16 bit tag using cross loop resonator

The bit encoding capacity of the Chipless RFID tag in the last section can be increased by increasing the number of resonators. A 16 bit tag based on cross loop resonator and the geometry of the fabricated tag is shown in figure 4.22. The resonant frequencies and guided wave lengths of resonators constituting the tag are shown in table 4.6 in ascending order of frequency.

Table 4.6: Mean perimeter and the resonant frequencies of the resonators in 16 bit Chipless RFID tag shown in figure 4.22

Resonator	λ_g (mm)	F(GHz)
1	68	3.67
2	66	3.75
3	64	3.93
4	62	4.09
5	60	4.20
6	58	4.24
7	56	4.55
8	54	4.65
9	52	4.93
10	50	5.03
11	48	5.35
12	46	5.59
13	44	6.01
14	42	6.26
15	40	6.52
16	38	6.95

As it is done for the 8 bit tag, first the range of frequencies for the tag is selected between lowest resonator frequency and its first harmonic frequency.

Then resonators are arranged in to 4 sets of nested groups, each containing four resonators. Again, utmost care is taken to provide maximum separation between the adjacent resonant frequency resonators. L and W dimensions of each resonator are chosen suitably for the nesting.

Response of tag for different codes is shown in the figure 4.23. Since the frequency band available or that can be used is limited and predetermined, as the number of resonators increases, the resonances representing bits come closer. As a result, interference between adjacent frequencies or coupling in between them become dominant and dependence of resonance bits between each other becomes more evident. Another observation made is the frequency shift is more in the absence/presence of outermost resonators in each nested set. Coding should be done by comparing the measured results with the predetermined combinations.

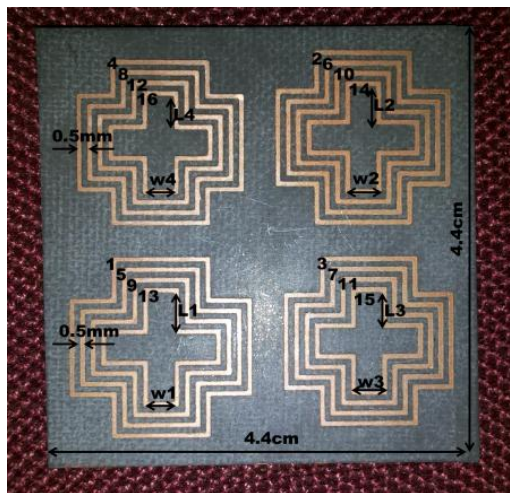


Figure 4.22: 16 bit tag using cross loop resonator, $\epsilon_r = 2.2$ substrate height = 1 mm, $L_1 = 4$ mm, $w_1 = 3.5$ mm, $L_2 = 3.75$ mm, $w_2 = 3.5$ mm, $L_3 = 3.5$ mm, $w_3 = 3.5$ mm, $L_4 = 3.25$ mm and $w_4 = 3.5$ mm

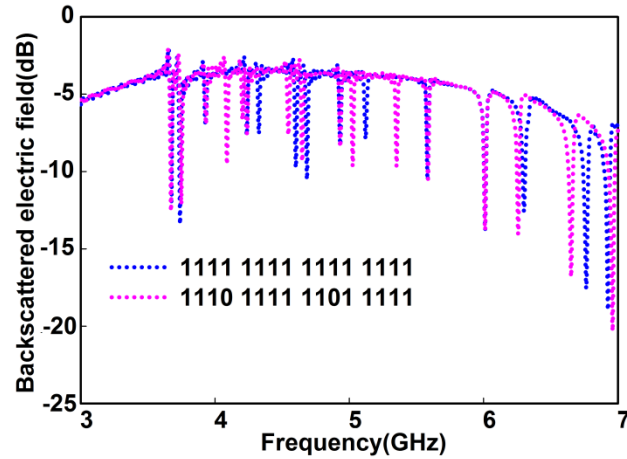


Figure 4.23: Different coding combinations simulated using 16 bit Chipless RFID tag shown in figure 4.22

The measured backscattered power is plotted in figure 4.24. The performance for different reading ranges is also shown. All the 16 bits are identifiable within 20 cm range from the reader antenna. The tag can ‘tag’ 65,536 items and it has dimensions of $4.4 \times 4.4 \times 1 \text{ cm}^3$. The surface encoding capacity is 1.71 bits/cm^2 .

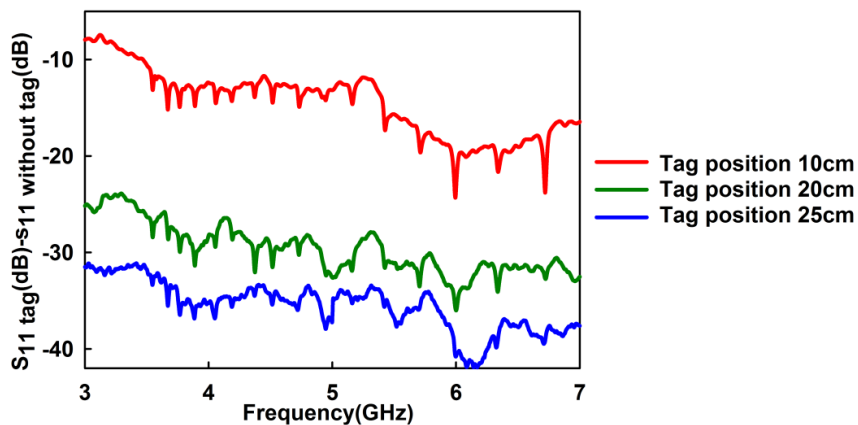


Figure 4.24: Measured backscattered power of 16 bit cross loop resonator tag (Shown in figure 4.22) for different distances

4.7. Polarization independent Chipless RFID tag using Stepped impedance resonators

Polarization or orientation independency to the incident interrogation signal is always an advantage to the Chipless tags. The tag proposed in the above section offers polarization insensitivity and is very compact. But the disadvantage of it as other multiscatterer based tags reported in the literature is that they don't have any mechanism to control the harmonic frequencies. Stepped impedance resonator as discussed in the previous chapter are structures that have control over higher harmonic frequencies. This control can be used in different ways in RFID applications. Nijas et.al utilized this property to define multiple bits with a single scatterer by using the fundamental and first harmonic frequencies [10].

By orthogonally and symmetrically aligning two identical SIRs, polarization independency can be achieved and is demonstrated in the proposed work. This particular arrangement retains all the other properties of SIRs. The entire UWB band can be used without the presence of harmonic frequencies of lowest frequency resonator. This can be effectively utilized to increase the coding capacity.

4.7.1. Basic scatterer characteristics

4.7.1.1. Selection of K and α

Impedance ratio (K) and length ratio (α) of SIR are defined in the previous chapter and are very important aspects of the resonator which adds flexibility in the design. They are selected individually for each resonator in such a way to ensure maximum compactness and separation between fundamental and first harmonic frequency. The selection is made based on

the figure 4.25 shown below. To get maximum compact structure, only $K < 1$ SIR is considered in this thesis [23].

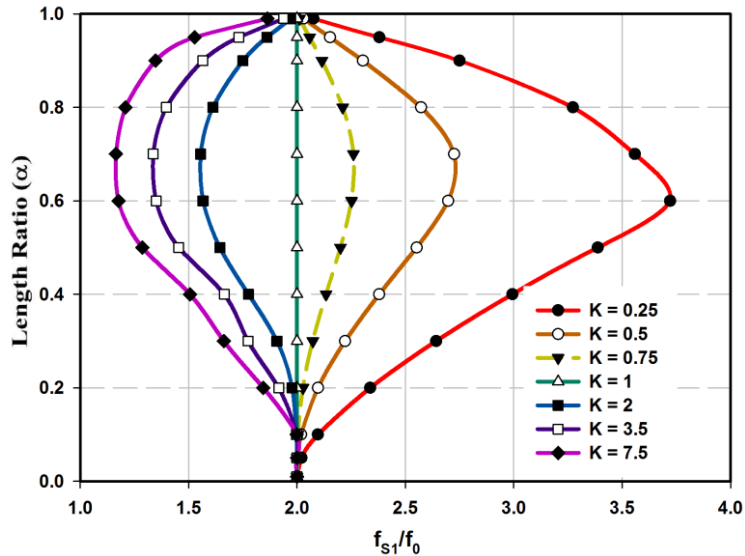


Figure 4.25: Relation between SIR's impedance ratio, length ratio and separation between Fundamental and 1st harmonic frequency. Courtesy C.M Nijas et al [10]

4.7.1.2. Backscattering from basic scatterer SIR

The basic scatterer, as discussed in the previous section is an orthogonal and symmetrical arrangement of two identical $\lambda/2$ SIRs. The performance of the tag for different polarizations of incident wave is demonstrated in Figure 4.26. Both simulation and measurement results are included to support the finding that the scatterer is polarization insensitive. It is seen that the scatterer presents its resonance for all orientations with respect to the axis of tag surface.

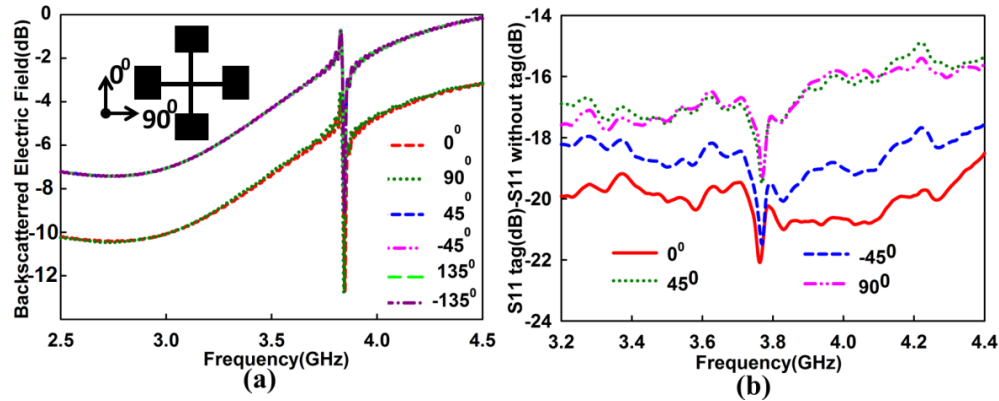


Figure 4.26: (a) Simulated backscattered electric field from a single scatterer for different orientations in x-y plane (b) Measured Backscattered signal from the scatterer for different orientations in x-y plane. Dimensions of SIRs are detailed in Table 4.7 and the parameters are defined according to figure 4.27(a).

When two SIRs joined as mentioned earlier there would be a shift in resonant frequency of the resultant scatterer. The resonances of single SIR and the scatterer designed with two SIR are shown in figure 4.27(b). Slight frequency shift is present owing to the coupling effects between two orthogonally joined SIRs.

Table 4.7: Dimensions of SIR shown in Figure 26(a)

L_1 (mm)	L_2 (mm)	W_1 (mm)	W_2 (mm)
5.4	2.42	0.5	5.89

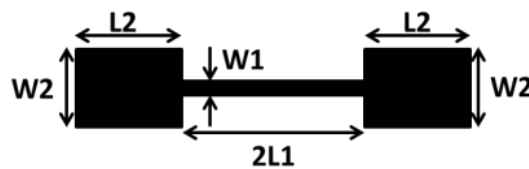


Figure 4.27(a): Dimensions of SIR forming the scatterer. Parameter values are given in table 4.7

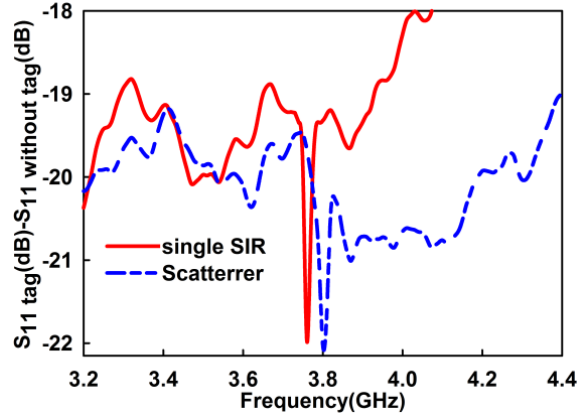


Figure 4.27(b): Measured response from single SIR and scatterer. Dimensions are given in Table 4.7 with respect to figure 4.27(a).

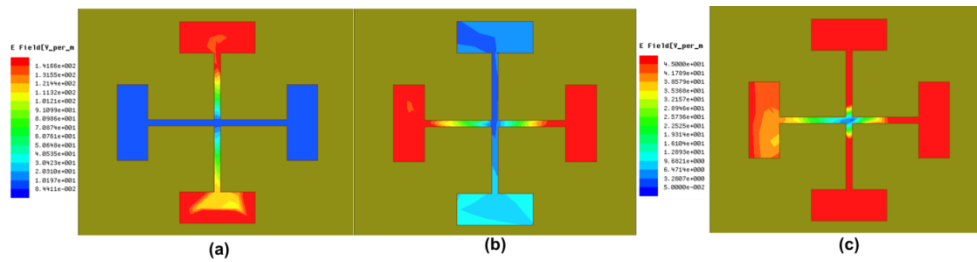


Figure 4.28: Electric field distribution of Orthogonally joined SIR (a) X polarized wave (b) Y polarized wave (c) 45° tilted wave. Dimensions are given in Table 4.7 with respect to figure 4.27(a).

The electric field distribution of scatterer formed by orthogonally joining identical SIRs are shown in figure 4.28. For X polarized incident wave and X aligned SIR shows a $\lambda/2$ distribution like a single SIR (figure 4.28(a)). For the Y polarized wave, the distribution is same as earlier one but on the Y oriented SIR (figure 4.28(b)). If the wave polarization is tilted 45° with respect to the scatterer, both SIRs will contribute to the resonance which will appear as a single resonance because of the identical nature of the SIRs (figure 4.28(c)).

4.7.1.3. Effect of substrate height

Performances of the SIR based scatterer for different substrate heights are shown in figure 4.29. The resonance becomes more identifiable as the height increases. But the bandwidth of individual resonances also increases with substrate height. Reduced or narrow bandwidth is very important for frequency domain Chipless RFID tags. Compact or thin tags are needed to compete with the advantages of barcodes. A height of 1 mm is selected as a compromise between the bandwidth and size.

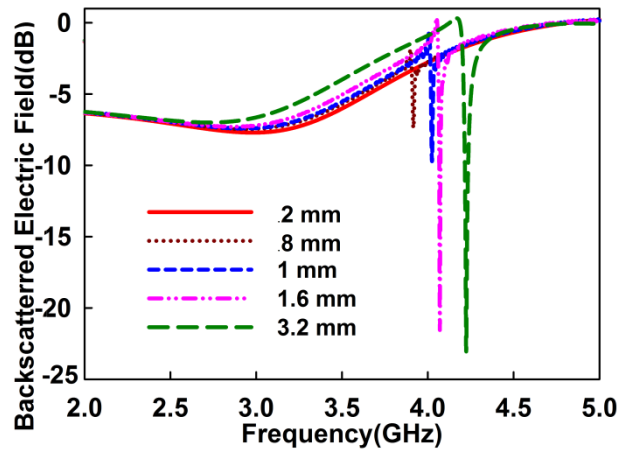


Figure 4.29: The performance of SIR based scatterer for different substrate heights. $\epsilon_r = 2.2$, $L_1 = 4.74$ mm, $L_2 = 3.81$ mm, $W_1 = 0.5$ mm and $W_2 = 3.73$ mm (Dimensions are specified with respect to Figure 4.27(a)).

4.7.1.4. Effect of coupling from adjacent scatterers

Coupling effect between resonators is the main challenge in multiresonator applications. Unlike the case of cross loop resonator based RFID tag, cross SIR based tag can have some isolation. Due to the scattered nature of resonators on tag surface rather than nested nature, designer can

choose suitable location of the resonators. Maximum care has taken to position the resonators so that adjacent frequency resonators are well separated. The parametric study to find out the minimum distance for maximum isolation is shown in figure 4.30. The distance between two scatterers designed at 3.2 GHz and 5.2 GHz is considered. It is seen from the figure that for distances less than 0.3 mm, there is a tendency of merging of these resonances. As distance increases, the resonances become more independent and isolated. Though 1 mm separation is sufficient for moderate performance, for the ease of fabrication and to ensure maximum isolation between resonators, 3 mm distance is selected for the current design.

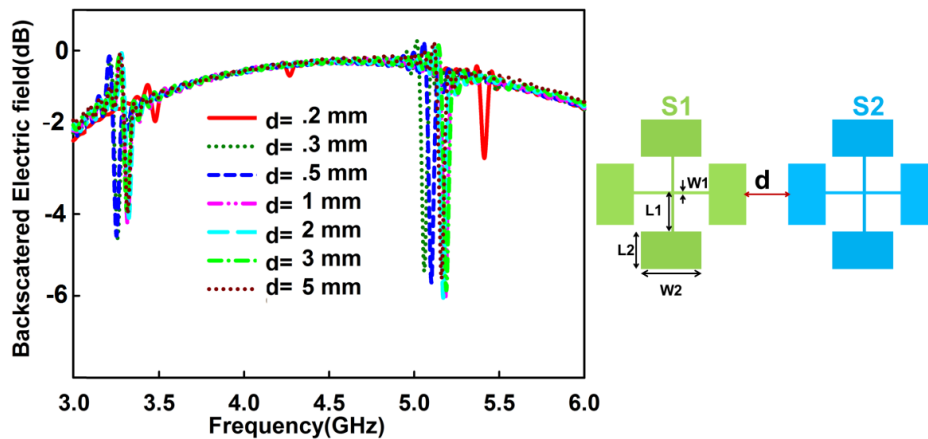


Figure 4.30: Optimization of distance between two scatterers. S1 dimensions: $L_1 = 5.27$ mm, $W_1 = 0.5$ mm, $L_2 = 3.99$ mm, $W_2 = 5.89$ mm, **S2 dimensions:** $L_1 = 5.2$ mm, $W_1 = 0.5$ mm, $L_2 = 2.83$ mm, $W_2 = 2.16$ mm

4.7.2. Method of Coding

Due to the flexible design of SIRs and the scattered nature of resonators on the tag surface, frequency shift coding can be applied for these tags.

Presence/absence technique is also applicable as well. Frequency shift coding technique achieves the same/more coding capacity than presence/absence technique with less number of resonators. This in turn reduces the interferences between resonances, offers more freedom to the positioning of resonators and most importantly enhances coding capacity with significant size reduction. So in the proposed tag frequency shift coding is used [7,9, 13,24].

4.7.3. Polarization insensitive Chipless RFID tag using Stepped impedance resonator

By virtue of the properties of stepped impedance resonator studied in the previous sections, a polarization insensitive Tag is designed with eight stepped impedance resonators. The basic scatterer is formed by orthogonally and symmetrically aligned $K < 1$ SIRs to ensure polarization insensitivity and compactness. Most of the tags reported in the literature [9,11,16] put stringent limits on the frequency band to be used. The entire UWB range from 3.1 GHz to 10.6 GHz is used for the current tag by using the harmonic control of stepped impedance resonators. By carefully selecting the impedance ratio and length ratio of the resonators, the first harmonic frequency of all the resonators are made to occur outside the UWB limit. The scatterer I is designed at 3.2 GHz. Referring the figure 4.25 the K value is chosen as 0.25 and α between 0.5 and 0.6 to move its first harmonic frequency above 10.1 GHz. Similar selection is used for other resonators also.

The geometry of the tag is shown in figure 4.31. The substrate used is RT Duroid 5880 ($\epsilon_r = 2.2$, $\tan\delta = 0.0009$, $h = 1$ mm). A minimum spacing of 3 mm between scatterers is ensured to mitigate the coupling effects and

the difficulties of in house fabrication. The scatterers are arranged non-uniformly on the tag surface to ensure minimum coupling effects between them. Starting from the lowest frequency resonator, in the ascending order of frequency the scatterers are labelled as I, II... VIII and represents frequencies 3.2 GHz, 4.1 GHz, 5.2 GHz, 6.3 GHz, 7.4 GHz, 8.4 GHz, 9.3 GHz and 10.5 GHz. The dimensions and design parameters are tabulated in table 4.8.

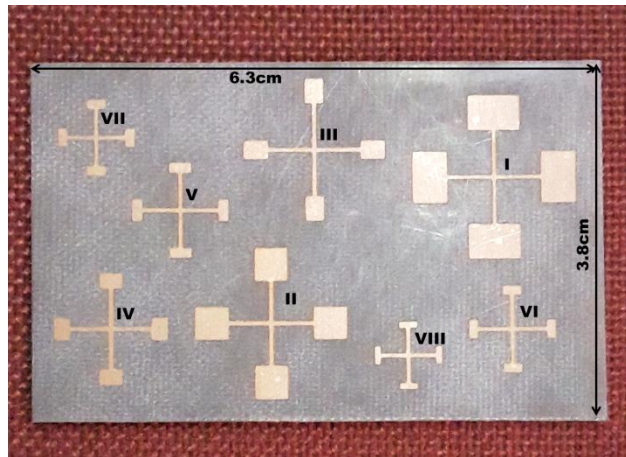


Figure 4.31: Geometry of the 8 bit polarization independent tag.
Tag dimensions are $6.3 \times 3.8 \times 0.1 \text{ cm}^3$. $\epsilon_r = 2.2$
Resonator dimensions are given in table 4.8

Frequency shift coding technique is used to enhance coding capacity and to use UWB efficiently. The entire UWB (3.1-10.6 GHz) is divided into 8 bands. First seven bands are having 1 GHz each, while the eighth or the last band is 600 MHz to limit the spectrum to 10.6 GHz. Each band is divided into subsections of 100 MHz each. These divisions are assigned codes 0 through 9. Position of the resonance in a particular Δf determines the digit assigned to it. So the first seven bands consist of 10 divisions while the last one has only six divisions. This non-uniform distribution is selected

to cover the entire UWB. This tag can tag 6, 0064,115 items. The overall dimension of the tag is $6.3 \times 3.8 \text{ cm}^2$. The tag has a surface encoding capacity of $1.08\text{bit}/\text{cm}^2$.

Table 4.8: Design parameters of the presented tag (Figure 4.31)

Parameters	Scatterers							
	I	II	III	IV	V	VI	VII	VIII
F(GHz)	3.2	4.1	5.2	6.3	7.4	8.4	9.3	10.5
K	0.25	0.35	0.5	0.45	0.45	0.5	0.5	0.5
α	0.5	0.5	0.4	0.35	0.3	0.3	0.35	0.3
$L_1(\text{mm})$	5.27	4.74	5.2	4.52	4.22	3.85	3.18	3.08
$L_2(\text{mm})$	3.99	3.81	2.83	1.78	1.18	1.08	1.13	0.754
$W_1(\text{mm})$	0.5	0.5	0.5	0.5	0.5	0.5	.5	0.5
$W_2(\text{mm})$	5.89	3.73	2.16	2.56	2.56	2.16	2.16	2.16

4.7.3.1. Measurements and discussions

Agilent PNA E8362B is used for the measurement as described earlier. The tag is read using continuous sweep from 3.1 GHz to 10.6 GHz. The magnitude response and group delay are shown in figure 4.32. Measurements for different orientations are also shown in figure 4.32. For different polarizations of reader signal or for different orientations with respect to the tag surface, the tag presents the same characteristics. As the coding technique used is frequency shift coding, there would be eight resonances always in the detected spectrum (unlike in the presence absence coding) which would be tuned in the assigned bandwidth. As mentioned before the backscattering from the tag should be greater than the noise floor shown in figure 4.19.

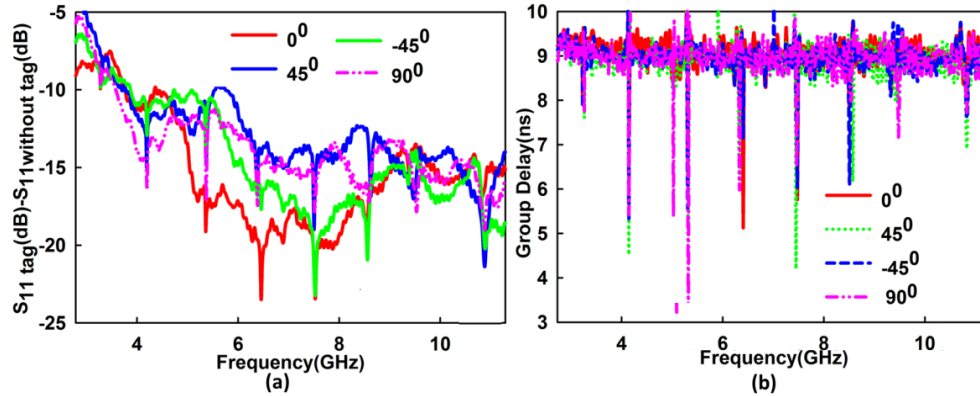


Figure 4.32: Measured backscattered response of 8 bit tag of figure 4.31
 (a) Magnitude response (b) Group delay

Tag measurement for different distances is shown in figure 4.33. Up to 40 cm from the reader, the tag is readable. After that the backscattering from the tag become insufficient to compete with the noise floor mentioned earlier.

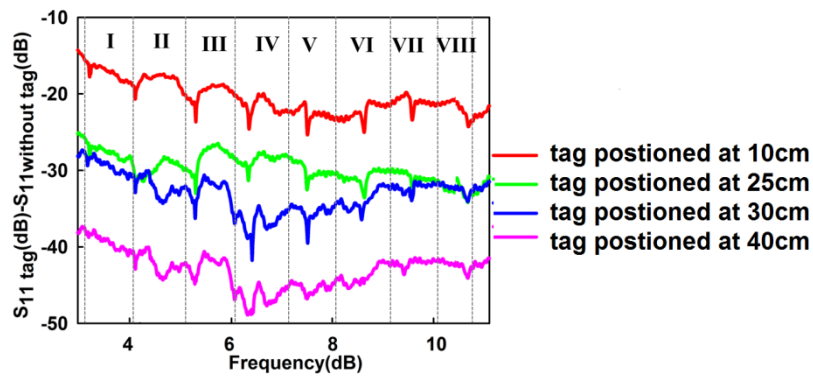


Figure 4.33: Performance of the tag (Shown in Figure 4.31) for different distances

Frequency division for each scatterer is also shown in figure 4.33. 3.1 GHz to 4.1 GHz is assigned to scatterer I, 4.1 GHz to 5.1 GHz for Scatterer II, ..., 9.1 GHz to 10.1 GHz for scatterer VII and finally 10.1 GHz to 10.6

GHz is assigned to scatterer VIII. The resonator is assigned a resolution bandwidth of 100 MHz. The tag has a bit encoding capacity (with respect to Equation 3.1) of 25.84 (6,0064,115).

4.7.4. High bit encoded Chipless RFID tag using SIR

Data encoding capacity can be increased by using resonators in vertical and horizontal directions. This concept is effectively demonstrated by A. Islam et.al [6]. The tag consists of metallic patches loaded with slots. Slots in the metallic patches are aligned in two polarizations that are mutually perpendicular to each other. The tag can be read by using dual polarized antenna or by two separate linearly polarized antennas aligned orthogonally. Besides increased data encoding, this concept offers reduced coupling effects between adjacent frequencies. This is possible by arranging adjacent frequency resonators in different polarizations just like orienting transmitting and receiving antennas at the reader side in orthogonal directions to reduce channel interference.

The proposed tag is a modification of the polarization independent tag discussed in the previous section. The basic scatterer is formed by two different stepped impedance resonators instead of identical ones in the former case. So that it can represent two data bits, one in x polarization (Horizontal) and the other in y (vertical) polarization. The scatterer geometry is shown in figure 4.34(a) and the frequency response in figure 4.34(b). The scatterer is formed of two SIRs designed at 3.8 GHz and 4.1 GHz. The dimensions of SIRs constituting the scatterer are detailed in table 4.9.

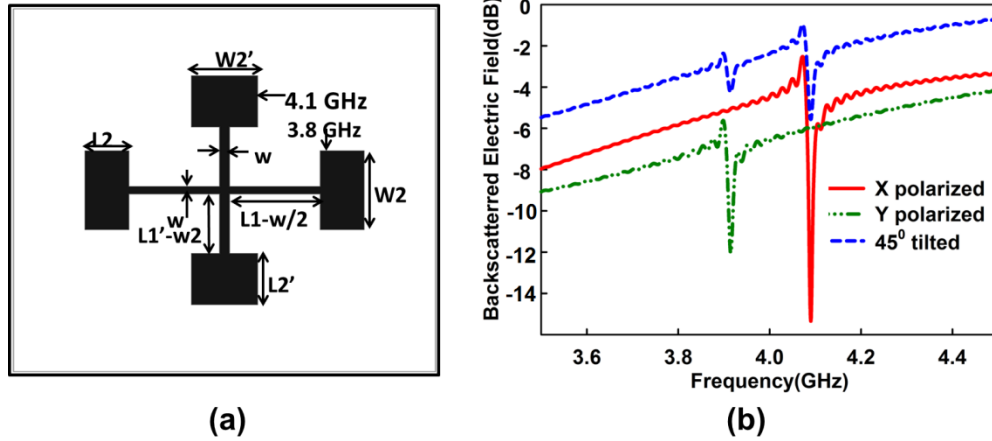


Figure 4.34: (a) Geometry of a single scatterer of high bit encoded tag. Substrate height = 1 mm and $\epsilon_r = 2.2$. Dimensions of SIRs constituting the scatterer are given in Table 4.9 (b) Response of the scatterer of Figure 34(a) for different polarizations of incident wave

Table 4.9: Dimensions of SIRs constituting the scatterer shown in figure 4.34(a)

L_1	5.39 mm
L_1'	4.74 mm
L_2	2.42 mm
L_2'	3.81 mm
W	0.5 mm
W_2	5.89 mm
W_2'	3.73 mm

The response of the scatterer for different polarizations of incident wave is shown in figure 4.34(b). For X polarized wave, the X directed SIR operating at 4.1 GHz is excited and for Y polarized wave SIR designed at 3.8 GHz is excited. For a 45° tilted orientation both SIRs present their resonances in the frequency spectrum.

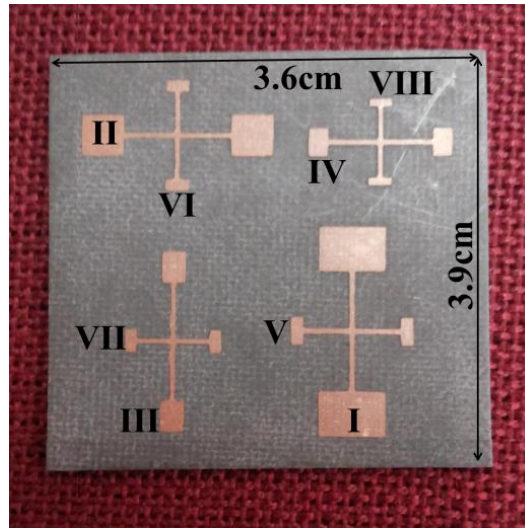


Figure 4.35: Geometry of the high bit encoded tag Dimensions: $3.9 \times 3.6 \times 0.1 \text{ cm}^3$. $\epsilon_r = 2.2$. Resonator dimensions are given in table 4.8

Here by encoding data in both polarizations, the tag achieve high surface encoding capacity. Present tag has double the coding capacity than the previous tag. The reduction in number of scatterers leads to compactness. All the other criterions for the arrangement of scatterers on the tag surface are as described earlier.

The geometry of the tag is shown in figure 4.35. The resonators in each scatterer are selected such that no consecutive resonances came in a given polarization. A random arrangement of scatterers is also done to reduce coupling effects. As discussed earlier a minimum distance of 3 mm is ensured in between the scatterers. The SIR dimensions, K and α value are same as detailed in table 4.8.

Frequency shift coding as discussed for the previous tag is also used to enhance coding capacity. The spectrum assigned for each resonator (the scatterer in the previous case) and the resolution bandwidth are identical for this case also. The tag can access 6, 0064,115 items and has an area of $3.9 \times 3.6 \text{ cm}^2$. The surface encoding capacity is 1.84 bits/cm^2 . So this tag attained double the bit encoding capacity and almost 50% reduction in tag surface area comparing the polarization insensitive RFID tag of previous section.

4.7.4.1. Measurement results

The backscattered signal from the tag is measured with two orthogonally placed horn antennas. A continuous sweep from 3.1 GHz to 10.6 GHz is employed. Each antenna reads the resonators aligned to its polarization. The entire frequency spectrum and each band is also subdivided in the same way.

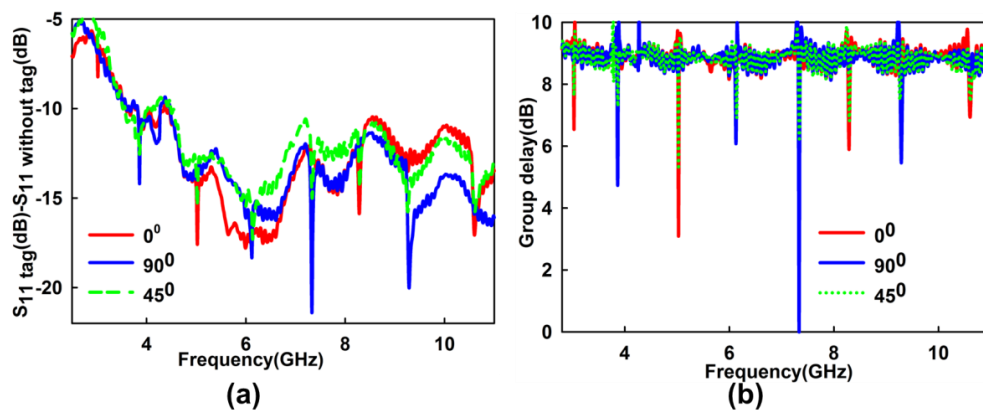


Figure 4.36: Measured responses of high bit encoded tag (shown in figure 4.35) (a) magnitude response for 3 different orientations (b) Group delay

The measured magnitude response and group delay are shown in figure 4.36. Three curves shown in the figure corresponds to the readings of

X (0°) oriented tag, Y (90°) oriented tag and for 45° oriented tag. scatterer I, III, V and VII are aligned in X direction (0°) and scatterer II, IV, VI and VIII are aligned in the Y direction (90°). The tag is readable up to 40 cm.

4.7.5. Modified Compact Chipless RFID tag using SIR

The polarization independency and high bit encoding capacity of the scatterer formed by two SIRs aligned orthogonally and symmetrically are discussed so far. Examining the Electric field distribution on the scatterer (figure 4.28), electric field is minimum/the current distribution is maximum at the intersection of the scatterers. The scatterer would perform identical even after shorting at the intersection and removing one symmetric section as shown in figure 4.37.

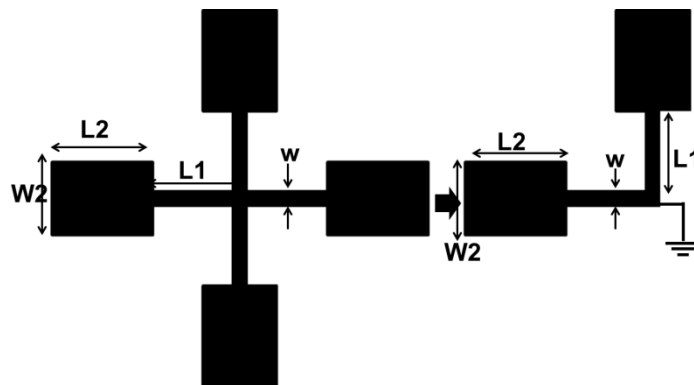


Figure 4.37: Transformation of the basic scatterer to compact form.
Substrate height = 1 mm and $\epsilon_r = 2.2$, $L_1 = 4.74$ mm,
 $L_2 = 3.81$ mm, $W_1 = 0.5$ mm, $W_2 = 3.73$ mm.

The theory of transformation of simple half wavelength resonator to quarter wave resonator by shorting at the current maximum point is applicable here also. The transformation doesn't alter the resonance frequency. The resonators

are quarter wave stepped impedance resonators. The short to ground ensures that the resonators provide the fundamental mode as per the SIR theory [23].

Backscattering from resonator shown in figure 4.37 and its compact form is shown in figure 4.38. The compact resonator's resonance shifts to lower side of spectrum. This is attributed to the increment in L_1 by length of the short to the ground. As seen from the figure 4.38, the backscattered power level is also reduced. This is due to the inverse relation between the size of the scatterer and the backscattered power level. This will also leads to the reduced range of detection of the Chipless RFID tag.

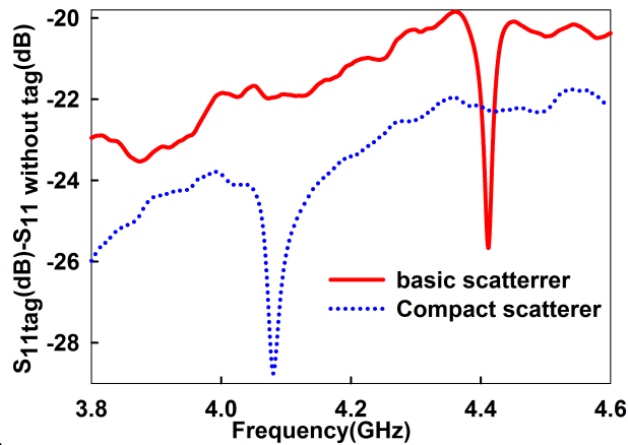


Figure 4.38: Comparison between the magnitude response of the basic scatterer and its compact form (figure 4.37). Substrate height = 1 mm and $\epsilon_r = 2.2$, $L_1 = 4.74$ mm, $L_2 = 3.89$ mm, $W_1 = 0.5$ mm, $W_2 = 3.73$ mm

The tag can be designed either for polarization insensitivity or for high bit encoding capacity depending on the application. Geometry of the compact polarization insensitive tag is shown in figure 4.39. Dimensions of

SIRs on the tag are same as those detailed in Table 4.8. The overall dimension of the tag is $3 \times 4 \times 0.1\text{cm}^3$.

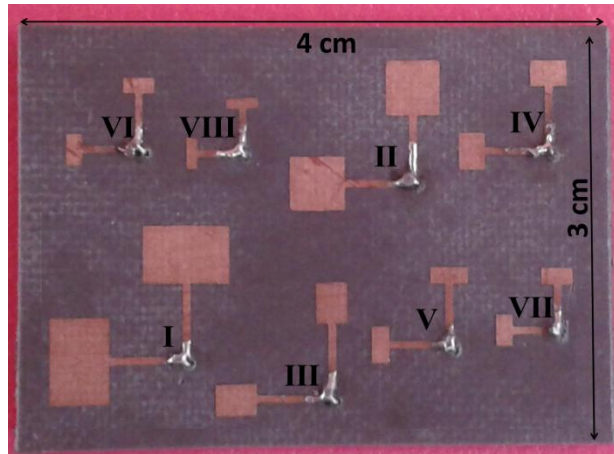


Figure 4.39: Geometry of compact polarization independent tag. Resonator dimensions are tabulated in table 4.8. Dimension of the tag is $3 \times 4 \times 0.1\text{cm}^3$.

The measured backscattered response is shown in figure 4.40. All the 8 resonances for the 8 resonators are seen in the figure. Measured responses for different orientations are also shown to prove the polarization insensitivity. With the same FSC technique, the tag can tag 6, 0064,115 items. The bit encoding capacity of the tag is 25.84. The surface encoding capacity is 2.15 bit/cm^2 . The tag attained double the surface encoding capacity than the orthogonally joined SIR tag.

The performance of the tag at different distances is shown in figure 4.41. The compactness of the tag reduces its readable range. The tag is readable only up to 10 cm. The tag is best suited for applications involving very near field communication.

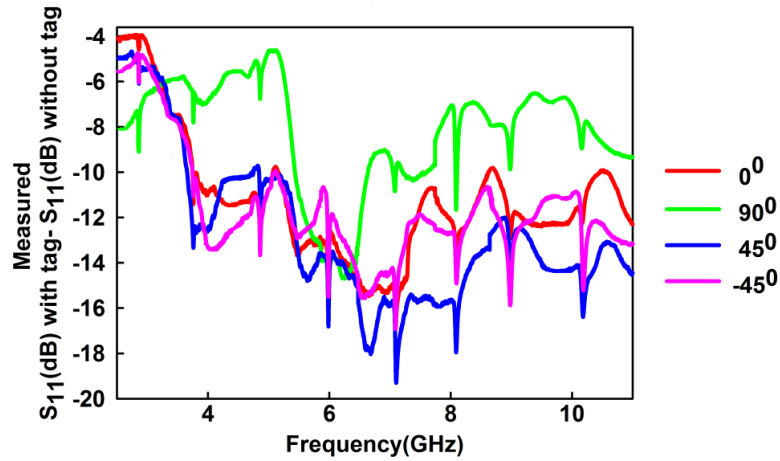


Figure 4.40: Measured backscattered response of the compact polarization independent tag shown in 4.39. Dimensions are shown in table 4.8.

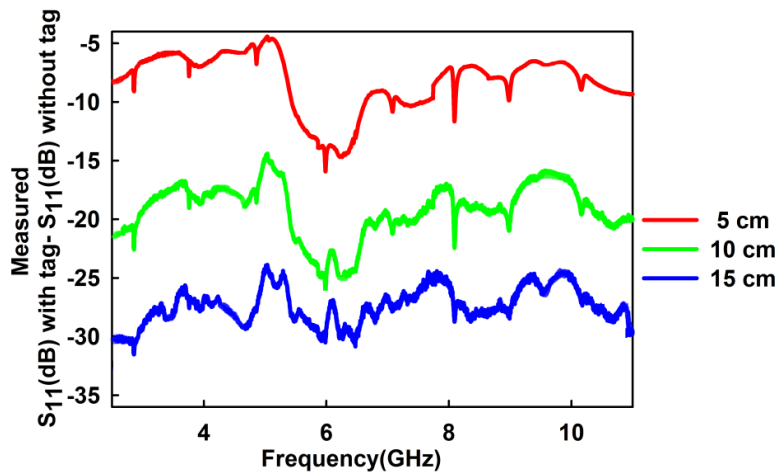


Figure 4.41: Performance of compact polarization independent tag (Figure 4.39) at different distances

The tag can also be arranged for high bit encoding applications. The scatterer in this case has two different quarter wave SIRs joined together with a common short to the ground. Here the bits/scatterer is 2 which will increase the bit encoding capacity. A tag designed in such a way is shown in

figure 4.42. The measured backscattered response is shown in figure 4.43. The tag has an overall dimension of $3 \times 2.5 \times 0.1 \text{ cm}^3$. The surface encoding capacity of the tag is 3.45 bits/cm^2 , which is approximately double the orthogonally joined $\lambda/2$ SIR case.

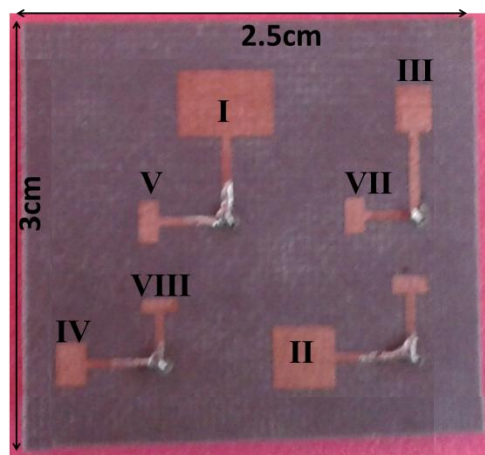


Figure 4.42: Geometry of compact high bit encoded Chipless RFID tag whose resonator dimensions are given in Table 4.8. Dimension of the tag is $3 \times 2.5 \times 0.1 \text{ cm}^3$.

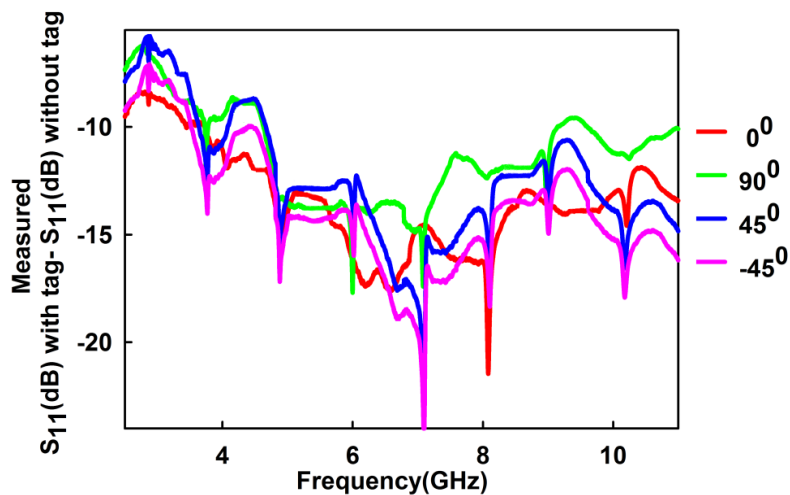


Figure 4.43: Measured response of high bit encoded Chipless RFID tag shown in figure 4.42 for different orientations

4.8. Comparison of different Chipless RFID tags in literature with the tags developed

Different frequency domain Chipless RFID tags reported in literature are compared with the tags developed in table 4.10. Freedom in orientation, bit encoding capacity and control over harmonic frequencies are the main achievements of the tags developed in the chapter

Table 4.10: Comparison of different Chipless RFID tags

Tag	Surface coding capacity(bit/cm ³)	Freedom in orientation	Control over harmonic frequency
Dipole barcode[25]	1.01	No	No
Multiband dipole[26]	0.81	No	No
SRR Array[27]	2.8	No	No
Coplanar strip[28]	3.3	No	No
Letter ID[29]	4.6	No	No
Slotted monopole[30]	1	No	No
Elliptical dipole[31]	0.36	No	No
SLMPA[9]	0.18	No	No
Multilayer Patch[32]	0.61	No	No
Dual polarized slot loaded tag[6]	>7	No	No
Multibit SIR tag[10]	>7	No	Yes
Cross loop resonator based tag	0.82	Yes	No
SIR based polarization independent tag	1.08	Yes	Yes
SIR based high bit encoded tag	1.84	No	Yes
SIR based compact polarization independent tag	2.15	Yes	Yes
SIR based compact High bit encoded tag	3.45	No	Yes

4.9. Conclusion

Multiscatterer based Chipless RFID tags are discussed in this chapter. Polarization insensitivity is emphasized in the presented tags. Two types of scatterers suitable for polarization independent application are presented. The former is a cross loop resonator which is more compact structure than the circular ring and support nesting. An 8bit and 16 bit tag are fabricated and the measured results are presented. Presence and absence coding is preferred for this particular case. The coding capacity is $0.83\text{bits}/\text{cm}^2$ and $1.71\text{bits}/\text{cm}^2$, respectively for 8 bit and 16 bit tag. The tag is readable up to 20 cm from the reader.

SIR based scatterer is the other structure proposed in this thesis. Due to flexible design and reduced coupling effects, Frequency Shift Coding is employed for this type of scatterer based tag. The tag can be designed for polarization independency or high bit encoding capacity depending on the application. The polarization independent tag has a surface encoding capacity of $1.08\text{ bits}/\text{cm}^2$ and the high bit encoded tag has a surface encoding capacity of $1.84\text{ bits}/\text{cm}^2$. The tag can be read up to 40 cm from the reader antenna. Finally a compact version of the SIR based tag is presented. The modified compact tag has a surface encoding capacity of $2.15\text{ bits}/\text{cm}^2$ for polarization insensitive tag and $3.54\text{ bits}/\text{cm}^2$ for high bit encoding capacity tag.

The tags presented in this chapter are given in table 4.11 along with their properties.

Table 4.11: The tags presented in this chapter

Tag	Surface coding capacity with present/absent coding(bit/cm ²)	Surface coding capacity with FSC(bit/cm ²)	Detection range	Freedom in orientation
Cross loop resonator based tag	0.82	NA	20	Yes
SIR based polarization independent tag	0.33	1.08	40	Yes
SIR based high bit encoded tag	0.57	1.84	40	No
SIR based compact polarization independent tag	0.67	2.15	10	Yes
SIR based compact High bit encoded tag	1.07	3.45	10	No

References

- [1] S. Preradovic, I. Balbin, N. Karmakar and G. F. Swiegers, “Multiresonator-based chipless RFID system for low-cost item tracking”, *IEEE Transactions on Microwave Theory and Techniques*, Vol.57, No.5, pp.1411-1419, 2009.
- [2] C. M. Nijas, R. Dinesh, U. Deepak, A. Rasheed, S. Mridula, K. Vasudevan, and P. Mohanan, “Chipless RFID Tag Using Multiple Microstrip Open Stub Resonators,” *IEEE Transactions on Antennas and Propagation*, Vol. 60, No. 9, pp. 4429-4432, Sep. 2012.
- [3] M. Sumi, R. Dinesh, C.M. Nijas, S. Mridula and P. Mohanan, “Frequency Coded Chipless RFID Tag using Spurline Resonators”, *Radioengineering*, Vol. 23, pp.203-208, April 2014.

- [4] R. Dinesh, P.V. Anila, C. M. Nijas, M. Sumi and P. Mohanan, “Open loop multi-resonator based chipless rfid tag”, General Assembly and Scientific Symposium (URSI GASS), Beijing XXXIth URSI , 16-23 August 2014, pp 1-4
- [5] Md. Shakil Bhuiyan, AKM Azad and Nemaï Karmakar, “Dual-band Modified Complementary Split Ring Resonator (MCSRR) Based Multi-resonator Circuit for Chipless RFID Tag” 2013 IEEE Eighth International Conference on Intelligent Sensors, Sensor Networks and Information Processing, Melbourne, VIC, 2-5 April 2013, pp- 277 – 281.
- [6] A. Islam and N. C. Karmakal, “A Novel Compact Printable Dual Polarized Chipless RFID System,” IEEE Transactions on Microwave Theory and Techniques, Vol. 60, No. 7, pp. 2142-2151, Jul. 2012
- [7] Arnaud Vena, Etienne Perret and Smail Tedjini, “Chipless RFID Tag Using Hybrid Coding Technique”, IEEE Transactions on Microwave Theory and Techniques, Vol. 59, No. 12, pp 3356-3364 December 2011.
- [8] Arnaud Vena, Etienne Perret and Smail Tedjini, “A Depolarizing Chipless RFID Tag for Robust Detection and Its FCC Compliant UWB Reading System”, IEEE Transactions on Microwave Theory and Techniques, Vol. 61, No. 8, pp. 2982-2994 August 2013.
- [9] A. Vena, E. Perret and S. Tedjini “A Fully Printable Chipless RFID Tag With Detuning Correction Technique,” IEEE Microwave and Wireless Components Letters, Vol. 22, No. 4, pp. 209-211, April 2012.
- [10] C. M. Nijas, U. Deepak, P. V. Vinesh, R. Sujith, S.Mridula and K.Vasudevan, “Low-Cost Multiple-Bit Encoded Chipless RFID Tag” IEEE Transactions On Antennas And propagation, Vol. 62, No. 9, pp. 4762-4770, September 2014.
- [11] Md. Shakil Bhuiyan, N. Karmakar,” Chipless RFID tag based on split-wheel resonators”, 7th European Conference on Antennas and Propagation (EuCAP) 2013, Gothenburg, 8-12 April 2013, pp 3054-3057
- [12] I. Balbin, N. Karmakar, “Phase-Encoded Chipless RFID Transponder for Large-Scale Low-Cost Applications”, IEEE Microwave And Wireless Components Letters, Vol. 19, No. 8, pp. 509-511, August 2009

- [13] A. Vena, E. Perret, and S. Tedjini, "Design rules for chipless RFIDtags based on multiple scatterers," *Ann. Telecommun. - Ann. DesTélécommunications*, Vol. 68, No. 7–8, pp. 361–374, Feb. 2013.
- [14] K.C. Gupta, R.Garg, I. Bahl, P. Bhartia, "Microstrip lines and slotlines" 2nd edition, Artech House, Boston London.
- [15] M. A. Islam, Y. Yap, N. Karmakar, A. Azad, "Orientation independent compact chipless RFID tag", *Progress In Electromagnetics Research C*, Vol. 33, 55-66, 2012
- [16] D. Laila, R. Thomas, C. M. Nijas, and P. Mohanan, "A novel polarization independent Chipless RFID tag using multiple resonators," *Progress In Electromagnetics Research Letters*, Vol. 55, 61-66, 2015
- [17] A. Vena, P. Etienne and S. Tedjini, "High-capacity chipless RFID tag insensitive to the polarization", *IEEE Transactions on Antennas and Propagation*, Vol 60, no.10, 2012,pp 4509-4515, 2012
- [18] R. Rezaiesarlak and M. Mantaghi, "Chipless RFID- Design Procedure and Techniques", Springer, Virginia Tech, Blacksburg, VA, USA
- [19] P. Kalansuriya, N. Karmakar and E. Viterbo, "On the Detection of Frequency-Spectra-Based Chipless RFID Using UWB Impulsed Interrogation" *IEEE Transactions On microwave Theory And Techniques*, Vol. 60, No. 12, pp 4187-4197, December 2012.
- [20] K. Chang, Lung-Hwa Hsieh "Microwave Ring Circuits and Related Structures", 2nd edition. Wiley-Interscience, A John Wiley and Sons, INC, Publication
- [21] C. A Balanis, *Antenna Theory Analysis and Design*, 3rd edition, Wiley Interscience, A John Wiley & Sons. INC, Publication.
- [22] R. Anee and N. C. Karmakar, "Chipless RFID Tag Localization,"*IEEE Transactions on Microwave Theory and Techniques*, Vol. 61, No. 11, pp 4008-4017 November 2013.
- [23] M. Makimoto and S. Yamashita, "Microwave Resonators and Filters for Wireless Communication, Theory, Design and Application" *Springer Series in Advanced Microelectronics*, Vol. 4, 2001.

- [24] Vena A, Perret E, Tedjini S, Novel compact RFID chipless tag. Proc. Progress Electromag. Res. Symp, p. 20–23, 2011
- [25] I. Jalaly and I. D. Robertson, “Capacitively-tuned split microstrip resonators for RFID barcodes,” in Proc. Eur. Microw. Conf., Oct. 4–6, 2005, Vol. 2, p. 4.
- [26] I. Jalaly and I. Robertson, “RF barcodes using multiple frequency bands,” in IEEE MTT-S Int. Microw. Symp. Dig., 2005, Vol. 1–4, pp. 139–142.
- [27] J. Hyeong-Seok, L. Won-Gyu, O. Kyoung-Sub, M. Seong-Mo, and Y. Jong-Won, “Design of low-cost chipless system using printable Chipless tag with electromagnetic code,” IEEE Microw. Wireless Compon. Lett., Vol. 20, pp. 640–642, 2010
- [28] A. Vena, E. Perret, and S. Tedjini, “Novel compact RFID chipless tag”, Progr. Electromagn. Res. Symp. Proc., Morocco, Mar. 20–23, 2011, pp. 1062–1066.
- [29] T. Singh, S. Tedjini, E. Perret, and A. Vena, “A frequency signature based method for the RF identification of letters,” in Proc. IEEE Int.Conf. RFID, Apr. 12–14, 2011, pp. 1–5.
- [30] I. Balbin and N. Karmakar, “Radio Frequency Transponder System,” Australian Provisional Patent, DCC, Ref: 30684143/DBW, Oct. 20, 2008.
- [31] M. Manteghi, “A novel approach to improve noise reduction in the Matrix Pencil Algorithm for chipless RFID tag detection,” in Proc. IEEE Antennas and Propagation Soc. Int. Symp., Jul. 11–17, 2010, pp. 1–4.
- [32] S. Mukherjee and G. Chakraborty, “Chipless RFID using stacked multilayer patches,” in Proc. Appl. Electromagn. Conf., Dec. 14–16, 2009, pp. 1–4.

.....✉.....

**TIME DOMAIN ANALYSIS OF
FREQUENCY DOMAIN CHIPLESS RFID TAGS**

Contents	5.1. Introduction
	5.2. Backscattering from frequency domain tags in time domain
	5.3. Tag performance in time domain using Numerical methods
	5.4. Steps to Extract Spectral Signature from the Backscattered Signal
	5.5. Time Domain Analysis of Measured Time Domain Data from Different Practical Environments
	5.6. Conclusion

An analysis of backscattered signal from frequency domain Chipless RFID tag in time domain is presented in this chapter. Clear distinction between the structural mode and antenna mode are demonstrated and the tag ID is extracted by processing the antenna mode. The chapter also emphasis on the importance of time domain reading techniques of frequency domain tags. Simulations in CST microwave studio software are used for the initial studies on extraction of structural and antenna modes from the backscattered signal. Measurements of time domain reading have been conducted using the Agilent PNA E8362B by enabling the time domain option. A simple algorithm employing Hamming window and sliding windows is used to extract tag ID and it enhances the reading range and decoding of encoded bits in the tag. The tag information is extracted for different practical scenarios.

5.1. Introduction

Two important classes of Chipless RFID tags are frequency domain based and time domain based tags. Peaks/dips in magnitude of resonant frequency define tag ID in frequency domain tags whereas in time domain tags the delay between the reflections of transmitted pulse define the tag ID. Both classes of tags have its own advantages and disadvantages and are narrated in the introduction chapter. As this thesis is concerned with frequency domain based Chipless RFID tags, here it is specifying only the enhancements for frequency domain Chipless RFID system. The duality between time and frequency domain leads the researchers to think about using methods of time domain in frequency domain and thus bringing its advantages to frequency domain tags [1-6].

The main disadvantage of frequency domain based Chipless RFID tags reported in literature is its expensive reader using wide band Voltage Controlled Oscillator (VCO). Moreover, their long distance reading requires adequate orientation and calibration to remove interference arising from clutter and antenna coupling [7-11]. A solution for this disadvantage is deployment of time domain analysis and reading techniques that are simple and less expensive. Moreover, they do not require complicated calibration and stringent orientation requirements [12-15]. With the adoption of time domain techniques, the benefits seen in time domain tags can be realized for frequency domain tags in addition to their inherent high bit encoding capacity.

The advantages of time domain analysis in the interrogation of frequency domain tags are

- Low cost Reader: Commercially available low cost UWB-IR (Ultra-Wide Band Impulse Radar) reader can be easily employed.
- Low power requirement: Low power is required since the reader is active only for a short duration of time.
- Easy tag position: Freedom in tag positioning and enhanced reading ranges.
- Calibration free: No calibration tags or reference ground planes are required.

5.1.1. Chipless RFID Reader based on UWB IR

As previously stated, the time-frequency duality can be exploited to read frequency domain tags using Ultra-Wide Band Impulse Radar (UWB-IR) technology based reader [16-20]. UWB IR modules are available in markets and are in compliance with Federal Communications Commission (FCC) standards [19]. The frequency modulated continuous wave (FMCW) based reader signal has extremely low power amplitude as per the FCC standards whereas the UWB IR approach employs a very low duty cycle short pulse having high power.

Gaussian pulse (or its higher order derivatives) of short duration (a few picoseconds) is used in the UWB IR approach for interrogation. These are preferred in UWB applications because they could be generated easily and they have no direct current component. The absence of direct current component is desired in the transmitter antenna to radiate efficiently.

Derivatives of Gaussian pulses are used as they fit to the FCC emission mask with a better performance and safe level. In the time domain, derivatives of Gaussian pulse look like sinusoids modulated by a Gaussian pulse shaped envelop. The number of zero crossings in time increases with the order of the derivative. Also, with the order of derivatives energy moves to higher frequencies. Figure 5.1 shows different Gaussian pulses and their frequency spectrum for UWB systems.

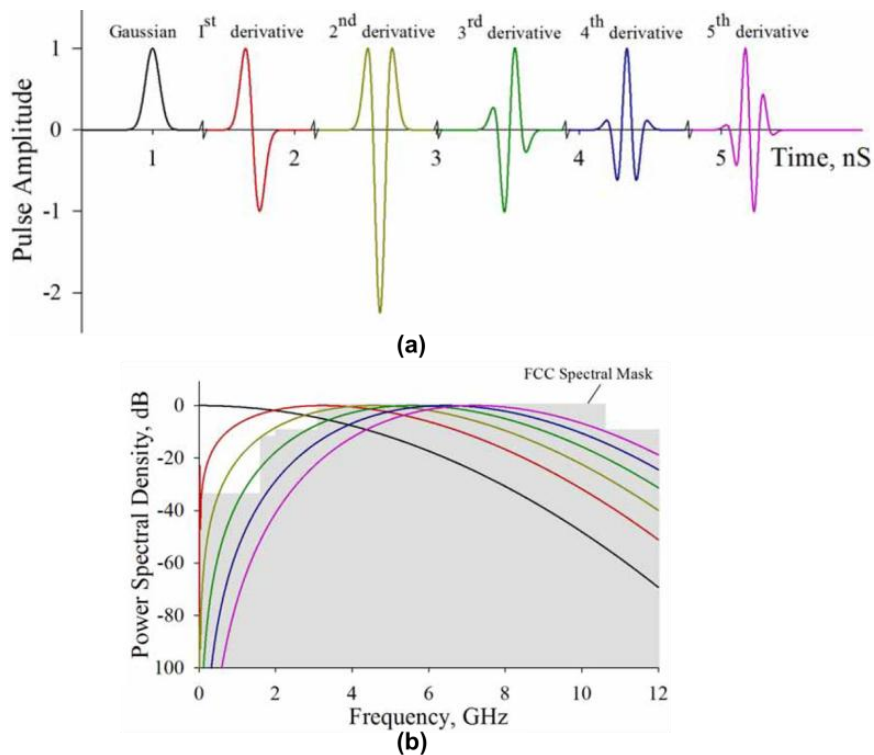


Figure 5.1: Gaussian pulse and its derivatives (a) waveforms in the time domain and (b) Power spectral densities

Fabrication expense of UWB IR transmitter is low compared to the FMCW transmitter [21]. The only complication is with the high sampling

in equivalent-time sampling based readers to replace expensive high sampling rate ADCs. Delay generator (producing delays of tens of picoseconds) is required to activate the sampling circuit during the assigned slot of time only. The modified block diagram with time sampling feature is shown in figure 5.3. Other approaches based on commercially available UWB IR to read Chipless RFID tags are also reported [2], [18]. Averaging method over hundreds of measurements can also be used to enhance signal to noise ratio of the reader [23].

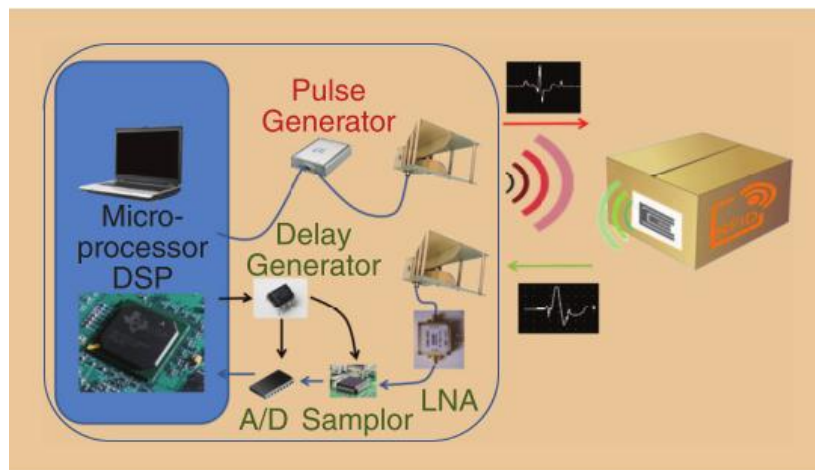


Figure 5.3: Block diagram of a Chipless reader based on equivalent time sampling. Courtesy: Smail Tedjini et al. [26].

5.2. Backscattering from frequency domain tags in time domain

A Chipless RFID tag excited with an impulse is shown in figure 5.4. Single antenna used in the reader ensures more freedom in tag-reader orientation and serves for reception and transmission. The Chipless RFID tag consists of different microstrip scatterers that are resonating at distinct

frequencies. The scatterers used for this system are two orthogonal $\lambda/2$ crossed SIRs.

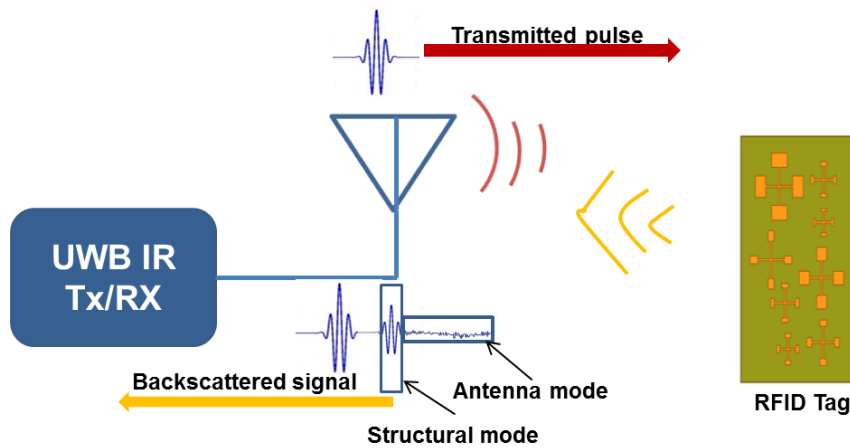


Figure 5.4: UWB IR based Chipless RFID system

The UWB pulse $x_i(t)$ is transmitted by the reader for interrogating the Chipless tag. In time domain, three components can be distinguished [4] in the received signal ($y_r(t)$) in a noise free environment. The first component ($y_R(t)$), constituting the major part is the reflected part of the transmitted pulse. The second component is the structural mode of the backscatter ($y_S(t)$). This is followed by the weakest and last component of backscatter named as antenna mode $y_A(t)$ [24], [25]. The structural mode occurs only after the complete transmission of $x_i(t)$ by the reader antenna and is due to the specular reflections from the scattering centers on tag geometry. And the antenna mode arises due to the interaction between local resonances in the early time that leads to the energy storage in the scatterers at their resonant frequencies. So the total received energy is expressed as

$$y_r(t) = y_R(t) + y_S(t) + y_A(t) \dots\dots\dots (5.1)$$

The return loss of the reader antenna without Chipless tag measured in frequency domain is denoted as $S_{11}(f)$. From the definition of return loss, the reflected part of input pulse by the antenna is given by

$$y_R(t) = f^{-1}\{S_{11}(f).X(f)\} \dots\dots\dots (5.2)$$

Where f^{-1} operator defines inverse Fourier transform. Lower case letters are used in time domain representation and upper case letters in frequency domain representation. So $X(f)$ is the transmitted signal in frequency domain. In the case of practical measurement, the backscattered signal without tag contains not only the reflected part of transmitted pulse but also noise components like reflection from surrounding objects ($y_0(t)$) and white noise ($y_n(t)$). Thus the backscattered signal without tag ($y_1(t)$) can be expressed as

$$y_1(t) = y_R(t) + y_0(t) + y_n(t) \dots\dots\dots (5.3)$$

The backscattered signal with the Chipless tag can be expressed as modified S_{11} of the antenna that comprise of rejection from antenna, reflection from surrounding objects, white noise and the backscattered signal from the tag ($y_S(t)$ and $y_A(t)$). The total received signal in frequency domain can be written as

$$y(t) = f^{-1}\{S_{11}^{loaded}(f).X(f)\} \dots\dots\dots (5.4)$$

where $S_{11}^{loaded}(f)$ is the return loss of the reader antenna with Chipless tag measured in frequency domain. Total received signal in the case of practical measurement scenario expressed in time domain is given as

$$y_r(t) = y_R(t) + y_0(t) + y_n'(t) + y_S(t) + y_A(t) \dots\dots\dots (5.5)$$

where $y_n'(t)$ is white noise signal at another instance of time. Subtraction of signal measured without the tag from that with tag eliminates effect of reader antenna and reflections from stationary objects. So this subtraction can be done as a calibration and the calibrated signal can be expressed as

$$y_C(t) = y_S(t) + y_A(t) + y_n''(t) \dots\dots\dots (5.6)$$

where $y_n''(t)$ is the white noise signal contributing after calibration. The same procedure can be used in the frequency domain by subtracting measurement without tag from that with tag and is expressed below.

$$y_C(t) = f^{-1}\{[S_{11}^{loaded}(f) - S_{11}(f)].X(f)\}\dots\dots\dots (5.7)$$

The $y_C(t)$ is free from all reflection due to the antenna and environment.

5.3. Tag performance in time domain using Numerical methods

CST microwave studio simulation software is used for the transient analysis of Chipless RFID tag. The interrogation is provided with a plane wave excitation polarized along X axis. The simulation setup in CST microwave studio is shown in figure 5.5. The simulation is carried out with a chipless RFID tag having two scatterers. The scatterers are formed by orthogonal $\lambda/2$ SIRs and are operating at 3.2 GHz and 4.1 GHz. The design parameters and dimensions of the basic SIRs are given in table 5.1. The scattered field is captured using an electric probe oriented along the polarization of plane wave excitation (here X direction) and it is placed 10 cm away from the tag. The vector K in figure 5.5 shows the direction of propagation of transmitted signal.

The interrogation signal is a modulated Gaussian pulse and can be represented as

$$x_t(t) = A_0 \cos(2\pi f_c t) \exp\left(-\frac{(t-\tau)^2}{2\sigma^2}\right) \dots\dots\dots (5.8)$$

where τ is the time index for peak value of pulse and σ is the variance. A_0 and f_c (Hz) are the amplitude and frequency of the sinusoidal carrier signal, respectively. The excitation pulse and its normalized frequency spectrum are shown in figure 5.6. The time duration of the transmitted signal is the order of 0.5-1 ns and its frequency spectrum is centered around 6.5 GHz.

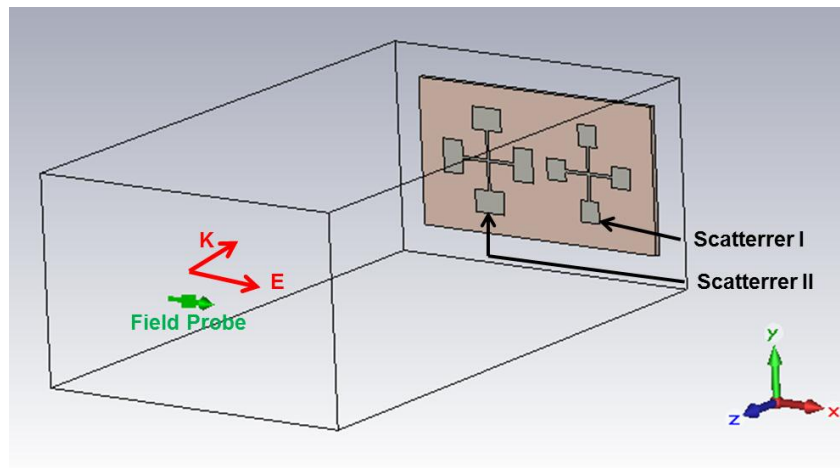


Figure 5.5: Simulation setup used in CST for time domain analysis of frequency spectra based RFID tag with two Polarization independent scatterers. The probe is placed at 10 cm away from the tag. The dimensions of scatterers are detailed in table 5.1.

Table 5.1: Dimensions of the scatterers used in the CST simulation setup. Tag substrate: RT Duroid 5880, $\epsilon_r = 2.2$, height = 1 mm

Scatterer	F(GHz)	K	α	L ₁ (mm)	L ₂ (mm)	W ₁ (mm)	W ₂ (mm)
I	3.2	0.25	0.5	5.27	3.99	0.5	5.89
II	4.1	0.35	0.5	4.74	3.81	0.5	3.73

As stated previously, the backscattered signal from the tag picked up by the probe is characterized by structural mode and antenna mode. Structural mode arises due to the specular reflection of the transmitted pulse by tag geometry and will be a delayed transmitted pulse with decreased amplitude. While the antenna mode is due to the resonators on the tag surface and the overall time domain response from the tag is expressed as

$$y_c(t) = A_s \cos(2\pi f_c t) \exp \left[-\frac{(t - \tau - \tau_{tag})}{2\sigma^2} \right] + \sum_{n=1}^N A_n \exp(a_n + j\omega_n t) + n(t) \dots\dots\dots (5.9)$$

The summation of exponentially decaying signals on the RHS of the expression represents the tag's resonance information. The number of exponentials depends on the number of resonances present on the tag. A_n is the complex amplitude and $(a_n + j\omega_n t)$ are the poles corresponding to predefined resonant frequencies [4], [11]. τ_{tag} is the delay involved in the structural mode of backscattered signal and is determined by the distance between the tag and the transmitter (reader). N is the number resonators and $n(t)$ is the noise measured in time domain.

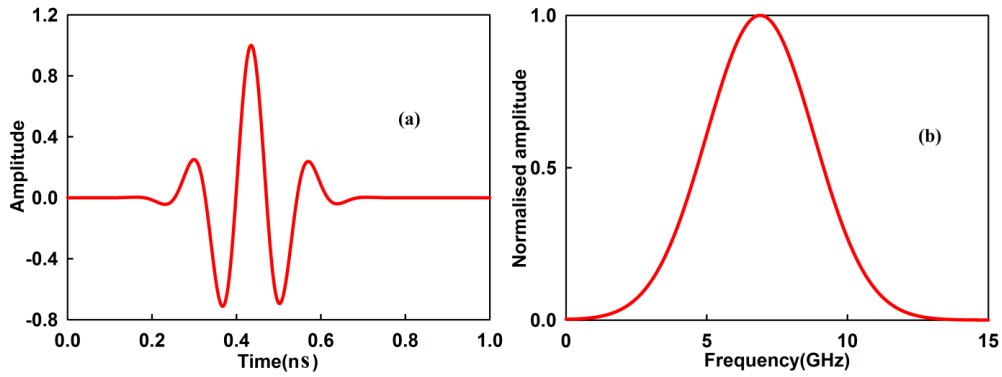


Figure 5.6: (a) Modulated Gaussian excitation pulse (b) Normalized amplitude spectrum of the pulse shown in figure 5.6(a)

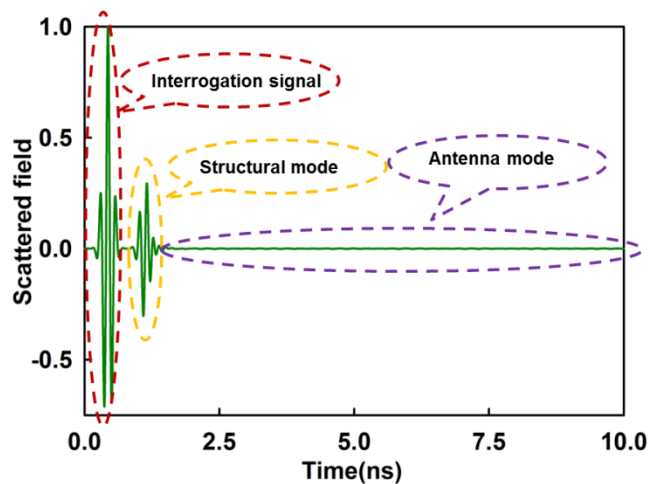


Figure 5.7: Signal picked up by the electric probe placed in front of the source and 10 cm away from the tag

The backscattered signal from the tag picked up by the electric field probe oriented along the polarization of excitation signal (X direction) at 10 cm away from the tag is shown in figure 5.7. In the figure, two earlier signals follow the shape of transmitted signal. The first one with higher amplitude is the transmitted signal itself, which is picked up by the probe

placed in front of the source. Enlarged view of backscattered signal showing structural and antenna modes alone is shown in figure 5.8. The structural mode is similar in shape to the interrogation pulse. The antenna mode or tag ID carrying part is spread in the late time after the structural mode and has smaller amplitudes compared to structural mode. The duration for which antenna mode exists depends on the quality factor of the resonators, i.e., higher the stored energy longer will be the existence of antenna mode [11].

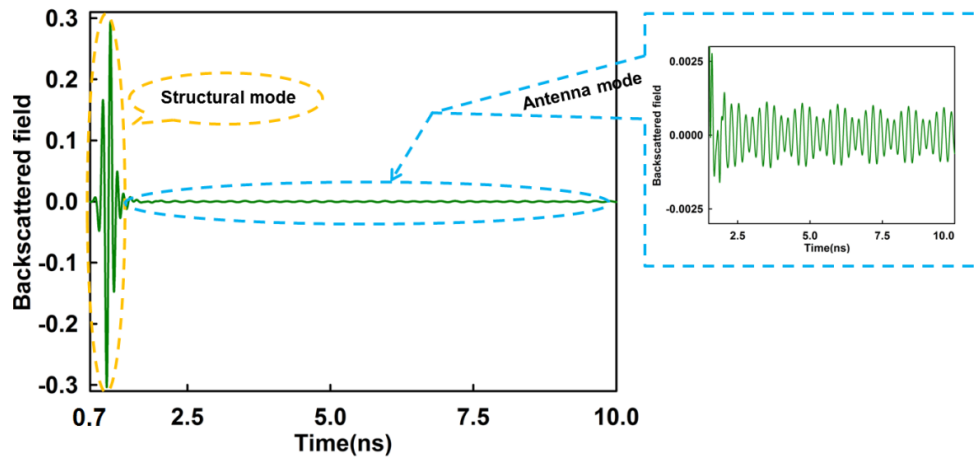


Figure 5.8: Structural mode and antenna mode in the backscattered signal from the tag. An enlarged view of antenna mode is shown on the right side.

5.3.1. Analysis of Structural Mode and Antenna Mode Scattering

Structural mode and antenna mode are separately analyzed in time domain in this section. Backscattering from the Chipless tag with two scatterers is filtered to get structural mode and antenna mode and to avoid the high amplitude forward transmitted pulse. The filtering is done by windowing the backscattered data according to the time of occurrence of

different components in it. That is, here the first component; the forward transmitted pulse occurs between 0 and 0.7 ns, and the structural mode occurs in between 0.7 ns and 1.4 ns. The antenna mode is spread over a long time after the structural mode. For this case, a simple rectangular window is used to filter out different components. Fourier transform of the so separated backscattered signal is performed to get frequency domain response and the obtained response is shown in figure 5.9.

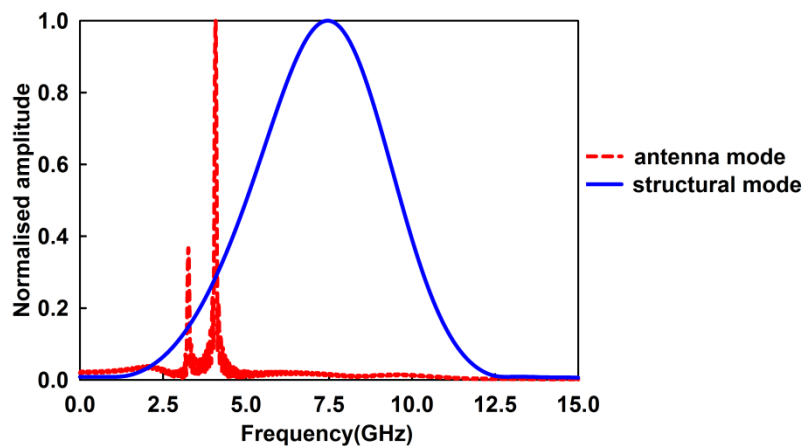


Figure 5.9: Normalized frequency spectrum of structural mode and antenna mode filtered from the backscattered signal from a 2scatterer tag (Table 5.1) placed 10 cm away from the source

Structural mode as narrated before is a simple reflection of the reader signal from the tag due to the shape and size of metallic structure in the tag. For this reason it resembles the transmitted pulse in shape as it is seen in its normalized spectrum shown in figure 5.9. The structural mode does not contain any information regarding the encoded data on the tag and hence of tag's ID. The frequency spectrum of the antenna mode is obtained by taking

FFT of the backscattered signal in the time 1.5 ns to 10 ns. The frequency spectrum clearly shows the resonances corresponding to the scatterers on the tag. The simulated resonant frequencies are at 3.2 GHz and 4.1 GHz. The variation in transmitted power spectrum over the frequency spectrum accounts for difference in amplitude peak of the two resonances [4].

As a proof to the readability of frequency domain Chipless tags from its response in time domain, responses obtained from frequency and time domain analysis are shown in figure 5.10. Exact tag ID (resonant frequency) is obtained from both the methods. In practical measurement, there would be a component of noise other than the structural and antenna modes in the backscattered signal. Depending on the interference between these components resonance can be detected as either a dip or a peak in the backscattered signal. In time domain analysis, it is possible not only to extract the resonant part but also to remove the unwanted noise.

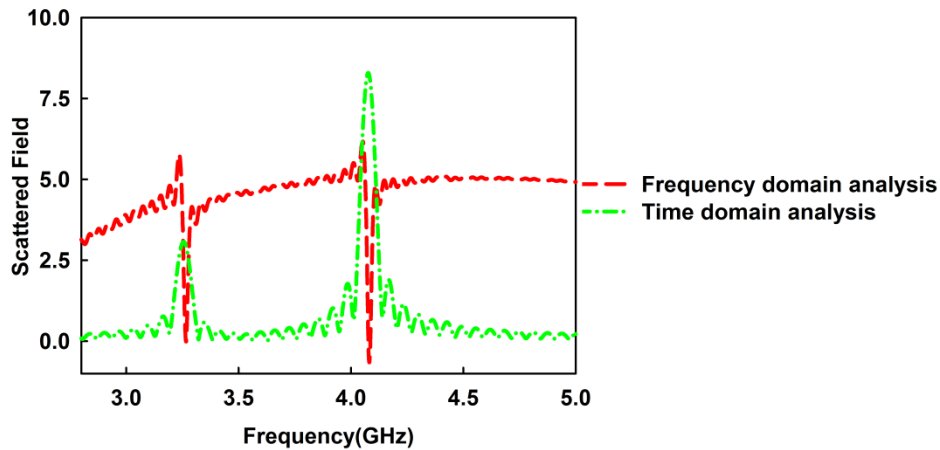


Figure 5.10: Spectral signature of the tag (Detailed in table 5.1) obtained from time and frequency domain analysis

The result by time domain analysis in figure 5.10 is obtained by taking Fast Fourier Transform (FFT) of a selected portion (antenna mode) in the time domain signal. Absence of any kind of delay line or transmission lines on the tag surface make it difficult to define the starting time of structural and antenna modes. The starting time of antenna mode can only be determined by observing the time domain signal and taking the time instance immediately after the structural mode. The structural mode would be the larger and first component of the measured backscattered signal which has a Gaussian amplitude spectrum similar to the transmitted UWB spectrum.

Backscattered signal collected by the probe when it is placed 50 cm away from the tag is shown in figure 5.11(a). A time Vs frequency plot is also used for better identification and is shown in figure 5.11(b).

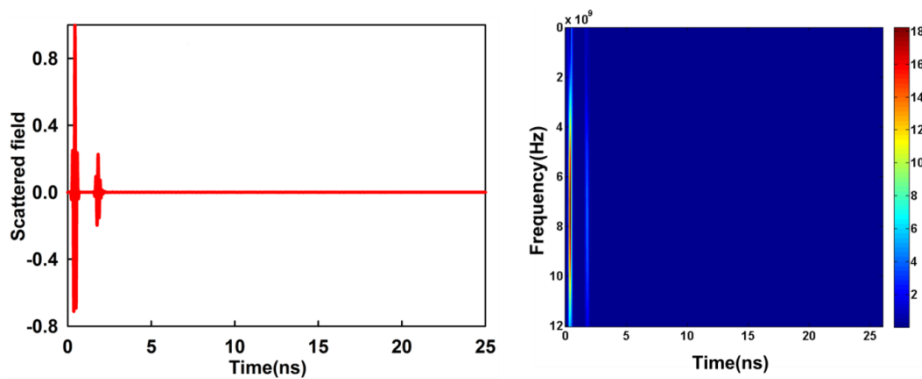


Figure 5.11: (a) Backscattered signal from the tag placed at 50 cm (b) Time Vs Frequency analysis of the backscattered signal in (a) when the resolution time is 0.09 ns and window size is 0.16 ns

The tag is placed at a distance of 50 cm away from the plane wave source. The forward transmitted signal occurs immediately after transmission,

within the same 0-0.7 ns. This is due to the fact that, in the simulation setup the probe is paced in front of the plane wave source. But the structural mode is delayed more than the 10 cm case narrated earlier. It occurs in between 3.5 ns and 4.2 ns. So the starting time of occurrence of structural mode is greatly influenced by the tag's distance from the excitation.

Accuracy of spectral contents is checked by two parameters named Resolution time and Window size. FFT of the data is taken by viewing the backscattered data through a sliding rectangular window. Resolution time is the time between two sliding window operations. Concepts of Window size and resolution time are demonstrated in figure 5.12.

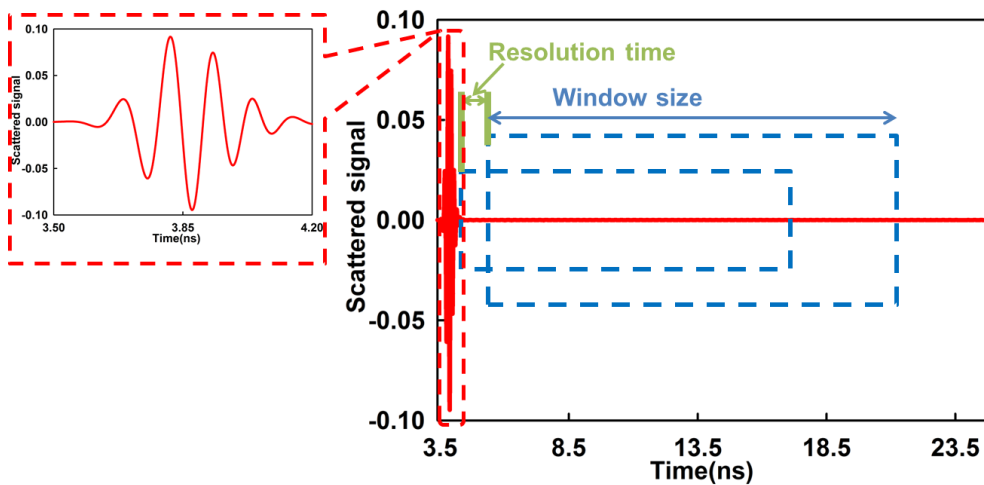


Figure 5.12: Backscattered signal from the tag (detailed in table 5.1) after removing the forward transmitted signal (Delay = 3.2 ns). Concept of window size and resolution time are shown.

In the figure, the forwarded transmitted pulse is removed by introducing a delay of 3.2 ns. This delay is fixed by observing the received backscattered signal in time domain. Forward transmitted pulse and structural mode in the

scattered signal picked by the probe exist only for a short duration (a few nanoseconds) determined by the width of interrogation pulse. For the successful detection of these components, the resolution time and window size should be less than the time period of the transmitted pulse. In figure 5.11(b) the forwarded transmitted pulse and structural mode are identifiable with a resolution time of 0.09 ns and window size of 0.16 ns.

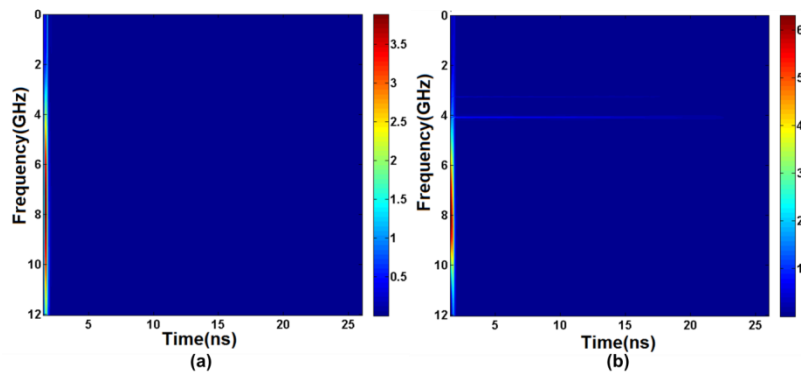


Figure 5.13(a): Time Vs Frequency analysis when the resolution time is 0.09 ns and window size is 0.16 ns. (b) Resolution time is 0.06 ns and window size is 19.8 ns, Delay = 3.2 ns

The resonant information of the tag (tag ID) is not identifiable in the presence of forwarded transmitting pulse. The remaining part of the backscattered signal after the removal of forwarded transmitted pulse (with a delay of 3.2 ns) is shown in figure 5.12. As already stated, the signal contains structural and antenna modes only. The spectral components of RFID tag obtained by post processing the signal in figure 5.12 are shown in figure 5.13(a). Exact time instance of structural mode is obtained when the resolution time and window size are smaller. But these smaller values are not sufficient for the visibility of antenna mode. So an increased window

size is needed and the result (with an increased window size of 19.8 ns and reduced resolution time of 0.06 ns) is shown in figure 5.13(b). Since the structural mode does not contain tag's resonance information like the forward transmitted signal, it is also be eliminated by extending the delay time. Again, starting time and duration of structural mode are needed to eliminate it effectively without affecting the antenna mode. Identification of structural mode is also easy as it follows the transmitted pulse in shape with reduced amplitude. By extending the delay time up to 4.2 ns, both forwarded transmitted signal and structural mode can be eliminated effectively.

Plots with and without structural mode are shown in figure 5.14. In both cases of figure 5.14(a) and (b), window size is 19.8 ns and resolution time is 0.06 ns. This selection of window size and resolution time is explained later in this section. In figure 5.14(a), the presence of structural mode is seen as a component spread over the entire spectrum with considerably high amplitude. It occurs for a short time and extends in the entire frequency band. No information can be encoded in frequency using this structural mode. After the structural mode, antenna mode is visible and is confined to the definite frequencies determined by the scatterers on the tag. But it is clear from the figure that spectral information is feeble in the presence of high amplitude structural mode. In figure 5.14(b), processed backscattered signal after removing the structural mode shows better clarity to antenna mode. The frequencies of the scatterers and the time of occurrence of their resonances are well identifiable without the structural mode. Hence the introduction of delay time to remove structural mode is significant.

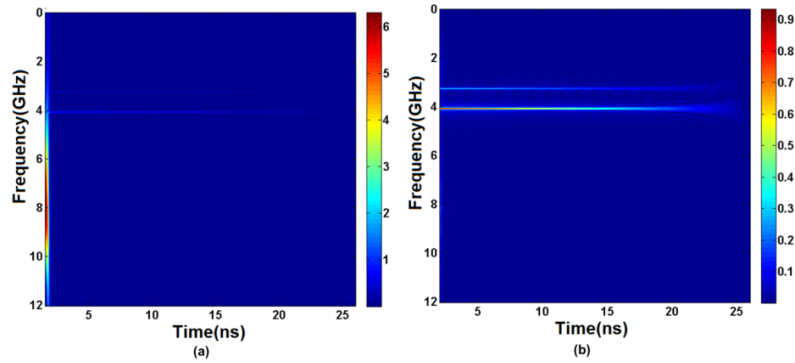


Figure 5.14: Frequency Vs Time plot for a 2 scatterer tag (Table 5.1) at 50 cm from the source (a) with structural mode., delay = 3.2 ns (b) Without structural mode, delay = 4.2 ns. In both cases window size is 19.8 ns and resolution time is 0.06 ns

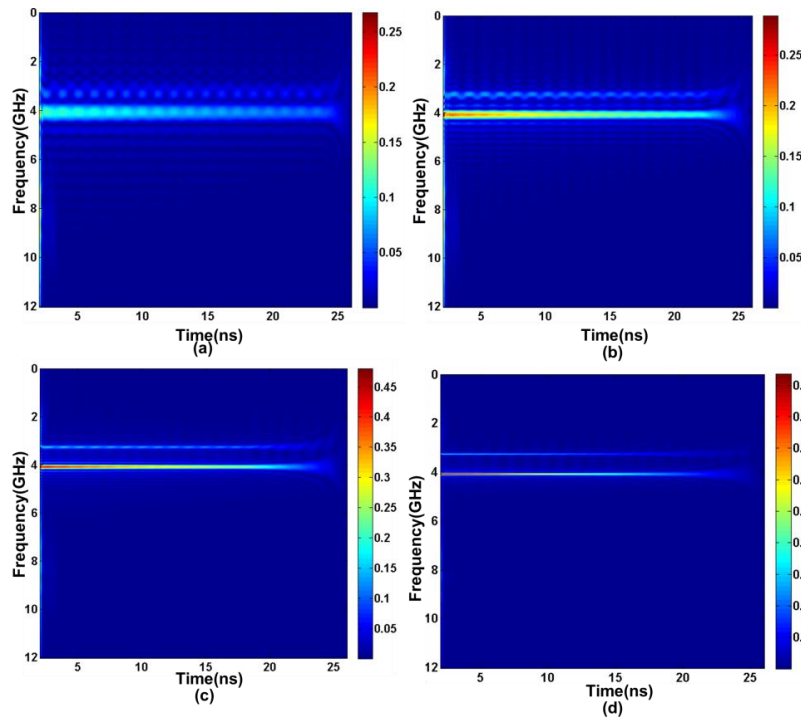


Figure 5.15: Frequency Vs Time plot for a 2 scatterer tag (Table 5.1) at 50 cm from the source, Delay = 4.2 ns (a): Window size = 1.98 ns. (b) Window size = 3.96 ns. (c) Window size = 7.92ns. (d) Window size = 19.8 ns. In all the cases resolution time is 0.06 ns

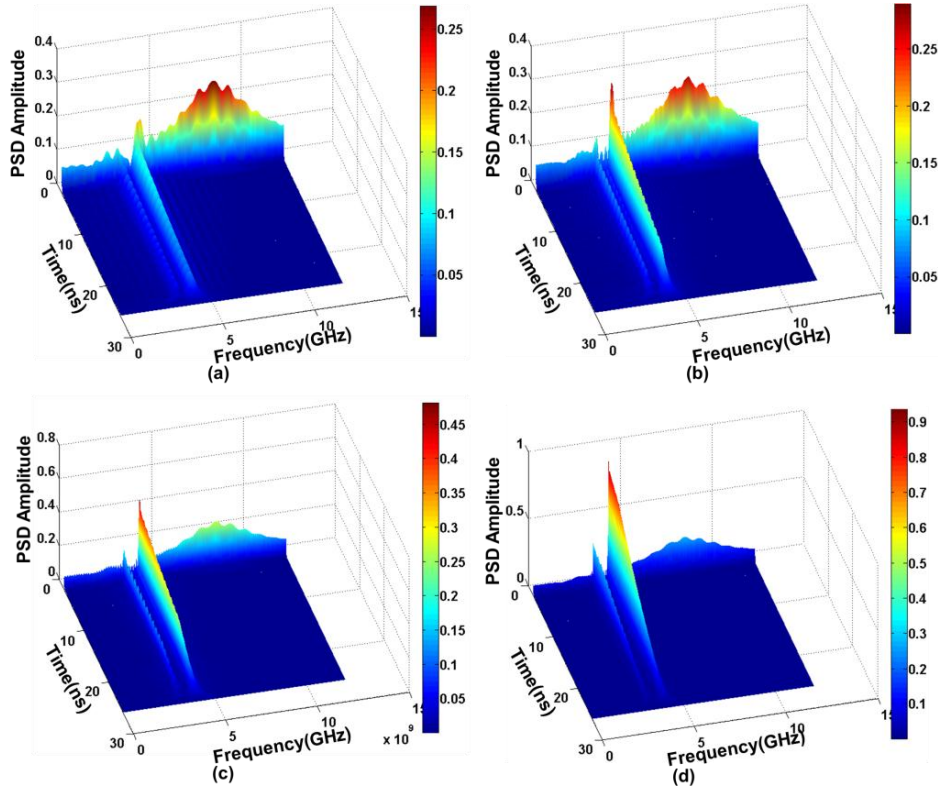


Figure 5.16: PSD Vs Frequency- Time plot for a 2 scatterer tag (Table 5.1) at 50 cm from the source, Delay = 4.2 ns. (a): Window size = 1.98 ns. (b) Window size = 3.96 ns. (c) Window size = 7.92 ns. (d) Window size = 19.8 ns. In all the cases resolution time is 0.06 ns

For accurate antenna mode extraction, possibly small resolution time and large window size in time is needed. Significance of window size in antenna mode extraction is demonstrated in figure 5.15. Antenna mode extraction for different window size [(a) 1.98 ns (b) Window size = 3.96 ns (c) 7.92 ns. (d) 19.8 ns] with constant resolution time (0.06 ns) is presented. In all the cases, the structural mode is removed by introducing a delay time of 4.2 ns. It is clear from the figure that the antenna mode is well identified in the magnified view provided with large window size. The optimum

performance is shown in Figure 5.15(d) for the largest window size (19.8ns). With a small window size (figure 5.15(a)), resonance information could not be seen exactly as the plot shows a spreaded appearance. As window size is increasing, the resonances become clearer. Starting time of antenna mode is also clearly identifiable with large window size. Power spectral density variation with time of backscattering from the same tag is provided in figure 5.16. Largest window size gives the most clear power spectral variation. Here also, starting and duration of existence of antenna mode is clearly identifiable. Time of existence of antenna mode depends on the power of incident wave and on the quality factor of the resonator.

Large window size is always good for the better clarity of results at the expense of computational complexity. The optimum value for window size depends on the reading environment. Larger values are needed for noisy surrounding and to provide better reading range. It will be clear later in this chapter while examining the data from practical scenario.

5.3.1.1. Hamming window

Better identification of tag ID is achieved when a hamming window is applied to the backscattered signal instead of a simple rectangular window. Increased read range and small window size is achieved by using the technique. The coefficients of Hamming window are computed from the following equation.

$$w(n) = 0.54 - 0.46\cos\left(2\pi\frac{n}{N}\right), 0 \leq n \leq N$$

Where the window length, $L = N+1$ and N is the number of points

The frequency time plot with and without hamming window is shown in figure 5.17. In both cases the window size is 7.92 ns and resolution time is 0.06 ns, Delay time = 4.2 ns. A more clear response is obtained for the latter case. The variation in power spectral density with time is shown in Figure 5.18. Here also, with hamming window the plotted resonant information is clearer than without it. Figure 5.19 shows that by using hamming window it is possible to obtain a better response with a reduced window size than the earlier one. In the figure two cases are shown. Figure 519(a) shows the result obtained using hamming window and the window size is 7.92 ns while Figure 519(b) shows the response without hamming window and the window size is 19.8 ns. The former figure shows a better response with reduced window size. This in turn increases computational efficiency. So the application of hamming window has improved the quality of time domain analysis.

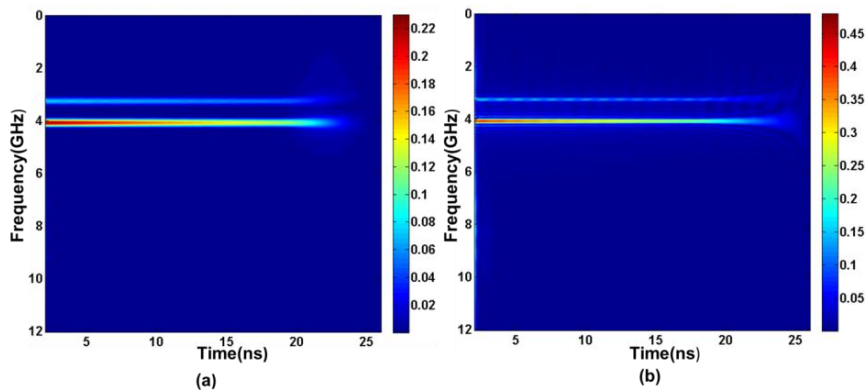


Figure 5.17: Frequency time Plot of backscatter analysis (a) with hamming window. (b) Without hamming window. In both cases the window size is 7.92 ns and resolution time is 0.06 ns, Delay = 4.2 ns

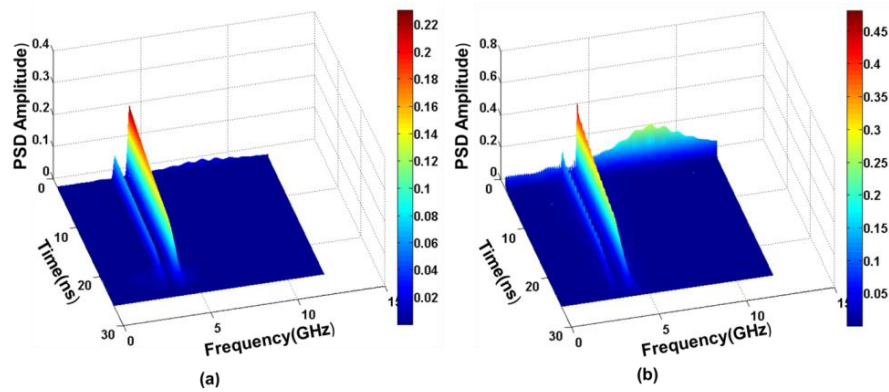


Figure 5.18: Power Spectrum Density plot of backscatter analysis (a) with hamming window. (b) Without hamming window. In both cases the window size is 7.92 ns and resolution time is 0.06 ns, Delay = 4.2 ns

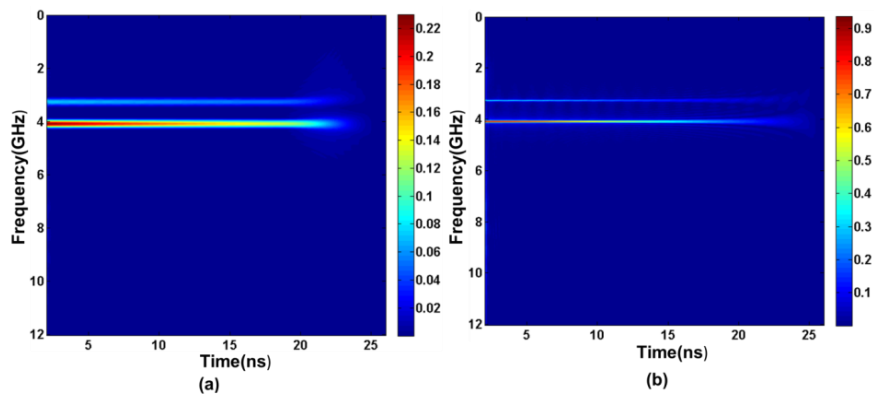


Figure 5.19: Frequency time Plot of backscatter analysis (a) with hamming window, window size = 7.92 ns. (b) Without hamming window, window size = 19.8 ns. Resolution time for both cases is 0.06 ns, delay = 4.2 ns.

Frequency Vs time plot and power spectral density variation plot with hamming window is shown in figure 5.20 for different window size. More clarity to the results would happen with increased window size. In this figure two window sizes are plotted; 7.9 ns and 19.8 ns (figure 5.20(a) and

figure 5.20(b)) to validate the concept. As it is seen, resonances are more clear with 19.8 ns. Similar is the case of power spectral density variation with time (figure 5.20(c) and (d)).

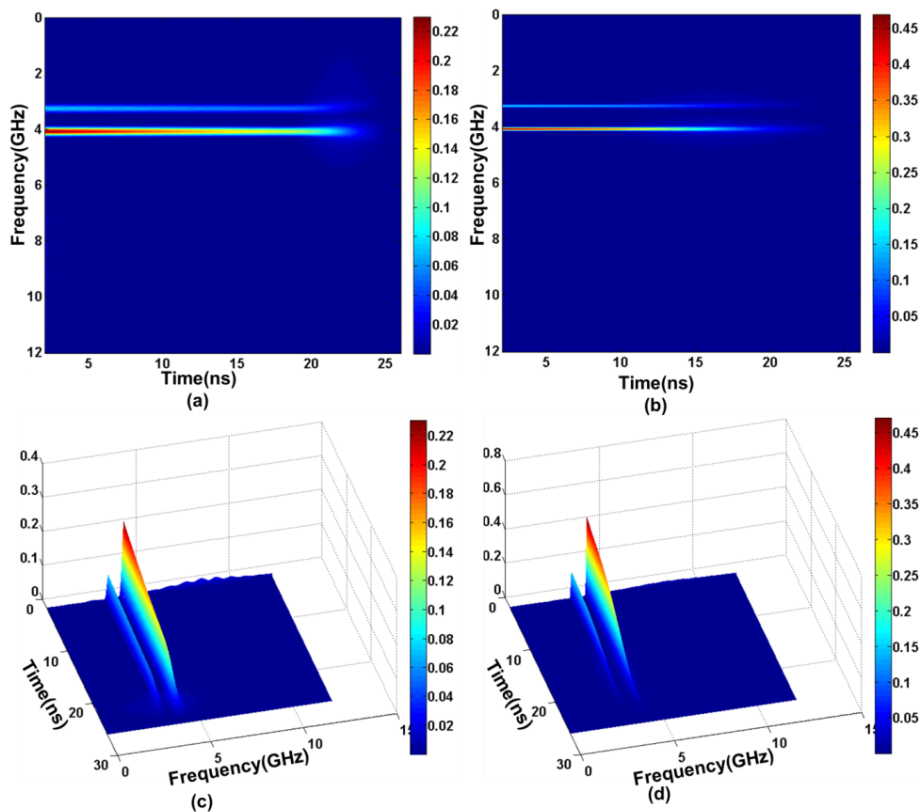


Figure 5.20: (a) frequency Vs time plot, window size = 7.96ns, resolution time = 0.06 ns. (b) Frequency Vs time plot, window size =19.8 ns, resolution time = 0.06 ns, (c) PSD amplitude variation with frequency and time, window size = 7.96 ns, resolution time = 0.06 ns. (d) PSD amplitude variation with frequency and time, window size = 19.8 ns, resolution time = 0.06 ns

The performance of the tag with two resonators mentioned above for an increased distance, say 100 cm from the source is analyzed without hamming window and is shown in figure 5.21. The case is tested for two different window sizes; (a) window size = 7.96 ns, (b) window size = 39.6 ns. Resolution time is 0.06 ns in both cases. As it is seen in figure 5.21, even for a window size of 39.6 ns the spectral information is not identifiable. The antenna mode is not well visible even for large window size. The frequency time plot of the same with hamming window is shown in figure 5.22. The two window sizes are tested with the same resolution time as the case without hamming [Figure 5.22(a) and (b)]. The spectral ID is well visible in both cases and sharper in figure 5.22(b) with larger window size. From this, it is clear that the application of hamming window improves quality of backscattering analysis in time domain for large reading range.

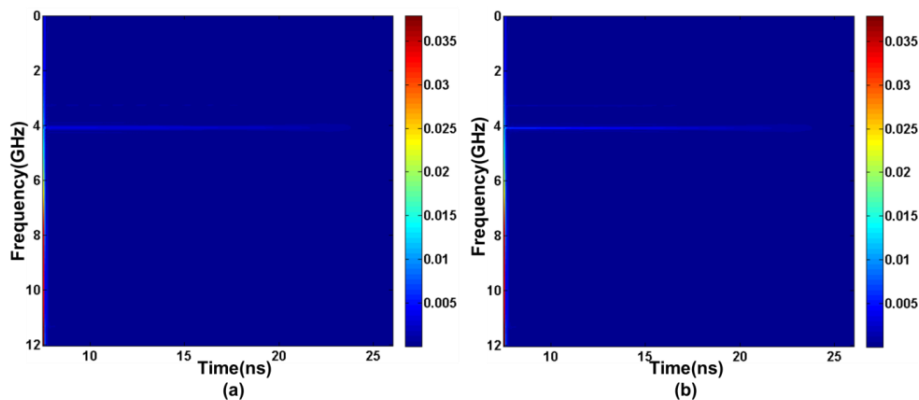


Figure 5.21: Frequency time plot of backscattering from the 2 scatterer tag placed 100 cm from the source (processed without hamming window) (a) Window size = 7.96 ns, resolution time = 0.06 ns (b) window size = 39.6 ns, resolution time = 0.06 ns

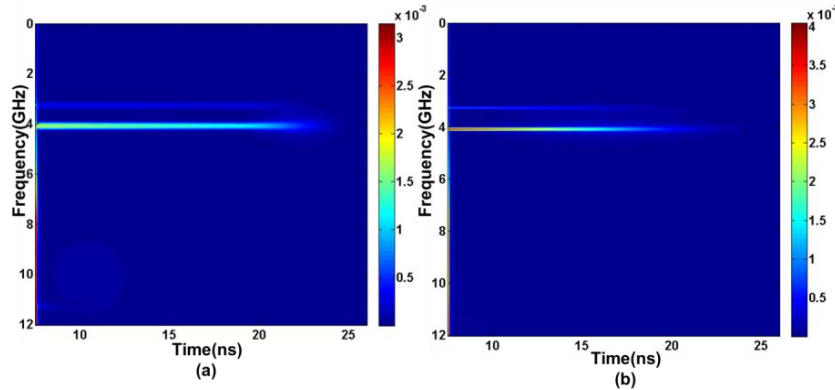


Figure 5.22: Frequency time plot of backscattering from the 2 scatterer tag placed 100 cm from the source (processed with hamming window) (a) Window size = 7.96 ns, resolution time = 0.06 ns (b) window size = 19.8 ns, resolution time = 0.06 ns

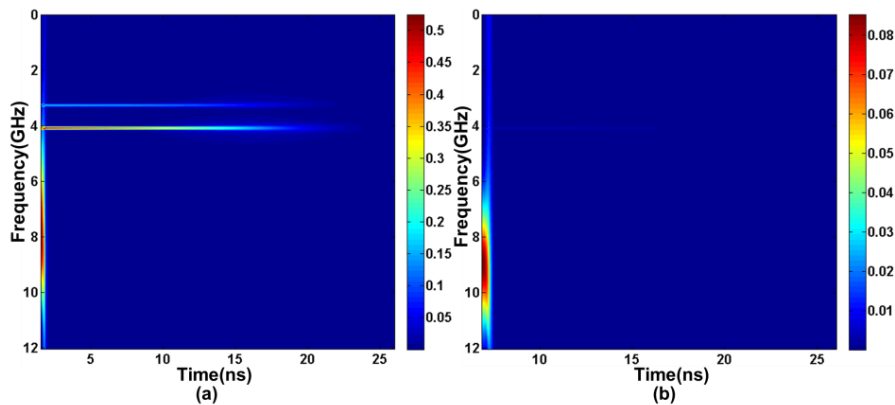


Figure 5.23: Frequency time plot of backscattering from the 2 scatterer tag with structural mode, window size = 19.8 ns, resolution time = 0.06 ns (a) tag placed at 20 cm (b) tag placed at 100 cm

The elimination of structural mode from the backscattered signal becomes more significant as the distance of tag from the source increases. It is demonstrated in figure 5.23 and figure 5.24. Frequency time plot of back scattered signal for two different distances, say 20 cm and 100 cm without

removing structural mode is shown in figure 5.23. The window size used is 19.8 ns and resolution time is 0.06 ns. For the first case (20 cm) the tag is identifiable and for the 100 cm case antenna mode is not distinguishable.

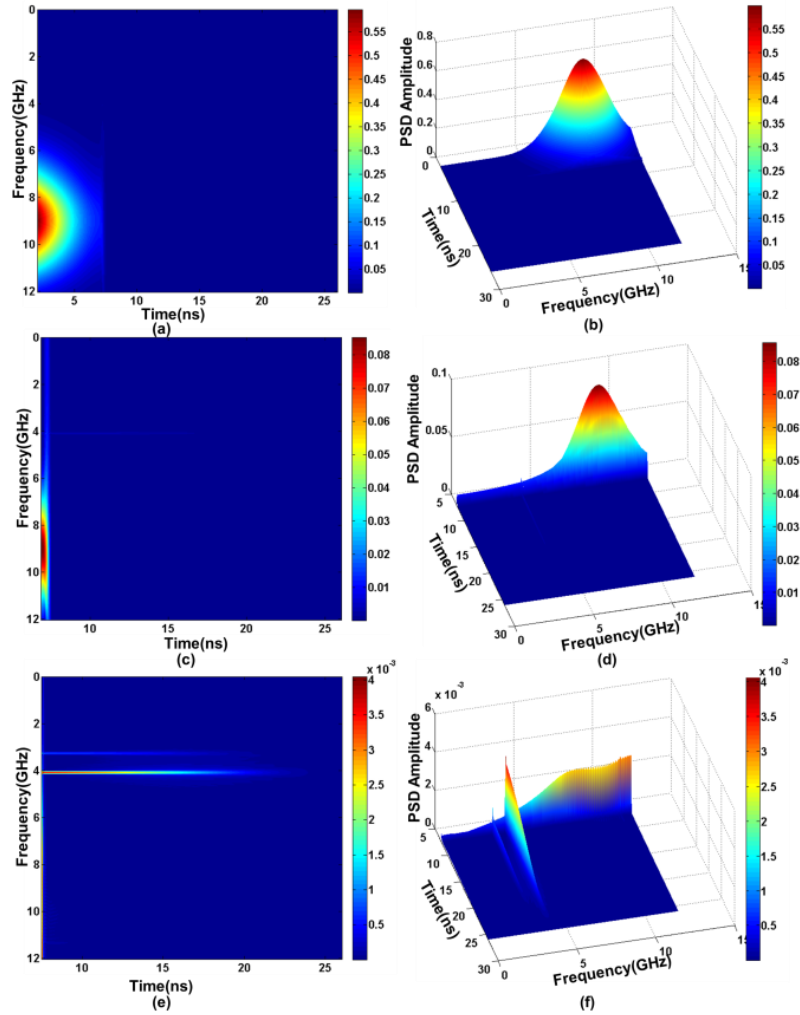


Figure 5.24: Frequency Vs time plot and PSD amplitude Vs time-frequency plot of backscattering from the 2 scatterer tag placed at 100 cm from the source for different delay time. Window size = 19.8 ns, resolution time = 0.06 ns (a), (b) delay = 2.04 ns. (c), (d) delay = 6.93 ns. (e), (f) delay = 7.52 ns

Response after introducing different delay time is shown in figure 5.24. Both frequency time plot and variation of power spectral Density plot are shown. When the delay is equal to 2.04 ns, the resonant information is not visible (figure 5.24(a) and (b)) as the structural mode is not fully removed. With a delay of 6.93 ns, the structural mode is not fully removed and hence the visibility of antenna mode is not good. The antenna mode is clearly visible with the same window and resolution time as that in figure 5.23 when the structural mode is completely removed with a delay time of 7.52 ns (Figure 5.24 (e) and (f)). The best way to filter out the structural mode completely is to detect the time of peak amplitude of structural mode and set the delay time equal to peak time plus half of transmitted pulse time period.

The overall procedure to extract antenna mode from backscattered signal recorded in time is summarized in the next section in relation to practical measurement.

5.4. Steps to Extract Spectral Signature from the Backscattered Signal

As detailed in the above section, the backscattered signal recorded in time can be processed with different signal processing methods to yield spectrum of antenna mode which contains the resonant information concerned with the tag ID. The antenna mode occupies a small portion of backscattered signals and follows the structural mode. The steps to find the spectral ID from backscattered signal in time domain can be summarized as,

- 1) Calibrate the tag response: subtract the return loss without tag from that with tag so that the received signal will consists of the

structural mode, antenna mode and the noise. Reflections from the reader antenna and all surrounding stationary objects can be removed by performing calibration.

- 2) Removal of structural mode containing no resonant information about the RFID tag: The signal before antenna mode can be removed completely before the FFT analysis. As a first step, calculate a delay time which should be equal to the peak time of structural mode plus half the transmitted pulse period. The entire signal before the delay time could be removed without affecting the tag ID calculation.
- 3) Proper resolution time and window size should be selected so that all the spectral information regarding the tag ID could be extracted with utmost accuracy. Small values for resolution time and large values for window size are preferred for the successful extraction of antenna mode.
- 4) Use a hamming window function to separate antenna mode before the application of FFT which will enhance the quality of results.
- 5) FFT analysis of so extracted antenna mode and then 2D & 3D plotting of extracted spectral contents.

Performance of resonators at different frequencies is different. The high frequency resonators with low Quality factor have very feeble response which will decay very faster than low frequency resonators. To

identify such resonances, FFT window should start from the beginning of antenna mode.

5.5. Time Domain Analysis of Measured Time Domain Data from Different Practical Environments

Chipless RFID tag based on orthogonally placed identical stepped impedance resonators presented in chapter 4 (Figure 4.31) is selected for the time domain analysis. The tag has eight scatterers (Dimensions are given in Table 4.8). The PNA E8362B with time domain option enabled performs the UWB IR reader function. Same transmitted power throughout the entire band is ensured by using rectangular window option in the analyzer.

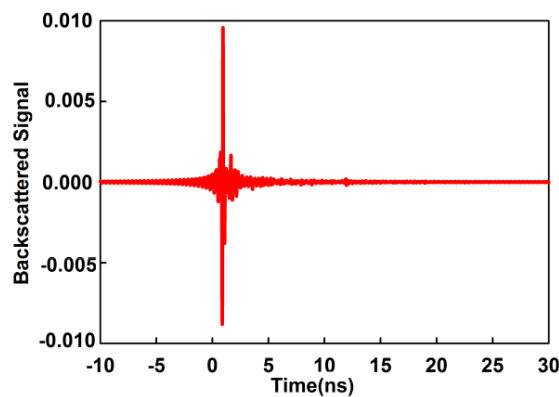


Figure 5.25: Backscattered signal in time domain measured from an 8bit Tag (Figure 4.31 and table 4.8) placed at 50 cm from the reader antenna

The backscattered time domain signal from the RFID tag positioned at 50 cm from the reader antennas is shown in figure 5.25. The measurement is taken in a practical environment and the averaging option in the network analyzer is disabled. The backscattered signal contains structural mode, antenna mode and white noises. Frequency domain response of the tag

placed at different distances is also shown in figure 5.26 for comparison. The signal is too small to identify the tag beyond a distance of 40 cm due to the reflections from the surroundings.

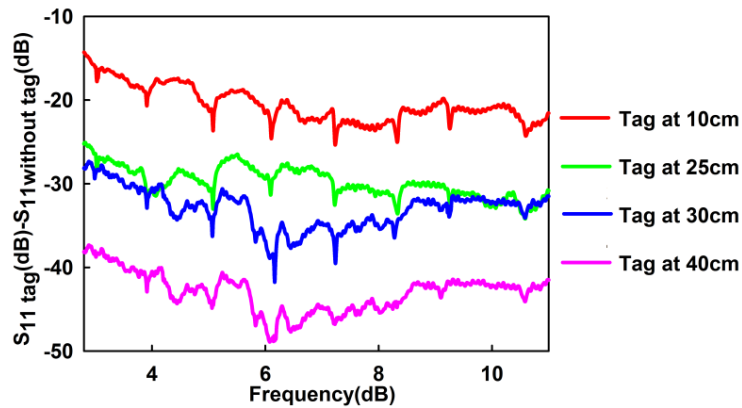


Figure 5.26: Backscattering from the tag (Figure 4.31 and table 4.8) at different distances measured in frequency domain

As explained in previous sections, the basic concept in the time domain analysis of these frequency domain tags is to slide a time window of proper duration (window size) over the entire signal by small time steps (resolution time) and then applying FFT on each time window. To improve the quality of extracted antenna mode spectrum hamming window function is used. Exact beginning of antenna mode should not be missed as it may result in unidentifiable higher frequency resonances. Delay time of 11.26 ns is used which is equal to peak time of structural mode plus half of transmitted pulse period to ensure the identification of higher order resonances and also to remove the structural mode containing no information regarding the tag ID. Backscattered signal measured in time domain with and without delay is shown in figure 5.27.

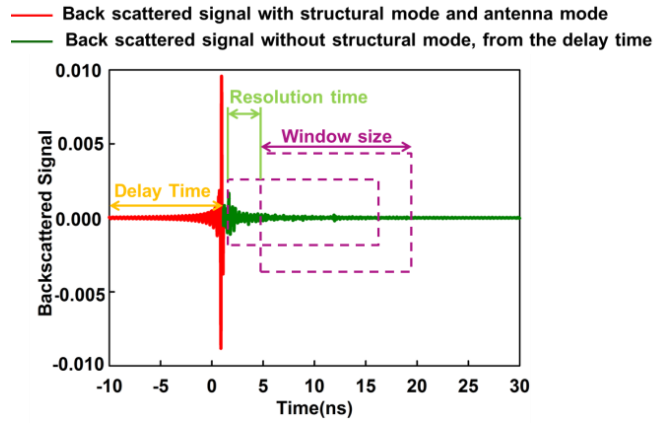


Figure 5.27: Backscattered signal from the above mentioned 8 bit tag with and without delay time. Delay = 11.26 ns

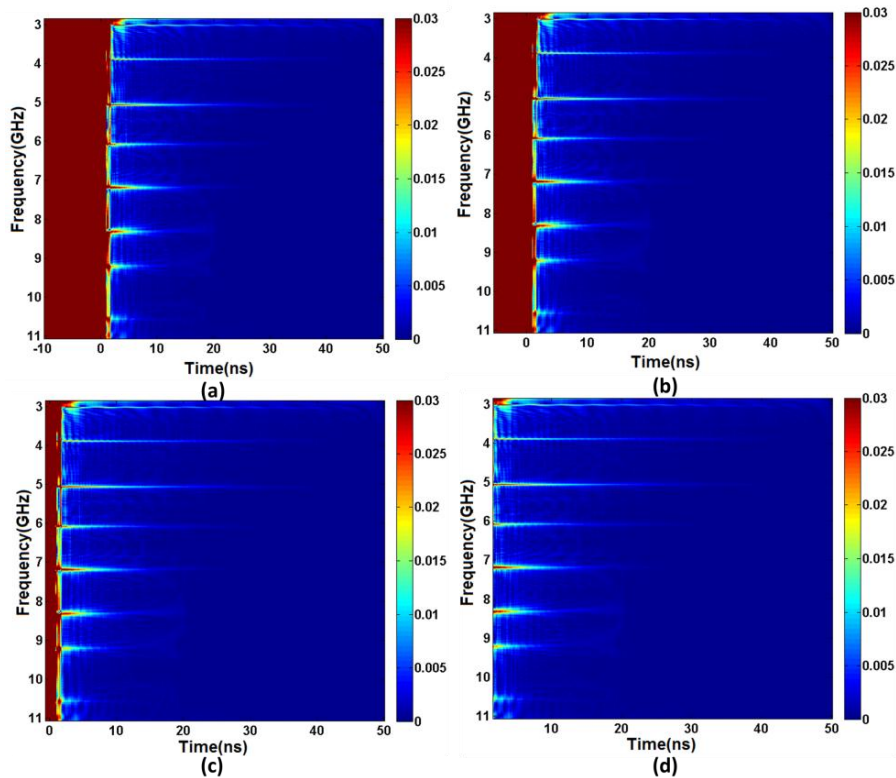


Figure 5.28: Frequency-time plot of figure 5.27 for different delay time. Window size = 94 ns, resolution time = 0.14 ns (a) No delay (b) delay = 4.7 ns (c) delay = 9.4 ns (d) delay = 11.28 ns

The results when different delay is applied are shown in figure 5.28. The best results are obtained when the structural mode is fully removed from the received signal. Four cases are plotted in figure 5.28. The structural mode is fully removed with 11.28ns and the spectral signature of the 8 bit tag is clear. Presence of higher amplitude structural mode lasting for a short duration extends over the entire frequency spectrum which deteriorates the detection of lower amplitude antenna mode.

The advantage of time domain method over direct frequency domain is verified by observing the extracted spectrum of antenna mode (which is actually the tag ID) at different distances of tag from the reader antenna. The positions selected are 20, 30 cm and 50 cm and resonant information regarding the tag ID is easily identifiable (figure 5.29).

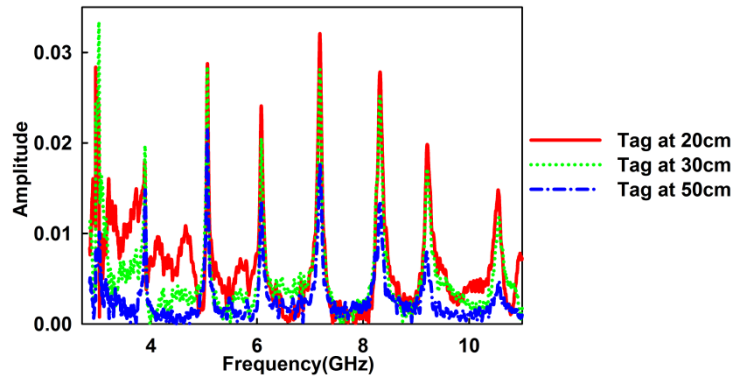


Figure 5.29: Spectrum of antenna mode extracted using time domain analysis when tag is placed at different distances

Since the practical situation is noisy comparing the simulation setup, large window size and small resolution time is needed for the successful detection. Significance of window size and resolution time is studied and

the results are shown in figures 5.30 to 5.33. Frequency–time plot and power spectral density plot are shown for different window sizes (18.8 ns, 47 ns, 94 ns and 470 ns) in figure 5.30 and figure 5.31. The resolution time in all the cases is 0.14 ns. As already stated, large window size yields better clarity to the resonance information of the tag. With the highest window size 470 ns, almost all the noise frequencies are removed (figure 5.31(d) and figure 5.32(d)) and clear resonances are seen in both time and power spectral density plots.

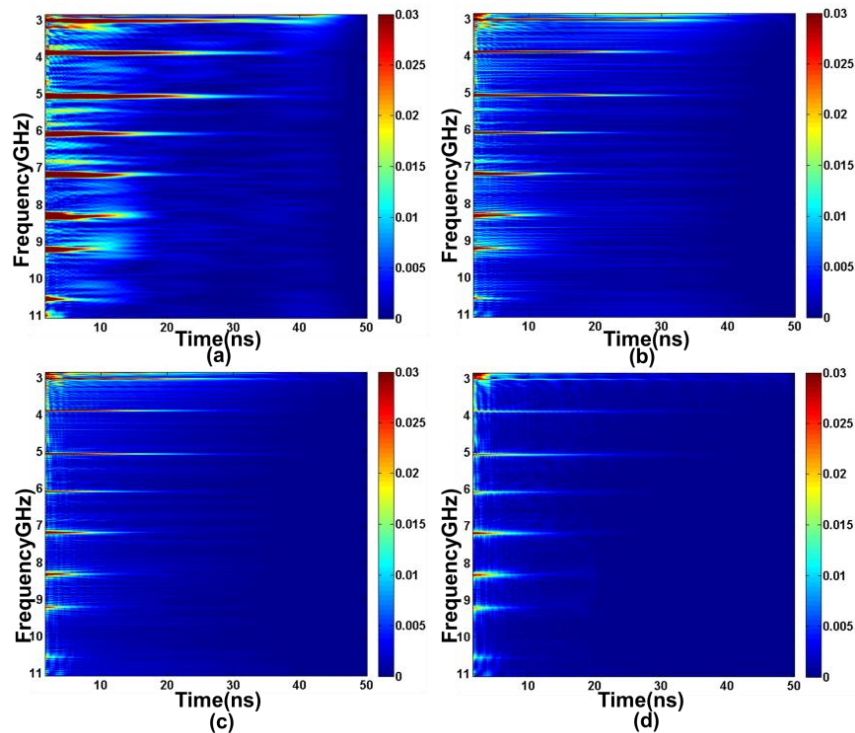


Figure 5.30: Frequency-time plot of extracted antenna mode of the 8bit tag for different window sizes, Resolution time = 0.14 ns, Delay time = 11.28 ns. (a) window size = 18.8 ns (b) window size = 47 ns (c) window size = 94 ns (d) window size = 470 ns

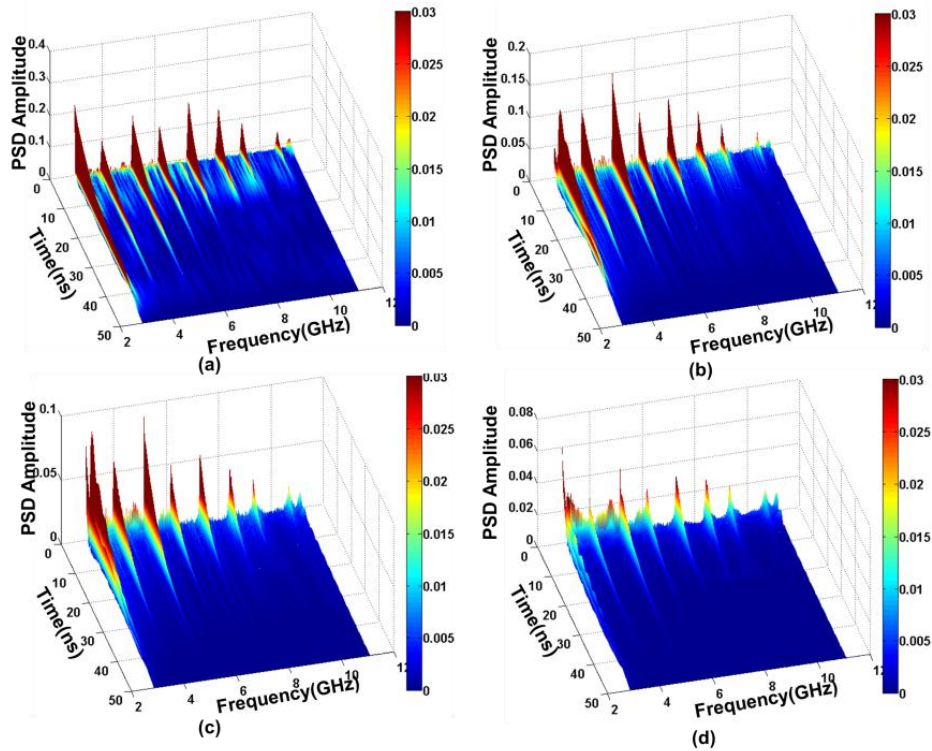


Figure 5.31: Power Spectral Density variation plot of extracted antenna mode of the 8bit tag for different window sizes, Resolution time=0.14ns, Delay time = 11.28 ns. (a) window size = 18.8 ns (b) window size = 47 ns (c) window size = 94 ns (d) window size = 470 ns

The results (both frequency-time plot and power spectral density variation) of varying resolution time for a fixed window size of 94 ns are shown in figure 5.32 and 5.33. Smaller resolution time is preferred for the better extraction of spectral signature. But with a larger window size, variation in resolution time is insignificant.

As discussed earlier, large window size and small resolution time are always preferred to get optimum results but will result in increased

computational time. Low frequency resonances are available over a larger time than the higher frequency resonators. First three resonances from the lower frequency band are available for more than 30 ns. Period of existence is decreasing with increasing frequency. The highest frequency resonance exists less than 10 ns. Degradation of the quality factor at higher frequency due to microstrip losses can be accounted for this short duration existence of high frequency resonances.

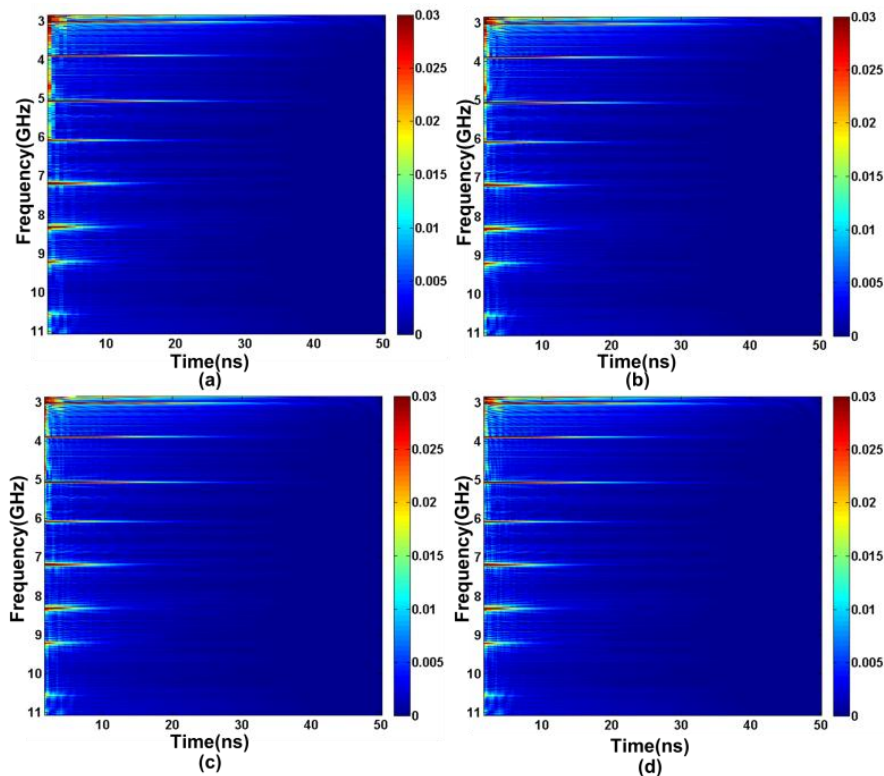


Figure 5.32: Frequency-Time plot of extracted antenna mode of the 8bit tag for different, Resolution time. Window size = 94 ns, Delay time = 11.28 ns. (a) Resolution time = 0.56 ns (b) Resolution time = 0.42 ns (c) Resolution time = 0.28 ns (d) Resolution time = 0.14 ns

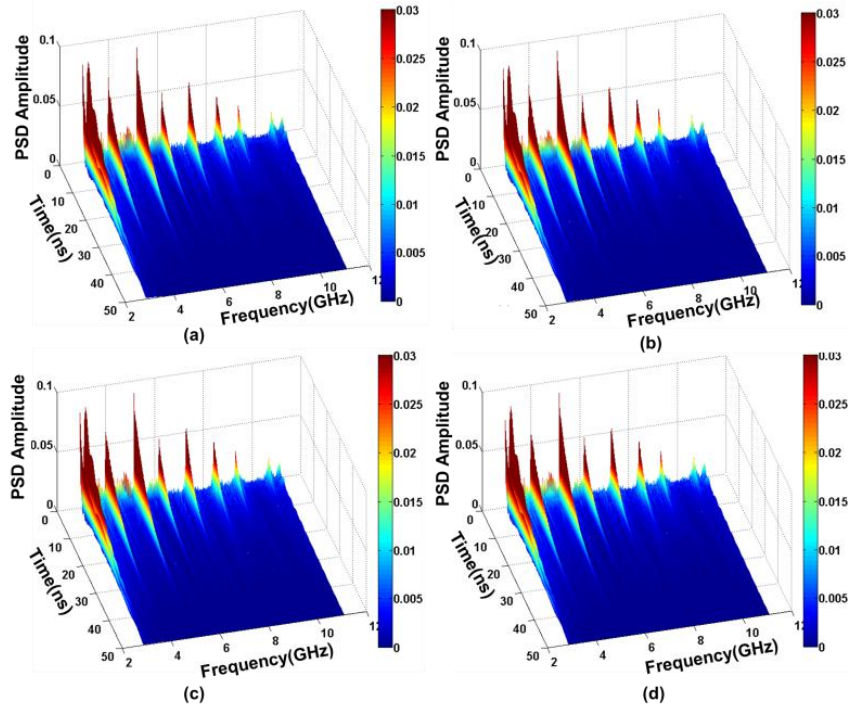


Figure 5.33: Power Spectral Density variation plot of extracted antenna mode of the 8bit tag for different, Resolution time. Window size = 94 ns, Delay time = 11.28 ns. (a) Resolution time = 0.56 ns (b) Resolution time = 0.42 ns (c) Resolution time = 0.28 ns (d) Resolution time = 0.14ns

Measurements of tag performance in Practical scenario are discussed in the next part of this thesis.

5.5.1 Tag on plastic box

Figure 5.34 shows the measurement setup inside the laboratory to test the validity of the 8 bit tag (mentioned in the above sections) placed on a plastic box. As stated earlier, the reader function is performed by the PNA E8362B and a medium gain horn antenna. Time domain analysis of the backscattered signal is performed and the extracted antenna mode spectrum is plotted in figure 5.35.

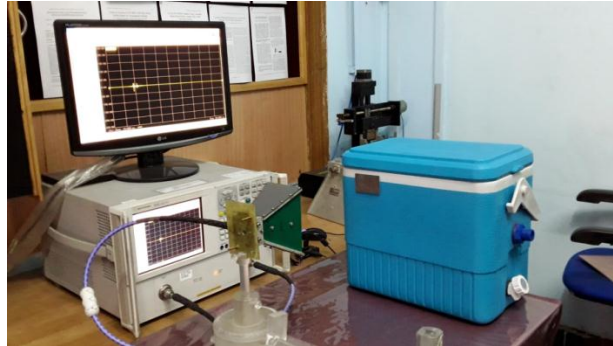


Figure 5.34: Measurement setup of tag fixed on plastic box

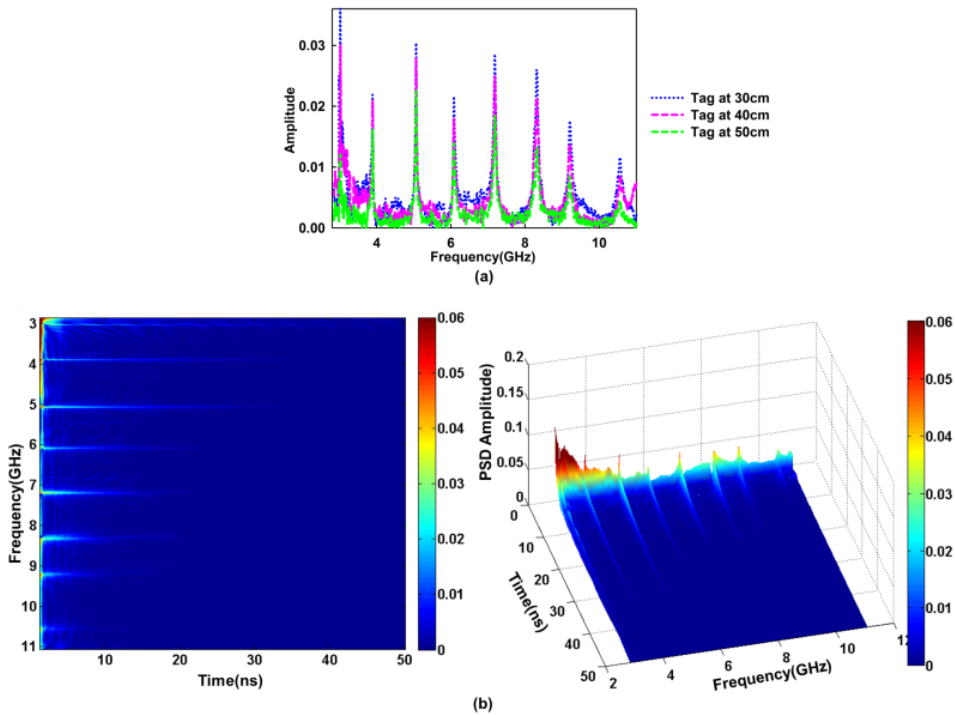


Figure 5.35: Extracted antenna mode spectrum of tag fixed on a plastic box using time domain analysis (a) tag response at different distances (b) Frequency time plot and PSD variation plot of antenna mode spectrum. Window size = 93.8 ns, resolution time = 0.14 ns.

From the figures, it is clear that the tag is well detected on objects like plastic box. Successful detection is possible up to 50 cm. Higher frequencies

are fading tremendously from the spectrum than the lower frequencies. Frequency-time plot and PSD variation plot are also shown in figure 5.35(b) with a window size equal to 93.8 ns and resolution time equal to 0.14 ns. The spectral signature of the 8bit tag is clear in the plots. The higher frequencies exist for a short duration (<10 ns) while the lower frequencies exist comparatively for a longer time (up to 30 ns).

5.5.2 Tag on metal sheet

The advantage of microstrip tags comparing the uniplanar tags is that its resonant characteristics are less affected by the material on which it is fixed. However, the extraction of structural mode and antenna mode is difficult when the tagged object is a metal sheet or any conductive materials. This is due to the fact that such materials will reflect the entire incident wave with higher amplitude than the structural mode signal from the RFID tag. The performance of the RFID tag on a metal sheet extracted using the presented time domain analysis is discussed in this section.

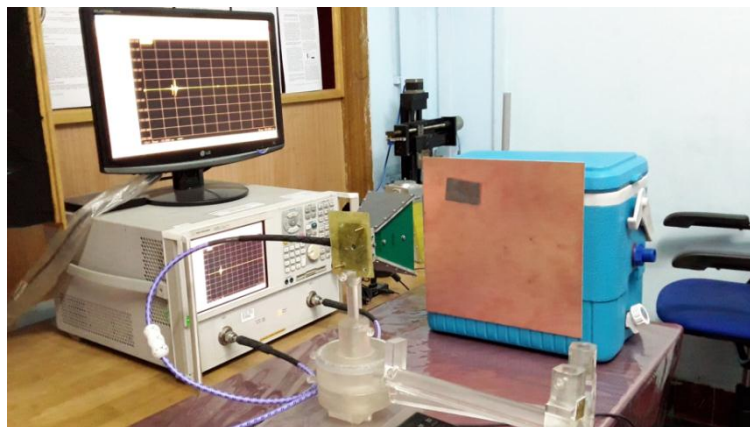


Figure 5.36: Measurement setup of tag fixed on metal sheet

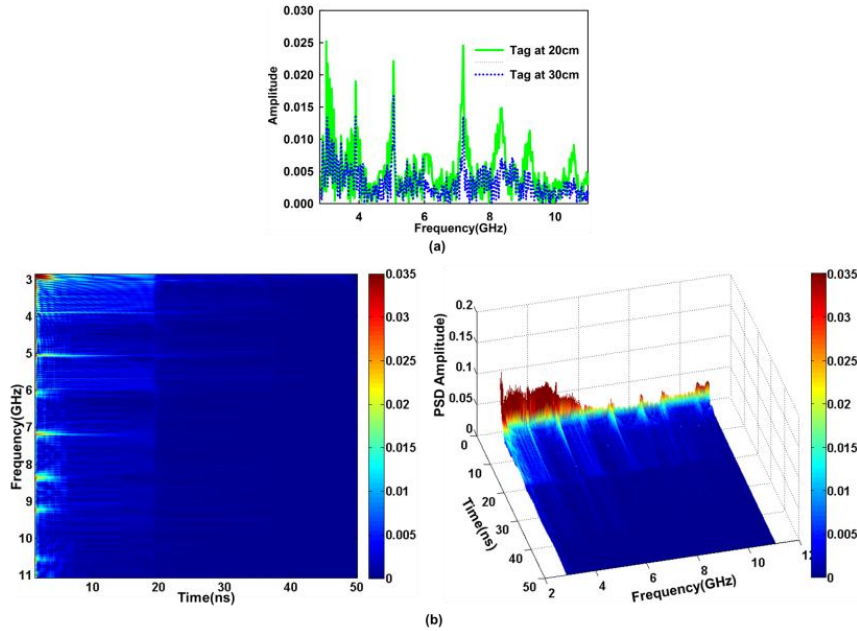


Figure 5.37: Extracted antenna mode spectrum of tag fixed on a metal sheet using time domain analysis (a) tag response at different distances (b) frequency – time plot and PSD plot of antenna mode spectrum. Window size = 93.8 ns, resolution time = 0.19 ns.

The measurement set up is shown in figure 5.36. The results are plotted in figure 5.37. Reflections from the metal sheet degrade tag performance considerably and the tag is detectable only up to 20 cm. Beyond that the extraction of antenna mode from the backscattered signal is very difficult.

5.6 Conclusion

This chapter presents UWB IR technology based time domain analysis of Chipless spectral signature tags. CST microwave studio is used to simulate time domain interrogation of the tags. Time domain measurements are conducted using PNA E8362B. An algorithm to improve the quality of

extraction of antenna mode is proposed and is validated with measured data. All measurements are carried out outside the anechoic chamber and further validations are conducted by attaching the tag on plastic box and metal sheet. The backscattered signal recorded in time domain is decoded successfully for a distance of 50 cm.

References

- [1] P. Kalansuriya and N. Karmakar, "Time domain analysis of a backscattering frequency signature based chipless RFID tag," 2011 Asia-pacific Microwave Conference proceedings (APMC), 2011, pp. 183–186.
- [2] R. Rezaiesarlak, S. Member, M. Manteghi, and S. Member, "Short Time Matrix Pencil Method for Chipless RFID Detection Applications," IEEE Transactions On Antennas And Propagation, Vol. 61, No. 5, pp. 2801–2806, May 2013..
- [3] M. Manteghi, "A novel approach to improve noise reduction in the matrix pencil algorithm for chipless RFID tag detection", IEEE International Antennas Propagation and CNC-USNC Symp./URSI Radio Science Meeting., Toronto, ON, Canada, Jul. 11–17, 2010.
- [4] P. Kalansuriya, N. C. Karmakar and E. Viterbo, "On the Detection of Frequency-Spectra-Based Chipless RFID Using UWB Impulsed Interrogation," IEEE Transactions on Microwave Theory and Techniques, Vol. 60, No. 12, pp. 4187– 4197, December 2012.
- [5] P. Kalansuriya and N. Karmakar, "UWB-IR based detection for frequency-spectra based chipless RFID," in IEEE MTT-S Int. Microw. Symp. Dig., 2012, pp. 1–3.
- [6] M. I. Skolnik, Radar Handbook, 3rd edition New York, NY, USA: McGraw-Hill, 2008.
- [7] S. Preradovic and N. Karmakar, "Design of fully printable planar chipless RFID transponder with 35-bit data capacity," Proceedings of 39th European Microwave Week, Rome, Italy, Sept. 2009, pp. 13–16.

- [8] Nijas C M, Dinesh R, Deepak U, Abdul Rasheed, Mridula S, K. Vasudevan and P. Mohanan, “Chipless RFID Tag using Multiple Microstrip Open Stub Resonators,” *IEEE Transactions on Antennas and Propagation*, Vol. 60, No. 9, pp. 4429-4432, Sep. 2012.
- [9] David Girbau, Javier Lorenzo, Antonio Lázaro, Carles Ferrater and Ramón Villarino, “Frequency-Coded Chipless RFID Tag Based on Dual-Band Resonators”, *IEEE Antennas and Wireless Propagation Letters*, Vol. 11, No.4, pp. 126-128, 2012.
- [10] RFSAW Inc, “The global SAW tag – a new technical approach to RFID”, internet white paper, 2004. Available: <http://www.rfsaw.com/pdfs/SAW%20RFID%20Whitepaper.pdf>
- [11] I. Jalaly and D. Robertson, “RF barcodes using multiple frequency bands,” in *IEEE MTT-S Microwave Sysmp. Dig.*, Long Beach, CA, Jun. 2005, pp. 139–141.
- [12] Y. Shen, C. L. Law, S. Hu, and J. Xia, “IR-UWB-based chipless RFID system,” *Ann. Telecommun. - Ann. Des Télécommunications*, Vol. 68, No. 7–8, pp. 375–383, Jun. 2013.
- [13] A. Ramos, D. Girbau, A. Lazaro, and S. Rima, “IR-UWB Radar System and Tag Design for Time- coded Chipless RFID,” 6th European Conference on Antennas and Propagation (EUCAP2012) Prague - 26-30 March 2012, pp. 2491–2494.
- [14] A. Ramos, D. Girbau, A. Lazaro, and D. Kit, “Influence of materials in time-coded chipless RFID tags characterized using a low-cost UWB reader”, 42nd European Microwave Conference (EuMC 2012) 29, October - 1 November 2012, Amsterdam, Netherlands, pp. 526–529, 2012.
- [15] A. Ramos, A. Lazaro, D. Girbau, and R. Villarino, “Time-Domain Measurement of Time Coded UWB Chipless RFID Tags”, *Progress In Electromagnetics Research*, Vol. 116, pp. 313-331, 2011.
- [16] A. Vena, T. Singh, S. Tedjini, and E. Perret, “Metallic letter identification based on radar approach,” in *Proc. General Assembly Scientific Symp. 2011 URSI*, pp. 1–4.

- [17] A. Vena, E. Perret, and S. Tedjini, “Novel compact RFID Chipless tag”, Progress Electromagnetics Research Symposium, Marrakesh, Morocco, 20-23 March 2011, pp. 1062–1066.
- [18] A. Ramos, D. Girbau, A. Lazaro, and S. Rima” IR-UWB radar system and tag design for time-coded chipless RFID”, Proc. 6th Eur. Conf. Antennas Propagation, EuCAP, 2012, pp. 2491-2494, 2012.
- [19] A. Vena, E. Perret, and S. Tedjini, “Chipless RFID tag using hybrid coding technique,” IEEE Trans. Microwave Theory Tech., Nol. 59, no. 12, pp. 3356–3364, 2011.
- [20] P. Kalansuriya and N. Karmakar, “UWB-IR based detection for frequency-spectra based chipless RFID,” in IEEE MTT-S Int. Microw. Symp. Dig., 17-22 June 2012, Montreal Convention Center Montreal, QC, Canada, pp. 1–3.
- [21] Y. Shen, C. L. Law, S. Hu, and J. Xia, “IR-UWB-based Chipless RFID system,” Ann. Telecommun. -Springer, Vol. 68, No. 7–8, pp. 375–383, Jun. 2013.
- [22] E. Perret, M. Hamdi, G. E. P. Tourtollet, R. Nair, F. Garet, A. Delattre, A. Vena, L. Duvillaret, P. Martinez, S. Tedjini, and Y. Boutant, “THID, the next step of chipless RFID,” 7th IEEE RFID Conf., April 30-May 2 Orlando, FL, 2013, pp. 292–299.
- [23] Novelda Impulse Radar. [Online]. Available: <http://www.novelda.no/>
- [24] C. A. Balanis, Antenna Theory Analysis and Design, 3rd ed. Hoboken, NJ: Wiley, 2005.
- [25] N. Karmakar, Handbook of Smart Antennas for RFID Systems. Hoboken, NJ: Wiley, 2010 [Online]. Available: <http://books.google.com/books?id=WgcSH4G86YAC>.
- [26] Smail Tedjini, Nemaï Karmakar, Etienne Perret, Arnaud Vena, Randika Koswatta, and Rubayet E-Azim, “Hold the Chip” IEEE microwave magazine, pp. 56–65 August 2013.



<i>Contents</i>	6.1 <i>Introduction</i>
	6.2 <i>Chipless RFID tags with reception/transmission antennas</i>
	6.3 <i>Multiscatterer based Chipless RFID tags</i>
	6.5 <i>Time domain analysis of backscattering from frequency domain Chipless tags</i>
	6.6 <i>Comparison of the tags developed in the thesis</i>
	6.6. <i>Future Work</i>

This chapter summarizes the research work presented in this thesis and highlights the conclusions of each chapter. A comparison of different tags developed is presented in tabular form. Scope for future work is also narrated at the end of the chapter.

6.1. Introduction

The study presented in this thesis is focused on the design and development of planar Chipless RFID tags. The frequency domain Chipless RFID tags designed on low loss substrates can provide high data encoding capacity with compact and simple structure. Also, frequency domain tags can incorporate the advantages of time domain tags by adopting time domain techniques to read the frequency domain tags utilizing the time-frequency duality.

The thesis presents two classes of frequency domain based Chipless tags. The first class of tags need Tx and Rx antennas to interact with the interrogation signal from the reader. The second class is the multiscatterer based Chipless tags in which the Tx and Rx antennas are absent. Tags belonging to both classes are developed during the research period. Tags presented in the thesis uses comparatively larger frequency spectrum and offer more freedom in orientation with respect to the reader antenna. Time domain analysis of backscattering from frequency domain tags using sliding windows and Fourier transform is also included in the research work.

The salient features in the research works detailed in this thesis are summarized in the following sections

6.2. Chipless RFID tags with reception/transmission antennas

Quarter wave stepped impedance resonator coupled to microstrip transmission line is the key element of the first type of tag presented in this section. Characteristics like control over harmonic frequencies, flexibility in design and compactness of resonator are effectively utilized in the development

of the Chipless tag. The tag is able to operate over a large spectrum comparing similar tags in literature. The resonators coupled to the transmission line are seen to be more effective than resonators connected to the transmission line and the tag design is completed with resonators coupled to transmitted line. A total bit encoding capacity of 18 bits achieved for the tag with an area of $5.5 \times 2.2 \text{ cm}^2$. The corresponding surface encoding capacity is 1.68 bits/cm^2 .

6.3. Multiscatterer based Chipless RFID tags

Multiscatterer based tags presented in the thesis is an attempt to bring more flexibility in the positioning of tags with respect to the reader and the properties like compactness and high bit encoding are also given special attention. Two types of scatterers; a cross loop resonator and orthogonally joined SIR based scatterers are presented in this context. Both scatterers constitute polarization independent Chipless tags. The cross loop resonator tag offers a compact structure by using the nesting property of resonators and a surface encoding capacity of 1.71 bits/cm^2 is obtained. SIR based tag is very flexible in its design and can use a wide band of frequencies for data encoding. The polarization independent tag offers a surface bit encoding capacity of 1.08 bits/cm^2 . The tag can also be designed for high bit encoding capacity (1.84 bits/cm^2) by employing data encoding elements in both vertical and horizontal polarizations. With a modification to the geometry, the tag is made more compact (3.54 bits/cm^2).

6.4. Time domain analysis of backscattering from frequency domain Chipless tags

Time domain analysis conducted on backscattered signal from the frequency domain tag shows that the tag is having better readability in time

domain than in frequency domain. Also, time domain readers are available in markets under the UWB IR technology and are low cost compared to the frequency domain readers. The time domain analysis employing sliding windows (spectrogram) and Fast Fourier transform is applied. Hamming window is employed in the analysis which offers better performance than with simple rectangular window.

6.5. Comparison of the tags developed in the thesis

Chipless frequency domain tags developed during the research work is compared in the table below.

Table 6.1: Different tags developed and their properties

Tag	Surface coding capacity with presence/absence coding(bit/cm ²)	Surface coding capacity with FSC(bit/cm ²)	Detection range	Freedom in orientation	Control over harmonic frequency
$\lambda/4$ SIR based tag with antennas	0.73 (tag antennas are not considered in the area)	1.69 (tag antennas are not considered in the area)	10	No	Yes
Cross loop resonator based tag	0.82	NA	20	Yes	No
SIR based polarization independent tag	0.33	1.08	40	Yes	Yes
SIR based high bit encoded tag	0.57	1.84	40	No	Yes
SIR based compact polarization independent tag	0.67	2.15	10	Yes	Yes
SIR based compact High bit encoded tag	1.07	3.45	10	No	Yes

6.6. Future Work

The Chipless RFID tag presented in chapter 3 with Tx and Rx antennas is operating over a wide band of frequency exploiting the harmonic control property of SIRs. But the advantage is not attained fully due to the inconsistency of antenna radiation characteristics throughout the spectrum. So realization of the tag with UWB antennas with more stable characteristics throughout the operating bandwidth will improve the detection range of the tag.

Multiscatterer based tags of chapter 4 offer better performances than multiresonator based tags in terms of detection range, freedom in orientation and structural complexity. The high bit encoded tags requiring two cross polarized antennas at reader side can be read by a single highly directional and circularly polarized reader antenna. Development of the whole Chipless RFID system proving the practicability of the presented tags is very significant and the performance can be enhanced with the new generation reader. Studies on the practicability frequency domain Chipless RFID reader should be concentrated along with the realization of much more effective scatterers (having properties like compactness with high Q, multibit encoding per resonator etc.).

Post processing of backscattered energy from the frequency domain tags read in time domain is proved to be effective in chapter 5. Application of more advanced communication techniques and mathematical algorithms to the backscattering to enhance Chipless RFID system performance is under active research and is very important.

Realization of thin, low cost and flexible low loss substrates is also very important in the development of Chipless RFID tags and should be included in the future developments. Also, research in conductive polymers can also be combined with the Chipless RFID.

Incorporation of sensing elements in the tags proposed will be very effective due to their compactness and other properties like polarization independent, high bit encoding capacity etc.. Chipless RFID functions can be enhanced by using them in conjunction with chipped technologies. Scope of this hybrid technology can also be included in the future work.

.....❧.....

COMPACT CHIP INDUCTOR LOADED MULTIBAND ANTENNA

Contents

- A.1. Introduction*
- A.2. Antenna Geometry*
- A.3. Results and Discussions*
- A.4. Conclusion*

A compact chip inductor loaded microstrip patch antenna for multiband application is proposed. The antenna is fabricated on a substrate of dielectric constant 4.4 and thickness 1.6 mm. The proposed circular antenna is of radius 7 mm surrounded by four different inductors which are connected to small rectangular metal patches. The obtained resonant frequencies are 2.28 GHz, 2.82 GHz, 3.96 GHz and 5 GHz. Optimization of the proposed antenna along with simulation and experimental results are presented.

A 1. Introduction

Multiband antennas are highly demanded as services operating in multiple bands are widely used in today's communication. Microstrip antennas are commonly used for this purpose because of their planar structure, low profile, light weight, moderate efficiency and ease of integration with other active and passive devices. Many multiband radiators in planar arrangement have been proposed for mobile communication devices [1-4].

Standard multiband techniques are stacking, addition of parasitic elements, modification of patch by introducing suitably shaped perturbing elements such as slots and notches etc. In [5], a floral shaped patch antenna is designed to resonate at multiple bands by introducing slits on a rectangular patch. The parasitic elements in the design provide a simple and efficient method for obtaining low profile, broadband and high gain antennas. A comparative study of four different multiband planar antennas is presented in [6]. Multiband operation is achieved by etching perturbation slots on the patch. Other techniques such as the use of pin diodes, switches and varactor diodes are also used for multiband operation [7-9]. A new reconfigurable multiband microstrip antenna is proposed in [10]. Slots were cut on a hexagonal to provide the shape of a 6 armed star and further rectangular slots were inserted for achieving multiband operation. The antenna was made reconfigurable by the use of switches. But the use of active components increases complexity in the design and needs extra biasing circuits.

A compact printed monopole antenna with a chip inductor embedded on radiating element is presented in [11-12]. The antenna has one resonant

element and the dual band operation is achieved by embedding one chip inductor to bring down the resonant modes of original antenna. Here it is demonstrated that with chip inductor, the resonant frequency and hence electrical length of the antenna can be reduced considerably.

In this appendix, we are proposing a compact multiband antenna in which the multi band operation is achieved by loading chip inductors in between the central circular patch and surrounding outer rectangular patches. The flower shaped antenna shows four bands of operation. 44% of size reduction is obtained in the lowest resonant frequency of the antenna. The radiation characteristics of the antenna such as return loss, radiation pattern and gain are presented. Parametric optimization method for obtaining desired frequency bands are also addressed in this chapter.

A.2. Antenna geometry

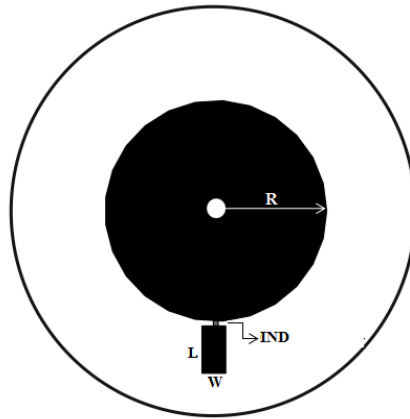


Figure A.1: Coaxial fed antenna with single rectangular patch connected to circular patch through chip inductor (IND). $R = 7$ mm, $L = 3$ mm, $W = 1.5$ mm, substrate height = 1.6 mm and $\epsilon_r = 4.4$

The antenna is fabricated on FR4 substrate of relative permittivity 4.4, loss tangent 0.02 and height 1.6 mm. As shown in Figure A.1, when a single outer patch is connected to the central circular patch through chip inductor (ind =1.8 nH) a lower resonance is generated at 4.48 GHz. The designed frequency band can be easily generated by choosing an appropriate inductor value. Parametric study of the above mentioned structure with different inductor values is shown in Figure A. 2.

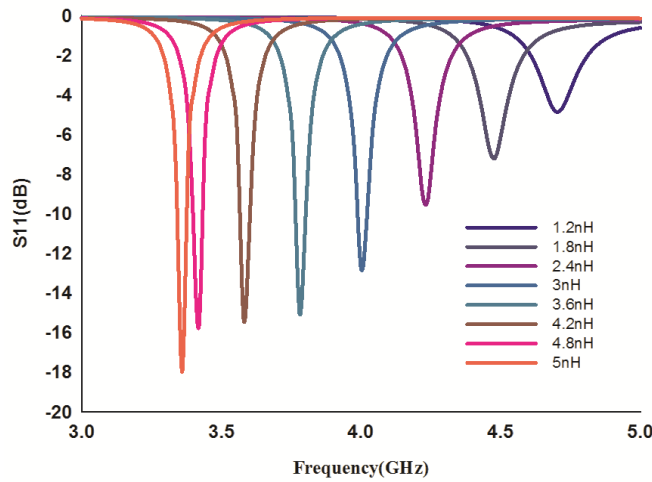


Figure A.2: Different S11 characteristics for different inductor values. Central circular and outer rectangular patch dimensions are same as figure A.1.

The dimensions of rectangular patch can also be used to tune the resonant frequency of the antenna. Resonant frequency variation due to rectangular patch width (W) and length (L) are plotted in Figure A.3. An additional frequency tuning of 1GHz can be achieved by changing the dimensions (L&W) of the rectangular patch. This yields the antenna to operate at any frequency by changing the above parameters.

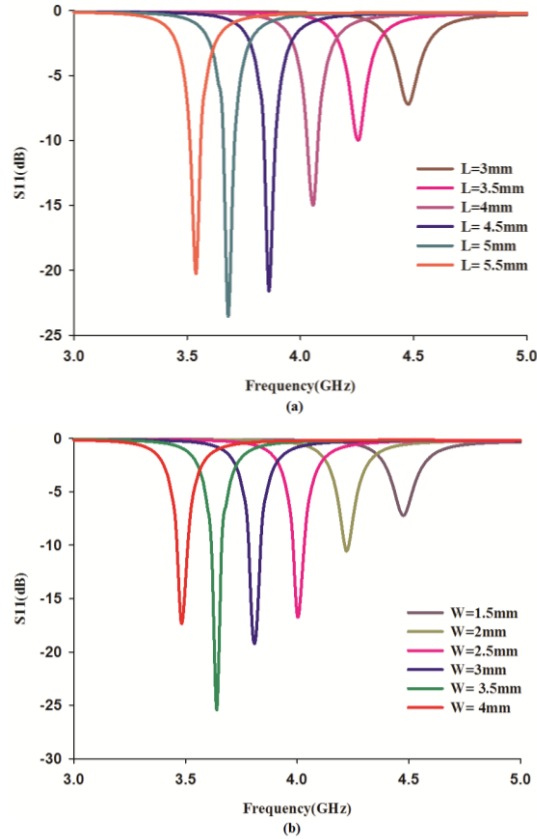


Figure A.3: (a) Effect of different length of outer rectangular patch on reflection coefficient for a width of 1.5 mm. (b) Effect of different width on reflection coefficient for a length of 3 mm. In both cases chip inductor value is 1.2 nH.

The proposed quad band antenna geometry is shown in Figure A.4. The antenna is fed centrally with a coaxial connector to a circular patch of radius 7 mm. The four surrounding outer rectangular patches are of different dimensions. Between the outer rectangular patches and the inner circular patch different chip inductors are loaded to establish different resonant frequencies.

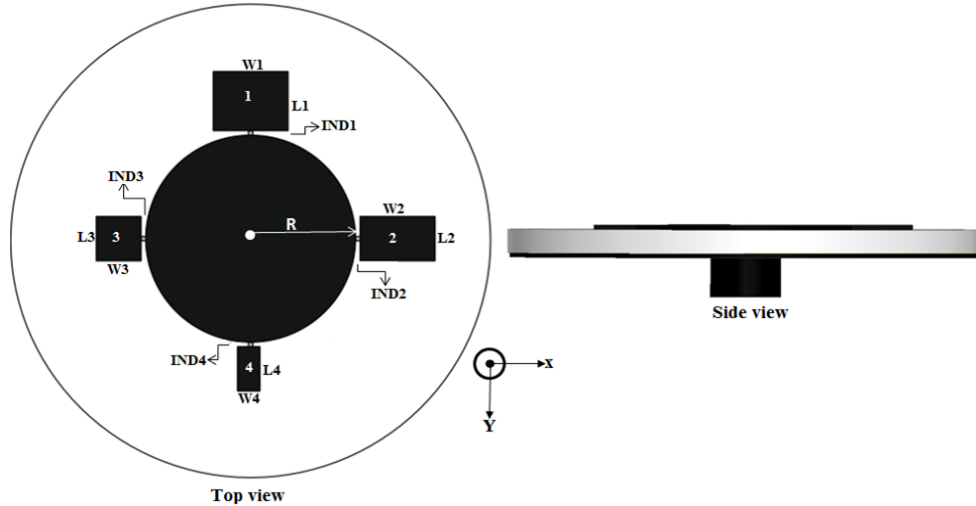


Figure A.4: Geometry of the proposed multiband antenna. $R = 7$ mm, $W1 = 5$ mm, $L1 = 4$ mm, $W2 = 5$ mm, $L2 = 3$ mm, $W3 = 3$ mm, $L3 = 3$ mm, $W4 = 1.5$ mm, $L4 = 3$ mm, $IND1 = 4.7$ nH, $IND2 = 3.3$ nH, $IND3 = 2.2$ nH, $IND4 = 1.8$ nH.

The outer rectangular patch dimensions are also shown in figure A.4. Chip inductors from Coilcraft are used in the fabrication of the antenna and the inductor values are 4.7 nH, 3.3 nH, 2.2 nH, 1.8 nH as shown as IND1, IND2, IND3, IND4 respectively in Figure A.4.

A.3. Results and discussions

Parameters of the antenna are optimized using Ansoft HFSS (High frequency structural simulator). Based on the design parameters and the optimization mentioned above, the prototype of the proposed antenna is fabricated and tested. The antenna is analyzed on RFS ZVB20 network analyzer.

The proposed geometry has 4 outer rectangular patches. Each rectangular patch and the associated chip inductor corresponds to individual

resonances. The dimensions of rectangular strips and inductor values are adjusted to get optimum results. Rectangular patch1 dimensions are adjusted as 5 mm × 4 mm to get the lower resonant frequency. Similarly patch 2, patch 3 and patch 4 dimensions are set as 5 mm × 3 mm, 3 mm × 3 mm, and 1.5 mm × 3 mm, respectively to get the second, third and fourth resonant frequencies.

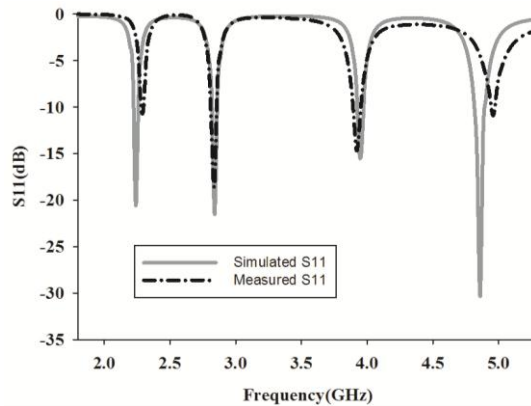


Figure A.5: Simulated and measured reflection coefficient of the multi band antenna shown in figure A.4

Measured and simulated reflection coefficient of the quad band antenna are shown in Figure A.5. The obtained resonances are 2.28 GHz, 2.82 GHz, 3.96 GHz and 5 GHz. The lowest resonance is due to the highest chip inductor value and its associated rectangular patch, i.e., here it is due to IND1 and the rectangular patch connected. Similarly, resonance at 2.82 GHz is the result of current path provided by IND2 to its associated rectangular patch. 3.96 GHz and 5 GHz resonances correspond to IND3 & IND4 and their associated patches, respectively. The measured radiation patterns at the four obtained frequencies are shown in Figure A.6.

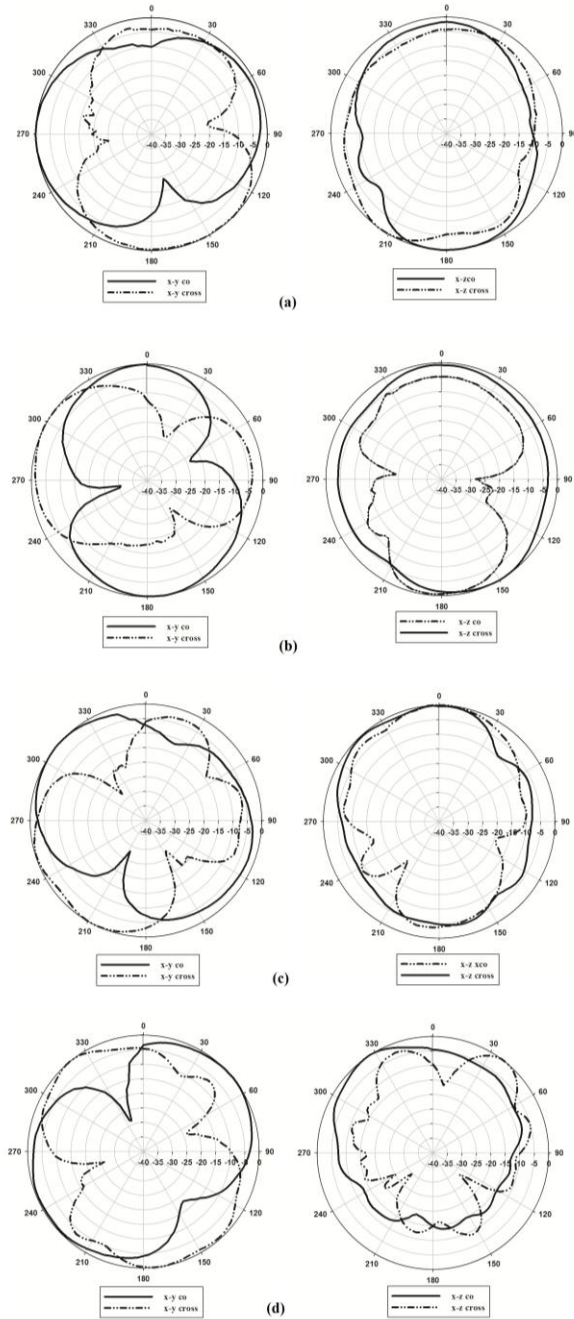


Figure A.6: Measured radiation pattern of the proposed antenna on two planes (x-y & x-z) (a) 2.28 GHz (b) 2.82 GHz (c) 3.96 GHz (d) 5 GHz

The gain of the antenna is calculated using two antenna method and is found as 3 dB at the higher frequency. A size reduction of 44% is obtained compared to the standard circular patch antenna resonating at the same frequency.

A.4. Conclusion

A compact chip inductor loaded quad band flower shaped antenna for microwave applications is presented in this chapter. The obtained resonances are 2.28 GHz, 2.82 GHz, 3.96 GHz and 5 GHz. The VSWR of the proposed antenna is ≤ 2 . The maximum gain of the antenna is observed as 3dB at the highest resonant frequency. A size reduction of 44% is also obtained.

References

- [1] K. Raj, M. Joseph, B. Paul and P. Mohanan, "Compact Planar multiband antenna for GPS, DCS, 2.4/5.8GHz WLAN applications", *Electronics Letters*, Vol.41, No.6, March 2005.
- [2] A. Mehdipour, A. R. Saebak, C. W. Trueman, Tayeb and A. Dendni, "Compact Multiband planar antenna for 2.4/3.5/5.2/5.8GHz Wireless applications", *IEEE Antennas and Wireless Propagation letters*, Vol.1., 144-147, 2012
- [3] Sd. Ashan Ali, Umair Rafique, Umair Ahmad and M. Arifkhan, "Multiband Microstrip Patch Antenna for Microwave Applications", *IOSR Journal of Electronics and Communication Engineering (IOSR-JECE)* ISSN:2278-2834, ISBN: 2278-8735, Vol.3, No. 5, pp. 43-48, Sep-Oct2012
- [4] K. Vyas, A. K. Sharma and P. K. Singal; "A Novel CPW Fed Multiband Circular Microstrip Patch antenna for Wireless Applications", 2012 4th International Conference on Conference on Computational Intelligence and Communication Networks, MATHURA, UTTAR PRADESH, INDIA (3-5 Nov, pp.1-4.

- [5] A. Agrawal and A. Jain; "Effect of Directly coupled parasitic patch on Floral shaped Patch Antenna", International Journal of Engineering Research and applications (IJERA). Vol.2, No.4, pp.954-957, 2012
- [6] C. Ales, Z. RAIDA, E. Las, H. Pacmero and R. C. Ruiz; "Multiband Planar antenna: A Comparative Study, Radio Engineering", Vol.14, No.4, pp.11-20, Dec 2005
- [7] H. Okabe and K. Takeji; "Tunable antenna system for 1.9GHZ PCS handsets", IEEE antennas and propag. Int. Symposium Boston, Massachusetts, 8-13 July 2001, Vol.1 pp.166-169.
- [8] D.Peroulis , K. Sarabandi and L. B. P Katechi; "Design of reconfigurable slot antennas", IEEE antennas and propagation, Vol. 53, No.7, pp. 645-654, 2005
- [9] F.Yang and Y. R Sami; "A reconfigurable patch antenna using switchable slots for circular polarization diversiry", IEEE antennas and propag. Int. Symp., Vol.12, No.3, pp.96-98, 2002.
- [10] J.Constantine, C.G, Christodoulou and S.E. Barbi; "A new Reconfigurable Multiband Patch Antenna", 2007 SBMO/IEE MTT-s International Microwave and Optoelectronics conference (IMOL2007), 29 Oct - 01 Nov 2007, Pestana Bahia Hotel Salvador, Brazil, pp.75-78
- [11] Qi Luo, J. R Pereira and H. M Salgado; "Compact Printed monopole Antenna with Chip inductor for WLAN", IEEE Antennas and Wireless Propagation letters, Vol.10, pp. 880-883, Aug 2011
- [12] Qi Luo, H. M Salgado and J. R Pereira; "Compact Printed C Shaped Monopole Antenna With Chip inductor", IEEE Antennas and Wireless Propagation letters, Vol.10, pp.156-159, 2011

.....❧.....

||| List of Publications |||

International Journals

- [1] **V. R. Sajitha**, C. M. Nijas, T.K. Roshna, Kesavath. Vasudevan and P. Mohanan, “Compact Cross Loop Resonator Based Chipless RFID Tag with Polarization Insensitivity” *Microwave and Optical Technology Letters* Vol. 58, No. 4, April 2016 ,pp. 944-946
- [2] **V.R. Sajitha**, C. M. Nijas, T.K. Roshna, R. Vivek, Kesavath. Vasudevan and P. Mohanan, “Polarization Independent Chipless RFID Tag”, *Microwave and Optical Technology Letters*, Vol-57, No.8, Aug2015, pp. 1889-1894.
- [3] **V. R. Sajitha**, C. M. Nijas, T. K. Roshna and P. Mohanan, “Compact Chip Inductor Loaded multiband Antenna”, *European Journal of Advances in Engineering and Technology (EJAET)*, Vol.2, No.4, pp.77-80.
- [4] **V. R. Sajitha**, C. M. Nijas, T. K. Roshna and P. Mohanan, “ Multiresonator Circuit Using $\lambda/4$ Sir For Chipless Rfid Tags” *International Journal on Cybernetics & Informatics (IJCI)* Vol. 5, No. 2, April 2016,pp .357-364
- [5] T. K. Roshna, U. Deepak, **V. R. Sajitha**, K. Vasudevan, P. Mohanan, “Modified Bowtie Antenna for Zeroth Order Resonance”, *Pier C*, Vol. 48, pp 45-52, 2014.
- [6] T. K. Roshna, Deepak u., Nijas C. M., **Sajitha V. R.**, Mohanan P., “A high gain Compact Coplanar Stripline fed Antenna for Wireless Application”, *Microwave and Optical Technology Letters* , Vol. 56, No. 8, August 2014.
- [7] T. K. Roshna, U. Deepak, **V. R. Sajitha**, and P. Mohanan, A coplanar stripline fed compact UWB antenna, *Electron. Letters*, Vol. 50, No. 17, pp. 1181-1182, Aug. 2014.
- [8] T. K. Roshna, U. Deepak, **V. R. Sajitha**, K. Vasudevan, and P. Mohanan, “A Compact UWB MIMO Antenna with Reflector to Enhance Isolation”, *IEEE Transactions on Antennas and Propagation*, Vol.63. No.4, April 2015,pp. 1873-1877

Conferences

- [1] **V.R. Sajitha**, C.M. Nijas, T. K. Roshna and P. Mohanan, “ Chipless Rfid Tag Based On Stepped Impedance Resonators”, APSYM Dec 2014, Department of Electronics, CUSAT, Kochi-22, INDIA
- [2] **V R Sajitha**, Nijas C M, Roshna T K and P. Mohanan, “Multiresonator circuit using $\lambda/4$ SIR for Chipless RFID Tags”, International Conference on computing and Communication 2016 (ICCC'2016), Mar Athanasius College of Engineering Kothamangalam, Kerala, INDIA.
- [3] C.M Nijas, **V.R Sajitha** and P Mohanan, “Properties of Stepped Impedance Resonator and its Application in the Design of Chipless RFID Tag”, EuCAP2015, Lisbon, Portugal on 12-17 April 2015.
- [4] C M Nijas, **V R Sajitha**, R Vivek, P Mohanan, Binu Paul and dS Mridula, “Spectral extraction of chipless RFID tag using time domain analysis”, Antennas and Propagation & USNC/URSI National Radio Science Meeting, 2015 IEEE International Symposium, Vancouver, BC, Canada pp: 169 – 170.
- [5] C. M. Nijas, P. V. Vinesh, **V. R. Sajitha**, P. V. Anila and P. Mohanan “Optimisation of Quarter Wave Microstrip Open Stub Resonators for Chipless RFID Applications” IEEE International Symposium on Antennas and Propagation and USNC-URSI National Radio Science Meeting, July 7-12, 2013, Orlando, Florida, USA
- [6] Shari Mohan, P.R. Harikrishnan, **V.R. Sajitha**, C. M. Nijas and P. Mohanan “Chipless RFID Tag with SMD Inductors” International Conference on Information Science 2014 (ICIS'14), July 4-5, 2014 at Cochin, Kerala, India.

..........

Resume of Author

Sajitha V R

Senior Research Fellow

Centre for Research in Electromagnetics and Antennas

Department of Electronics

Cochin University of Science and Technology

Cochin-682022

Kerala, India.

Email: svrk1989@gmail.com

Ph: +91-9744631699



Experience

- 5 years of research experience in Microwave Antennas, Chipless RFID, Electromagnetics and Dielectric measurements.
- International Publications – 7
- 1 year teaching Experience

Achievements

- UGC-NET
- KSCSTE Research Fellowship 2011
- University First Rank Holder in BSc. Electronics from Calicut University, Kerala, India
- Second Prize Winner in Inter zone Archery competition during graduation

Areas of Interest

- Microwave Antennas, Multiband antennas, Implantable and Wearable antennas, MIMO Antennas, Microwave Sensors, Biological effects of Microwaves, Chipless RFID, Filters, Microwave material characterization etc..

Technical Skills

- Experience in using HP 8510C Vector Network Analyzer, PNA E8362B Network Analyzer, R&S ZVB20 Network Analyzer, Spectrum Analyzer, Anechoic chamber etc..

- Experience in Antenna and RF/Microwave circuit design tools like Ansoft HFSS, CST MWS, Agilent ADS, etc..
- Experience in Microwave Material Characterization measurement using the Cavity Perturbation Method.
- Hands-on experience in building of antenna prototypes using photolithography and CNC Machine, and antenna experimental work.
- Experience in the design and development of microstrip antennas and Chipless RFID tags
- MATLAB
- Computer Languages- C,C++, VB
- Documentation- MS Office, LATEX

Scholarly Works and Services

- Active participant and Member in the Organizing Committee of International Biennial Symposium on Antennas and Propagation Symposium (APSYM), from 2012 to 2014.
- Active Member in the Organizing Committee of Biennial International Symposium on Ocean Electronics (SYMPOL) from 2013-2015.
- Actively engaged in organizing various events and workshops
- Attended various National and International conferences and presented research papers

Educational Qualification

Course	Year	University	Institution	Class
PhD	Doing	Cochin University of Science and Technology, Cochin(CUSAT), Kerala, India	Centre for Research in Electromagnetics and Antennas Department of Electronics, CUSAT, Kerala, India	---
M.Sc Electronics	2009-2011	Cochin University of Science and Technology(CUSAT), Cochin, Kerala, India	Department of Electronics,CUSAT, Kerala, India	First class CGPA 8.51/10

Personal Details

Date of birth : 30th May 1989
Sex : Female
Languages Known : English, Hindi and Malayalam
Nationality : Indian
Marital status : Married
Adhaar card Number : 3618 7246 8998
Father's Name : V K Radhakrishnan
Mother's Name : M B Anjanavathi
Permanent Address : W/o Dipu K. Dilip
"Kizhakkanoor"
Kottavathil, Kottamuri P O
Thrissur
Kerala India 680732

.....*✍*.....